



HAL
open science

Engineering microchannels for vascularization in bone tissue engineering

Bruno Aor

► **To cite this version:**

Bruno Aor. Engineering microchannels for vascularization in bone tissue engineering. Polymers. Université de Bordeaux; Université catholique de Louvain (1970-..), 2018. English. NNT: 2018BORD0430 . tel-02090853

HAL Id: tel-02090853

<https://theses.hal.science/tel-02090853v1>

Submitted on 5 Apr 2019

HAL is a multi-disciplinary open access archive for the deposit and dissemination of scientific research documents, whether they are published or not. The documents may come from teaching and research institutions in France or abroad, or from public or private research centers.

L'archive ouverte pluridisciplinaire **HAL**, est destinée au dépôt et à la diffusion de documents scientifiques de niveau recherche, publiés ou non, émanant des établissements d'enseignement et de recherche français ou étrangers, des laboratoires publics ou privés.



THÈSE EN COTUTELLE PRÉSENTÉE

POUR OBTENIR LE GRADE DE

DOCTEUR DE

L'UNIVERSITÉ DE BORDEAUX

ET DE L'UNIVERSITÉ CATHOLIQUE DE LOUVAIN

ÉCOLE DOCTORALE DES SCIENCES CHIMIQUES

ÉCOLE POLYTECHNIQUE DE LOUVAIN

SPÉCIALITÉ POLYMÈRES

Par Bruno AOR

Engineering microchannels for vascularization in bone tissue engineering

Sous la direction de Mme. Marie-Christine DURRIEU
et de Mme. Sophie DEMOUSTIER-CHAMPAGNE

Soutenu le: 17 décembre 2018

Membres du jury :

M. Landoulsi Jessem	Maître de Conférences de Sorbonne Université, France	Rapporteur
M. Laroche Gaetan	Professeur de l'Université Laval, Canada	Rapporteur
M. Pauthe Emmanuel	Professeur de l'Université de Cergy-Pontoise, France	Examineur
Mme. Migonney Veronique	Professeur de l'Université Paris 13, France	Examineur
Mme. Bordenave Laurence	Professeur de l'Université de Bordeaux 2, France	Examineur
M. Jonas Alain	Professeur de l'Université catholique de Louvain, Belgique	Président
Mme. Demoustier-Champagne Sophie	Professeur de l'Université catholique de Louvain, Belgique	Directeur
Mme. Durrieu Marie-Christine	Directeur de Recherche INSERM Bordeaux, France	Directeur

This thesis work was carried out in the European Joint Doctorate in Functional Materials Research (EJD-FunMat) framework, and is the results of a collaboration between:

Université de Bordeaux

CNRS, Chimie et Biologie des Membranes et des Nanoobjets UMR5248

1 Allée Geoffroy Saint-Hilaire 33600 Pessac, France

Under the supervision of

Dr. Marie-Christine DURRIEU

and

Université catholique de Louvain

Institut de la Matière Condensée et des Nanosciences

Bio- and Soft Matter

Croix du Sud, 1

B-1348 Louvain-la-Neuve, Belgique

Under the supervision of

Pr. Sophie DEMOUSTIER-CHAMPAGNE

and

it4ip, Belgium (industry partner)



Acknowledgements

The path, which is life, often reserves unexpected surprises. We are constantly overwhelmed by stimuli, emotions, newness, problems, and worries. All mixed together to give strong emotions that radically change you deeply. The combination of places, people, experiences, passions, pains, joys, worries and much more was the Ph.D. for me. I do not regret any of my choices, because it is precisely my choices that have made me grow in the person I am now. And indeed, I feel the need to thank each of the special people with whom I have shared beautiful moments of my life, private and academic.

First of all my journey started thanks to the European Joint Doctorate for Multifunctional Materials (EJD-FunMat) funds, which allowed a collaboration between the University of Bordeaux (UBX) in France and the Catholic University of Louvain (UCL) in Belgium. First of all, I would like to thank my two supervisors, Marie-Christine Durrieu at UBX, and Sophie Demoustier at UCL. Thanks to the patience and joint support, they immediately made me feel welcome in the new environment. In particular, Marie, with her timeless positivity, has spurred me every day to see the best even when it does not seem possible. His patience in trying to understand, and his inestimable strength of spirit, pushed me to always look for the best or at least not get me into the constant world of problems and failures, such as scientific research. Sophie, with her kindness, guided me and supported me during the Bordeaux-Belgium work transitions, helping me a lot during the early stages to find accommodation and then giving me precious advice on the world of polymers and LbL.

In Belgium, I also want to thank Alain Jonas who assisted me in the first part of the characterization of the material and the LbL, through new techniques (for me at least new) and has always had a good dose of patience with me. I also want to thank Karine Glinel, who gave me much practical advice, transferring my ability to work meticulously, with precision and scientific rigor. I also want to thank her, especially because, even if not being strictly part of my project, she has always been very helpful, patient and sympathetic towards me.

In addition, I would like to thank UBX, Laurent Plawinski for the help I received on cellular culture and other methodologies concerning work in sterility and biological tests, and also Christel Chanseau for help in the chemistry lab and chemical management. I would also like to thank the Bordeaux Imaging Center for the fundamental help given to me for experiments and confocal microscope.

During the early stages, in France, our group was the host of the IECB, and we were able to share, albeit in small part, the joys, and adventures of the research world. I would like to thank Reiko Oda for her vivacity, her energy, her desire to have fun, and the feasts organized at her house to celebrate the most important parties all together internationally.

As for the working group in France, what to say ... they have become like a family for me! We laughed, we cried, we rejoiced and we were desperate. An explosive mix that has formed indissoluble bonds over time. I am aware that, unfortunately, over time these bonds will become less intense and will become memories, but it is precisely the experiences and memories that we carry within our hearts every day, and it is these little new elements, jealously guarded, that they grow and mature in the person you want to be in your future. I, therefore, thank Laurence Padiolleau, Caroline Royer, Emilie Prouve, Luce le Gat, Marion Petitet, Julie Lavie, Jian-Quiao, Noemie Dubuc, and Catarina Pedrosa. I especially want to thank Catarina Pedrosa, not only for sharing with me the joys and sorrows in the world of work, but because she had the (crazy) idea of sharing the house for almost two years in Bordeaux. This makes her particularly important for the huge amount of patience needed to share the same roof with me (I am fully aware ^.^). But I do not want to limit my thanks only to the members of my workgroup, in fact, the family that I created in France goes much further! I want to thank whom has hard-worked (more or less: p) with me in the open space! Manon Jaffredo, Myriam Abarkan, Karen Leal Fischer, Mathieu Coudert, Antoine Baudin (yes, everyone should try the thesis in 180 seconds), Coralie Croissant and Adeline Evrard. I thank all of them for their insatiable desire for sweets, which led me to discover new recipes and new ways of cooking! I want to thank Adeline also for giving me the chance, together with Tarik, to discover new dance styles like Kizomba! I really loved this new experience! Also, I particularly want to

thank Coralie for sharing with me the passion for ballroom dancing, rock, salsa, and Argentine tango! These are all experiences that I will bring with me in the future, and I hope one day, to be able to improve and practice better and better this beautiful adventure that is the dance.

In Belgium, I had the opportunity to share daily experiences with my colleagues, and I would like to thank Delforge Jean-Marc, D'haese Cécile, Douchamps Colette, Ferain Etienne, Lipnik Pascale, Magnin Delphine, Van Velthem Pascal, Bahrami Amir, Chattaway Claire, Horion Jérémy, Gribova Varvara, Lefevre Damien, Lemaitre Matthieu, Somville Eleana, Cai Ronggang, Chandra Prakash, Fernandes Antony, Moshkunov Konstantin, Abreu Araujo Flavio, Giol Diana, Kuterbekov Mirasbek, and Ciardi Moira. Moira helped me since the early days in Belgium, creating a connection between connotations, making me feel part of the new group. With Mirasbek, I immediately linked a lot, and we shared many experiences thanks to the meetings organized by the EJD-FunMat program, organized twice a year. With regard to these meetings, I also want to thank Francesco Naccarato and Danila Amoroso with whom I have spent wonderful moments of complicity.

In Belgium, I have had wonderful moments with the "Belgian family" who gave me hospitality and cordiality during my long stay. We spent wonderful moments together, despite the differences, and this really touched me a lot. So I want to thank Gudrun, Muriel, Benjamin, and Antoine. I also want to thank my dance partners in Belgium, who shared the room with me with energy, liveliness, and passion, making it possible to have fun even in the most stressful moments. I, therefore, thank Alain, Eleonore, Shara, Melanie, Christine, Aïda, Arnaud, Marco, and Mathilde.

I also want to thank my friends left in Italy, who despite all have had the desire and the patience to keep in touch even at a distance. A heartfelt thanks then to Sabrina, Andrea, Elena, Alessandra, Michele, and Calogero.

Fundamental was the help and support of my girlfriend Sophie, who with me have endured stress, distance, loneliness, long waits, and countless journeys to be together despite the distances and the work.

Infine un ringraziamento particolare alla mia famiglia, la quale mi ha donato ali per volare lontano, ed un cuore per amare tutto il mondo. Grazie quindi a Mamma

Acknowledgements

Rita, Papa Silvano, Nonne Nini e Marica, la mia piccola sorellina Elisabetta e la mia sorellona Giorgia con Andrea ed i "Piccoli" Alice e Francesco.

To all of them, I wish a long life, prosperity and may the force be with them all!

Summary

Engineered microchannels for vascularization in bone tissue engineering

Tissue engineering is an always-evolving field, which aims to restore the physiological functions of damaged tissues and organs. It uses the most advanced techniques and methodologies to develop always-new biomaterials and engineered tissues with unique properties and characteristics. This challenging goal can be achieved through the combination of cells, biological factors, and biomaterial scaffolds. Those last do not work uniquely as supportive elements for the cells but thanks to their physicochemical properties they can drive the cell into adhesion, migration, morphology change, differentiation and so on, to develop the new tissue. In this fundamental context of biomaterial development, the surface has to be optimized to increase the interaction of the biological components with the cells to favor the growth of the new tissue.

A very important limiting factor in the development of large and complex tissues is the impossibility to develop a rapid, stable, and organized micro-vascular network. This network is normally present in almost all the tissues and allows the exchange of oxygen and nutrient with the discarding metabolite products and carbon dioxide in each cell of the human body. Herein, we designed and developed micro-structured channels that, once biofunctionalized to mimic the physiological extracellular matrix, drive the development of capillary vessels *in vitro*.

We first created micro-channels bioactive surfaces by combining hot-embossing technique and surface functionalization technique. Those micro-channels were transferred on to a polycarbonate film using silicon line mold as the template (Figure i).

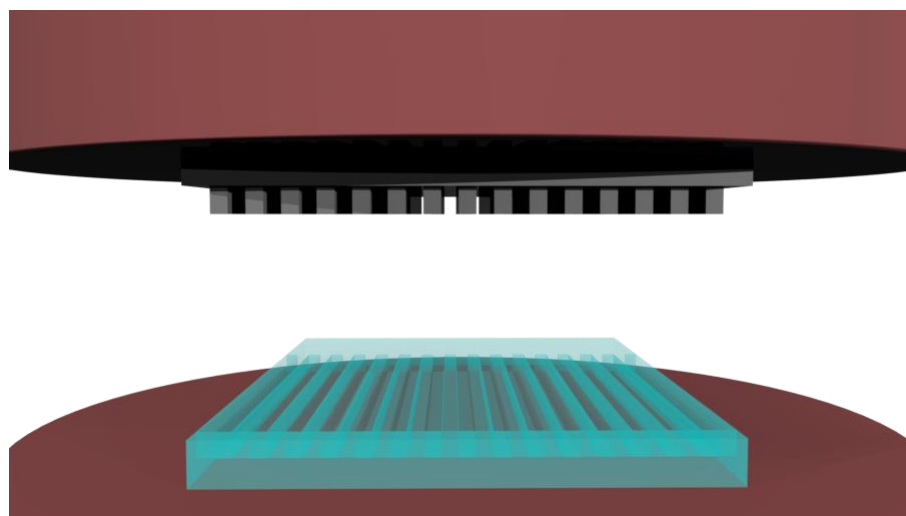


Figure i – Schematic of the imprinting process. On the upper part, in gray, the silicon mold (SiM) with the pattern line. On the bottom, in light blue, the polycarbonate micro-channels (PC- μ Ch). In red the two plates, on which the pressure is applied during the hot-embossing process.

An initial step of layer-by-layer (LbL) deposition of natural polysaccharides of chitosan and hyaluronic acid is used to develop a favorable environment for the endothelial cells, and at the same time, provide a rich surface for peptides immobilization. We characterize the micro-channels development using a combination of scanning electron microscopy and profilometry. Later, LbL deposition was investigated with ellipsometry and confocal laser scanning microscopy (CLSM). Finally, the immobilization of the adhesive peptide RGD and the angiogenic peptides SVV and QK were characterized with fluorescence microscopy to quantify the number of each type of peptides present on the material's surface and localize their penetration into the layer-by-layer cushion.

Next, we studied human umbilical vein endothelial cells (HUVECs) behavior on the biofunctionalized surfaces, identifying which combination of LbL and peptide would promote cellular adhesion and increased metabolic activity. The combination of adhesive and angiogenic peptide represents a good support for HUVECs to adhere and grow. The aim was to develop capillary vessels inside the functionalized micro-

channels (Figure ii). For this reason, we studied HUVECs behavior on the functionalized micro-channels using a combination of time-lapse CLSM and fixed-time CLSM. We found how the combination of micro-channels, LbL, RGD, and QK or SVV peptides provide the best conditions for the development of capillary-like structures already after 2 hours of incubation. In the case of RGD+QK combination, the capillary-like structures were observed also for the next two hours of the experiment.

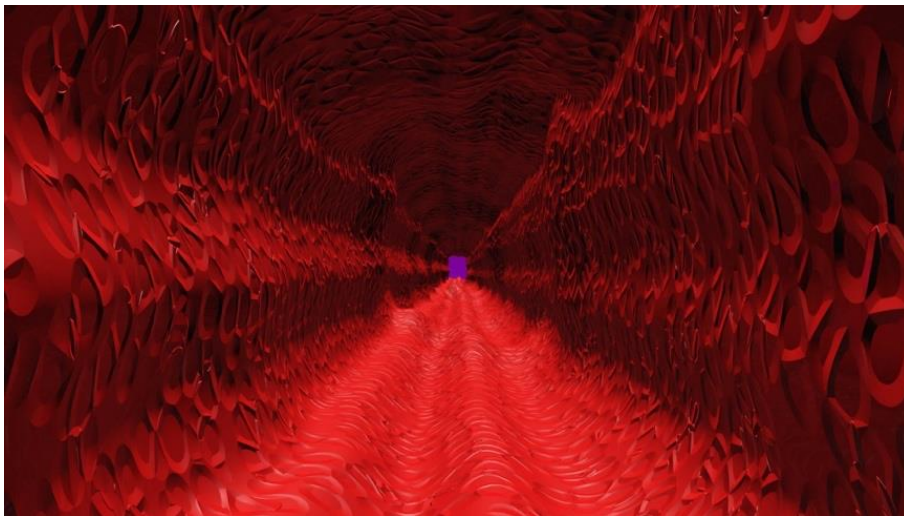


Figure ii – Schematic of the tubular structure of the capillary vessel. In red the capillary vessel seen from inside composed of HUVECs.

Finally, we investigated a co-culture system using HUVECs combined with human pericytes derived from placenta (hPC-PL) to assess the stabilization of the capillary-like structures in the micro-channels (Figure iii) with LbL, RGD, and SVV peptides. For this, we used CLSM and different markers to identify and localize both cells at the same time in the biofunctionalized material. We found how the presence of hPC-PL influence positively the stability of the capillary-like structures, showing a clear formation of the empty-lumen structure for two hours longer than the control with HUVECs monoculture.

To summarize, the combination of micro-channels and surface functionalization is a unique way of capillary development after only two hours in both monocultures of HUVECs or co-culture of HUVECs with hPC-PL.

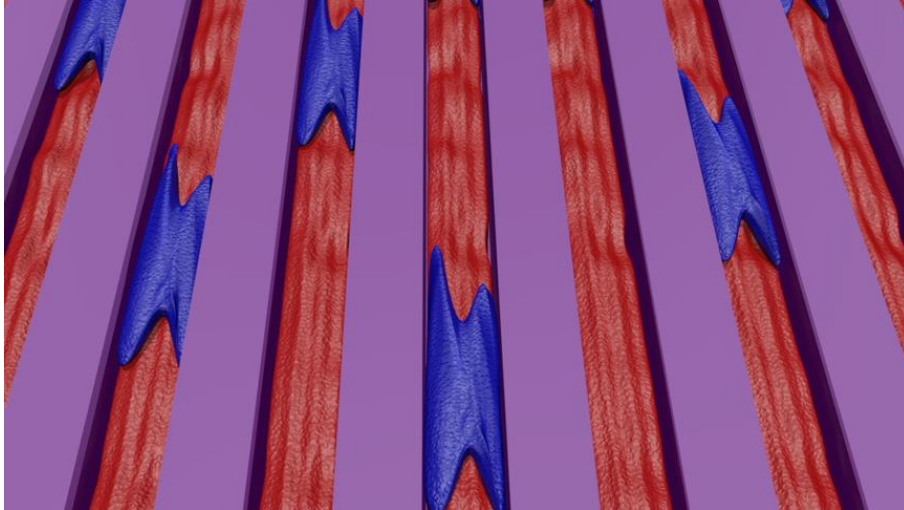


Figure iii – Schematic of the pericytes stabilization. Pericytes (in blue) wrapping the HUVECs (in red) as one possible mechanism of stabilization. All of this, inside the micro-channels of the biofunctionalized material (violet).

Keywords: hot-embossing, surface functionalization, micro-channels, layer-by-layer, bioactivity, human umbilical vein endothelial cells, human pericytes, peptides, capillary structure.

Résumé (long)

Synthèse de microcanaux bioactifs pour la vascularization

L'ingénierie tissulaire est un domaine en constante évolution qui vise à restaurer les fonctions physiologiques des tissus et organes endommagés. Il utilise les techniques et les méthodologies les plus avancées pour développer des biomatériaux toujours nouveaux et des tissus techniques dotés de propriétés et de caractéristiques uniques. Cet objectif ambitieux peut être atteint en combinant des cellules, des facteurs biologiques et des échafaudages de biomatériaux. Ceux-ci ne fonctionnent pas uniquement comme éléments de soutien pour les cellules, mais grâce à leurs propriétés physico-chimiques, ils peuvent conduire à l'adhésion, la migration, le changement de morphologie, la différenciation, etc., et au développement du nouveau tissu. Dans ce contexte fondamental du développement des biomatériaux, la surface doit être optimisée pour augmenter l'interaction des composants biologiques avec les cellules afin de favoriser la croissance du nouveau tissu.

Un facteur limitant très important dans le développement de tissus volumineux et complexes est l'impossibilité de développer un réseau micro-vasculaire rapide, stable et organisé. Ce réseau est normalement présent dans presque tous les tissus et permet l'échange d'oxygène et de nutriments avec les produits métabolites et le dioxyde de carbone rejetés dans chaque cellule du corps humain. Dans le présent travail de recherche, nous avons conçu et développé des canaux micro-structurés qui, une fois biofonctionnalisés pour imiter la matrice extracellulaire physiologique, entraînent le développement de vaisseaux capillaires *in vitro*.

Nous avons d'abord créé des surfaces bioactives micro-structurées en combinant la technique d'estampage à chaud et des techniques de fonctionnalisation de surface. Les microcanaux ont été transférés sur un film de polycarbonate en utilisant un moule en silicium comme gabarit (Figure iv).

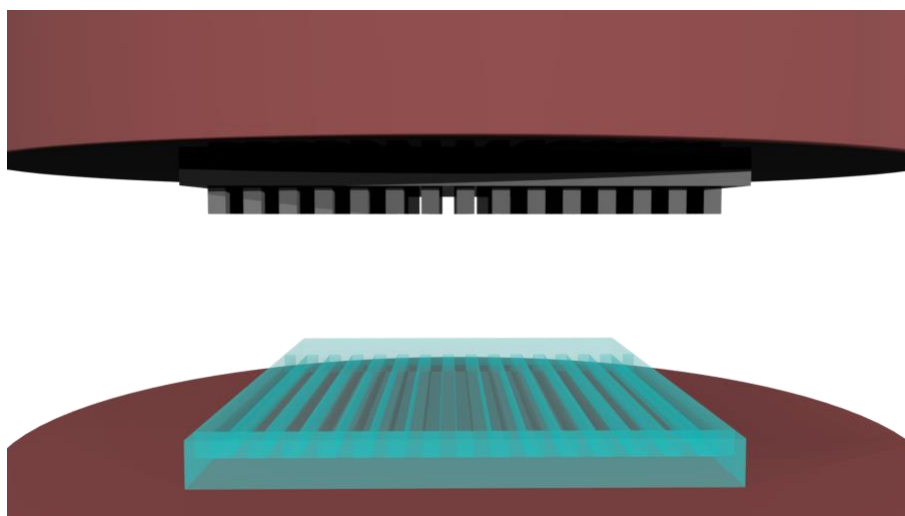


Figure iv - Schéma du processus d'impression. Sur la partie supérieure, en gris, le moule en silicium (SiM) avec la ligne de motif. En bas, en bleu clair, les micro-canaux en polycarbonate (PC-μCh). En rouge, les deux plaques sur lesquelles la pression est appliquée pendant le processus de gaufrage à chaud.

Une première étape de dépôt couche par couche (LbL) de polysaccharides naturels de chitosane et d'acide hyaluronique est utilisée pour développer un environnement favorable aux cellules endothéliales, tout en fournissant une surface riche pour l'immobilisation des peptides. Les dimensions des micro-canaux ont été caractérisés en combinant la microscopie électronique à balayage et la profilométrie. Dans un second temps, la croissance du dépôt LbL a été étudié par ellipsométrie et microscopie confocale à balayage laser (CLSM). Enfin, l'immobilisation du peptide adhésif RGD et des peptides angiogéniques SVV et QK a été caractérisée par microscopie à fluorescence afin de quantifier le nombre de chaque type de peptides présents sur la surface du matériau et localiser leur pénétration dans le coussin LbL.

Ensuite, nous avons étudié le comportement des cellules endothéliales de la veine ombilicale humaine (HUVEC) sur les surfaces biofonctionnalisées, en identifiant la combinaison de peptides qui favoriserait l'adhésion cellulaire et augmenterait l'activité métabolique. La combinaison du peptide adhésif et du peptide angiogénique représente un bon support pour que les HUVEC adhèrent et se développent. L'objectif était de développer des vaisseaux capillaires à l'intérieur

des micro-canaux fonctionnalisés (Figure v). Le comportement des HUVECs sur les micro-canaux fonctionnalisés a ensuite été étudié à l'aide d'une combinaison de CLSM time-lapse et de CLSM à temps fixe. Nous avons montré comment la combinaison de micro-canaux, LbL, RGD, et les peptides QK ou SVV fournissent les meilleures conditions pour le développement de structures de type capillaire déjà après 2 heures d'incubation. Dans le cas d'une combinaison RGD + QK, les structures de type capillaire ont également été observées pendant les deux heures suivantes de l'expérience.

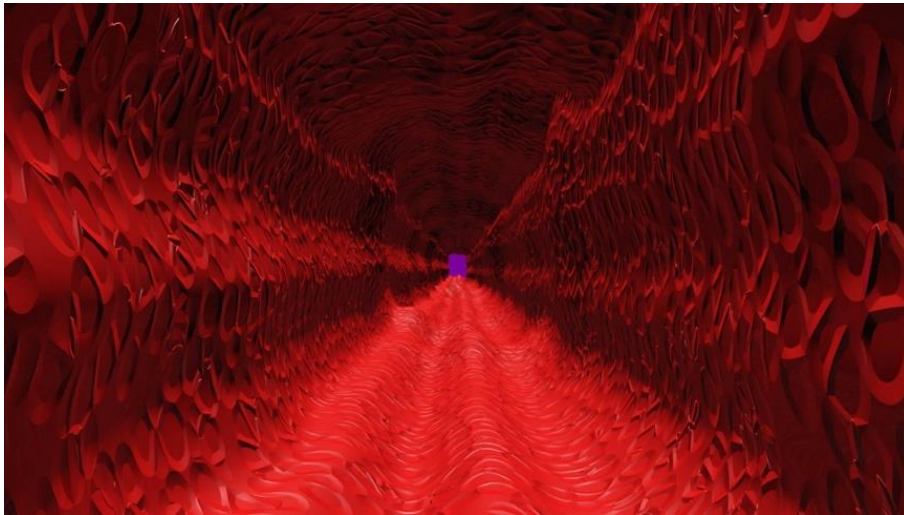


Figure v - Schéma de la structure tubulaire du vaisseau capillaire. En rouge, le vaisseau capillaire, vu de l'intérieur, composé de HUVEC.

Enfin, nous avons étudié un système de co-culture utilisant des HUVEC combinées à des péricytes humains dérivés du placenta (hPC-PL) pour évaluer la stabilisation des structures capillaires dans les microcanaux (Figure vi) avec les peptides LbL, RGD et SVV. Pour cela, le CLSM et différents marqueurs pour identifier et localiser les deux types cellulaires simultanément dans le matériel biofonctionnalisé ont été utilisés. Nous avons trouvé comment la présence de hPC-PL influençait positivement la stabilité des structures de type capillaire, montrant une

nette formation de la structure à lumière vide pendant deux heures de plus que la monoculture de HUVEC.

En résumé, la combinaison de micro-canaux et de fonctionnalisation de surface est un moyen unique de développement de capillaires après seulement deux heures de monocultures de cellules HUVEC ou de co-culture de cellules HUVEC avec le hPC-PL.

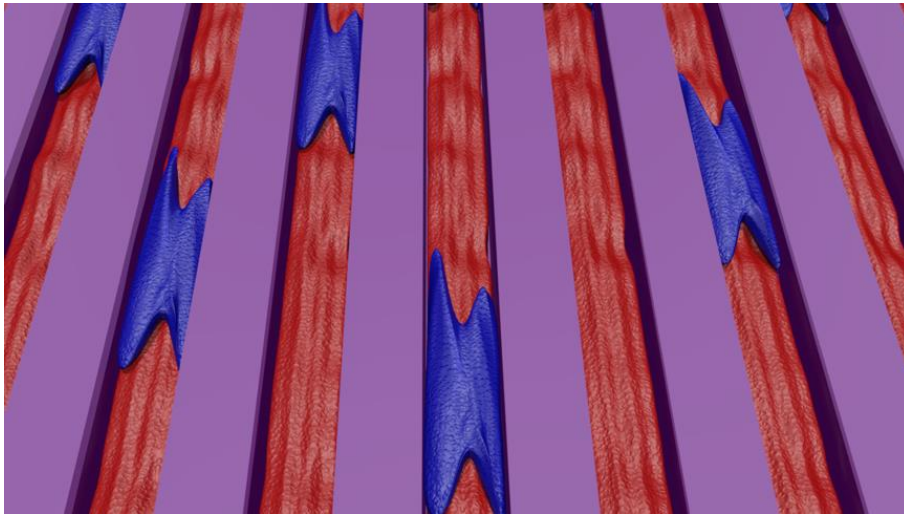


Figure vi - Schéma de la stabilisation des péricytes. Les péricytes (en bleu) enveloppent les HUVEC (en rouge) comme possible mécanisme de stabilisation. Tout cela dans les micro-canaux du matériau biofonctionnalisé (violet).

Mots-clés: estampage à chaud, fonctionnalisation de surface, microcanaux, dépôt couche par couche, bioactivité, cellules endothéliales de la veine ombilicale humaine, péricytes humains, peptides, structure capillaire.

Résumé (bref)

Titre: Synthèse de microcanaux bioactifs pour la vascularization

Résumé: *In vitro*, la formation de structures de type tubulaire avec des cellules endothéliales de veine ombilicale humaine (HUVEC) a été étudiée en combinant la fonctionnalisation de la chimie des matériaux et le développement de la géométrie tridimensionnelle. Le polycarbonate (PC) a été utilisé comme modèle pour le développement de l'échafaud. Le film de polysaccharide naturel, basé sur un dépôt alternatif couche par couche (LbL) d'acide hyaluronique (HA) et de chitosane (CHI), a d'abord été appliqué sur une surface PC et caractérisé en termes de croissance d'épaisseur microscopie à balayage laser (CLSM). Cette première fonctionnalisation se traduit par un revêtement complet de la couche PC. Une biofonctionnalisation supplémentaire avec un peptide adhésif (RGD) et deux peptides angiogénétiques (SVV et QK) a été étudiée, immobilisant ces peptides sur le groupe carboxylique de HA précédemment déposé, en utilisant la chimie bien connue du carbodiimide. La version marquée de chaque peptide a été utilisée pour caractériser l'immobilisation et la pénétration des peptides dans les couches de polyélectrolytes, aboutissant à une greffe réussie avec une pénétration complète dans toute l'épaisseur du LbL. Des tests *in vitro* ont été effectués à l'aide de cellules HUVEC pour évaluer leur efficacité d'adhésion et leur activité métabolique sur la LbL avec et sans immobilisation de peptides, ce qui a permis d'améliorer l'activité préliminaire lorsque des combinaisons de peptides sont utilisées. Enfin, les microcanaux PC (μ Ch) ont été développés et caractérisés pour la première fois, et les autres expériences ont été réalisées sur un micromètre de 25 μ m de largeur, fonctionnalisé avec une architecture (HA / CHI) 12,5 (PC-LbL) avec des peptides RGD et QK -RGD + QK) ou avec des peptides RGD et SVV (PC-RGD + SVV). Notre première expérience de tubulogénèse a montré de manière surprenante la formation de structures de type tubulaire déjà après 2h d'incubation en utilisant la combinaison double-peptides, mais uniquement avec PC-RGD + QK. Les tubes étaient également présents après 3 et 4 heures de culture. L'expérience de co-culture avec des péricytes humains dérivés du placenta (hPC-PL) montre comment la stabilisation des tubes a

été améliorée après 3 et 4 heures également pour l'échantillon de PC-RGD + SVV. Globalement, notre matériel bio-fonctionnel avec les peptides PC-RGD + QK et PC-RGD + SVV permet la formation d'une structure de type tubulaire à la fois dans une expérience de monoculture et de co-culture.

Mots-clés: estampage à chaud, fonctionnalisation de surface, microcanaux, dépôt couche par couche, bioactivité, cellules endothéliales de la veine ombilicale humaine, péricytes humains, peptides, structure capillaire.

Abstract

Title: Engineered microchannels for vascularization in bone tissue engineering

Abstract: *In vitro*, tubular-like structures formation with human umbilical vein endothelial cells (HUVECs) was investigated by combining material chemistry functionalization and three-dimensional geometry development. Polycarbonate (PC) was used as a template for the development of the scaffold. Natural polysaccharide's film based on alternate layer-by-layer (LbL) deposition of hyaluronic acid (HA) and chitosan (CHI), was first applied to PC surface and characterized in terms of thickness growth both, in dry conditions using ellipsometry, and confocal laser scanning microscopy (CLSM). This first functionalization results in a complete coating of the PC layer. Further biofunctionalization with one adhesive peptide (RGD) and two angiogenic peptides (SVV and QK) was investigated, immobilizing those peptides on the carboxylic group of HA previously deposited, using the well-known carbodiimide chemistry. The labeled version of each peptide was used to characterize the peptides' immobilization and penetration into the polyelectrolyte layers, resulting in a successful grafting with complete penetration through the entire thickness of the LbL. *In vitro* tests were performed using HUVECs to assess their adhesion efficiency and their metabolic activity on the LbL with and without peptide immobilization, resulting in a preliminary improved activity when peptide-combinations is used. Finally, PC micro-channels (μCh) were first developed and characterized, and the rest of the experiments were performed on μCh of $25\mu\text{m}$

width, functionalized with (HA/CHI)_{12.5} architecture (PC-LbL) with RGD and QK peptides (PC-RGD+QK) or with RGD and SVV peptides (PC-RGD+SVV). Our first tubulogenesis experiment surprisingly showed the formation of tubular-like structures already after 2h of incubation using the double-peptides combination but only using PC-RGD+QK the tubes were present also after 3 and 4 hours of culture. The co-culture experiment with human pericytes derived from placenta (hPC-PL) demonstrates how the stabilization of the tubes was improved after 3 and 4 hours also for the PC-RGD+SVV sample. Globally our bio-functional material with PC-RGD+QK and PC-RGD+SVV peptides allow the formation of tubular-like structure in both mono and co-culture experiment.

Keywords: hot-embossing, surface functionalization, micro-channels, layer-by-layer, bioactivity, human umbilical vein endothelial cells, human pericytes, peptides, capillary structure.

UNITÉS DE RECHERCHE

CBMN – UMR 5248 Chemistry And Biology Des Membranes Et Des Nano-Objets
3Bio's Lab; 1 Allée Geoffroy Saint-Hilaire, 33600 Pessac (France)

IMCN - Institut de la Matière Condensée et des Nanosciences

Bio- and Soft Matter lab; Croix du Sud, 1 B-1348 Louvain-la-Neuve, (Belgique)

Table of Content

ACKNOWLEDGEMENTS	IV
SUMMARY.....	VIII
RÉSUMÉ (LONG).....	XII
RÉSUMÉ (BREF).....	XVI
ABSTRACT	XVII
TABLE OF CONTENT.....	XX
LIST OF FIGURES.....	XXIV
LIST OF TABLES	XXVI
LIST OF ACRONYMS.....	XXVII
I. LITERATURE REVIEW	1
1. NEEDS FOR TISSUE REPLACEMENT: THE GOLD STANDARDS	2
1.1. <i>Autografts</i>	6
1.2. <i>Allografts</i>	7
1.3. <i>Xenografts</i>	9
2. TISSUE ENGINEERING: THE FUTURE OF ORGANS REGENERATION	10
2.1. <i>Biomaterial grafts and biocompatibility</i>	12
2.2. <i>Limitation of large-size graft: vasculature importance</i>	13
3. VASCULAR NETWORK: PHYSIOLOGICAL ARCHITECTURE AND FUNCTION	14
3.1. <i>Function and physiology of blood vessels</i>	14
3.1.1. Capillaries	19
3.2. <i>Blood circulation, a combination of flow, pressure and resistance</i> ..	21
3.3. <i>Capillaries exchange</i>	21
3.4. <i>Development of blood vessels: vasculogenesis, angiogenesis and</i> <i>vascular remodeling</i>	23
3.5. <i>The bone tissue: an example of intimate vessel integration</i>	24
3.5.1. The structure of the bone	24
4. MICROVASCULAR TISSUE ENGINEERING	27
4.1. <i>Key-role of pre-vascularization: the future of large tissue creation</i> .	27
4.2. <i>Cellular importance: the players</i>	29
4.2.1. Molecular perspective of cell signaling: cell adhesion.....	29
4.2.2. Molecular perspective of cell signaling: angiogenesis	34
4.2.3. Cell mono-culture: capillary formation	39
4.2.4. Cell co-culture: vascular stability	45

4.3.	<i>Biomaterials: more than just a supportive element</i>	54
4.3.1.	Naturally derived biomaterials.....	55
4.3.2.	Synthetic biomaterials.....	60
4.3.3.	Hybrid materials	63
4.3.4.	Surface chemistry: biochemical and physical modifications	63
4.4.	<i>Small molecules: the signaling messengers</i>	67
4.4.1.	Growth factors	67
4.4.2.	Peptides.....	71
4.5.	<i>Surface topography and micro patterning: advance mimicking of natural ECM</i>	74
4.5.1.	Photolithography.....	75
4.5.2.	Soft lithography.....	78
4.5.3.	Hot embossing.....	78
4.6.	<i>Vascular tissue engineering approached</i>	81
4.6.1.	<i>In vivo</i> approach	82
4.6.2.	<i>In vitro</i> approach	85
4.6.3.	Micro engineering technique: the use of micro scale pattern or structures	86
II.	OBJECTIVES AND STRATEGY	89
1.	OBJECTIVE #1: FABRICATION OF PC MICROCHANNELS	91
2.	OBJECTIVE #2: BIOFUNCTIONALIZATION	92
3.	OBJECTIVE #3: CAPILLARIES DEVELOPMENT	93
4.	OBJECTIVE #4: CAPILLARIES STABILIZATION	94
5.	STRATEGY AND APPROACH.....	95
III.	MATERIALS AND METHODS	101
1.	MATERIALS.....	102
1.1.	<i>Molecular structures</i>	103
1.2.	<i>Materials preparation</i>	106
1.3.	<i>Material functionalization</i>	109
1.3.1.	Layer-by-layer deposition and crosslinking.....	109
1.3.2.	Peptide grafting.....	111
1.3.3.	Biofunctionalized material sterilization	113
1.4.	<i>Materials characterization</i>	114
1.4.1.	Profilometry	114
1.4.2.	FE-SEM.....	114
1.4.3.	Ellipsometry.....	114
1.4.4.	Spectrometry (TBO).....	115
1.4.5.	Fluorospectrometer (peptide grafting)	116
1.4.6.	CLSM (LbL swelling)	116
1.4.7.	Fluorescence microscopy (scratching test)	117
2.	CELL CULTURE	118
2.1.	<i>Mono culture (or HUVEC)</i>	118
2.1.1.	Expansion	118
2.1.2.	Cell detachment and counting	118
2.1.3.	Culture on PC-LbL.....	118
2.1.4.	Culture on PC- μ Ch-LbL	119

2.2.	<i>Co-culture (or hPC-PL)</i>	119
2.2.1.	Expansion	119
2.2.2.	Culture on PC- μ Ch-LbL	119
3.	BIOLOGICAL CHARACTERIZATION.....	121
3.1.	<i>Metabolic activity (XTT)</i>	121
3.2.	<i>DNA content (Pico green)</i>	121
3.3.	<i>CLSM (tubulogenesis)</i>	121
3.3.1.	Mono-culture tubulogenesis.....	121
3.3.2.	Co-culture stabilization	122
4.	SOFTWARE AND STATISTICAL ANALYSIS.....	123
4.1.	<i>ImageJ / Fiji</i>	123
4.2.	<i>IMARIS</i>	123
4.3.	<i>PRISM (statistical software)</i>	123
4.3.1.	μ Ch development.....	123
4.3.2.	LbL growth.....	124
4.3.3.	TBO	124
4.3.4.	Peptide grafting.....	125
4.3.5.	Scratching test.....	125
4.3.6.	Metabolic activity (XTT).....	126
4.3.7.	DNA content (Pico Green).....	126
IV.	RESULTS AND DISCUSSION	127
1.	PART I: FABRICATION OF PC MICROCHANNELS	130
1.1.	<i>25K-125K geometry</i>	132
1.2.	<i>25K-75K geometry</i>	132
1.3.	<i>25K-50K geometry</i>	133
2.	PART II: BIOFUNCTIONALIZATION	134
2.1.	<i>Layer-by-layer biofunctionalization</i>	134
2.2.	<i>Immobilization and penetration of peptides on materials' surface</i>	138
2.3.	<i>Quantification of RGD, SVV and QK peptides on PC-LbL</i>	142
2.4.	<i>Preserving a selective functionalization into μCh</i>	146
3.	PART III: CAPILLARIES DEVELOPMENT.....	148
3.1.	<i>Sterilization protocol for HUVEC adhesion</i>	148
3.2.	<i>Counting of HUVEC. Malassez vs Pico green (sonication tests also)</i> 150	
3.3.	<i>Metabolic activity of HUVECs</i>	153
3.4.	<i>Centrifuge-based seeding approach of HUVECs</i>	155
3.5.	<i>Time lapse epi- fluorescence microscopy</i>	157
3.6.	<i>Time-lapse confocal microscopy</i>	157
3.7.	<i>HUVECs on functionalized PC-μCh: late time-point investigation ..</i>	159
3.8.	<i>HUVECs on functionalized PC-μCh: wide time-point investigation .</i>	160
3.9.	<i>HUVECs on functionalized PC-μCh: early time-point investigation .</i>	162
4.	PART IV: CAPILLARIES STABILIZATION	166
4.1.	<i>HUVECs and hPC-PL stabilize tube-like structures</i>	166
V.	CONCLUSION AND PERSPECTIVES	171

1.	CONCLUSIONS.....	172
1.1.	<i>Regarding materials preparation and surface functionalization....</i>	172
1.2.	<i>Regarding mono-culture on functionalized PC materials</i>	174
1.3.	<i>Regarding co-culture on functionalized PC materials.....</i>	175
2.	PERSPECTIVES AND FUTURE WORK	176
2.1.	<i>Comparison with single-peptide functionalization</i>	176
2.2.	<i>Investigate genetic pathways involved in angiogenesis</i>	176
2.3.	<i>Time-lapse analysis for tube-like formation</i>	177
2.4.	<i>Choice of cell line for the endothelial line and supporting cells.....</i>	177
2.5.	<i>Application of microfluidic system</i>	178
2.6.	<i>Moving towards clinical application</i>	179
	APPENDICES	181
1.	APPENDIX 1: SCIENTIFIC COMMUNICATION.....	182
	REFERENCES	185

List of figures

FIGURE I – SCHEMATIC OF THE IMPRINTING PROCESS.	IX
FIGURE II – SCHEMATIC OF THE TUBULAR STRUCTURE OF THE CAPILLARY VESSEL.	X
FIGURE III – SCHEMATIC OF THE PERICYTES STABILIZATION.	XI
FIGURE IV - SCHEMA DU PROCESSUS D'IMPRESSION.	XIII
FIGURE V - SCHEMA DE LA STRUCTURE TUBULAIRE DU VAISSEAU CAPILLAIRE.	XIV
FIGURE VI - SCHEMA DE LA STABILISATION DES PERICYTES.	XV
FIGURE I.1 – REGENERATION VS. REPAIR:	3
FIGURE I.2 – WHAT IS A STEM CELL?:	4
FIGURE I.3 – SOURCES FOR TISSUES TRANSPLANTS:	6
FIGURE I. 4 – ALLOGRAFTS AND IMMUNE SYSTEM:	8
FIGURE I. 5 - THE CYCLE OF TISSUE ENGINEERING:	11
FIGURE I. 6 – TISSUE-CAPILLARIES DIFFUSION:	15
FIGURE I. 7 – VASCULAR SYSTEM IN THE HUMAN BODY:	16
FIGURE I. 8 – SUMMARY OF ARTERY AND VEINS TUNICA:	18
FIGURE I. 9 – DIFFERENCES BETWEEN CAPILLARIES:	19
FIGURE I. 10 – FILTRATION AND REABSORPTION IN CAPILLARIES:.....	22
FIGURE I. 11 – BLOOD VESSELS DEVELOPMENT.....	24
FIGURE I. 12 – BLOOD VESSELS AND BONE:.....	26
FIGURE I. 13 – CAPILLARIES REMODELING:	29
FIGURE I. 14 – FOCAL ADHESION IN CELLS:	30
FIGURE I. 15 – INTEGRINS ACTIVATION DURING FOCAL ADHESION:	31
FIGURE I. 16 – CELL ADHESION PHASES <i>IN VITRO</i> CONDITIONS:	32
FIGURE I. 17 – CELL ADHESION <i>IN VIVO</i> CONDITIONS:	34
FIGURE I. 18 - FIVE MECHANISM OF EPITHELIAL TUBULOGENESIS.....	36
FIGURE I. 19 – INTRACELLULAR CASCADE OF CELL MIGRATION:	38
FIGURE I. 20 – ENDOTHELIAL CELL SEEDING IN MICRO-CHANNELS:	40
FIGURE I. 21 – SINGLE ENDOTHELIAL TUBE FORMATION.	42
FIGURE I. 22 – CAPILLARY NETWORK DEVELOPMENT:	43
FIGURE I. 23 – CONTINUOUS CURVED CAPILLARY STRUCTURE:.....	44
FIGURE I. 24 – ENDOTHELIAL MICRO-TUBULAR STRUCTURE FORMATION:	45
FIGURE I. 25 – ENDOTHELIAL CELLS AND PERICYTES <i>IN VIVO</i> SPATIAL ORGANIZATION:	46
FIGURE I. 26 - ANGIOGENETIC STUDIES ON CO-CULTURE OF HUVECS AND PCs:	48
FIGURE I. 27 - IMMUNE FLUORESCENT STUDIES FOR CO-CULTURE:	49
FIGURE I. 28 – CO-CULTURE IMMUNOFLUORESCENCE IMAGES:	50
FIGURE I. 29 – TIME-LAPSE CONFOCAL MICROSCOPE HUVECS	51
FIGURE I. 30 – MICROFLUIDIC STRUCTURE FOR ENDOTHELIAL SEEDING:	52
FIGURE I. 31 - ORGANIZATION OF PCs AND HUVECS IN PRESENCE OF INHIBITORS:.....	52
FIGURE I. 32 – ANGIOCHIP MICROFLUIDIC STUDIES:	54
FIGURE I. 33 - CHITOSAN CHEMICAL STRUCTURE.....	57
FIGURE I. 34 – HYALURONIC ACID MONOMERIC STRUCTURE.	58
FIGURE I. 35 – STUDIES ON POLYELECTROLYTES LBL GROWTH:	59

FIGURE I. 36 – LAYER-BY-LAYER ASSEMBLY:.....	60
FIGURE I. 37 - CHEMICAL STRUCTURE OF POLYCARBONATE:.....	61
FIGURE I. 38 – STABILIZATION OF IMMOBILIZED PROTEINS:.....	62
FIGURE I. 39 – CARBODIIMIDE CHEMISTRY FOR PEPTIDES IMMOBILIZATION:.....	66
FIGURE I. 40 - MODEL OF VEGF PROTEIN AND RECEPTOR INTERACTION:	68
FIGURE I. 41 - DOSE-RESPONSE CURVE FOR PDGF AND ANGIOTENSIN-2 IN AORTIC CONTRACTION:	71
FIGURE I. 42 - NUCLEAR MAGNETIC RESONANCE OF QK STRUCTURE:.....	73
FIGURE I. 43 – <i>IN VIVO</i> STUDIES ON QK PEPTIDE:.....	74
FIGURE I. 44 – PHOTOLITHOGRAPHY FOR PEPTIDES IMMOBILIZATION:	76
FIGURE I. 45 – DEVELOPMENT OF PATTERN-LINE ON PEGDA HYDROGELS:.....	77
FIGURE I. 46 – HOT-EMBOSSING PROCESS:.....	79
FIGURE I. 47 - SEM IMAGES OF MICRO-CHANNELS MOLDED ON PMMA:	81
FIGURE I. 48 – EXTRINSIC AND INTRINSIC VASCULARIZATION MODELS:	84
FIGURE II. 1 – THE OBJECTIVES OF MY WORK:.....	99
FIGURE III. 1 – SILICON MASTER WITH MICRO-LINE PATTEN:	107
FIGURE III. 2 – HOT-EMBOSSING SETUP:	108
FIGURE III. 3 – IMPRINTED POLYCARBONATE MICRO-CHANNELS:.....	109
FIGURE III. 4 – LAYER-BY-LAYER FUNCTIONALIZATION:.....	111
FIGURE III. 5 – PEPTIDE IMMOBILIZATION STEP:.....	113
FIGURE IV. 1 – SILICON MASTER AND POLYCARBONATE MICRO-CHANNELS GEOMETRIES.....	131
FIGURE IV. 2 - ELLIPSOMETRY MEASUREMENTS FOR PC-SPIN COATED ON THE SILICON WAFER. ..	135
FIGURE IV. 3 - LAYER-BY-LAYER DEPOSITION CHARACTERIZATION.....	136
FIGURE IV. 4 - CHARACTERIZATION OF IMMOBILIZED-PEPTIDES.....	140
FIGURE IV. 5 - CALIBRATION CURVE OF FLUORESCENT RGD, SVV AND QK.....	143
FIGURE IV. 6 - SELECTIVE FUNCTIONALIZATION OF MICRO-CHANNELS.	146
FIGURE IV. 7 - TWO STERILIZATION APPROACHES.....	149
FIGURE IV. 8 - NUMBER OF HUVECS COUNTED AFTER 24H SEEDING USING TWO TECHNIQUES..	151
FIGURE IV. 9 - BIOLOGICAL EVALUATION ON METABOLIC ACTIVITY.....	154
FIGURE IV. 10 - INVESTIGATION OF CENTRIFUGATION SEEDING APPROACH.	156
FIGURE IV. 11 – TIME-LAPSE ACQUISITION OF HUVECS ON PC- μ CH-QK.	158
FIGURE IV. 12 – FIXED HUVECS CULTURED ON PC- μ CH-RGD+QK.	160
FIGURE IV. 13 - FIXED HUVECS CULTURED ON PC- μ CH-RGD+SVV.	161
FIGURE IV. 14 – TUBE-LIKE STRUCTURE FORMATION ON FUNCTIONALIZED BIOMATERIALS.	164
FIGURE IV. 15 – TUBE-LIKE STRUCTURE STABILIZATION BY CO-CULTURE.	167

List of tables

TABLE I. 1 - SUMMARY OF FEATURES, SIZES AND POLYMERS USED FOR HOT EMBOSsing PROCESS:. 80

TABLE IV. 1 – QUANTIFICATION OF IMMOBILIZED PEPTIDES 143

TABLE IV. 2 – CORRELATION OF HUVECS COUNT AND SONICATION POWER USED. 151

List of Acronyms

ANOVA:	Analysis of variance
BIC:	Bordeaux imaging center
CHI:	Chitosan
CLSM:	Confocal laser scanning microscopy
CMFDA:	Green cell tracker
CMTPX:	Red cell tracker
COC:	Cyclic olefin copolymer
DAPI:	4',6-diamidino-2-phenylindole
dsDNA:	Double-stranded Deoxyribonucleic Acid
EBM-2:	Endothelial basal media-2
ECs:	Endothelial cells
EDC:	1-Ethyl-3-(3-dimethylaminopropyl)carbodiimide
EDTA:	Ethylenediaminetetraacetic acid
EGM-2:	Endothelial growth medium-2
FBS:	Fetal bovine serum
FE-SEM:	Field emission scanning electron microscopy
FGF:	Fibroblast growth factor
FITC:	Fluorescein isothiocyanate
HA:	Hyaluronic acid
HCl:	Hydrochloric acid
HEPES:	(4-(2-hydroxyethyl)-1-piperazineethanesulfonic acid)
hPC-PL:	Human pericytes derived from placenta
HUVECs:	Human umbilical vein endothelial cells
LbL:	Layer-by-Layer
MES:	2-(N-Morpholino)ethanesulfonic acid
NaOH:	Sodium hydroxide
PC:	Polycarbonate
PC-LbL:	Polycarbonate with LbL architecture of PEI(HA/CH) _{12.5}

PC-PEI(HA/CH)_n: Polycarbonate with biofunctionalization of LbL with different architecture (n)

PC-QK: Polycarbonate with LbL and immobilized QK peptide

PC-RGD: Polycarbonate with LbL and immobilized RGD peptide

PC-RGD+QK: Polycarbonate with LbL and immobilized RGD and QK peptides

PC-RGD+SVV: Polycarbonate with LbL and immobilized RGD and SVV peptides

PC-SVV: Polycarbonate with LbL and immobilized SVV peptide

PC- μ Ch: Polycarbonate with micro-channels

PC- μ Ch-LbL: Polycarbonate with micro-channels functionalized with LbL architecture of PEI(HA/CH)_{12.5}

PC- μ Ch-QK: Polycarbonate with μ Ch and LbL and immobilized QK peptide

PC- μ Ch-RGD: Polycarbonate with μ Ch and LbL and immobilized RGD peptide

PC- μ Ch-RGD+QK: Polycarbonate with μ Ch and LbL and immobilized RGD and QK peptides

PC- μ Ch-RGD+SVV: Polycarbonate with μ Ch and LbL and immobilized RGD and SVV peptides

PC- μ Ch-SVV: Polycarbonate with μ Ch and LbL and immobilized SVV peptide

PCs: Pericytes

PDMS: Polydimethylsiloxane

PEI: Polyethylenimine

PET: Polyethylene terephthalate

PFA: Paraformaldehyde

PGM: Pericytes growth medium

PMMA: Poly(methyl methacrylate)

poly-HEMA: Poly(2-hydroxyethyl methacrylate)

PS: Polystyrene

PVC: Polyvinyl chloride

QK: Ac-KLTWQELYQLK(Ac)YK(Ac)GI-amide aminoacidic sequence

RGD: GRGDS aminoacidic sequence

RT: Room temperature

S-NHS: (N-hydroxysulfosuccinimide)

List of Acronyms

SEM:	Scanning electron microscopy
SiM:	Silicon mold
SVV:	GDSVVYGLRK aminoacidic sequence
TBO:	Toluidine blue
VEGF:	Vascular endothelial growth factor
XTT:	(2,3-Bis-(2-Methoxy-4-Nitro-5-Sulfophenyl)-2H-Tetrazolium-5-Carboxanilide)
μCh:	micro-channels

I. Literature review

1. Needs for tissue replacement: The gold standards

Traumas, injuries, and diseases can lead to the failure of our vital organs, leading to death unless properly replaced or regenerated. The always increasing population and aging lead inevitably to face an increasing number of traumas, degenerative diseases, and congenital abnormalities and disorders. Before encounter organ failure and death, the human body tries to find a solution to restore the architecture and the function of the damaged tissue/organ [1, 2]. This restoration is generally named tissue repair and it can follow two different mechanisms: regeneration or replacement (Figure I.1). Briefly, regeneration is the process in which the damaged tissue undergoes healing through the formation of newly-growth tissue which restores the damaged portion of the tissue until it returns to a physiological healthy state (Figure I.1) [2]. Instead, replacement is the process in which severely damaged, or largely damaged tissues are repaired by the formation of connective tissue, a process named scarring (Figure I.1) [2]. The type of mechanisms which body will use to heal the damaged tissue depends mostly on the size and severity of the damage, as well as the type of tissue. In fact, each tissue responds differently to damaged caused by trauma and injuries and certain tissues of the body contain a subset of cell population more active and capable of proliferation (which lead intrinsically to regeneration) than other tissues [3]. According to this difference in cellular proliferation capability, tissues can be divided into three categories: continuously dividing tissues, quiescent tissues and non-dividing tissues [2].

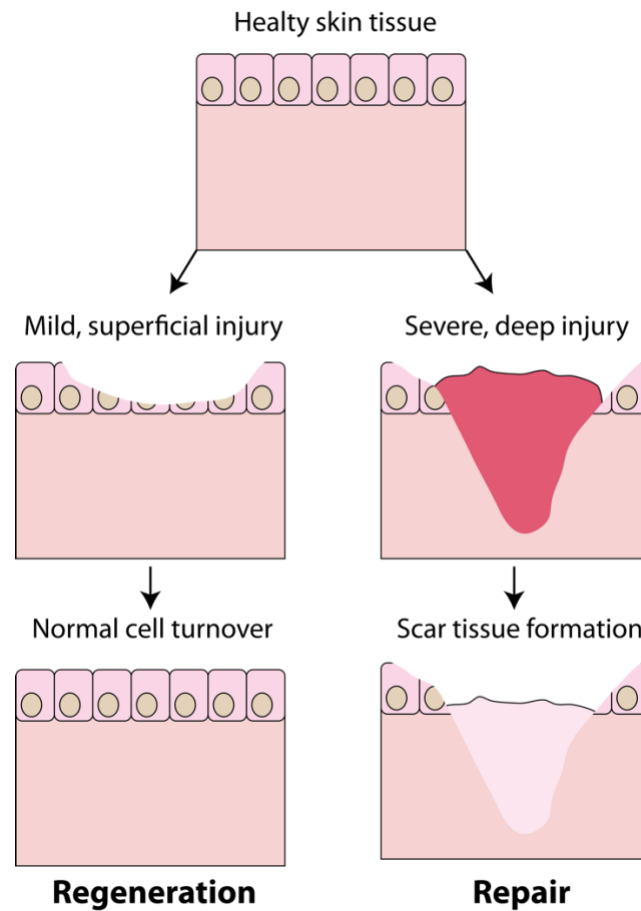


Figure I.1 – Regeneration vs. repair: Schematic representation of the two processes of regeneration (left part) or repair (right part) depending on the severity of the occurred injury.

Continuously dividing tissues contain a subpopulation of cells which are constantly proliferating to replace dead cells, termed as stem cells (Figure I.2). This peculiar type of cells has the capability to self-renew or differentiate. Self-renew mean that during the cell division, the originated daughter cell is identical to the mother cell under all aspects (genetic content, morphology, gene expression, and more). Differentiation is the process in which mother cell originate daughter which are different, generating multiple type of cells' types (Figure I.2) [3]. According to the definition of stem cells, is now quite clear how the regenerative potential of a tissue

is directly linked to the proliferative capacity of those stem cells, as well as the variety of cells which they are able to generate from a single starting cell. Thinking about everyday life, there are few clear examples of those continuously dividing tissues such as skin tissue, in which dead cells of the skin are completely replaced every two weeks, or also the gastrointestinal epithelium [2].

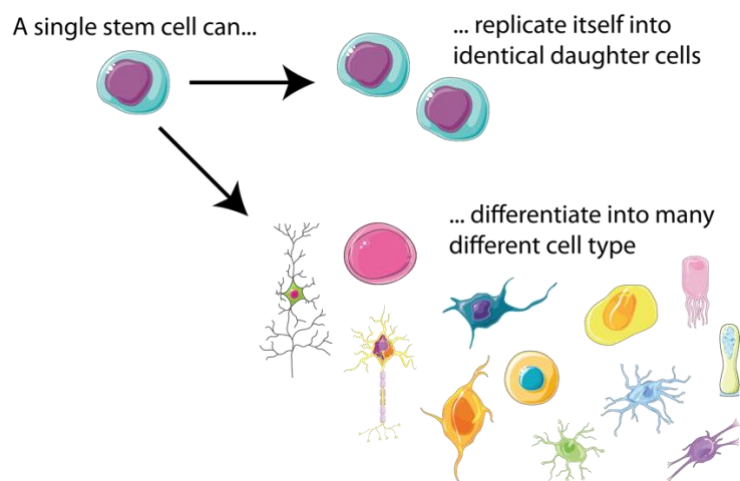


Figure 1.2 – What is a stem cell?:Schematic representation of the replicative potential of a stem cells. In fact a stem cell can replicate itself an undefined number of time, originating an identical daughter cell, or originate a different cell type after a process named differentiation.

Quiescent tissues contain a subpopulation of cells which normally exist in a non-dividing state, quiescent, but when certain stimuli are applied such as an injury or a trauma, the stem cells may enter the cell cycle again in order to regenerate the damage. Few examples of this type of tissues are liver, kidney, and pancreas. Thinking about liver tissue is well-known how the resection of a part of the liver, for donation purpose, for example, is capable of regrowth thanks to the massive proliferation rate of the remaining liver cells [2, 3].

Non-dividing tissues are composed uniquely of cells which permanently left the cell cycle process, and so unable to proliferate. An example of this tissue, with dramatic effect in case of injuries, is the cardiac and skeletal muscles. The only

mechanism in which these tissues will be normally healed is by the formation of a scar tissue, thus replacement mechanism [2], [4].

Even if some tissues preserve a good capability to self-regenerate themselves through the proliferation and differentiation of stem cells, this potential is very limited and all the tissues/organs once seriously damaged, or with severe pathological dysfunctions, will undergo to tissue/organ dysfunctions with devastating effects which can lead to death [5].

One critical and largely studied tissue for regenerative capability improvement is the bone tissue [6]. Patients with defects in the bone structure, or with osteoporosis, or with arthritis, or with a bone infection, or with spinal fusion, or with a metabolic bone disease, or with osseous-related tumors like osteosarcoma are unable to use the self-regenerative properties of the bone itself to properly heal [7]. The bone loss and repairs have, still nowadays, a great impact on both clinical and economic importance. The non-union cases in the USA arrive at 100'000 fractures and the average cost of treatments is about 11'333 US dollars. In addition, the bone becomes more fragile and with reduced regenerative capability while aging, rising the senile osteoporosis up to 50% for women and 25% of men with more than 50 years [7].

When the two mechanisms of repair are not sufficient to avoid tissue/organ collapse, in order to preserve the tissue/organ function, transplantation is one of the few possible solutions. Transplantation can be considered as the gold standard for organs substitution, especially in the case of bone, and the procedure consists in the replacement of a damaged organ or tissue with the same organ or tissue, provided by a donor. Transplantation is currently used as the first line of action to overcome this ever-increasing number of patients (Figure I.3) [1] [5].

Depending on the nature of the donor, three main categories can be identified: autograft transplant, allograft transplant, and xenograft transplant (Figure I.3). The difference between those approaches derives from the source of the organ or tissue to transplant [1] [7]. For the single case of bone transplantation, 2.2 million surgeries occur worldwide per year, mostly done by using autografts or allografts. This very large number of patients increases the complexity and the time required to have availability of such grafts and the medical care at the hospital [7].

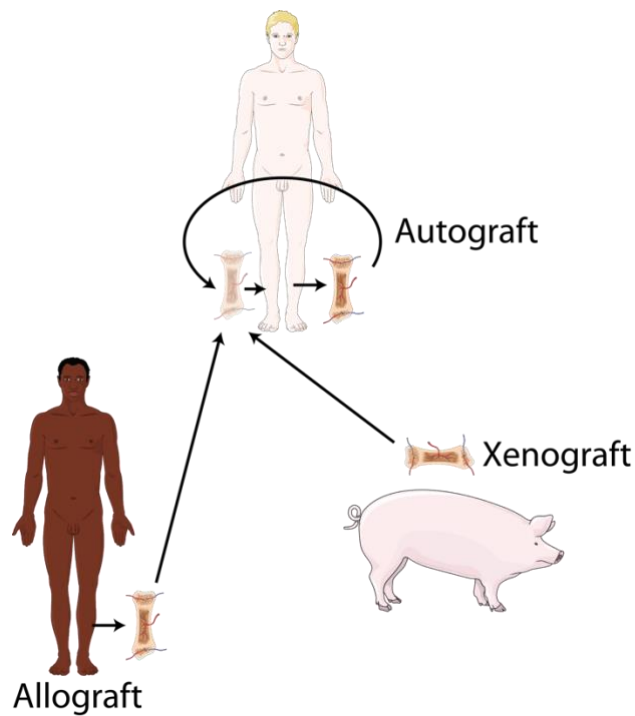


Figure 1.3 – Sources for tissues transplants: Schematic of the possible sources for transplantation indicating the autograft, isograft, allograft and xenograft.

1.1. Autografts

Autograft, named also autologous tissue graft, was the first approach used to successfully replace an organ or tissue. It consists of the extraction of a tissue or organ from one site to another, within the same individual [1]. Nowadays it is still considered the best approach for the reconstruction of most tissues or organs defects and is still used as the main control to compare the efficiency of other implantable biomaterials since autografts retain large masses of living cells and have all the required properties for new tissue development and structural reconstruction [5, 8]. Additionally to their success in tissue and organs reconstruction, autograft does not present any antigenicity since it comes from the patient's own body.

The use of autograft transplant, for bone tissue applications are largely investigated and practiced in regular base. In fact, as the first line of action for a bone

transplant, autograft present a success rate over 90% compared to other clinically-available substitutes [5]. This high rate of autograft-transplant success is linked to the peculiar properties of the autograft tissue itself, which retains superior osteoinductive and osteoconductive properties [5]. Osteoinduction is a physiological phenomenon which implies the recruitment of immature cells which differentiating in osteoblast would induce osteogenesis (formation of new bone) [9]. Osteoconduction is the process in which new bone growth on the surface of a material, for example, a newly implanted bone substitute [9].

However, even if autograft presents a series of clinical benefits, the approach suffers from drawbacks such as unpredictable graft resorption which can be too fast or slow, limited availability, short-term viability because of stressful cellular conditions during and after transplantation, and most important a second surgery [5]. In fact, the harvesting procedure in order to collect the bone tissue from another site of the donor can induce pain, morbidity, and risk of postoperative complications such as infections [5]. Another important aspect, neglected in the past, is the importance of a vascular tissue in large graft surgery, in fact, in the best material conditions such as cancellous graft, the vascular response after the surgery can take weeks to completely revascularized the implanted bone in large animals model [5, 10].

1.2. Allografts

Allograft, named also allogenic tissue graft, was investigated as a potential solution to avoid the disadvantages of autografts in terms of morbidity and tissue availability of the donor/host [5]. Contrarily to autograft, the origins of those tissues or organs comes from another individual of the same species but with different genotype [1]. This important difference is, unfortunately, at the base of the tissue or organs rejection, which is the main risk and drawback for allograft transplantations. The rejection is mostly due to the response of the host's immunity system against the allogeneic tissue graft, which plays a pivotal role in the tissue/organ integration, or rejection (Figure I. 4) [5]. However, the allografts transplants are always followed

by immunosuppressive medication to avoid an extensive immune rejection of the new tissue, and in addition to this, human leukocyte antigen (HLA) matching between donors and recipients is fundamental [5].

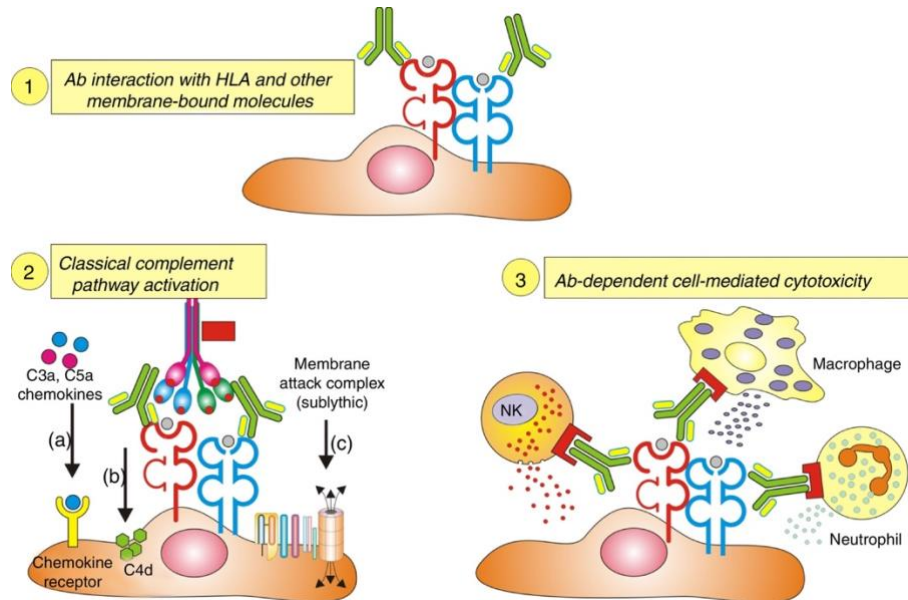


Figure 1.4 – Allografts and immune system: Schematic of the immune rejection between (1) the antibodies of the host and the cells of the donor which trigger (2) the classical pathways of complement activation which (3) lead to cellular-mediated cytotoxicity. From [11].

In the special case of bone allograft, the allogenic bone tissue grafts are cadaveric in origin and available from commercial vendors such as bone banks. Those type of grafts has been largely used in the field of reconstructive surgery when the autograft was not possible or available [5]. This approach removes completely the drawbacks of a second surgery and limitations of tissue availability in quantity and size. In addition, the product is ready-to-use and, theoretically, always available in the required sizes and shapes, matching the recipient constitutional elements and architecture of the original bone. Although, the complete absence of living cells into the tissue, to reduce the immune response of the host, provide a poor osteoinductive and osteoconductive properties. In addition to those problems, another one concern about potential infectious agents transmission, which can be minimized by strategies of tissues processing, sterilization and freezing that,

unfortunately, decrease even more the already poor osteogenic properties of the graft and reduce the mechanical strength of the original tissue [5]. To regulate the commercial of this allograft bone tissue, the food, and drug administration (FDA) of the United States develops a series of tissues process and medical screening that each material has to perform before the approach on the market. The medical screening concerns mostly about infectious diseases such as HIV-1, HIV-2, hepatitis B, and hepatitis C, while the tissue process applied are blood removal, freeze drying or gamma irradiations [5]. Using bone allograft, in comparison to bone autograft, the remodeling and revascularization are slow and inefficient, another drawback for a quick and rapid integration of the graft with the host's tissue [5]. In this case, the bone transplant failure rate approaching 25%, mostly due to an inadequate revascularization and mineralization of the bone graft.[12] [13].

1.3. Xenografts

Xenograft named also xenogeneic tissue graft consists in the use of tissues or organs acquired from another species than the final host. This procedure is the less common and less practice, however, it is possible to find few applications in which is currently used in clinics [14]. When the component to replace is small, and the transplant could decide the life of the patient, a xenograft can be used as the last option. From ancient Greek, Xeno indicates "foreign, alien", and in this case, represents a tissue from an animal donor, to be implanted into a human patient. This approach presents severe implications for immune compatibility due to inter-species transplant but could save the life of the patient, which cannot wait any longer other donor-sources and would encounter death due to organ failure [14]. A major concern with animal-derived graft is the potential transmission of zoonotic diseases and prions infections which can lead to a more aggressive form of rejection and increase the morbidity of the patients [14].

Similarly to allografts, xenografts lose partially their osteoinductive properties during the processing to counteract the strong antigenic properties, therefore xenografts produce poor clinical outcomes [14].

2. Tissue engineering: the future of organs regeneration

Even if the potential of the three described graft could save countless lives, the enormous imbalance between grafts availability and graft need, together with tissues/organ compatibility, push numerous patients in a waiting list, leading often to their death.

Tissue engineering (TE) is the research field that aims to create biological substitutes which can restore, repair and replace damaged or diseased tissues and organs, resolving the problems related to availability and potentially being applied without compatibility or immune rejection issues. The term was first introduced back in 1988 at the national science foundation meeting at the Massachusetts Institute of Technology (MIT) during the keynote. Four years later, Vacanti J.P. and Langer R. published a work containing the first definition of TE: "Tissue engineering is an interdisciplinary field that applies the principles of engineering and the life science toward the development of biological substitutes that restore, maintain or improve tissue functions" [15 J.P. "Tissue Engineering." *Science* (1993): 260, 920]. Figure I. 5 show the TE cycle which corresponds in 5 different phases: first cells are extracted from the patients, expanded in culture conditions and seeded into a scaffold in the presence of growth factor and other small molecules to generate a tissue. Later the newly developed engineered tissue is extracted and implanted into the patients' body.

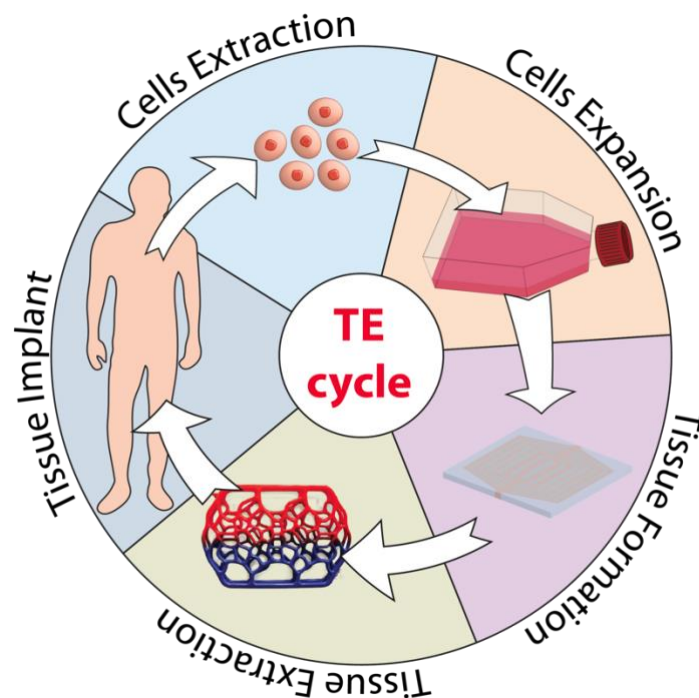


Figure 1. 5 - The cycle of tissue engineering: Cells are extracted from the patient and expanded in culture. Later, cells are implanted into a scaffold with (or without) other growth factors to generate a tissue. Last the engineered tissue is extracted and implanted into the patients' body.

Most of the living tissues are composed of repeating parts, assembled together in a hierarchical way with a precise three-dimensional architecture and micro-architecture. The possibility to reproduce those micro-architecture features and tissues functionalities have a huge interest in the fast-growing TE field [5]. Although the technology and knowledge nowadays do not allow us to develop complex organs de novo, more and more studies suggest that is possible to trigger the body's innate (even if limited) capacity of regeneration, increasing the potential of tissues and organs regenerative cascade [5]. The potential of TE is not limited at only one type of tissue or organ but it could potentially lead to the regeneration of each tissue in the human body, however, even if in the modern medicine multitude of studies were performed in several tissues' type, there is not easy access to achieving regeneration in clinics [5].

Thanks to technological and knowledge progress and achievements, the original definition of TE nowadays can be defined as “a substance that is able, or has been engineered, to take a form which, alone or as part of a complex system, is used to direct, by control of interactions with components of living systems, the course of any therapeutic or diagnostic procedure, in humans or veterinary medicine”[5, 16] [17].

Biomaterials in TE play a fundamental role for a successful tissue integration and regeneration by the creation of a neo-tissue *in vitro* with similar or identical properties of the native body tissue. In addition to the structural properties, biomaterials are often used as a template/scaffold for cellular guidance, growth, differentiation, etc. together with *in situ* release of specific molecules, growth factors, chemokines, etc. to improve the regenerative potential of the scaffold in the damaged tissue.

2.1. Biomaterial grafts and biocompatibility

Biomaterial grafts differ from autograft, allograft, and xenograft since they are artificially or manufactured materials. In the past, but still, nowadays, the problem of a severe and persistent shortage of tissue and organs for worldwide transplantation persists. An innovative solution must be considered in order to decrease the number of people which populate the waiting list, which is ever growing due to population expansion and increased aging [5]. The goal of biomaterial design for tissue engineering application is to develop an engineered construct capable of both provide a three-dimensional microenvironment for cellular functions and guide the formation of the new tissue.

Biomaterials must possess biocompatible surfaces to reduce or eliminate host responses. The definition of this term remains ambiguous in literature, with different possible interpretations and definitions. However, I will refer to the definition of Williams D.F. which for me better represents the complexes requirements that a biomaterial should possess: Biocompatible “refers to the ability of a biomaterial to perform the desired function with respect to a medical therapy, without eliciting any

undesirable local or systemic effects in the recipient or beneficiary of that therapy, but generating the most appropriate beneficial cellular or tissue response in that specific situation, and optimizing the clinically relevant performance of that therapy”[18]. Therefore, the materials used should provide a structural support for a predictable period of time (according to the tissues’ need) in order to ensure the formation and the maturation of the new tissue, even under stress conditions, like in the case of bone constructs constantly loaded by the body weight [5]. In addition to structure, the design of biomaterials should approximate the many critical features of the extracellular matrices of the healthy tissue counterpart, mimicking the myriad of cellular and molecular events and signaling which are involved in the regeneration of the tissue/organ. For this purpose, the combination of supporting materials, adequate cells and bioactive factors must be in harmony in order to promote the, natively limited, regeneration of the damaged tissues [5].

2.2. Limitation of large-size graft: vasculature importance

Even if enormous steps have been made from the origins of tissue engineering until nowadays, many of those engineered tissues do not fully match the chemical, functional and structural properties of their native counterparts. This failure is certainly due to the complexity of the living organisms with their organs and tissues, and in addition to that, our knowledge and understanding of this complexity are far from being sufficient to understand the mechanisms behind tissues growth, remodeling and healing [5].

What is missing in all the previously presented procedure is an integration between the biomaterial developed and a functional vasculature network, pre-installed into the device and ready to be linked to the patient’s circulatory system [10].

3. Vascular network: physiological architecture and function

In this chapter, we are providing a quick preview of the fundamental components of the complex circulatory system focusing on capillaries architecture, role, and physiology. The main differences between the three types of capillaries, the mechanism of oxygen exchange and the intimate connection between bone and blood vessels will be presented.

3.1. Function and physiology of blood vessels

The main function of blood vessels is to transport blood around the entire body, to properly supply each cell in the human body with oxygen and nutrients, removing at the same time the discarding products such as carbon dioxide and metabolite waste (Figure I. 6) [19].

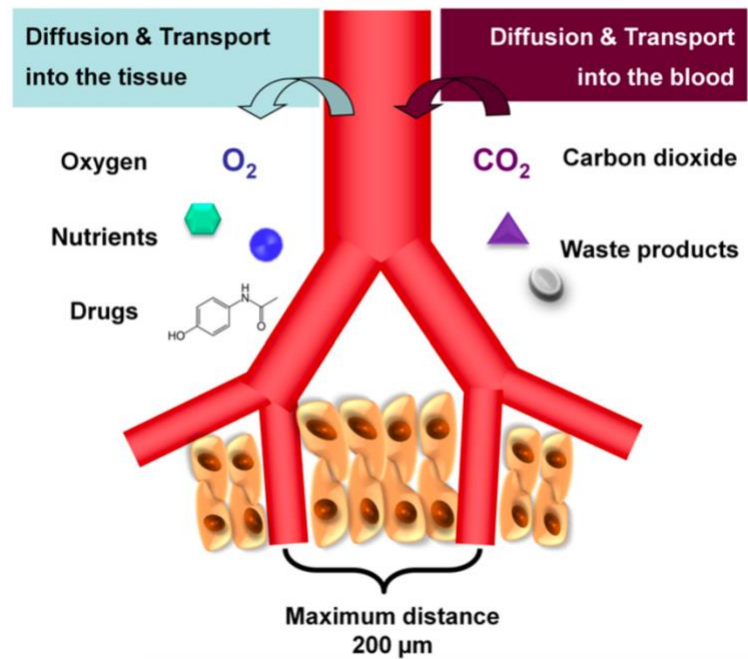


Figure I. 6 – Tissue-capillaries diffusion: Schematic representation of molecules exchange between the capillary vessels and the surrounding tissues with a particular focus in the maximum distance between two capillaries found in healthy tissues in order to avoid hypoxic conditions. From [20]

As the general overview the blood is pumped from the heart to the lungs, through the pulmonary vein, to release the carbon dioxide and recharge with new oxygen, then it returns to the heart, through the pulmonary artery. From the heart, oxygenated blood is pumped in the rest of the body, through the aorta, other arteries and arterioles until it reaches capillaries. At the level of capillaries, the blood exchanges oxygen with the surrounding tissue and it collects CO₂ and waste products which will be driven back to the heart through venules and finally veins (Figure I 7) [19]. From this general overview, it is possible to identify two distinct circuits: the pulmonary circuit and the systemic circuit.

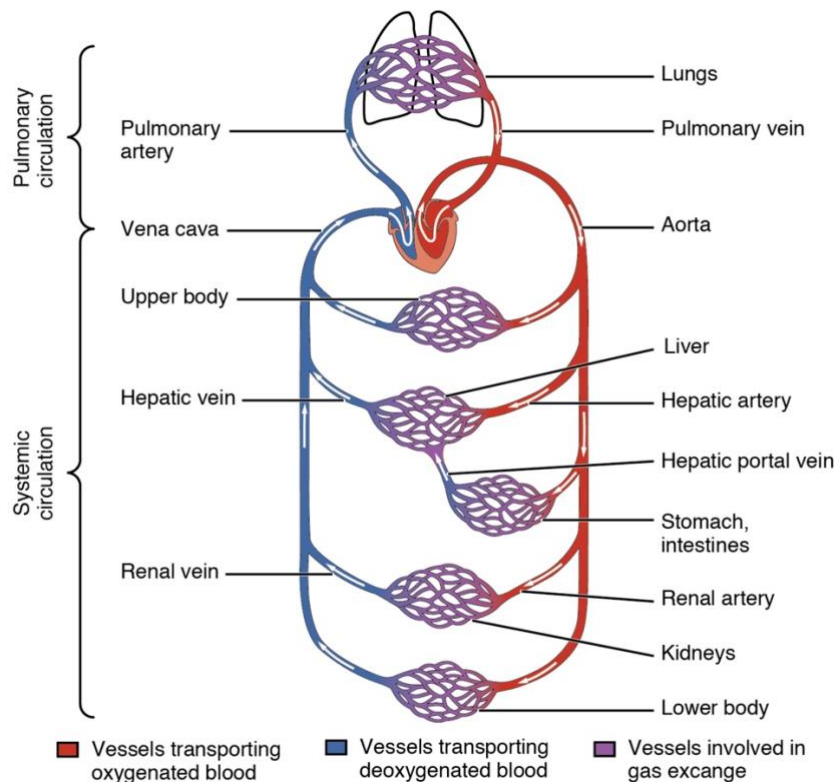


Figure 1. 7 – Vascular system in the human body: The blood is pumped from the heart to the lungs in which the gas exchange occur enriching the quantity of oxygen. Then the oxygenated blood travel back to the heart to be pumped to the system circulation through the intricate system of arteries. Later gas exchange occurs in the capillaries releasing the oxygen present in the blood and enriching it in carbon dioxide. Finally exhausted blood travel back to the heart through the intricated system of veins. From [19].

The different vessels type in the body differ for composition, but they share some structural features. For example, each blood vessel has a lumen, a hollow passage through the length of the vessel which allows the passage of blood, and in addition, almost all the vessels are composed of three layers: tunica intima, tunica media, and tunica externa. The tunica intima is located most internally, at the level of the lumen, and is made of a continuous layer of endothelial cells present in all the vessel's type

in the entire cardiovascular system (Figure I. 8) [19]. The tunica media is located around the tunica intima and consists mostly of smooth muscle cells and connective tissues. Especially in arteries, but also arterioles, this layer plays a fundamental role in sustaining the high blood pressure pumped from the heart through an expansion-contraction mechanism which regulates the blood flow, avoiding a pressure drop. Venules and veins preserve the tunica media but in reduced thickness and importance, since there are no variations in the blood pressure at this level (Figure I. 8) [19]. Last, the tunica externa is a sheath of connective tissue made of collagenous fibers which plays two important functions in providing nutrients through the vasa-vasorum and maintaining the vessels in their relative position thanks to the connection with surrounding connective tissue. Arteries and arterioles present a thinner tunica externa, compared to venules and veins (Figure I. 8) [19].

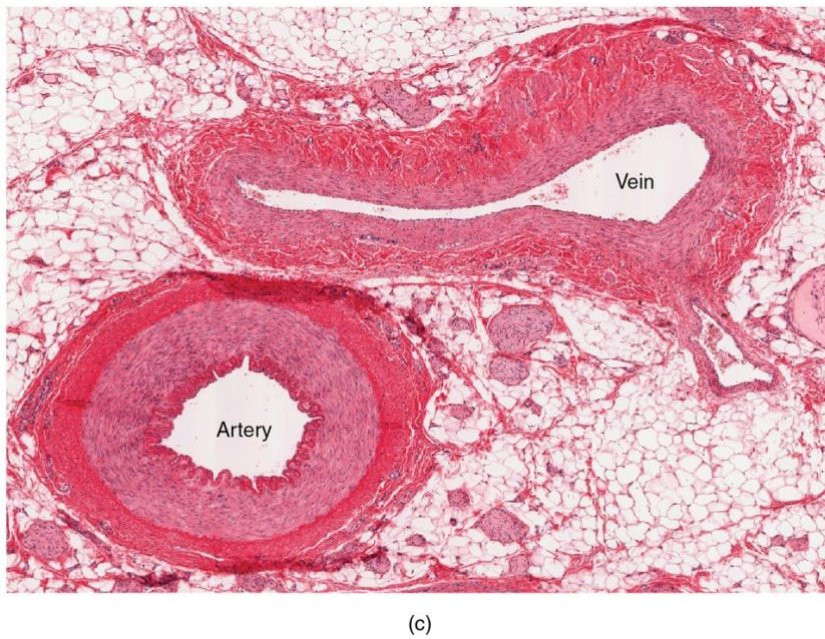
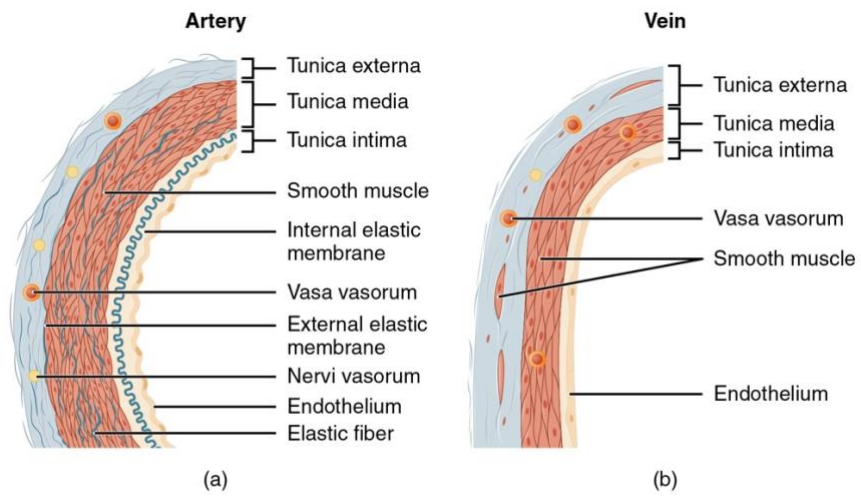


Figure I. 8 – Summary of artery and veins tunica: Detail of the three tunica layers on artery (A) and on vein (B). Histological sample of artery and vein (C). From [19].

3.1.1. Capillaries

Compared to the previously described architecture of larger vessels, capillaries are microscopy channels composed uniquely of the tunica intima and play the fundamental function of supply oxygen and nutrients to all the tissues in the body through an exchange process of gases and other substances between blood and surrounding cells, and interstitial fluid, a process called perfusion. Lumen diameter for capillaries is the smallest in the body and range from 5 to 10 μm making erythrocyte to squeeze during passage through. Globally the flow through capillaries takes the name of microcirculation. Depending on the size of capillaries, there might be some occasional smooth muscle cells, but mostly capillaries are composed of endothelial cells arranged to form the endothelium, surrounded by the basement membrane. In capillaries, the lumen can be formed by several cells bounded to each other and wrapped with a cylindrical orientation, or even formed by a single cell layer that wraps around and bound itself. Due to their fundamental perfusion function, the wall of capillaries must be leaky to allow gases and molecules to cross the endothelium and diffuse outside. According to their leaking characteristic, three types of capillaries can be identified: continuous, fenestrated and sinusoid (Figure I. 9).

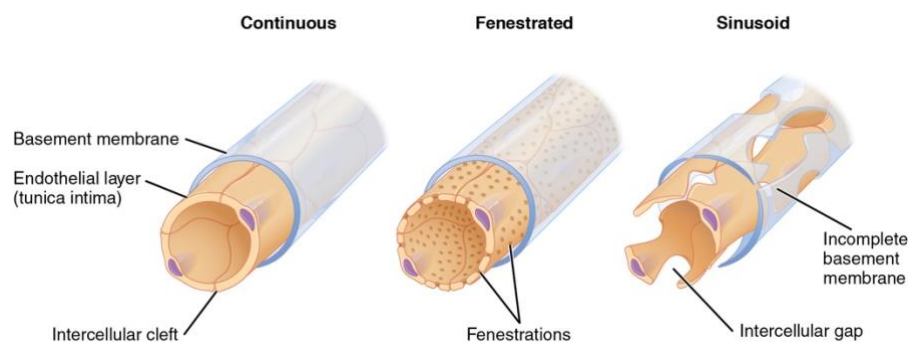


Figure I. 9 – Differences between capillaries: Schematic representation of the three types of capillaries, indicating the peculiarity of each like the continuous basement membrane for continuous capillaries (left), the presence of fenestrations in the fenestrated capillaries

(center) and the intracellular gap with incomplete basement membrane in the sinusoid capillaries (right). From [19].

Continuous capillaries represent the most common type of capillaries present in the body tissues, characterized by a continuous and complete endothelial lining with tight junctions between endothelial cells. Those tight junctions normally would not allow passage of molecules, making an almost impermeable layer, however, in capillaries, those junctions are often incomplete, leaving some intracellular clefts which allow small molecules such as metabolic products, glucose, water, and hormones to freely be exchanged with the surrounding tissue. An exception of this leaking capacity is given by capillaries forming the blood-brain barrier, in fact, those capillaries do not present intracellular clefts and show a thicker basement membrane to prevent the exchange of nearly all substances (Figure I. 9).

Fenestrated capillaries, in addition to the tight junctions and intracellular clefts, show pores that make them permeable to large molecules. Those type of capillaries is more common in the small intestine for nutrient absorption and kidneys for blood filtration. In those capillaries, the basement membrane is preserved as a continuous layer which surrounds entirely the endothelial cells (Figure I. 9).

Sinusoid capillaries are the least common type of capillaries. They present the same characteristics of intracellular clefts and fenestration as the fenestrated capillaries, but in addition, they show large intracellular gaps and an incomplete basement membrane (Figure I. 9). Those large passages allow the passage of very large molecules such as plasma proteins and even cells. For example, after the formation of new blood cells from the bone marrow, those cells enter in the bloodstream through the large opening in those sinusoid capillaries, otherwise, the small pore of the fenestrated capillaries would not be sufficient to allow the passage. Another important organ that requires sinusoid capillaries is the liver. Large materials from the digestive tract and the spleen reach the spleen and are later processed.

3.2. Blood circulation, a combination of flow, pressure and resistance

The movement of the blood through the vessels of the circulatory system is defined as blood flow and it is expressed in volume of blood per time. The blood flow is originated from the ventricles of the heart that, after contraction, eject the blood to the major arteries increasing the pressure. When the blood needs to cross all the small vessels of the body such as arterioles, capillaries, and venules it encounters a physiological resistance and the flow is slow down, phenomenon defined as resistance. Blood pressure is the hydrostatic pressure which blood exerted on the walls of blood vessels. [19]

In order to maximize the nutrient and oxygen exchange, microvessels divide into numerous smaller branches increasing the total available area. The stasis of the blood flow, in those particularly small vessels with reduced pressure, is prevented by the Fahraeus-Lindqvist effect. In particular, the combination of repulsive charges between the blood cells and the wall in the capillary vessels, together with a thin layer of glycocalyx present on the endothelial layer [19].

3.3. Capillaries exchange

The cardiovascular system is responsible for the circulation of gases, nutrients, wastes, and other substances. Depending on the size of those elements they can diffuse directly through the membrane of endothelial cells in the continuous or fenestrated capillaries, such as gases, lipids, amino acids, sugars, and ions (Figure I. 10). Larger molecules like proteins in the blood plasma can exit through the great gaps of the sinusoids capillaries. Water, thanks to its properties can diffuse by osmosis in all the tissues [19]. The overall exchange between capillaries and surrounding tissue requires an efficient transport mechanism which is defined as bulk flow [21].

This important exchange exploits two pressures: the capillary hydrostatic pressure and the blood colloidal osmotic pressure. The first one represents the force that blood, confined within the blood vessels, exerts on the capillaries' tunica intima. The second one represents the force that a different osmotic gradient exerts. Briefly, the high concentration of plasma proteins into the capillaries (which cannot cross the tunica intima due of their large size) attracts water by osmosis from the surrounding tissue as compensation mechanism [21]. Therefore those two forces play together to drive the two exchange mechanisms present in capillaries:

- filtration occurs when the fluids move from the higher pressure in the capillaries to the lower pressure inside the tissues.
- reabsorption occurring when the fluids move from the higher pressure in the surrounding tissues to the lower pressure inside the capillaries [21].

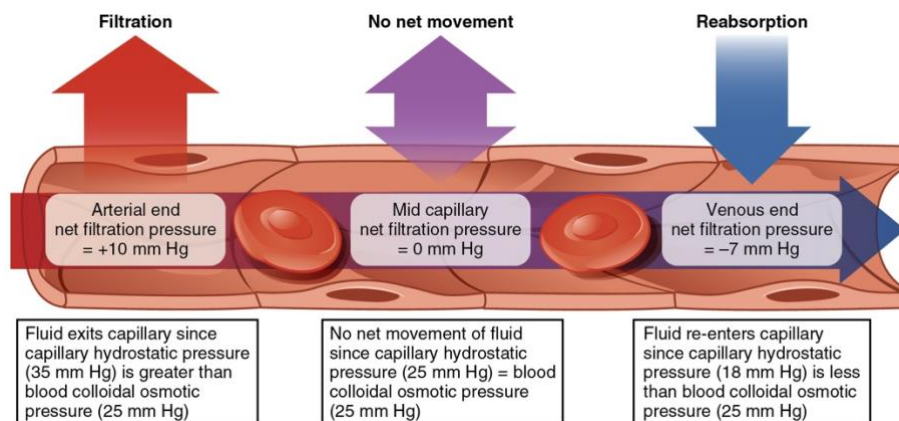


Figure I. 10 – Filtration and reabsorption in capillaries: Schematic representation of the effect of the pressure on the fluid homeostasis depending on the type of vessel, which regulate the capillary exchange in the tissues. From [19].

3.4. Development of blood vessels: vasculogenesis, angiogenesis and vascular remodeling

In human embryogenesis, heart began beating after 21 days post-fertilization and by the fourth week of development, the circulatory pattern is already established to allow an immediate supplement of nutrients, gases and remove the waste products. During the few weeks of vascular network development the blood vessels start their formation from the embryonic mesoderm, the cells' precursors are termed hemangioblast and they later differentiate into angioblasts. This cell type originates both the blood vessels and the pluripotent stem cells responsible, later one, for the differentiation in elements which compose the blood. Those cells groups together to form the blood islands which later open up to develop the vessel lumen (Figure I. 11) [19, 22]. Endothelium generates directly from the angioblast of the blood islands while surrounding mesenchymal cells will differentiate into smooth muscle and connective tissues. This initial formation of de novo vessels is termed vasculogenesis and after, based on guidance molecules in the extracellular matrix, the specific differentiation in arteries or veins begin [23, 24]. As soon as the blood vessels start to develop, pluripotent stem cells begin to produce the blood components. Those spare blood islands generate, each, a vascular tube which later merges to the neighbors to generate the vascular network (Figure I. 11) [19]. The formation of the complex system of vessels thus does not start from one vascular tube which elongates to form all the network but starts from several different vascular tubes which merge together to create one network, complex and ramified. The formation of new blood vessels from the existing one formally termed angiogenesis, continues during the whole life of the human being, during the grow and develop [19]. In this case, the coordinated migration of endothelial progenitor cells (EPC) and pericytes (PCs), from the existing vascular bed, lead to their maturation and stabilization creating new vascular network [25]. Two are the purposed models for angiogenesis: capillary sprouting is the first one, and involve the migration of endothelial cells from the existing vessel to a new region without vessels in order to develop the new one. Intussusception is the second one, and consist in the split of a vessel into two smaller

vessels which now can remodel and develop independently [26-28]. Micro-vascular remodeling is a different process which occurs during the entire life of a person in the skeletal muscle after exercise activities, in the female menstrual cycle or in the pathological situation like inflammation, wound healing and tumors, responding to hypoxia conditions [29].

The important role is played by the umbilical vein, which carries blood rich in oxygen from the mother to the developing fetus directly into the fetus heart which has the function to pump it in its circulatory system.

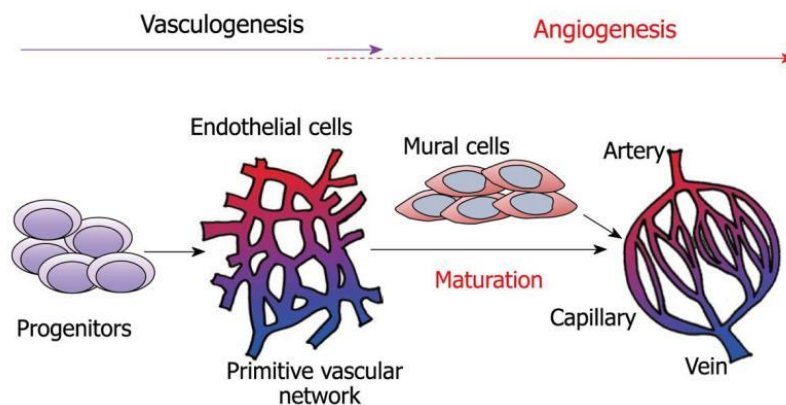


Figure I. 11 – Blood vessels development. Vasculogenesis occurring through the fusion of the blood island to develop the primary capillary plexus (left). Angiogenesis with the formation of new branches of an existing artery (right). From [30]

3.5. The bone tissue: an example of intimate vessel integration

3.5.1. The structure of the bone

In the bone, arteries enter through the compact bone using a natural cavity called nutrient foramen to properly supply oxygen and nutrients to the spongy bone and the medullary cavity. Once blood is inside the spongy bone in the bone marrow cavities is later collected by veins, and those veins exit from the bone using the same

nutrient foramina as arteries used to enter (Figure I. 12) [19]. The marrow cavity presents a range of vascular niches which play the important role of bone growth, differentiation and the development of hematopoietic lineage depending also on a gradient of oxygen tension [31]. The vascular supply in the bone tissue enables efficient growth and regulate bone remodeling, which are not possible in the avascular cartilage [31]. In fact, direct impairment of blood supply is linked with reduced bone growth and problems in the repair mechanisms of the bone, with consequent bone loss and, at last, necrosis [31]. The intimate connection between bone and vessels can be appreciated also considering the hematopoiesis process, which briefly is the development of new blood cells components. In fact, the marrow in the bone is the responsible site where hematopoiesis occurs, thanks to mechanisms which are also regulated by the pressure of oxygen in the tissue [31]. Moreover, as soon as the new cells' components of the blood are produced, they need to be perfused into the circulatory system through the sinusoidal capillaries. The vasculature in the bone tissue also provides an important role in the regeneration and healing process. A bone fracture, in fact, damages also the blood supply, resulting in a drop of oxygen level, and consequently hypoxia state, which triggers many signaling events for cells such as the inflammation process, prior to healing [31]. Last, the quality of vascular supply in bone tends to decrease during the aging, leading to pathological settings such as anemia, immobility, and bone loss [31].

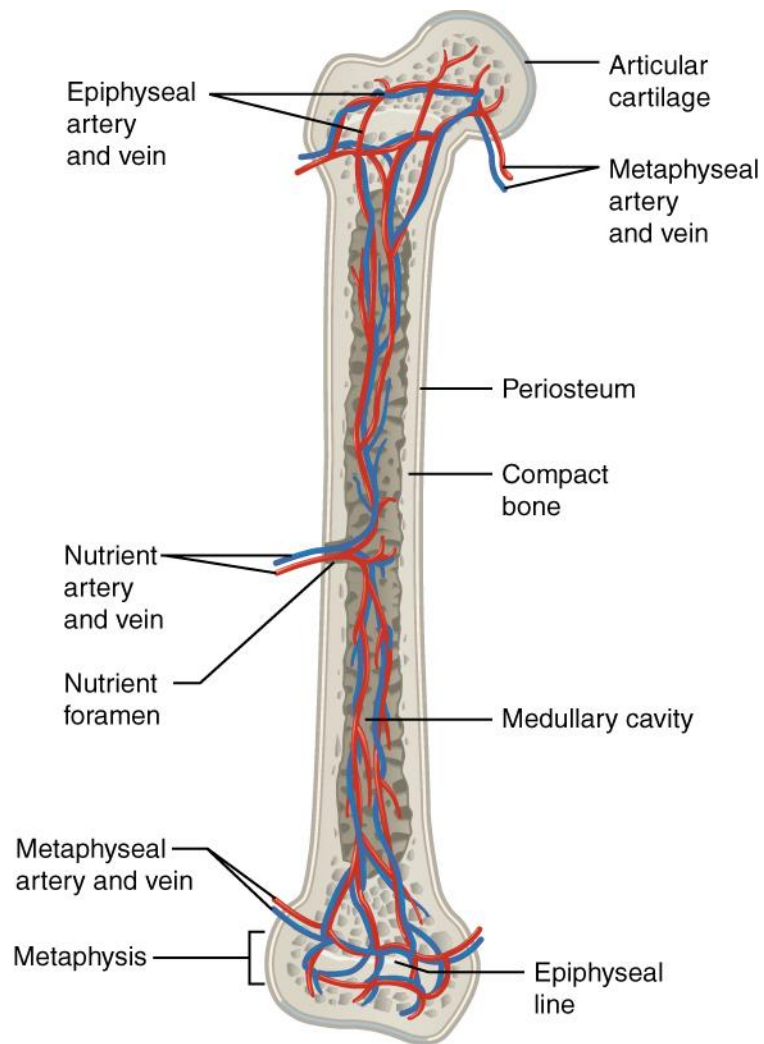


Figure I. 12 – Blood vessels and bone: Schematic of the intimate relationship between blood vessels on bone tissue with particular attention of the localization of the vessels. From [19].

4. Microvascular tissue engineering

The aim of this chapter is to review the most advanced (state-of-the-art) approaches and methodologies used to develop capillary-vessel structures. The focus will be given to the cellular component and the possibility to combine different cells, later in this chapter will discuss the different possible materials and composition which can be used to develop a properly defined and engineered supporting biomaterial. In addition, small molecules and factors will be reviewed to underline their potential to trigger cellular signals in the development of capillary vessels. Finally, the chapter will conclude with the two main procedures to develop capillaries using *in vivo* or *in vitro* approaches.

4.1. Key-role of pre-vascularization: the future of large tissue creation

Current status of vascular tissue engineering focuses mostly on the development of large diameters graft, to overcome death for cardiovascular disease (CVD)[32 2016, 33, 34] Despite those prostheses for vascular bypass grafts are currently used clinically, the absence of capillary network remains a missing part of the vascular tissue engineering [10, 35] [29, 36].

The importance of developing a functional capillary network into the engineered construct is fundamental when the size of such scaffolds is larger than a few mm³ in volume. Although largely ignored during the initial studies of tissue engineering, a major limitation for cell survival is the accessibility to oxygen and nutrients in order to properly perform the necessary metabolic activities [29, 37]. It is nowadays globally accepted that cells will encounter hypoxia and death when the closest capillary is further than 200 μm, which is the oxygen diffusion limit in living tissue [10] [29, 37],[38] [39]. As a consequence, the most successful engineered tissues produced nowadays, which can find a valid application in clinics, are based on the

constructions of thin layers such as skin, urinary tract, avascular cartilage and heart valves [40, 41] [42] [43] [44].

Only recently, engineered tissues start to implement microvascular capillary bed in order to achieve a better integration after implantation in the body of the host, however, there is no a well-defined procedure which can be used to obtain reliable results widely applied for a large variety of tissues [10] [35].

In adults' mammals, the body is physiologically capable to develop new capillaries, where required, within the tissues, regulating constantly the quantity of oxygen provided to each cell which is forming tissues and organs. Unfortunately, we are currently limited by technology, knowledge, and techniques for the development of complex and large scaffold, which would help the global health in replacing, repairing and restoring damaged tissue and organs.

Before discussing more in deep about cellular, material and growth factors importance, we need to define some terminology which is largely used, but often with a small difference between definitions. The terminology linked to capillary vessels remodeling or regression is not well-defined in the literature (Figure I. 13), and each research group defines their personal definition about it. In my study, I will refer to the definition reported by Lokmic *et al.*:

“

-Vascular remodeling is a process of reorganization of the engineered vascular network to achieve tissue homeostasis and maintain a fully functional construct. This process encompasses recruitment of pericytes and smooth muscle cells (SMCs) to the abluminal surface of the endothelial tubes (maturation) and at later stages a loss of individual blood vessels (pruning) of the microcirculatory network.

-Vascular regression is a process of complete loss of all cellular and structural components of a microcirculatory network through programmed cell death (apoptosis) resulting in the death of all of the construct's cellular components and loss of construct function.

“

[45].

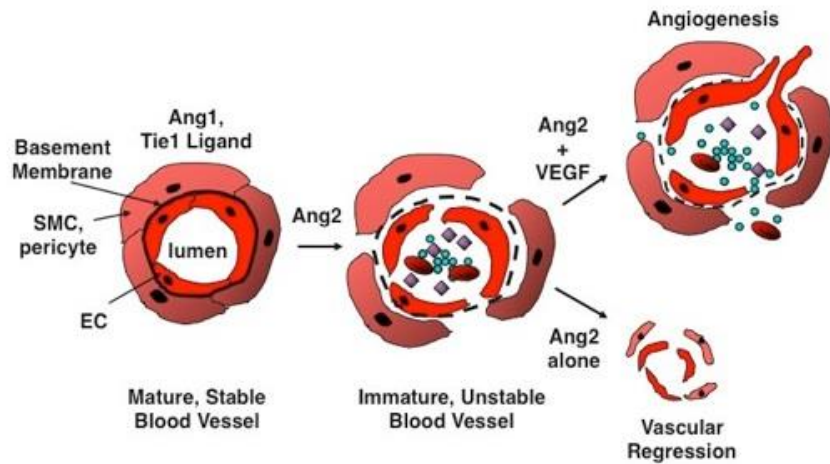


Figure I. 13 – Capillaries remodeling: Schematic of mature vessel, immature vessel, angiogenesis and vascular regression. [46]

Vascularization, applied for large tissue engineering constructs is an always-improving field and the interest of the scientific community is growing every year more [47 Heinz Redl, 2019].

4.2. Cellular importance: the players

4.2.1. Molecular perspective of cell signaling: cell adhesion

In this part, the most important cell signaling pathways for the development of capillary networks are investigated. The first cell signaling event is the cellular adhesion, which always occurs between cells and the surrounding environment [48].

Adhesion can be briefly described as the capability of the cells to be stable in contact with the surrounding ECM through the cell's receptor binding of the protein of the ECM (Figure I. 14). It has been demonstrated how cell adhesion is involved in the stimulation of other signals that regulate cell cycle, cell migration, cell differentiation, and cell survival [49]. The affinity between cell and substrate is fundamental in order to design and develop an optimal biomaterial for tissue engineering. In addition, cell adhesion plays a key role in cell communication and regulation, becoming essential for the development and the maintenance of a tissue [49].

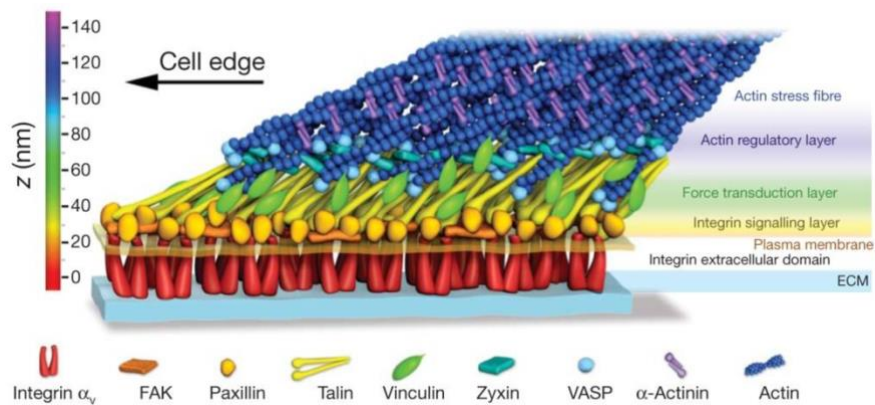


Figure I. 14 – Focal adhesion in cells: Schematic representation of the main components and architecture of focal adhesion such as integrins, actin, vinculin, and talin. From [48].

To properly trigger cellular signals, extracellular or intracellular forces are transmitted through localized sites at which cells adhered to other cells or the ECM [49]. In eukaryotic cells, this adhesion is occurring through a list of possible receptors such as integrins family, immunoglobulins, non-integrin collagen, glycolipids, glycosaminoglycans, and glycosylphosphatidylinositol-linked [48]. The integrin family covers a very important role in cellular adhesion, and their interaction with ECM is the most investigated. Integrins are capable of bind the main component of ECM proteins which are collagen, fibronectin, and laminin. Once the binding occurs, integrins are activated and cluster together into a nascent adhesion. Integrins are attached to actin filaments, which are the tensile members of the cytoskeleton,

through focal adhesion (FA) complex; a highly organized cluster of molecules. The cytoskeleton has the structural role to hold the nucleus and preserve the shape of the cell. Integrins, responsible for the transmission of forces to the cytoskeleton, are capable of mechanotransduction through the FA proteins, connecting the integrins to the actin filaments forming the adhesion complex. The FA complex formation is important not only for the cell adhesion but also for cell migration, proliferation, differentiation and for tissue organization, maintenance, and repair (Figure I. 15) [49].

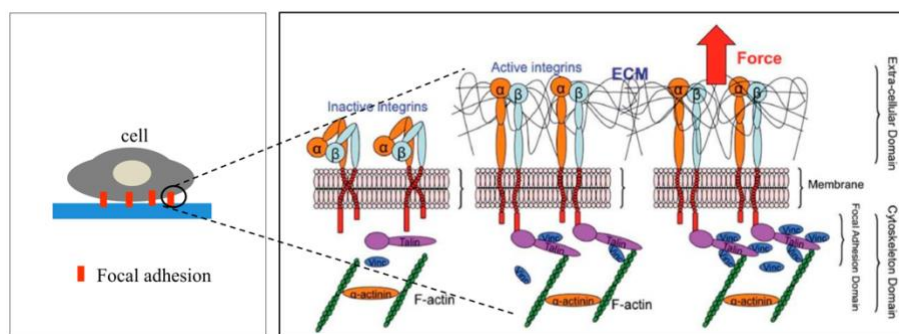


Figure I. 15 – Integrins activation during focal adhesion: Schematic representation of the intracellular receptors and the integrin connection. From the inactivated integrins, until the active form which would feel the extra-cellular forces and transfer the signal to the intracellular domain From [49]

Two main mechanisms are reported to explain the cell adhesion, the first one describes the *in vitro* cell adhesion defined as passive adhesion, the second one describes the *in vivo* cell adhesion defined as dynamic adhesion [49].

During *in vitro* condition in static medium cultures such as the culture flask or the Petri dishes, cells adhere through a mechanism defined as passive adhesion. Cells undergo attachment and spreading with a morphological alteration of their structure driven by passive deformation and active reorganization of the cytoskeleton (Figure I. 16) [49]. When integrins bind to ECM proteins, Rho GTPase proteins are activated such as Rho, Rac, and Cdc42. This activation is later responsible for cytoskeleton regulation which induces cells to spread, migrate and control the formation of stress fibers which assemble in focal adhesion complex [49]. Three stages can be identified

during the process of static *in vitro* cell adhesion: cell body attachment to the substrate (Figure I. 16 phase I), cell body flattening and spreading (Figure I. 16 phase II), reorganization of actin skeleton and focal adhesion formation (Figure I. 16phase III) [49]. During phase I, the interactions between cell and substrate are mostly electrostatic, thus weak interaction. The force which regulates the contact between cell and substrate is due to sedimentation effect and the morphology of the cell retain the round shape typical of cells in solution. During phase II, there is a change in morphology with a decrement in cell height and increment of the contact area spreading beyond the projected area of the spherical-cell contact. In this case, the contacts became stronger via adhesive interaction mediated by integrins. During phase III, the spreading process is continuous and evolving together with the reorganization and distribution of actin skeleton of the cell body. At this stage, the cellular spread reaches its maximum and the adhesive forces are the strongest via formation of focal adhesion (Figure I. 16) [49].

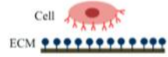
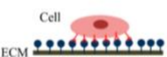
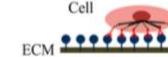
Cell Adhesion Phases	Phase I	Phase II	Phase III
Schematic diagram of cell adhesion			
Schematic diagram of the transformation of cell shape	Initial attachment	Flattening	Fully spreading and structural organization
Cell adhesion intervention	Electrostatic interaction	Integrin bonding	Focal adhesion
Adhesion stages	Sedimentation	Cell attachment	Cell spreading and stable adhesion

Figure I. 16 – Cell adhesion phases *in vitro* conditions: Evaluation of passive *in vitro* cell adhesion intervention and stages. Phase I represent the initial attachment, phase II represents the flattening of the cells with initial integrins bounding and last, phase III represents the strongest interaction with focal adhesion formation and spread cell-morphology. From [49]

During *in vivo* conditions, the adhesion of cells to extracellular matrix is an extremely dynamic process because involves fluid flow such as in the blood circulation, when migrating cells from the bloodstream need to pass through the endothelial layer and penetrate into the surrounding tissue, in response to environmental cues such as tissue remodeling [49]. Also in this model, the cell

adhesion cascade and signaling involve three basic steps: selectin-mediated rolling, chemokine-triggered activation, and integrin-dependent arrest (Figure I. 17). Those three-phased together, from the rolling of cells to the endothelial surface until cell arrest, are generally named docking phase [49]. Molecules responsible during this stage of adhesion are cell-surface conjugates selectins, chemokines, and immunoglobulins. The signal cascade for adhesion is triggered from the moment in which the cell starts to roll on the vessel's wall; molecular bonding between adhesion molecules must form rapidly, as well as break rapidly for cells to roll. The rolling cell are able to transduce those adhesive-braking signals from the receptors' surface to the cell nucleus in order to induce morphological changes which would slow down the rolling speed of the cell until its complete arrest, a fundamental prerequisite for cell migration through the vascular endothelium to reach the underlying tissue (Figure I. 17) [49].

The second part of the overall process to allow cells penetrating through the endothelium to reach the surrounding tissue takes the name of locking phase (Figure I. 17). This phase occurs after the ex-rolling cell established stable bonds with the endothelial cells mediated by integrins bonds. During this phase cell adhesion became stronger and spreading occurs in a similar approach to the static conditions, followed by cellular crawling to migrate into the endothelial lumen. Once the cell reaches the designed place, transmigration occurs, which is the process in which the cell emigrate out of the vasculature penetrating between two endothelial cells, paracellular transmigration, or through one endothelial cell, transcellular transmigration (Figure I. 17) [49].

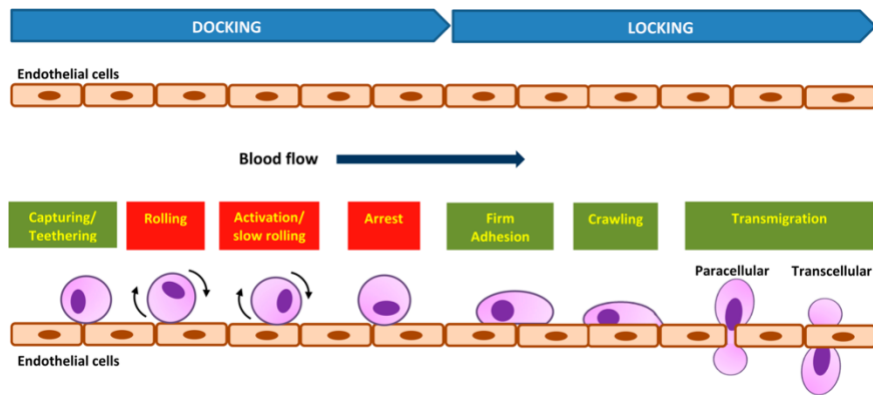


Figure I. 17 – Cell adhesion *in vivo* conditions: Schematic of the two steps docking and locking of cell adhesion when flowing in the blood circulatory system. From [49]

4.2.2. Molecular perspective of cell signaling: angiogenesis

The second cell signaling event is specifically involved in the formation of vessels structure, named angiogenesis or tubulogenesis [35].

Angiogenesis is a complex process in which tissues or organs involve multiple cells, from the same type or from different types, which guide the development of a new vessel from the angiogenic sprout formation until the vessel stabilization [35] [50-53].

In the human body, blood vessels differ from each other depending on their cellular composition, their diameter size and the functions they need to perform. Regardless of those differences, all blood vessels share a common characteristic which is the presence of a hollow center region, named lumen. The process which induces the formation of this lumen is extremely efficient and allows endothelial cells to cope with the force applied by the shear stress of the turbulent blood flow [54]. During the initial part of the process, when supporting cells are not yet bonded to the external surface of the endothelial cells, the cell-cell interaction of endothelial

cells are capable of supporting the physical forces exercised. While the size of the diameter of the vessels seems to be determined genetically, the blood flow is essential for the regulation and the maintenance of this lumen diameter [55]. Depending on the inner diameter of the blood vessels, the impact falls on the overall blood pressure and the perfusion of nutrients [54].

It has been already investigated the potential mechanisms by which lumen and tubular structure could be formed in epithelial cells, in the specific, five mechanisms were purposed: wrapping, budding, cavitation, cord hollowing, and cell hollowing (Figure I. 18) [54].

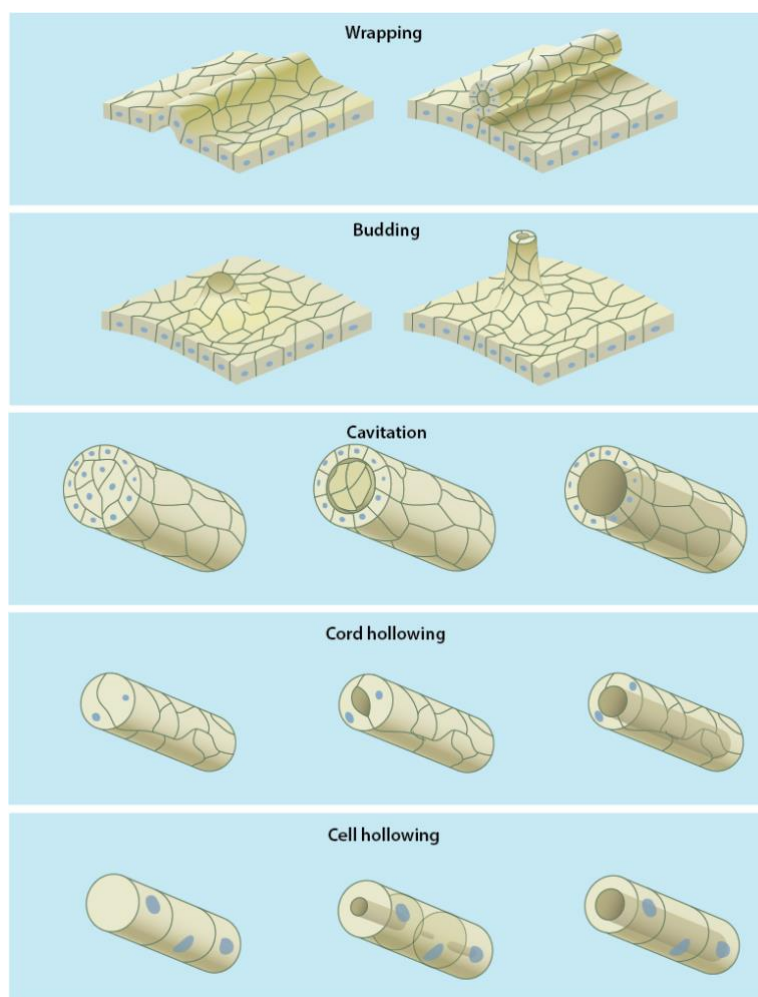


Figure I. 18 - Five mechanism of epithelial tubulogenesis. Wrapping, budding, cavitation, cord hollowing and cell hollowing. From [56]

Wrapping consists of planar cells sheet which wraps to form a tubular structure. Budding in which a vessel sprout from a pre-existing tube. Cavitation where space is created by the elimination of the central part of the cells from cell-cell aggregates in spheres or cylinder. Cord hollowing where a cord or cylinder of packed cells creates a central space by changing the cellular shape. Cell hollowing in which individual cells create an intracellular space within them to create a luminal structure (Figure I. 18) [54]. Number studies suggest how three out of five mechanisms purposed are used

by endothelial cells during developmental or postnatal angiogenic events: budding cord hollowing and cell hollowing. A common feature among those mechanisms is the necessity of the EC to create a physical space within the three-dimensional ECM to invade it and form lumen and tube networks [54]. EC can assume their characteristic cobblestone shape along the walls of the generate space into the ECM, to later create a tight connection with the adjacent cells through intercellular junctional adhesion. Matrix metalloproteinases (MMPs) are proteins secreted by EC, able to cleave proteins of the ECM to locally degrade the environment. Those MMPs play a key role during the formation of the empty space in the ECM where after EC will migrate to develop later one a new vessel. The physical space created by MMPs before the EC migration have been termed vascular guidance tunnels and influence both EC motility and vascular remodeling [54].

Previous studies in culture using three-dimensional ECM, as well as zebrafish and knockout mice, shown how integrins-ECM interactions play a critical role during vascular formation especially in the regulation of cellular sprouting, lumen development and tube stabilization [54]. Among the integrins identified to be responsible for the formation of new vessels, it is possible to identify $\alpha 1\beta 1$, $\alpha 2\beta 1$, $\alpha 4\beta 1$, $\alpha 5\beta 1$, $\alpha v\beta 3$, and $\alpha v\beta 5$. The binding of those integrins activates a downstream signaling which induces phosphorylation of Src and FAK kinases, which contributes to the process for the formation of the lumen and it's stabilization (Figure I. 19). Another important downstream path regulated by integrins is the Rho GTPases such as Cdc42 and Rac1, which regulate the endothelial cells' cytoskeleton activity, resulting in a morphogenic response for lumen development [54]. Already from its early formation during embryogenesis process, the vascular lumen has to sustain a large variety of physical forces such as plasma and blood cells circulation. In vertebrates, the heart starts to beat before the vasculature network is fully remodeled, thus endothelial tubes must be enough stable to sustain the pressure of the pumped flow [54]. These forces, from the moment they are applied to the vasculature network, will trigger morphological changes in the EC for the cytoskeleton orientation and the cell-cell junctional complexes formation and stabilization. In fact, in absence of flow perfusion, vessels naturally regress and, on

the contrary, when the pressure applied is higher than physiological, vessels undergoes an enlargement [54].

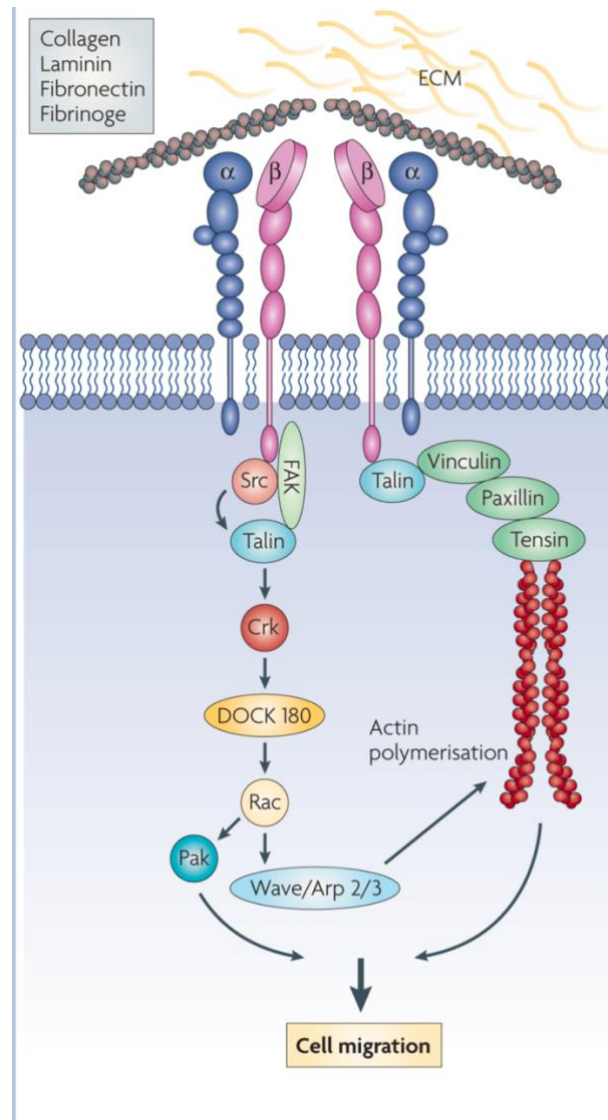


Figure I. 19 – Intracellular cascade of cell migration: Schematic representation of the intracellular cascade triggered by ECM-integrin link which lead to cellular migration. From [57]

Once the vasculature is newly-developed, a fundamental process takes place: vessel maturation. In this process, different cell types such as pericytes and vascular

smooth muscle cells are recruited to catalyze further remodeling events. Interestingly, some data suggest that during the maturation phase and the mural cell recruitment, genes involved in tube regression events are activated, without showing a visible regression in the morphology of the tubular structure [54].

4.2.3. Cell mono-culture: capillary formation

The oldest and most used cells for *in vitro* testing regarding vascularization is the endothelial cell extracted from the umbilical vein in humans since their isolation and characterization in 1973 [58 1973]. Human umbilical vein endothelial cells (HUVECs) have been extensively studied and used in research, both alone or with other supporting cells, to achieve vascularization *in vitro* and *in vivo* conditions [59]. HUVECs show an average lifespan about 10 passages and *in vitro* culture conditions for about 5 months [58], after which cells enter in a senescence stage: their proliferation stop and they develop giant multinucleated cells to undergoes death as the final stage [60]. HUVECs isolation in the clinic is a laborious process and, as most of the primary cells, there are differences between the donor-to-donor batch. Nevertheless, HUVECs becomes one of the most used sources for vascular studies in the field of tissue engineering for both large vascular scaffolds development and micro-vascularization studies since they preserve nearly all of the native-vascular endothelium features, normally found in physiological condition [59] [61]. After decades of studies, since their first isolation, HUVECs played a critical role in the development of *in vitro* model which help the understanding of mechanisms related to angiogenesis and neovascularization, inflammation and hypoxia response in tumors and embryogenesis [62-64]. HUVECs monolayer has been used also with microfluidic chambers to mimic shear stress and blood flow *in vitro*, in order to reproduce the physiological conditions and study cellular signaling, gene expression and cellular behavior [61]. Both *in vivo* and *in vitro* conditions, HUVECs express specific endothelial markers such as von Willebrand factor and CD31, making possible their identification and isolation. In addition, HUVECs are capable to bind a

large set of growth factor including VEGF, FGF, TNF-alpha, and angiopoietins, thanks to the abundance of specific cellular receptors [61].

Raghvan *et al.* introduce a novel method to combine three-dimensional structure micro-channels with collagen matrix and endothelial cells in order to promote de novo endothelial tubulogenesis *in vitro* (Figure I. 20) [65]. They seeded endothelial cells into the micro-patterned channels previously filled with unpolymerized collagen, applying a centrifugation step in order to drive the cells into the channels. After, gelling of collagen was performed with incubation at 37°C.

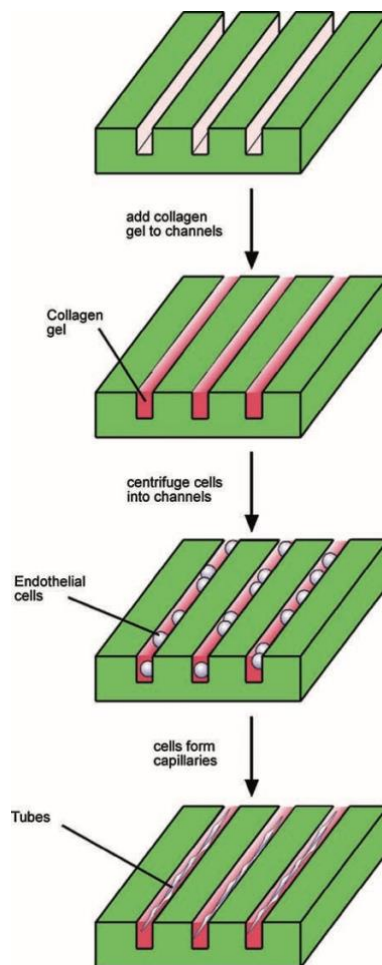


Figure I. 20 – Endothelial cell seeding in micro-channels: Schematic of the method used to seed endothelial cells into the micro-channels previously filled with collagen. From [65].

In their study, Raghavan *et al.* prove the self-assembled formation of tubular structure over 24h incubation with bFGF and VEGF, with the possibility to regulate the tube dimension using a combination of collagen concentration, channel width, and template pattern (Figure I. 21). Collagen was used at 1.3 mg/ml, 2.4 mg/ml, and 3.3 mg/ml, while channel width was ranging from 50 to 244 μm with a height between 50 and 100 μm . In addition, their approach also allows removing the developed tubes embedded into collagen, retaining spatial organization to be, possibly, further used as a component for more complex composite three-dimensional scaffolds for *in vivo* implantation [65]. Their studies investigated also the more complexes structure with a “T” or “Y” branch structure, showing after 48h incubation, a bifurcation of the endothelial cells to follow the channel design, and forming a lumen per each branch [65].

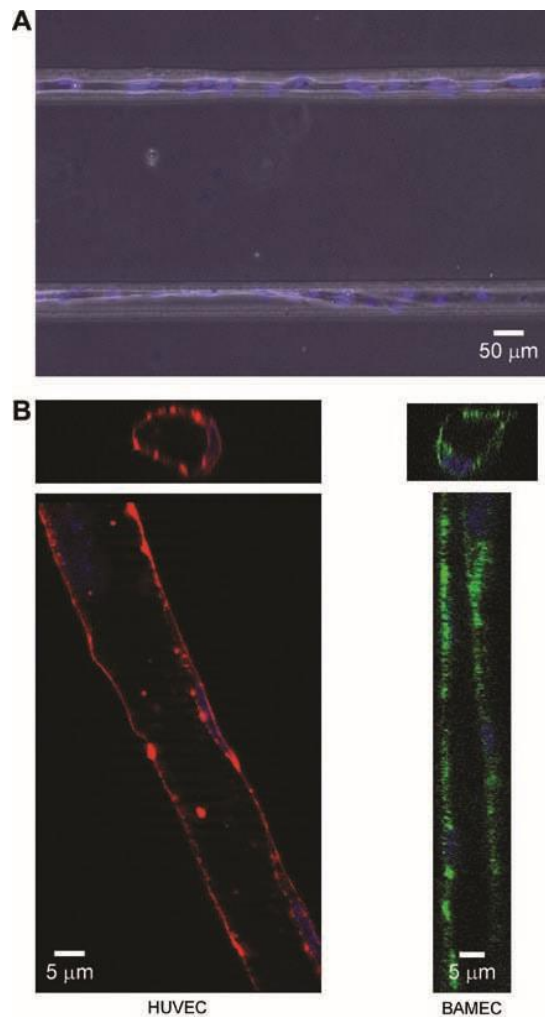


Figure I. 21 – Single endothelial tube formation. (A) phase contrast images after 24h HUVECs-collagen seeding in 50µm width channel. (B) Fluorescence images of HUVECs (red) and BAMEC (green) cultured in 50µm width and 50µm tall channels. From [65]

Sivarapatna A *et al.* established a microvascular platform based on PDMS to seed endothelial cells using microfluidic approach, studying the cellular gene expression change in response to shear stress to mimic *in vivo* physiological conditions [66]. The researchers were able to seed and growth HUVECs cells into the microfluidic platform up to 7 days of incubation, in micro-channels if about 200 µm in diameter developing intact microvessels *in vitro* (Figure I. 22) [66].

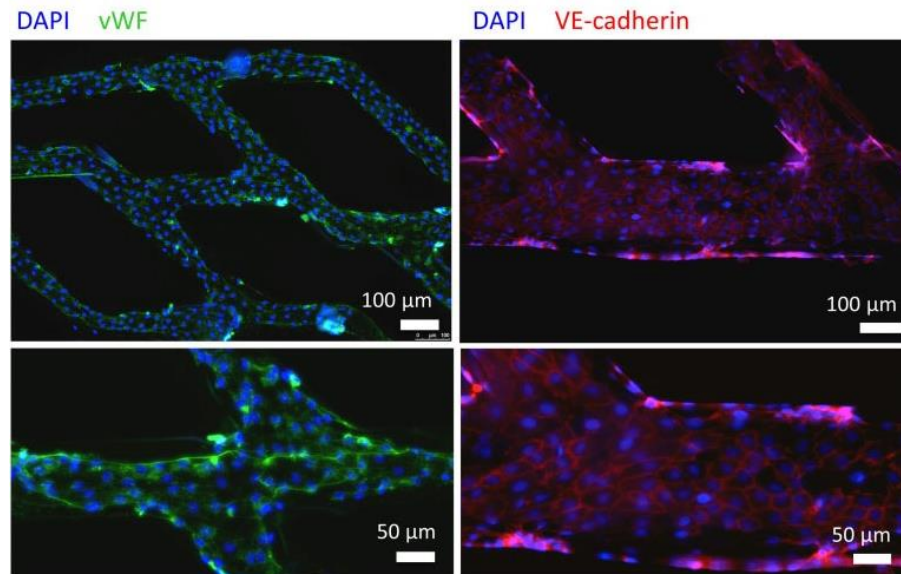


Figure I. 22 – Capillary network development: Immunofluorescence analysis of micro vessels generated using HUVECs after 4 days of culture under regular flow, marked with endothelial markers like vWF (left) and VE-cadherin (right). Adapted from [66].

Since HUVECs shows a great potential for the scientific community, several studies were done to transfect those cells with viruses carrying specific plasmids, to modify the original genetic content of HUVECs and develop a prolonged life-span cell line [60, 67]. Afterward, immortalized cell line, developed through the fusion between HUVECs and other cancer cells, was developed to generate a stable cell line which could mimic the characteristics of the original endothelial cells, without the drawback of the limited expansion [60]. In a previous study of Zheng et al, HUVECs were cultured into a spatial-defined microchannels network within matrices of type I collagen (Figure I. 23). After 1-2 weeks, endothelial morphology and barrier function were investigated as well as the behavioral change of HUVECs when exposed to flow stress [68].

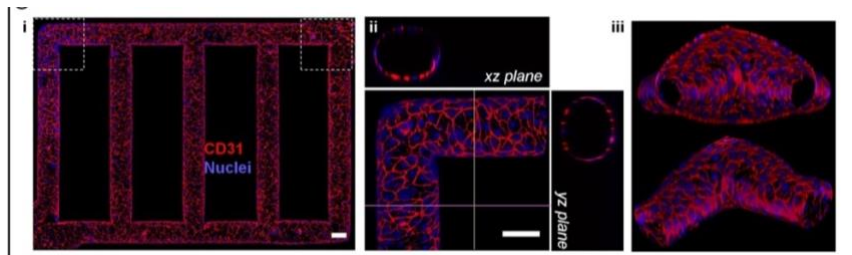


Figure I. 23 – Continuous curved capillary structure: CLSM of endothelialized micro-fluidic vessels. (i) General overview of the network, (ii) detail of the corner of the network in three different view sections. (iii) 3D reconstruction of the branching section. From [68]

The above-mentioned studies provide a more detailed understanding of the effort involved in the development of micro-vessels structures using an *in vitro* approach. However, according to the diameter size of each micro-vessel investigated so far, they cannot be classified as normal capillaries, but they can be defined as “giant” capillaries [69-71].

In a more recent publication Tsvirkun D. *et al.* developed micro-channels of 30-40 μm height from PDMS, creating a microfluidic device which approaches closer the size of capillaries in the human body. Once the device was developed, micro-channels were coated with fibronectin and later HUVECs were injected into the microchannel network in a pulse-wave manner for two consecutive days and cultured for two weeks, developing a continuous tubular structure inside the micro-channels (Figure I. 24) [72].

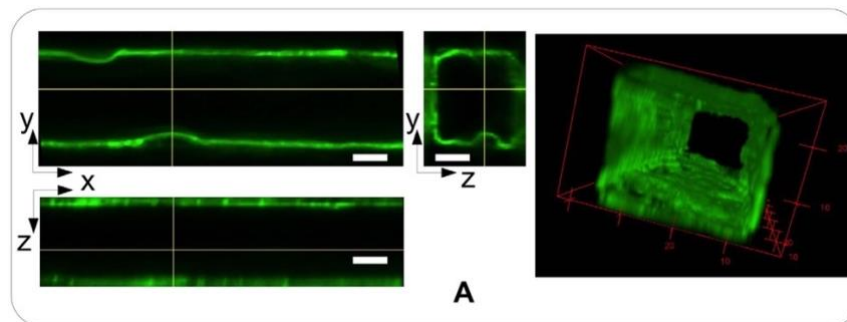


Figure I. 24 – Endothelial micro-tubular structure formation: Confocal images of HUVECs (green) from the top-, side, cross-section views and the 3D reconstruction. From [72].

4.2.4. Cell co-culture: vascular stability

In physiological *In vivo* conditions, blood vessels and especially capillary vessels, are surrounded by perivascular cells which aim to stabilize and mature the vascular structure. Pericytes (PCs) are perivascular cells already largely used in vascular tissue engineering and they present multipotential differentiation capacity (chondrogenic, myogenic, osteogenic, and adipogenic differentiation) expressing cell surface markers such as CD73, CD90, and CD105 [73] [74]. According to their characteristics in differentiation potential and cellular markers, Crisan *et al.* showed that PCs are the *in vivo* equivalent of cultured mesenchymal stem cells (MSCs) [75]. Therefore in my thesis, I will focus on the interest in PCs and their usage in literature for vascular tissue engineering applications. For more detailed information about the properties and functions of PCs in terms of cell isolation, culture and characterization methods, please refer to the review of Gökçinar-Yagci *et al.* [76]. Pericytes (also named as Rouget cells or mural cells) are perivascular cells that wrap around endothelial cells in capillaries and microvessels (Figure I. 25) [75].

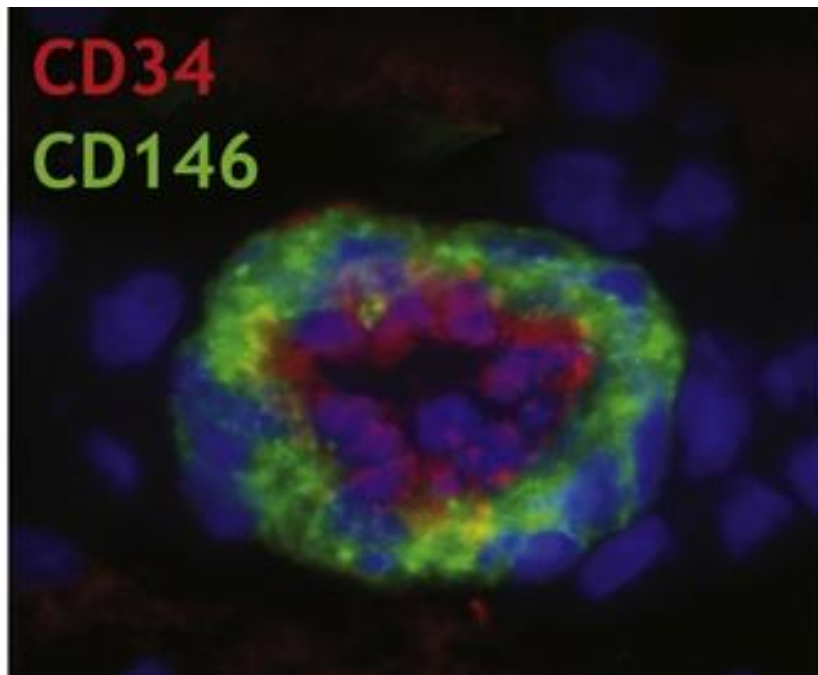


Figure I. 25 – Endothelial cells and pericytes *in vivo* spatial organization: Immunostaining image of Endothelial cells (CD34 +) forming a skeletal muscle small vessel (transverse section). Pericytes (CD 146 +) surround the structure. From [75].

Rouget described them in 1873 giving their initial name, and later in 1923 a German anatomist Zimmermann rename them as “pericytes” [77] [78]. *In vivo* physiological conditions, Pericytes can be found in capillaries, arterioles, venules, and also at the subendothelial region of large vessels [79]. Small blood vessels like capillaries are composed of endothelial cells surrounded by basal membrane, and PCs [76].

The newly developed vascular structures require a stabilization and perfusion in order to mature. Stabilization occurs by the application of flow-mediated shear forces, mimicking the physiological conditions, in addition, the basement membrane is produced and PCs are recruited [76]. The precise order of sequences of those events is not clear and can vary according to different conditions but in mature vessels, pericytes are embedded within the endothelial basement membrane [26].

In the field of micro-vascular tissue engineering pericytes are largely used since they are one of the main residents of small blood vessels and provide vessel stability [76].

The mechanism in which PCs are capable of stabilizing endothelial cells, like HUVECs, is not limited to a physical interaction between the two cells' type but involves as well as several signaling pathways [76]. Important pathways involved in the interaction between those two cell types are Transforming growth factor β (TGF- β) / activin-like kinase receptor (ALK5) [80], angiopoietin 1 (Ang1) / receptor tyrosine kinase of the Tie family (Tie2) [81, 82], and platelet-derived growth factor b (PDGF-B) / PDGF receptor beta (PDGFR- β) [83]. Zheng at al. studied the interactions between endothelial cells and pericytes when added to collagen bulk to form a long and stable vessel sprout [68]. Studies demonstrate how, during the angiogenic process, the absence of those cell-cell interactions due to the absence of supporting cells like pericytes leads to EC tube instability and regression [84]. An elegant experiment was performed developing a co-culture system between HUVEC and supportive cells grown in Matrigel, with and without direct contact between the two cell types. In both conditions, cells were able to communicate through soluble factors, but only in one case, the physical cell-cell interaction was involved. It was shown how the sample co-cultured without the physical cell-cell interaction was much less developed in term of capillary-like network formation [85]. The achievement of a stable co-culture system which would improve angiogenesis is not yet an easy task and the possible supporting cells such as pericytes, SMC not always lead to capillary network formation [86]. Co-culture experiments were performed trying to mimic the different type of tissues, such as in the case of engineered skin graft in which capillary network was introduced by co-culturing keratinocytes, dermal fibroblast and HUVEC on a 3D porous scaffold made of chitosan and collagen [51].

In the human body, the ratio between PCs and ECs differ from tissues to tissue ranging from 1:1 in the brain and retina, lower to 1:10 in skin and lung, and as low as 1:100 in striated muscle [76] [87]. PCs gained with the years more and more attention because it was demonstrated their role in regulators of vascular development, stabilization, maturation, and remodeling such as stabilization of

blood vessels permeability, blood pressure control, vasculogenesis and angiogenesis, contractility of vessels tone, and repair processes [76].

Tourovskaja A *et al.* developed an *in vitro* model for brain blood barriers using a combination of HUVECs and PCs seeded into microtubular channels made of PDMS (Figure I. 26 A-C) [88]. They report a successful angiogenesis in which PCs were recruited to the ECs vessels in presence of VEGF gradient with increasing sprout length (Figure I. 26 D) [88].

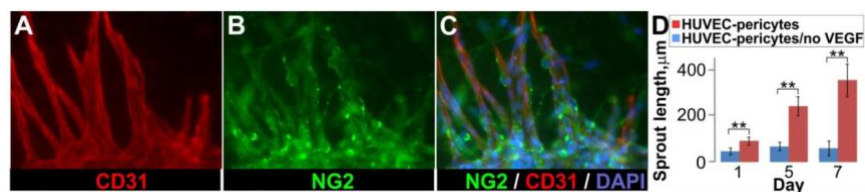


Figure I. 26 - Angiogenic studies on co-culture of HUVECs and PCs: (A) Immunofluorescence of HUVECs and (B) PCs with (C) merge of fluorescent signals. (D) determination of sprout length in presence or absence of VEGF for the co-culture system. From [88]

Morin KT *et al.* developed microvessels in fibrin gels to study the fundamental interactions between cells and matrix as well as align the microvessels for tissue engineering purpose [89]. The results reported in their work demonstrated the ability of HUVECs and PCs to form fully interconnected microvascular networks in fibrin gel developing longer structures with longer average length. In addition, the type of media used influence significantly the recruitment of PCs (Figure I. 27).

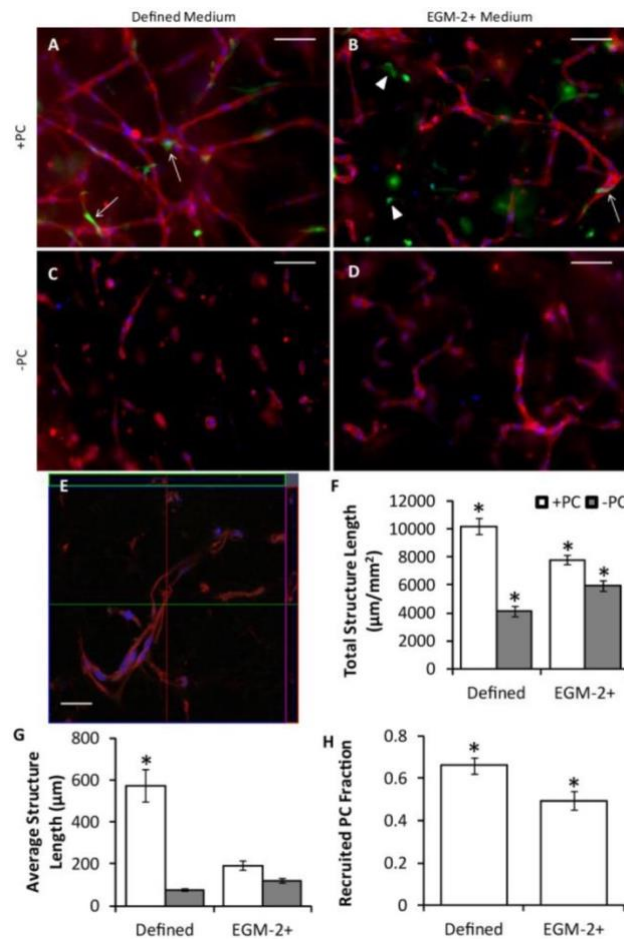


Figure I. 27 - Immune fluorescent studies for co-culture: (A, B) of HUVECs (red) and PCs (green) co-culture and (C, D) monoculture of HUVECs in two different media compositions indicating recruited PCs (white arrow-head). (E) confocal z-stack of construct. Scale bars = 30 μm . (F-H) quantification of micro vessels network properties in presence or absence of PCs. * $p < 0.05$. From [89].

Sudong Kim *et al.* developed a co-culture system into a single stromal cell culture channel filled with fibrin solution. Firstly, HUVECs were seeded using the microfluidic approach in endothelial growth medium-2, later PCs were mixed in fibrinogen solution and injected in the central channel. The incorporation of pericytes was then followed in the angiogenic sprout (Figure I. 28) [90]. They reported how after 4 days of co-culture, PCs were frequently found adjacent to the capillaries vessels with

stretched morphology to cover the abluminal surface of endothelium. The particular detail of the pericyte's adhesion to the endothelial-derived collagen IV basement membrane (Figure I. 28).

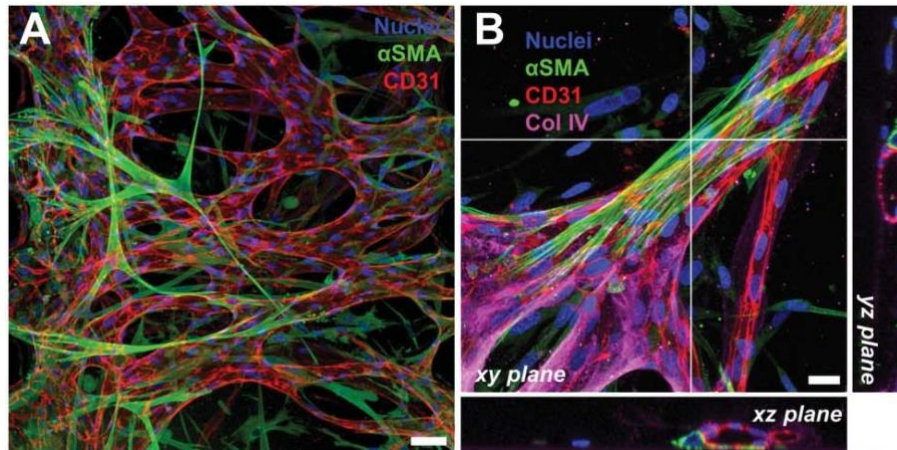


Figure I. 28 – Co-culture immunofluorescence images: HUVECs (red) and PCs (green) developing microvascular network. Scale bar 50 μ m. (B) Confocal sections of pericytes-decorated capillaries. Scale bar 20 μ m. From [90].

Moon *et al.* performed an experiment using a long time-lapse acquisition to follow the formation and the regression of capillary structure in PEG-hydrogels [91]. They investigated a monoculture of HUVECs and a co-culture of HUVECs with 10T1/2 (4:1 ratio) in PEG-hydrogels (Figure I. 29) [91]. 10T1/2 is a clonal mouse embryo cell line with multipotential [92]. For the monoculture investigation, they found how HUVECs were forming large clusters after 5 hours, then organizing in the primitive tubule-like structure after 21hour stable up to 50 hours. At later time-points between 53 and 69 hours, however, the structure lost their tubular morphology and rapidly regressed to form again the initial cluster (Figure I. 29). Contrarily, the co-culture experiment reported a rapid organization of tubule-like structure between 21 and 37 hours which were maintained stably even at later time-points of 52-69 hours (Figure I. 29) [91].

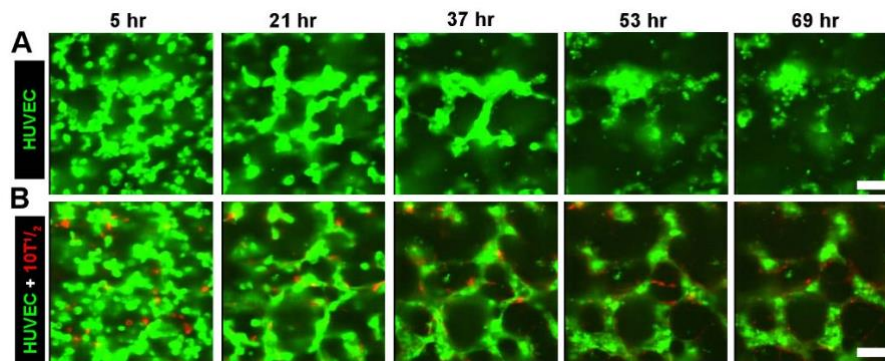


Figure I. 29 – Time-lapse confocal microscope HUVECs Cellular interactions in hydrogels encapsulated with either A) HUVECs only or B) HUVECs and 10T1/2 cells were visualized over about 70 hours with time-lapse confocal video-microscopy. A) In HUVECs mono-culture conditions, tubule-like structures initially formed by cells failed to maintain their networks and quickly regressed after about 50 hours of encapsulation in hydrogels. B) Tubule-like structures formed in co-culture conditions maintained their morphologies throughout the time-lapse experiments. From [91]

Andries D. van der Meer *et al.* developed microfluidic channels in PDMS to demonstrate the potential of blood-vessels-on-chip [93]. In their studies, they developed a three-dimensional construct inside a microchannel by injecting a mixture of HUVECs and PCs with collagen type I into PDMS channel of 500 μm width, 120 μm height and 1 cm length (Figure I. 30). After 12 hours cells were capable to organize themselves into a single tubular structure with a bifurcation. In addition, they demonstrate how the inhibition of the TGF- β pathway lead to disruption of normal vascular development with defective angiogenesis (Figure I. 31) [93].

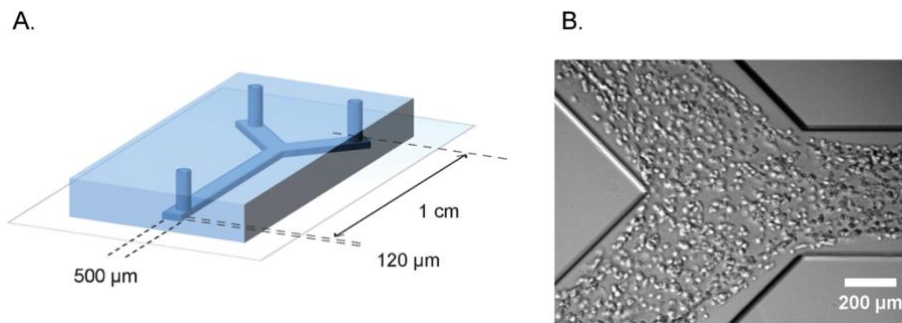


Figure I. 30 – Microfluidic structure for endothelial seeding: (A) Schematic representation of the microfluidic device with indicated measures. (B) Bright field image of cell suspension inside the microchannel after 1h of seeding. From [93]

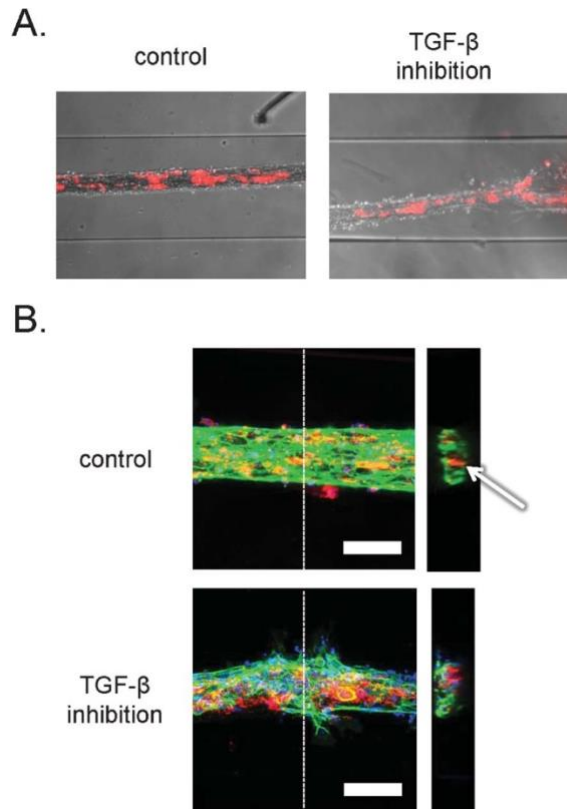


Figure I. 31 - Organization of PCs and HUVECs in presence of inhibitors: (A) brightfield microscopy and in (B) confocal microscopy in the presence of TGF-B inhibitors and the

control sample. Scale bar 100 μm , dashed lines denote the sections in the respective planes, arrow denotes lumen in control structure. From [93].

More recently Zhang *et al.* investigate a coculture system using a home-made scaffold which they term AngioChip. This AngioChip presents a symmetrical bifurcation of micro-channels which can be connected to a pump to provide a regular flow (Figure I. 32). The micro-channels were firstly seeded with EC using microfluidic approach, and later supportive cells were seeded on top of the micro-channels. The smart approach consists in the fabrication of micro-pores in the micro-channels, which allow the two cells type to communicate through specific factors (Figure I. 32). Later the chamber is sealed using a biodegradable gel system. The authors report how this approach provided no delay for the tissue endothelialization since the endothelial coverage was achieved within one day after perfusion. In addition, paracrine signaling between the two cells type can be sustained thanks to the 10-20 μm pores present on the micro-channels (Figure I. 32). In summary, the AngioChip was successfully used for *in vitro* and *in vivo* studies to generate a hepatic tissue model with a precise three-dimensional structure allowing a direct anastomosis to the host vasculature [94].

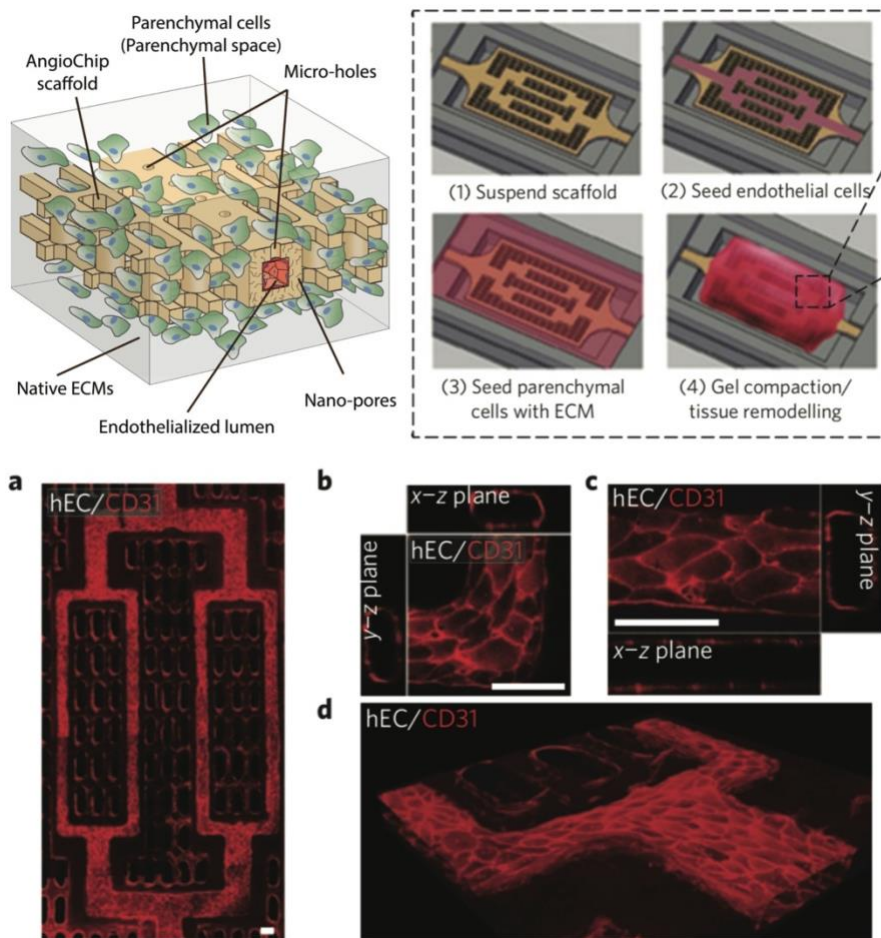


Figure 1.32 – AngioChip microfluidic studies: (Top left) Schematic of a part of an AngioChip tissue with particular attention on the co-culture system without direct contact but micro-holes connections. (Top right) Schematic of the assembly of the bioreactor and the assembly of vascularized tissue. (a-d) Immunostaining HUVECs (red) of the internal vasculature after 2 days of culture. (a) a view of the entire network (b) a view of a corner and (c) a straight segment and (d) a branch. Scale bar 100 μm . Adjusted from [94].

4.3. Biomaterials: more than just a supportive element

The basement membrane produced by endothelial cells (EC), in physiological conditions in the human body, is composed of several molecules such as laminins'

family, collagen IV, heparin-sulfate proteoglycans and nidogen. Altogether, these molecules play the important role of communication with the EC to induce proliferation, migration, differentiation, maturation, and adhesion [95]. Migration of EC during angiogenesis is driven by a well-known peptide motif sequence: arginine-glycine-aspartate (RGD). The binding of this motif sequence through integrin receptors, present on the EC membrane, results in modification of cellular shape and behavior [96]. In addition, some ECM proteins are able to interact and bind angiogenetic factors such as VEGF-A and FGF-2, providing a signaling-reservoir which trigger angiogenesis in the migrating EC [97, 98].

In tissue engineering field, the biological substitutes, which aim to support the seeded cells and guide them through biological function, are generally termed scaffolds or biomaterials [45]. Biomaterials play a key role in the engineered tissues constructs, in fact they serve as scaffolding to support the cells but also the mechanical properties of the tissue/organ to replace, they serve as reservoir for molecular signaling thanks to growth factors absorption or grafting, they serve to trigger signals to the cells in order to guide them through one intracellular pathway, or another.

In this sub-chapter, we will investigate the different materials largely used in vascular tissue engineering and the importance of their microscopical structures.

4.3.1. Naturally derived biomaterials

Natural biomaterials present the peculiar characteristic to resemble the native extracellular matrices of tissues, such as good bioactivity, biocompatibility and, tunable biodegradation. In order to preserve their original characteristics of natural biopolymers, they are often processed using aqueous solutions and environmental-friendly methods [5]. It is critical to avoid any release of cytotoxic products which could alter the delicate equilibrium of cellular and molecular signaling. Upon the real application in the complex biological systems, those biopolymers and their degradation by-products must be tested to verify the absence of harmful products and signaling [5]. Since natural biomaterials contain epitopes which can be

recognized and bounded by cells during their activity, they possess the innate ability to promote biological recognition which improves radically the functionality and regenerative properties of the final implantable device [5]. This class of biomaterials can be further divided into two larger groups, according to shared common properties: protein-based biomaterials and polysaccharide-based biomaterials.

Among the naturally derived biomaterials, and specifically in the polysaccharide-based biomaterials, it is common to find polyelectrolytes which are a macromolecule containing both cationic and anionic groups. Some of those polyelectrolytes are directly extracted from animals or derived from animals' components as reported by those two important examples of polyelectrolytes largely used in TE field: chitosan (CHI) and hyaluronic acid (HA).

Chitosan (CHI) is a natural-derived copolymer, originated from chitin (poly(N-acetyl-D-Glucosamine) by partial de-acetylation of the D-glucosamide groups (Figure I. 33). Chitin, the precursor of chitosan, is widely distributed in nature and it is the most abundant polysaccharide in nature, after cellulose. It was firstly isolated from fungi and later from beetle insects. However, nowadays the main sources of chitin are the crustaceans wastes of the fishing industry [99]. Chitin is not naturally present in the human body, nevertheless, it was proved how this would induce only a minimal immune response when implanted in other animals [100].

The biological properties of Chitosan are associated to its solubility in water and other solvents. Above pH 7 chitosan remains insoluble in aqueous solutions [101]. However, in the presence of a little amount of acid, the amino groups are protonated, facilitating the solubility of the macromolecule [101]. The pK_a of its primary amino groups depends on the deacetylation degree, as well as its solubility [101].

It was investigated in several studies, how the two monomers of the CHI copolymer behave differently in terms of biodegradability. In fact, while the de-acetylated residues of CHI are non-degradable, the acetylated residues can be slowly degraded by the action of lysozyme and other catabolic enzymes (Figure I. 33) [102]. The secretion from the body, via the kidney, works when the resultant fragments are smaller than 30 kDa, and thus soluble [103]. Previous studies demonstrate how a

change of deacetylation degrees from 60 % to 70 % can drastically change the leftover of implanted CHI film from < 5 % to > 90% respectively, after 12 weeks implantation *in vivo* by a subcutaneous implant in the back of rats [102]. This suggests that using a batch of CHI with de-acetylation degrees <60 % would allow a complete clearance of the degraded chains of CHI from the body [103].

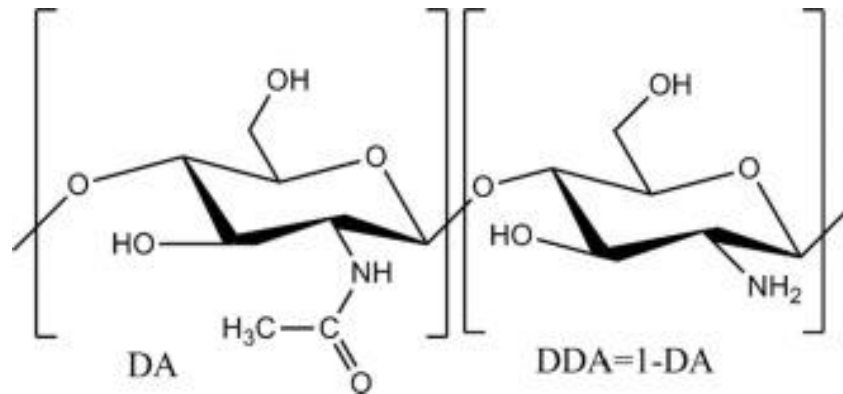


Figure I. 33 - Chitosan chemical structure. Notice the acetylated monomer on the left, and the deacetylated monomer on the right, in which an acetyl group was removed. From [104].

Hyaluronic acid (HA) is a copolymer, which alternates glucuronic acid and N-acetyl-D-glucosamine and is a major constituent of the extracellular matrix, present in many tissues in the body such as vitreous humor and synovial joint fluid (Figure I. 34) [105]. The pK_a of its carboxyl groups are around 3-4 and, therefore, at physiological pH (± 7) these groups are negatively charged [106]. HA is known to be non-adhesive for most proteins and so, represent an ideal material to be used natively or chemically modified [103]. Those characteristics make HA extremely attractive for various technologies concerned with body repairs such as wound healing [107], drug delivery [108] and visco-supplementation [109]. HA presents several advantages for tissue engineering applications such as biodegradability, biocompatibility, and bioresorbability and, moreover, HA is involved in the wound healing process, providing faster healing [105].

The appealing properties of HA, makes it largely used in tissue engineering, especially after chemical modification, easily performed thanks to the alcohol and carboxyl group present in each monomer. Several routes of chemical modification

are possible, such as esterification, hydrazide modifications, glutaraldehyde crosslinking, auto-crosslinking, and carbodiimides chemistry. In this last case, the crosslinking occurs via formation of anhydride on the polysaccharide through reaction with neighboring carboxyl groups, and this anhydride then reacts with nearby hydroxyls to give both inter- and intramolecular cross-links. In some studies, HA was crosslinked using EDC to enhance mechanical stability [110 Watson, & Cameron, 2010, 111]. Even when physicochemical properties of the new HA-based scaffold change, depending on the chemical change, most of the resulting derivate, retain the biocompatibility and biodegradability of the native HA [105].

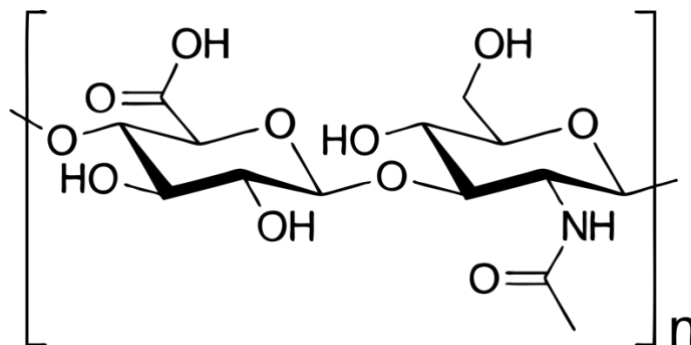


Figure I. 34 – Hyaluronic acid monomeric structure.

Those two polyelectrolytes can be used, not exclusively alone, but also in combination with each other and thanks to the electrostatic charges present on those two polyelectrolytes, is possible to deposit them in alternate way, in a process generally termed layer-by-layer deposition (LbL) to functionalize surfaces and make them (more) biocompatible [112-116]. Briefly, the technique involves the initial deposition of the polyanion, negatively charged species and, after several rinsing steps, the deposition of polycation, positively charged species [117]. The electrostatic interaction between those two species can be controlled and tuned thanks to the salt concentration used to dissolve them, the pH, the temperature and the deposition time [118, 119]. Polyelectrolytes growth in mass and thickness was found to follow either a linear equation [120, 121] or an exponential equation [122, 123] depending on the nature of the polyanion and polycation (Figure I. 35).

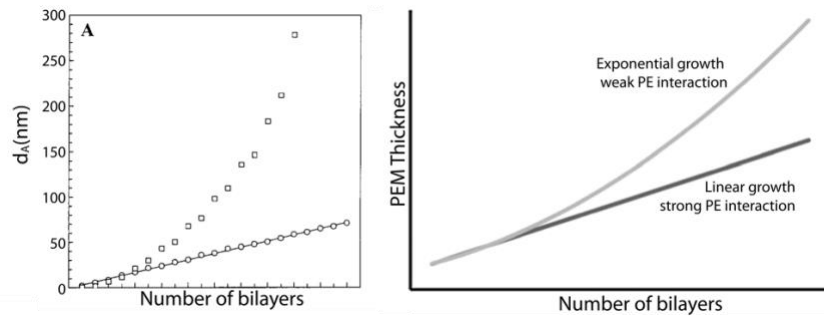


Figure I. 35 – Studies on polyelectrolytes LbL growth: (A) Evolution of the polyelectrolytes film thickness (d_A) for PEI-(PSS/PAH)_i or PEI-(PGA/PLL)_i. PEI: polyethylenimide, PSS: poly(styrenesulfonate), PAH: poly(allylamine hydrochloride), PGA: by poly(L-glutamic acid), PLL: poly(L-lysine). From [124]. (B) From Polyelectrolytes LbL film growth in linear or exponential manner, depending on the strength of interaction between the polyelectrolytes. From [125].

The combination of HA/CHI can be found in several biomedical applications such as guided tissues regeneration in periodontal applications [126], drug delivery [127], protein adsorption [128], cartilage tissue engineering [129], bone tissue engineering [130], or also microchip reactor for enzyme immobilization [131]. It was shown that HA/CHI deposition of about 20 cycles can reach the thickness of 10 μ m or more [119]. The deposition of the two alternate polyelectrolytes can be performed in an automatic manner using a dipping machine (Figure I. 36). Briefly, the preselected material is firstly dipped into the first polyelectrolyte solution and automatically rinsed several times, before the application of the second polyelectrolyte.

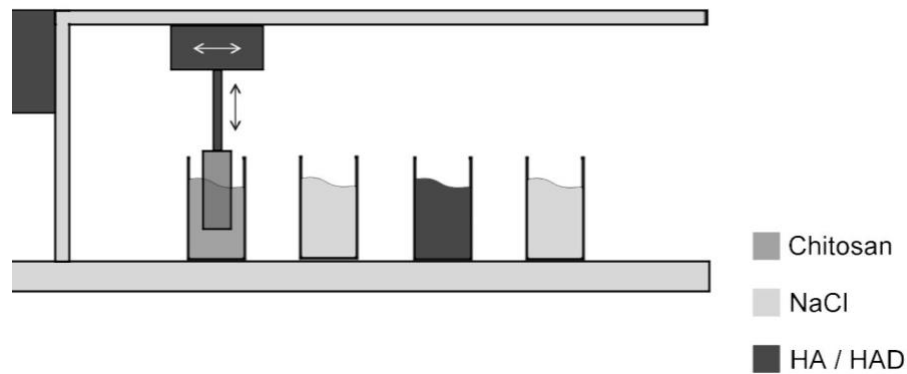


Figure I. 36 – Layer-by-layer assembly: Schematic representation of the LbL assembly through an automatic dipping machine, divided in 4 main parts. Part 1, deposition of the first polyelectrolyte in this case Chitosan. Part 2, rinsing in NaCl solution to remove the excess. Part 3, deposition of the second polyelectrolyte in this case hyaluronic acid. Part 4, rinsing in NaCl solution to remove the excess. Gently provided from [126 and João F. Mano. "Biomimetic polysaccharide/bioactive glass nanoparticles multilayer membranes for guided tissue regeneration." RSC Advances 6.79 (2016): 75988-75999.]

4.3.2. Synthetic biomaterials

On the other hand, synthetic scaffolds can be tuned to provide the desired biological functions such as vessels ingrowth, depending on chemistry, pore size, density, and interconnectivity [132, 133]. A disadvantage of some of those scaffolds is given by the degradation rate and the formation of toxic by-products during the break down of the polymeric chains [134]. It was shown how the fast degradation of poly d, l-lactic-glycolic acid copolymer (PLGA) negatively affects cell viability and migration due to significant acidification of the local environment during to polymer degradation [134].

Synthetic biomaterials can trigger a biological response, defined as the foreign body reaction. During this process, macrophages and foreign body giant cells develop a fibrotic tissue which surrounds the implanted material, negatively influencing its functionality in patients, with the undesired outcome, in some cases,

of device failure [135]. The foreign body reaction represents the end-stage of the inflammatory wound healing process, occurring after implantation of medical devices, prosthesis or materials [135]. The interactions between macrophages and foreign body giant cells with the synthetic material's surface play a role in modulating this inflammatory event [135]. The formation of fibrotic tissue all around the implanted material can, therefore, impair microvasculature formation and further development of the tissue [136-138]. Polytetrafluoroethylene (PTFE) membranes of various pore sizes were tested and implanted subcutaneously in rats resulting in the development of thick fibrotic tissue, typical of a foreign-body response when the pores size were below 5 μm in diameter [138].

Thermoplastic polymers were developed more than 80 years ago, and their usage nowadays became part of the routine life. Those materials start to be used also in the tissue engineering field as a template or scaffold materials, such as Polyethylene terephthalate, Polycaprolactone, and Polycarbonate. This last polycarbonate polymer was firstly synthesized at the beginning of 50's from the union of a carbonic acid with symmetrical aromatic 4,4 dihydroxy diphenyl (Figure I. 37) [139].

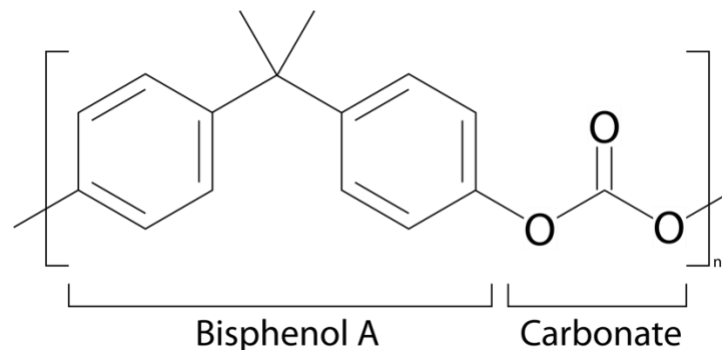


Figure I. 37 - Chemical structure of Polycarbonate: the two units which compose the polymer are represented; bisphenol A and carbonate.

This polymer is not soluble in aqueous solutions, but it is highly soluble in organic solvents such as dichloromethane. Key-characteristics of this material is the optical transparency to possibly work with cells and visualize them. In addition, it is resistant to reagents, it is mechanically and thermally stable and moreover, it can be used

easily for molding process like hot embossing. The glass transition temperature of this polymer is around 140-150°C and its capacity to absorb water is nearly zero [139]. Thanks to its transparency, resistivity, durability, and plasticity during the molding process, PC acquired an immediate interest for different applications. One example is the capability to transform the PC into a micro-reactor. Their small size and high control over parameters such as temperature, pH, salt solution and flow speed allow those micro-reactors to develop an efficiently biochemical reaction, otherwise impossible in the normal industrial processes. PC during the years was successfully functionalized with proteins [140] and nucleic acids [141]. In the work of Ogonczyk D *et al.*, alkaline phosphatase enzyme (ALP) was immobilized into the capillaries of polycarbonate, and enzymatic reaction was followed for several days to evaluate the stability of the immobilized enzyme over time at different flow rate speed (Figure I. 38) [140]. The recorded absorbance show how the enzyme was successfully immobilized onto a polyethyleneimine (PEI) layer through carbodiimide chemistry and stable up to 27 days (Figure I. 38). For more detailed works about the use of microfluidics for cell isolation and other biomedical application please refer to this review [142].

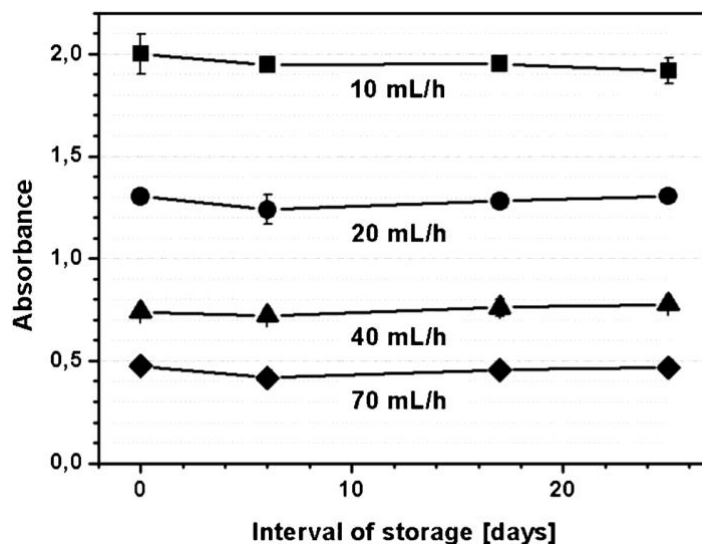


Figure I. 38 – Stabilization of immobilized proteins: Characterization of stability of ALP enzyme when immobilized in PC capillaries under constant flow rate. From [140].

4.3.3. Hybrid materials

To ameliorate the cellular function and improve the control over the material degradation, hybrid scaffolds composed of both natural and synthetic materials were developed. Those materials often incorporate angiogenic proteins [143] or peptide sequences [144-146]. Incorporating those factors results in a bio-recognition of the material from the body, avoiding the foreign body reaction effect and improving cell migration and growth [45]. Recent studies were done combining synthetic Polydimethylsiloxane (PDMS) and natural Collagen to develop microchannels [147, 148]. In the study of Alimperti S. *et al.*, they fabricated micro-channels of 160 μm diameter, made of PDMS coated with collagen type I to study the endothelial cells barrier integrity. Combination of HUVECs and human kidney pericytes was used or HUVECs with human bone marrow stromal cells (HBMSCs) [147]. Costa PF *et al.* developed instead one micro-channel of 700-800 μm diameter with a narrow constriction in the middle, to study arterial thrombosis. Channel made of PDMS was later coated with rat tail collagen type-I and finally, HUVECs were perfused in the microfluidic system for two days to ensure confluent monolayer [148]. Another study for atherosclerotic plaque formation was done using a combination of PDMS and vWF/fibrinogen [93]. In this study, they developed microfluidic chips from PDMS using parallel micro-channels of 300 μm width and 52 μm height and later immobilized vWF/fibrinogen. In addition, HUVECs were seeded into the precoated micro-channels and stenosis formation was investigated [93].

4.3.4. Surface chemistry: biochemical and physical modifications

Besides bulk properties, the control of the properties of the biomaterial surface used for medical applications is a key point. So, biomaterial surface is often modified with biomolecules that can stimulate different intracellular pathways in the cell, such

as adhesion, migration, growth, differentiation, angiogenesis and much more. The activation of these pathways depends not only on the type of biomolecules that is adsorbed or grafted on the surface of the biomaterial but is also strongly related to the quantity and density present on the surface.

The native extracellular matrix is a mixture of macromolecules self-assembled together, mostly composed of collagen proteins, glycoproteins, hyaluronan, and proteoglycans [149]. Like the ideal biomaterial should be, the ECM serves as a scaffold for cells, reservoir of growth factors and cytokines, and provide structural strength to tissues maintaining the intricate architecture around the cell and the shape of organs. The aim of the tissue engineering field is to transfer the characteristics of the physiological ECM into the biomaterials, controlling the environment for cells in a precise way [150-152].

In order to mimic the ECM environment, biomaterials' surface has been modified with a large variety of substances from the inorganic molecules to short peptides or complex proteins, tuning the cellular behavior. Coating of the biomaterials' surface before introducing the cellular component can increase significantly cellular adhesion, increasing the biocompatibility of the material [152]. Usage of natural proteins extracted from the ECM is a smart approach for the biomaterials' surface coating. However, sometimes the use of large proteins can be complicated due to the laborious and long procedure for their extraction from the ECM and purification with the high risk to alter the native conformational state of the protein itself [153, 154]. In fact, proteins are macromolecules with a defined three-dimensional structure which is fundamental for cellular-receptors recognition and binding. When the three-dimensional structure of a protein changes from its native state to an aberrant state, the process is defined as denaturation [153, 154]. Denaturated proteins lose their capability to bind cellular-receptors and thus to perform any biological function for the cell. When instead the sequence of the protein is altered due to sequence breakage, the process is named degradation [155, 156]. Proteins denaturation and degradations are an important drawback to consider during the development of a biomaterial, in fact, the process of integration of those macromolecules into the biomaterial, maintaining the native proteins' structure can

be challenging. In addition to this point, when a protein is covalently bonded to the biomaterials' surface is fundamental to provide the proper orientation, which would not affect the functionality of the protein in binding the cellular-receptor. As results, a precise control over protein dynamics can be extremely difficult.

A valid alternative solution to large macromolecules like proteins can be the usage of small and stable oligomers, named peptides. A peptide is a small molecule which reproduces the binding site, defined epitope, of larger proteins [157-159]. This allows scientist to use more stable molecules than the proteins, without affecting the biological recognition between epitopes and cellular-receptors. In addition to their stability during the biomaterials' surface functionalization, peptides can be easily synthesized with a moderate cost, can be easily characterized, present a slow enzymatic degradation, and in lyophilized conditions are extremely stable for transport and storage purposes.

In order to biofunctionalize the biomaterial's surface to enhance the overall material properties, several techniques are commonly used. The most simple but also least stable is the physical adsorption of biomolecules, such as peptides. In this case, the surface functionalization is performed by dipping the material into a peptide solution in order to allow a physical interaction between the materials' surface and the biomolecules in solution and allow their deposition [160, 161]. Since the forces of interaction in this technique are weak, environmental conditions such as temperature, pressure, pH, ionic strength and concentration must be stable and properly adjusted. Any change of those conditions might easily cause a molecules desorption and system instability.

When molecules are covalently immobilized to a surface they acquire the advantages to be more stable to environmental modifications and they are more stable over a longer period of time [161]. Several routes are possible in order to create a covalent bond between the molecule of interest and the biomaterials' surface. However, a common route, largely used for peptides grafting, consists in the use of carbodiimide chemistry (Figure I. 39).

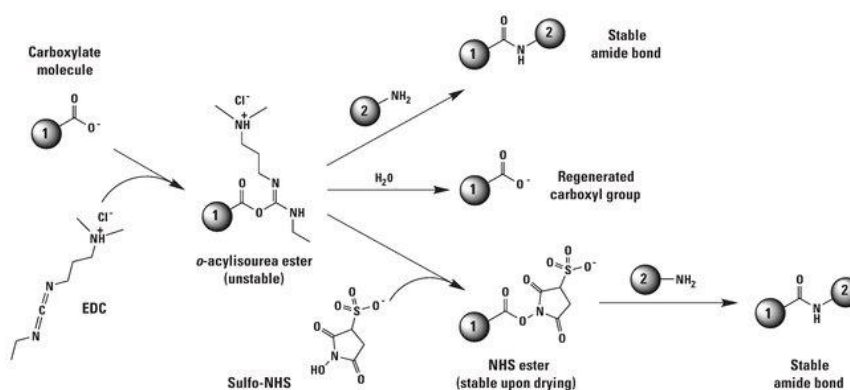


Figure I. 39 – Carbodiimide chemistry for peptides immobilization: General representation of the chemical reactions which occur between the molecule-presenting carboxylic group “1” and EDC to generate an unstable product. Later Sulfo-NHS will react with this unstable form to generate a stable ester that can react with the amine group of the molecule “2” in order to create a newly and stable amine bond linking molecule “1” and molecule “2”. From [162].

This route involves two chemicals: 1-Ethyl-3-(3-dimethylaminopropyl)carbodiimide (EDC) combined with N-Hydroxysuccinimide (NHS) or N-hydroxysulfosuccinimide (sulfo-NHS). In the specific, the carboxyl group on the materials’ surface reacts with EDC to form an unstable intermediate (Figure I. 39). Upon reacting with NHS (or sulfo-NHS), a more stable amine-reactive intermediate is formed (Figure I. 39). Finally, this intermediate is coupled to the amine groups found on the peptide group, finalizing the immobilization process (Figure I. 39). Previously in our group, carbodiimide chemistry was largely used to covalently graft peptides on to polyethylene terephthalate (PET) surface after a hydrolytic/oxidative step to increase the number of carboxylic groups [163-169, 170 2013, 3, 171 2009., 172 2010].

Many other methods of immobilizing biomolecules on materials’ surfaces are reported in the literature, and each of them, according to the conditions of reaction or the reactive group used, present advantages and drawbacks [173] [174]. Methods used include the biotin-avidin system, click chemistry and 3-

aminopropyltriethoxysilane (APTES). For a larger list of biomolecules immobilization methods, please refer to more detailed publications [173, 175] [176].

4.4. Small molecules: the signaling messengers

4.4.1. Growth factors

Growth factors are an important category of small molecules with a powerful effect. They can play the important role of initiators of vascularization process, and so, they have been largely used both *in vitro* and *in vivo* [177, 178]. In the body, they are able to activate endothelial progenitor cells (EPC) and guide their migration through gradient effect, based on the modulation of their concentration in the tissues. In addition, growth factors can guide cell assembly, the formation of new vessels and finally the stabilization of the tubular structure to preserve the shape and the function over the time, in a process termed vessel maturation [20].

To solve the instability problem of growth factors, due to their short-life, new materials were designed in order to preserve the growth factor functionality and at the same time allowing a slow-rate delivery strategy. Biomaterials with a different rate of biodegradability, thanks to natural or synthetic polymers characteristics, can be used to entrap the growth factors protein within the scaffold, and release them in a time-dependent manner, according to the biodegradability of the material [179-181]. Examples of those slow-rate-release materials are the encapsulation of growth factors in poly(lactic-co-glycolic acid) (PLGA) [182, 183]. Another innovative approach to constantly supply growth factor to the system, is the usage of transfected cells which overexpress angiogenic factors, like in the work of Geiger *et al.* in which mesenchymal stem cells (MSCs) transfected with VEGF plasmid, can provide significantly enhanced vascularization and osteogenesis [184] or the work of Yang *et al.* in which transfected MSCs improved heart function after myocardial infarction [185].

A key point in this growth factors strategies is not simply their production or release, but probably even more important is to control their dose. In fact, a high

level of growth factors in tissue might lead to vessel destabilization [186], endothelial hyperplasia [187] and even cancer development [188]. Therefore, to control the dose present on the material, their spatial localization and their stability, the focus of tissue engineering shifted to immobilization approaches in which growth factors (or derivatives) are covalently bonded to the scaffold and accessible to bind cells-receptors to trigger intracellular signals [189].

Successful vascularization was achieved using a group of well-known growth factors used to upregulate the endothelial cells signaling: vascular endothelial growth factor (VEGF), basic fibroblast growth factor (bFGF) and platelet-derived growth factor- β (PDGF- β) [35, 190-198].

VEGF is a family of homodimer glycoproteins which bind heparin, and the founding member of this family of polypeptides is named VEGF-A which present complex role both *in vitro* and *in vivo* for angiogenesis and vasculogenesis (Figure I. 40) [199, 200].

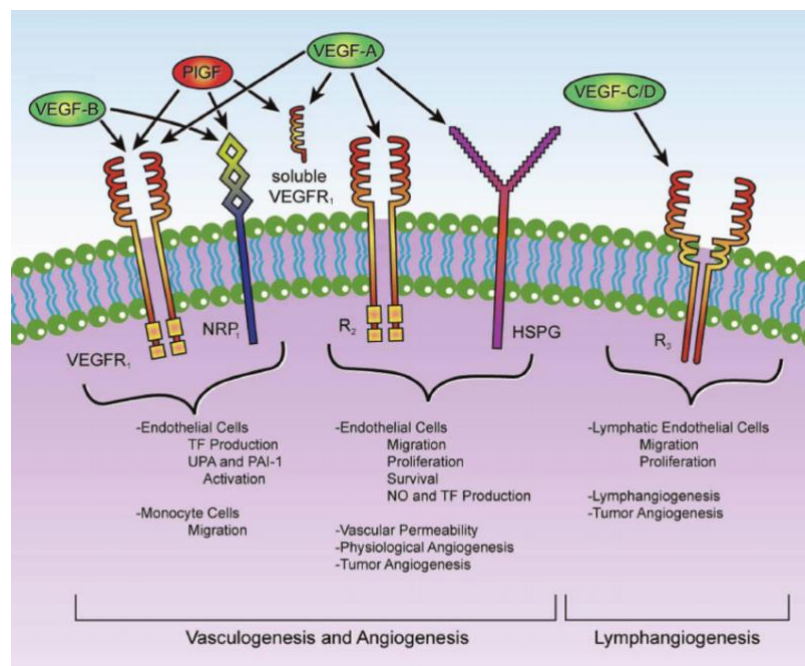


Figure I. 40 - Model of VEGF protein and receptor interaction: identifying the different classes of VEGF protein from A to D and of receptors from R1 to R3. From [201].

The gene encoding for VEGF-A is located in human on the chromosome 6 and encode for 8 exons [202] which undergoes different exon splicing, generating up to four different protein-variants: VEGF-A121, VEGF-A165, VEGF-A189 and VEGF-A209 [203]. Besides the type of spliced-variant of the VEGF-A protein, a key-role factor is a proper concentration to use within a body tissue to avoid hypertension, atherosclerotic plaque development [204], inappropriate vessels growth [205] and neovascularization in tumors [206]. In fact, the angiogenetic properties of this protein are strictly dependent on the dose applied in the tissue, and therefore the determination of the proper concentration to be used is crucial before applying it within engineered tissues [45]. In addition, this protein presents a short half-life (the time after which the protein is not functional anymore) and so, novel studies of encapsulation and controlled release have been examined [207].

During the process of angiogenesis, the concentration of the VEGF-A protein influences the rate and amount of new vessels development [208]. When the capillaries are formed, the migration of pericytes around the tubular structure is recognized as the synonym of vessel maturation, while the absence of pericytes often leads to capillary regression [209]. VEGF-A and pericytes cells work in collaboration to promote vessel remodeling and maturation, in fact, it was shown how the presence of pericytes in absence of VEGF-A do not prevent capillary vessels regression *in vivo* [210]. The mechanisms which drive the capillary vessels regression, as well as the EC shedding into the vessel lumen are unknown, however, there is a two-steps hypothesis: firstly, a quick cessation of blood flow and EC apoptosis with consequent destruction of the vessel wall, secondly, the degradation of the basement membrane [210]. Capillary vessels remodeling occurring within engineered tissues cannot be avoided either *in vitro* and *in vivo*. However, the capillary vessels regression can be prevented to obtain a functional scaffold that can benefit from the pre-vascularized network developed inside [45]. The VEGF protein is nowadays largely used in order to guide angiogenesis in bone tissue when combined with hydroxyapatite microspheres [211], or encapsulated into injectable cell macroaggregates [212], or again encapsulated into hydrogels [213].

FGF is a large protein family, composed of 23 members. The main actor for our studies is the FGF-2, which play an active role in angiogenesis [214]. Similarly to VEGF-A, also this factor, when overexpressed, is associated with dangerous side effects such as hyperplasia [215], atherosclerosis formation [216] and hypertension [217]. The half-life of FGF-2 is about 9 hours [218] and thus, development of controlled-release delivery systems is required for tissue engineering showing how slow-release system of FGF-2 in PLGA beads can improve up to 4 times the capillary penetration in rats [219]. FGF-2 has been also recently used to develop three-dimensional scaffolds to enhance skin regeneration and dermal neovascularization using a composite material of gelatin and silk fibroin [220] or to induce osteoblastic differentiation of bone marrow mesenchymal stem cells using up-regulated gene expression [211].

Platelet-derived growth factor- β was discovered back in 1974 when it was observed how the released material from platelets was able, alone, to induce cell growth of many cells which are serum-dependent [221, 222]. PDGF in human is normally a heterodimer of two subunits with related sequences, the two chains have been termed simply "A" and "B" [223]. In normal conditions, the human plasma contains a very low level of PDGF, and intravenous injection of it, is rapidly cleared from the body, indicating that the effect of this growth factor is most probably linked to a locally increased signal, then a systemic increase in the blood flow [224]. About its potential, PDGF is able to induce a cell migration of fibroblast and smooth muscle cells, through a chemotactic response [225, 226] This important property might be linked to the important role of wound healing process. It was also shown how PDGF is able to modulate cell growth in a direct way, by cellular-receptor binding, on specific cells sensitive to it such as chondrocytes, vascular smooth muscle cells, glial cells dermal and tendon fibroblasts [227]. In addition, PDGF works as potent vasoconstrictor showing a concentration-dependent mechanism of aorta contraction [228].

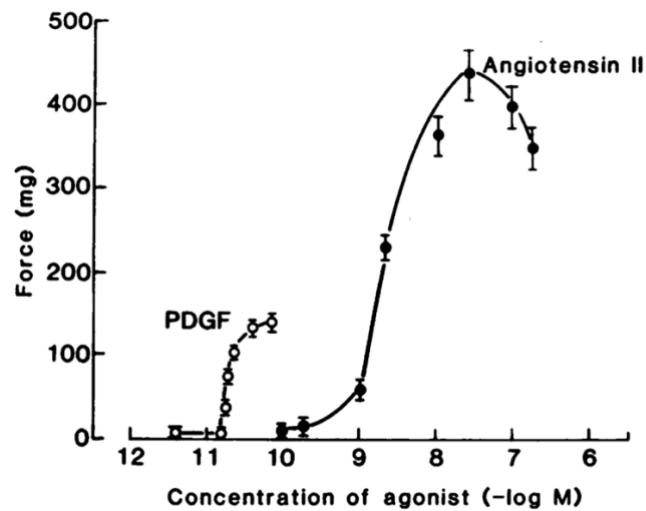


Figure I. 41 - Dose-response curve for PDGF and angiotensin-2 in aortic contraction: From [228]

4.4.2. Peptides

Even if the use of growth factors became a common approach to induce vascularization, some drawback has to be solved, such as the high instability and short active-life form *in vivo* [20]. This limitation requires several bolus injections over the time, to preserve the functionality of those expensive factors, resulting in inefficient approach [229].

Generally, the name of a peptide is indicated with the single-letter-code of the amino acid of which it is composed. The most well-known and largely used peptide sequence to improve cellular adhesion is a derivative from fibronectin, a protein which composes the extracellular matrix, and takes the name of "RGD" which represent the three mains amino-acids of the binding site of the protein: Arginine-Glycine-Aspartate (Arg-Gly-Asp for three-letter code or RGD for single-letter code)[152, 159, 166, 167, 230-235]. Cell adhesion is the process in which integrins form a cluster when bounded to both (which are intra-membrane cellular receptors)

the actin cytoskeleton of the cells (microfilament of cells) and proteins of the extracellular matrix [230].

In addition to cellular adhesion, as for RGD peptide, other sequences can be used to specifically target different cell functions, thanks to specific cell-receptor interaction, like in the case of "SVVYGLR" peptide. This sequence derived from osteopontin [236-238] and bind the integrins $\alpha 4\beta 1$ [239], $\alpha 4\beta 7$ [240], and $\alpha 9\beta 1$ [241]. It has been shown how this sequence has the potential to enhance endothelial cells adhesion, proliferation, migration, and tube formation both *in vitro* and *in vivo* [238, 241, 242] [243, 244]. Thanks to those characteristics of a potent angiogenic factor, this small peptide might be expected to stimulate angiogenesis when grafted on a surface.

Another more recent peptide sequence, to induce angiogenesis, is named "QK" peptide [245]. This peptide was designed to reproduce the vascular endothelial growth factor (VEGF) 17-25 helix region, which is responsible for the binding with the cell receptor (Figure I. 42). This peptide was developed *de novo* by mutagenesis of the sequence of amino acid, in order to find the best structural conformation which would provide stability maintaining its activity in terms of cell-receptor interaction and angiogenesis [245-248].

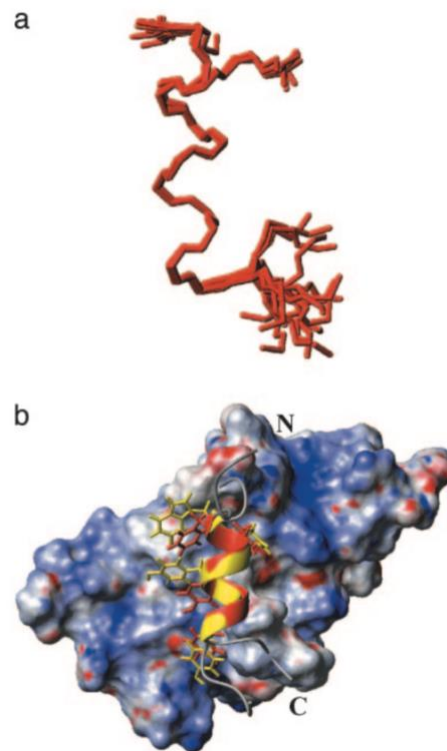


Figure I. 42 - Nuclear magnetic resonance of QK structure: (a) backbone representation of QK structure. (b) backbone superposition (yellow) with VEGF protein. Gently provided from [245]

It was shown how QK peptide, *in vitro*, is able to bind cell receptor-like KDR and Flt-1, which normally recognize and bind the complex VEGF protein [245] [246]. In addition, D'andrea proved how QK competes with VEGF for binding the endothelial cell's receptor, triggering the downstream intracellular signaling pathway such as ERK1/2 [245]. The novel peptide sequence was also tested *in vivo*, to ensure that the biological activity and the angiogenic potential was still triggered in animal models, comparable with the VEGF protein (Figure I. 43). Encouraging results indicate how QK peptide was able to increase capillaries density on the tibialis anterior muscle of rat model, accelerate healing by enhancing angiogenesis in the granulation tissues after wound formation and greater peripheral capillaries infiltration (Figure I. 43) [249].

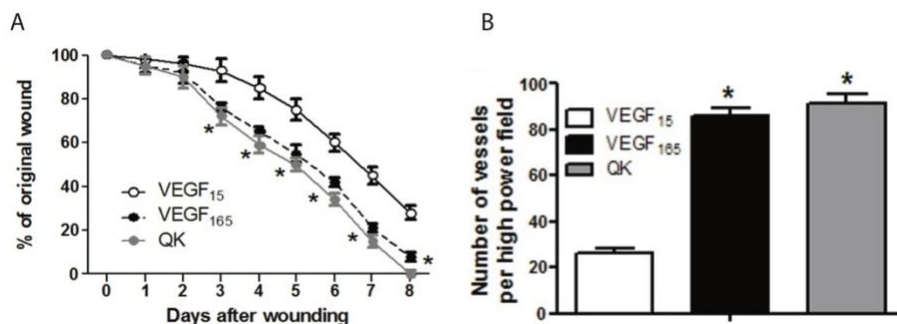


Figure 1. 43 – *In vivo* studies on QK peptide: (A) QK and VEGF165 accelerate the closure of wound in mice, compared to the negative control VEGF15. (B) Quantification of microvessels infiltrating Matrigel plugs. Adapted from [249].

4.5. Surface topography and micro patterning: advance mimicking of natural ECM

Scaffolds on tissue engineering provide primarily the needed three-dimensional structure specific for tissues, supporting tissues regeneration through adhesion, proliferation, cellular interaction, and communication [250]. Scaffolds can be fabricated using various techniques such as heat, light, and molding (or their combination) in order to develop a desired three-dimensional structure. Their design should be in all the three-dimensions, ranging from the centimeter to the micrometer sizes, in order to mimic not only the tissues features but also the micro-environment of the extracellular matrix (ECM) [250, 251]. Originally, micro-pattern technology was used for microelectronics industries, combining the knowledge of material science and surface chemistry, but nowadays those techniques can be applied in tissue engineering applications in order to mimic in a better way the ECM environment [252] [250].

4.5.1. Photolithography

Photolithography is a well-established method, largely used to fabricate semiconductors, which currently found useful applications in biomedical and tissue engineering fields for cells, proteins and peptides patterning [165-167, 253]. In brief, photolithography is used to transfer geometrical shape from a mask to a special surface, using exposition to light or ultraviolet wavelength (Figure I. 44) [254]. Firstly, a layer of photoresist is applied to the material surface (Figure I. 44). This photoresist is an organic solvent which has the characteristic to be sensitive to light exposition and thus change its characteristics and chemical bonding. Photoresists can be classified into two categories: positive and negative. Positive photoresists react positively to light exposition, breaking some chemical boundaries and becoming more soluble in the developer solution, a specific solution designed to wash away and remove the soluble form of the photoresists. In this case, photoresists positively exposed to light, are removed from the surface, generating a new pattern (Figure I. 44). Negative photoresists work in the opposite way, they react negatively to light exposure, becoming insoluble in the developer solution. This means that the photoresists exposed to light will not be removed by the developer solution, while all the rest of the photoresists will be efficiently washed away from the surface of the material [254]. Those newly developed patterns can now be used to specifically graft bioactive molecules with the desired spatial distribution (Figure I. 44). Regardless of the type of photoresist selected, the last step termed lift-off, involves the removal of the leftover of the photoresists, by dissolution in an organic solvent (Figure I. 44).

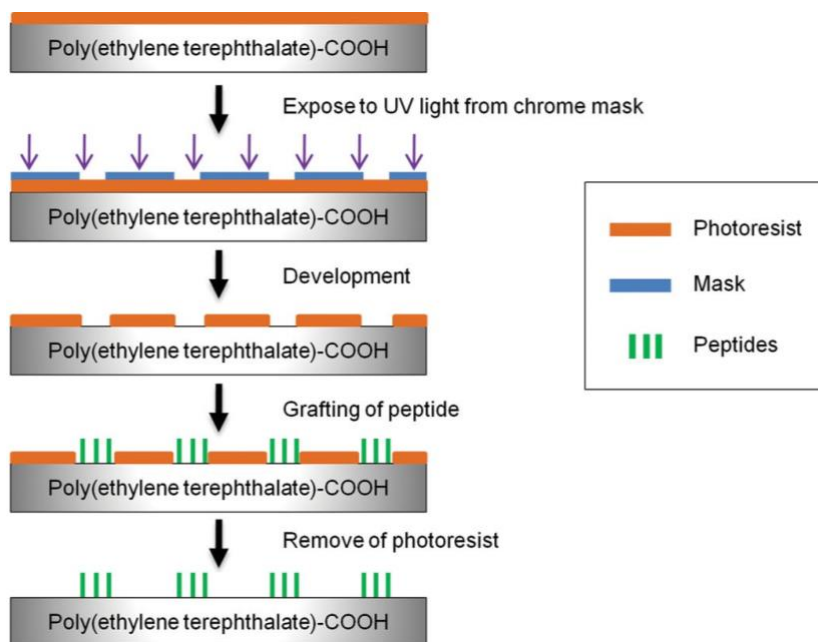


Figure I. 44 – Photolithography for peptides immobilization: (a) Schematic of photolithography approach to immobilize peptides on a polymeric substrate. First polymer is covered by photoresist and then exposed to light through a mask with a specific pattern. Then after the pattern transfer, peptides are grafted where the light remove the photoresist, and finally the leftover of the photoresist is removed, leaving immobilized peptides in a pattern-design. Gently provided by [167].

Possible applications in tissue engineering of this technique were investigated by several groups of research using different biomolecules and cells, such as the work of Moon *et al.* in which PEG-RGDs was patterned on poly(ethylene glycol)-diacrylate (PEGDA) hydrogels [253]. Endothelial cells, in this case, were seeded on the materials with a different linear pattern from 50 μm to 200 μm width (Figure I. 45). It was shown how ECs were able to develop capillary-like structure only in the smaller pattern-type while the larger show a continuous monolayer of spread cells (Figure I. 45). As well as the pattern condition, also biomolecules concentration play an important role. In the same work, researchers investigate RGD peptide concentrations ranging from $<10 \mu\text{g}/\text{cm}^2$ up to $>100 \mu\text{g}/\text{cm}^2$. They proved how lower concentration is not sufficient to reproduce the tubular-like structures as well as the

higher peptide concentration, only an intermediate concentration of about $20 \mu\text{g}/\text{cm}^2$ was able to reproduce tubular structures in the patterned material [253].

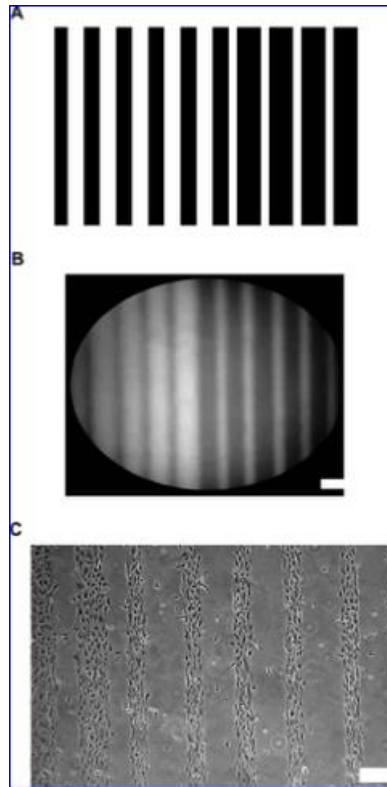


Figure 1. 45 – Development of pattern-line on PEGDA hydrogels: designed strips (A) from 50 to 200 μm . (B) Fluorescence image of pattern on the hydrogel and (C) HUVECs adhesion on such patterns. Scale bars = 200 μm . From [253]

Photolithography technique has a great potential for micro-patterning but it shows some limitations and drawbacks, such as the incompatibility to develop three-dimensional structures, or a poor patterning on a not-planar surface and last the organic solvents used to remove the photoresist, typically acetone can be harmful to proteins [255].

4.5.2. Soft lithography

To improve the micro-fabrication process, several non-photolithographic techniques have been developed to create high-quality micro- and nanostructures [256]. Those techniques are generally termed soft-lithography since each of them involve an elastomeric stamp or mold where the pattern is transferred. The main techniques under the definition of soft-lithography are the following: microcontact printing, replica molding, micro-transfer molding, micro molding in capillaries and solvent-assisted micro molding [256]. Those techniques collectively are cheap to process and simple to perform with a high reproducibility. In this session, among the possible soft lithography techniques, we will focus on the microcontact printing technique which allows reproducing three-dimensional structures.

4.5.3. Hot embossing

Hot embossing is a simple and highly reproducible process in which a polymeric material can be molded according to an initial master (most of the time made *in silicon*). Firstly, the design of the microstructure of the master is performed using photolithography. Then silicon can be used directly as an embossing tool reducing the cost of material production (no intermediate steps required), high reproducibility and aspect ratio in the developed structures and the possibility to deep dry etch the material [257, 258]. After the master preparation, the silicon master is mounted in the embossing machine and a combination of pressure and temperature will be applied to reach the temperature above the glass transition temperature of the selected polymer in order to penetrate within the master, into the polymer, to transfer the pattern shape. At the end of the process, when the pressure is still applied on the polymeric material, the temperature is decreased below the glass transition to allow the stabilization of the microstructure of the material, before the master removal [258].

Hot embossing is a promising process to transfer micro- or nanostructures pattern from a master mold onto a polymeric substrate with high precision and

quality features (Figure I. 46). This technology was developed more than 40 years ago and has been used for research applications, as well as industrial production. [259].

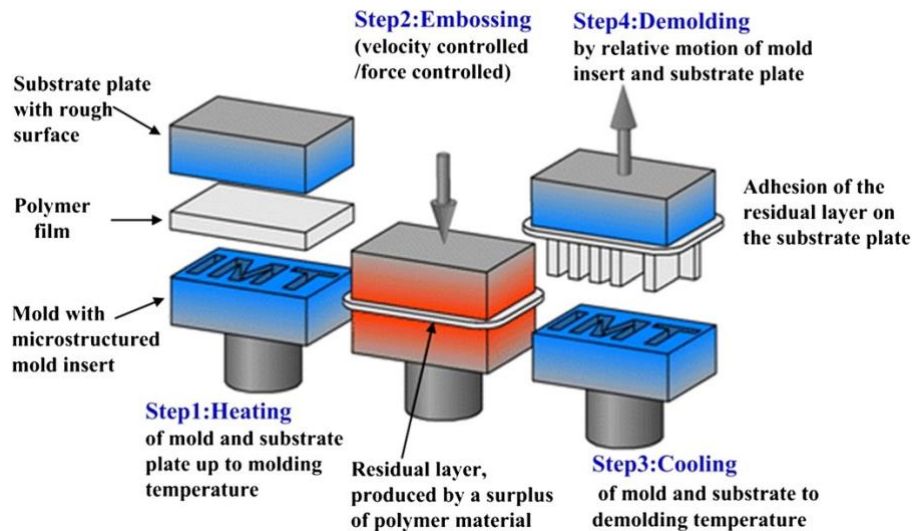


Figure I. 46 – Hot-embossing process: Schematic representation of an hot-embossing process which detailed the four main steps involved: the heating, the molding or embossing, the cooling, and the demolding. Reused from [260].

Four main steps characterize the hot embossing process (Figure I. 46):

Heating the mold and the substrate up to the molding temperature (usually close to the glass transition temperature of the polymer).

Embossing the microstructure patterns using pressure at the molding temperature.

Cooling the mold and the substrate to the demolding temperature, without releasing the pressure applied.

Demolding the component by opening the tools and removing the polymer from the mold.

During the process, two deformation stages occur: the first one is a stress concentration and strain hardening during heating and embossing steps. The second one is the stress relaxation and deformation recovery during the cooling and demolding steps. The main parameters for the hot embossing are the glass

transitions temperature (T_g), the pressure applied and the holding time (during embossing) [259].

Depending on the polymer used for the process, different sizes were exploited ranging from 6 mm down to 0.02 μm , as summarized by this review [259]. In addition, a wide variety of feature geometries were created and tested such as cuboids, channels, cavities, pyramid arrays, microlenses, pin arrays, and other more [259].

Table I. 1 - Summary of features, sizes and polymers used for hot embossing process: References per each work can be found on the work of Peng L. *et al.* [259]. PMMA = polymethyl-methacrylate, PC = polycarbonate, PS = polystyrene, COC = cyclic-olefin-copolymer, PVC = Polyvinyl chloride.

Feature geometry	Lateral (μm)	Height (μm)	Aspect ratio	Materials
Cuboids	0.5 and 20	1 and 25	2 and 1.25	PVC and PS
Channels	70	40	0.57	PMMA
Cavities	0.071–0.98	0.296	0.30–4.17	PMMA
Channels	50	30	0.60	PMMA
Line features	100	71	0.71	PMMA
Pyramid arrays	50	35.3	0.71	PMMA
Channels	100	37	0.37	COC
Channels	100	100	1.00	PMMA
Channels	100	50	0.50	PMMA
Channels	50	100	2.00	COC
Pyramids	100–530	260	0.49–2.60	PMMA
Microlens	150	35.88	0.24	PC
Nano-columns	0.1	0.26	2.60	PC
Microlens	150	25.15	0.17	PC
Line features	1.6	1	0.63	PS
Microlens	145	10.8	0.07	PC
Pin array	0.11	0.37	3.7	PMMA
Nano-columns	0.48	4.7	9.79	PMMA

Saha, Biswajit *et al.* developed complex micro-capillaries size using hot-embossing process in polymethyl-methacrylate (PMMA). They were capable to transfer the pattern from a silicon mold to PMMA material using the combination of the high temperature of the 130°C and constant force of 25 mN (Figure I. 47).

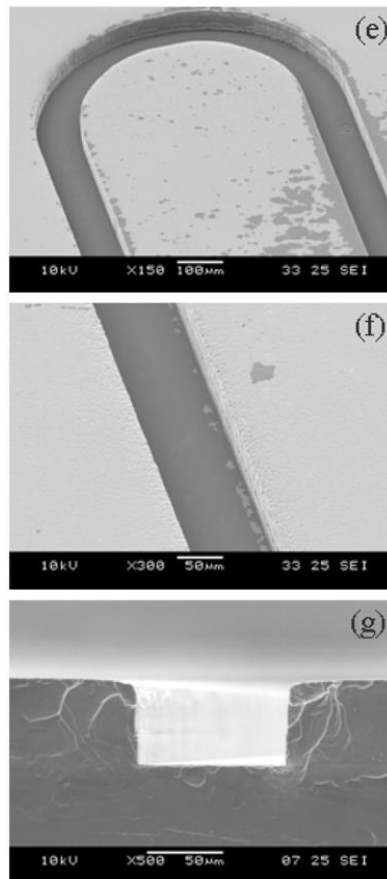


Figure I. 47 - SEM images of micro-channels molded on PMMA:(e) curve region, (f) straight region, and (g) cross-section of the micro-channel. From [261].

4.6. Vascular tissue engineering approached

Collecting all those precious details and knowledge about cell type, material properties, and growth factor potential is possible to combine the different expertise

to develop an engineered tissue with a desired pre-vascularized network within it. In order to develop this tissue, two main approaches are used:

-*In vivo* approach. The first approach involves a preliminary implantation under the skin of the patient, to induce the ingrowth of the capillaries. After some weeks, the pre-vascularized scaffold is surgically removed to be newly implanted in the desired region. This implies a double surgery procedure which carries pain, morbidity, and possibility to develop infections.

-*In vitro* approach. The second approach consists in the formation of CVN using in-vitro techniques to guide endothelial cells through the development of this network. This approach is more challenging since we need to mimic the complex signals and environment existing *in vivo*.

4.6.1. *In vivo* approach

Two techniques are used *in vivo* to create new vascular network into the implanted scaffold.

The first one termed extrinsic vascularization consists in the development of a micro-circulatory system through the capillaries ingrowth of the surrounding tissue in the host [35] [45, 262, 263]. In the human body, this process occurs every time there is an avascular region in physiological, pathological or surgical situations [45, 264]. The technique involves the initial implantation of the scaffold (without cells seeded) into highly vascularized tissues on the host, such as intermuscular tissue [265], adipose tissue, kidney capsule and subdermal areas [219, 266-273]. This first implantation, into an ectopic position of the host, will induce a *de novo* vascularization mediated by the host vessels which would migrate and infiltrate through the scaffold to build this vascular network [274-276].

Due to a slow capillaries ingrowth, a delay normally occurs between the implantation time and the full perfusion of oxygen and nutrients within the scaffold, resulting in inadequate for thick engineered construct larger than 3 mm [45]. It was proved that capillary ingrowth into an engineered tissue via extrinsic vascularization takes up to several weeks and depends on the size of the construct, leaving cells in

hypoxic conditions for several days if dimensions are larger than $400 \mu\text{m}^3$ [35] [277]. The nowadays technology integration depends initially on the diffusion, and later on extrinsic vascularization making impossible to avoid fibro-vascular ingrowth and formation of scar tissue. In addition, once the extrinsic vascularization is complete, the scaffold is surgically removed from the patient and newly implanted into the required target site. This triple-surgery requirement is the biggest drawback of this approach which would cause pain and morbidity to the patient [262] [177].

The second one, termed intrinsic vascularization, uses a similar approach as the extrinsic one, but exploit the intrinsic potential of a blood vessel to sprout and create new capillaries network [10, 262] [278, 279]. This approach can be divided into three phases:

- First, joint of a macrovascular component with a scaffold
- Second, implantation of the scaffold within an ectopic body part and surgically anastomosis
- Third, extraction of the vascularized scaffold and implantation in the region of interest

The most used macrovascular component for this type of approach, in order to generate intrinsic vascularization, is named arteriovenous loop (AVL) [280] [10]. In this case, an artery and a vein are connected together via a pedicle (which can be an autologous vein or another synthetic substitute) to create a loop in the blood flow, and placed inside a protected silicon chamber. This loop presents interesting characteristics of increased shear stress and wall tension due to blood perfusion of the host when the micro-surgical anastomosis is performed during the first implantation [280] [281]. Those characteristics induce a spontaneous formation of angiogenic sprouts from the pedicle which allow the formation of a capillary network both inside the silicon chamber and in the surrounding tissue. This preliminary network has been proven to remodel with the time to create arterioles, postcapillary venules and venules [279]. Similarly to the extrinsic vascularization approach, at least three surgeries are also required in this case. The first one would implant the scaffold in an ectopic region of the host, rich in vasculature where the surgical anastomosis can be performed. Once the scaffold would be vascularized

thanks to intrinsic vascularization process, a second surgery is needed to remove the implanted scaffold, while the third one would be needed to finally implant the scaffold in the designed region of interest [280].

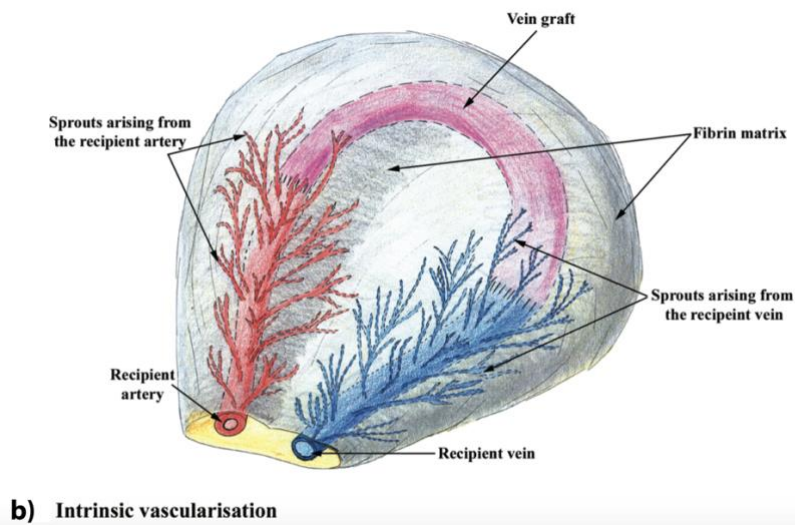
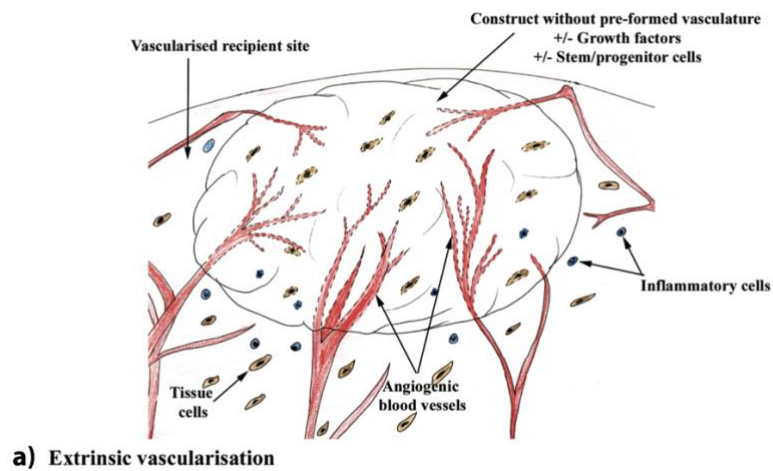


Figure 1. 48 – Extrinsic and intrinsic vascularization models: Schematic representation of (b) Extrinsic Vascularization and (c) Intrinsic vascularization used for TE pre-vascularization approach. From [45].

This method was largely used and investigated using different tissue materials [282-284], using artificial ECM such as Matrigel, collagen, gelatin, fibronectin and fibrin [20, 279, 285, 286] or even in the absence of additional ECM [278].

Despite the high potential of AVL method, the concerns related to multiple surgeries make this technique more complex and problematic.

4.6.2. *In vitro* approach

The efficient, rapid and sufficient vascularization for the large tissues and biomaterials remain the main obstacle for the wide implementation of TE into clinical practices. Even if nowadays is possible to vascularize some constructs by stimulation ingrowth of the host's vasculature, these approaches showed a slow development and a laborious surgical process [280]. The research field is trying to investigate in parallel another approach which is the pre-vascularization which aims to induce the formation of a sufficient vasculature within the engineered tissues before its implantation into the host. Such engineered tissue should allow the connection to the host's vasculature at the moment of the implant and provide an immediate perfusion through all the scaffold. However, the development of such functional vascular tree with hierarchical structures remains a long-lasting challenge [280].

Pre-vascularization *in vitro* consists in the seeding of endothelial cells (alone or with other vascular supportive cells) into a scaffold or gels before the implantation *in vivo*, in order to recreate a three-dimensional vascular network [10]. Human umbilical vein endothelial cells (HUVECs) are commonly used as a cell source to develop capillary-like structures [287]. This approach is a successful strategy to facilitate the survival of cells into engineered constructs after *in vivo* implantation. The efficiency of this approach does not only depend on the formation of capillary-like structures but also involves the functional join between the capillaries into the scaffold and one of the patients, a process called anastomosis or inosculation [10]. After the implantation, due to the formation of a wound to implant the material, oxygen and nutrients which are contained in the blood will diffuse into the scaffold as the initial step. Within 48h after the surgery, a close alignment and joining of capillaries of the graft with the patient's one occurs, facilitating blood perfusion. Later on, the blood flow is consolidated by extrinsic vascularization, the angiogenic

ingrowth of the patient's capillaries into the implanted scaffold. An example of the potential of this technique is provided by Trembley et al. in which they developed an endothelial-reconstructed skin with capillary-like structures, which after implantation in nude mice, anastomose after only 4 days, compared to the 14-days period to achieve a similar result without a pre-vascularized network structure [274]. The main drawback of the *in vitro* approach is the impossibility to surgically connect the small capillary network of the pre-vascularized scaffold, to the host vasculature, slowing down the perfusion of the nutrients and oxygen after implantation [20]. The possible strategies to induce the formation of a capillary network into a scaffold broad from the use of special cells type, to the use of small molecules such as growth factors, cytokines or the immobilization of molecules such as proteins or peptides.

4.6.3. Micro engineering technique: the use of micro scale pattern or structures

Development of a stable vascular network, with a designed pattern which can be integrated into engineered tissues, is of significant interest. In fact, endothelial cells cultured without a designed pattern will grow according to a random architecture, making more complex to integrate this network with the designed tissue of interest [65].

The highly structured microenvironment made of ECM guide and influence cells under a lot of aspects such as adhesion, morphology, and mechanical stimuli [288]. The cellular adhesion is driven by receptor-ligand interaction, which transfers the localized signal to the cytoskeleton of the cells, changing its entire architecture [289-291]. Those particular conditions differ largely from the culture-conditions in a petri dish and even if those artificial conditions can be practical for cell expansion, they would not mimic the more complex microstructure present in complex tissues. This leads to the development of new strategies and techniques to recreate a micro-scale environment which could lead cells into the desired fate [288]. Micro-patterning methods are now becoming more popular in the field of tissue engineering and biomedicine and three-dimensional micropatterning mimic better the physiological

environment than two-dimensional micropatterning, because cell behaves differently in those two conditions [292, 293].

II. Objectives and strategy

Tissue engineering is an emerging field with a great potential for the therapeutic goal of tissues and organs regeneration [294, 295]. The combined work of scientists, engineers, and physicians enable the development of very complex, sophisticated and innovative products, which can be implanted into the patients to heal the damaged tissue or replace some of their functions [296]. However, the enormous technological progress of materials, techniques, and analysis face the biological limitations of long cell culture time, reduced cell-source availability and especially low (or even absent) oxygen-nutrients perfusion. Especially, this last limitation impairs enormously the fabrication of large tissues or organs since the cells which compose those tissue/organ depend primarily on the proper level of oxygen and nutrient to accurately reproduce the physiological condition of such tissues/organs [297-299]. A particular tissue in which the interaction of blood vessels is exceptionally important is the bone tissue. In fact, inside the bone marrow, the blood-components are produced and have to be introduced immediately in the vascular system. Therefore it exists a close spatial relationship between the two tissues with a continuous interaction and remodeling to ensure a perfect function over the lifespan of the human being [19, 300].

In this context, the present Ph.D. research work focuses on an innovative approach to develop tubular-like capillaries micro-vessels using a combination of cellular component, biochemical factors, natural polysaccharides, and three-dimensional patterns. The overall goal is to guide human umbilical vein endothelial cells (HUVECs) to develop capillary vessels into a specific pattern structure in order to improve the basic knowledge about capillary development for future clinical applications such as the development of large pre-vascularized bone scaffolds.

HUVECs have been largely investigated for development of large vascular tissues, as well as basic studies of angiogenesis in 2D conditions or encapsulated into hydrogels [10, 301]. Nevertheless, there is no emerging definitive solution ready to be used at the clinic, and our study will investigate the potential of a novel approach aiming at developing capillaries with the smallest possible size.

The research work detailed in this thesis manuscript aims to determine the specific impact that polyelectrolytes, peptides, and geometrical cues can have on

HUVECs for the development of capillary vessels. In order to minimize the variable present in this work, a defined culture media without supplemented factors was chosen. This choice would prove how only the tested conditions can lead to the development of capillaries structures, without the influence of supplemented factors. Specifically, the effect of the surface's functionalization with hyaluronic acid (HA) and chitosan (CH), the impact of the adhesive peptide (RGD) and angiogenic peptides (SVV, QK) and the three-dimensional pattern of micro-channels on the HUVECs adhesion and tubulogenesis was investigated. We hypothesized that the interaction between the HUVECs with the surrounding artificial extracellular matrix (ECM) combined to the potency of peptides in the three-dimensional space would be sufficient to guide those cells into the development of capillary vessels.

1. Objective #1: Fabrication of PC microchannels

The first objective of this work is the development of a stable three-dimensional network. The native structure of capillary vessels is a tubular geometry ranging from 10 to 15 μm with the empty lumen in the middle.

In the present work micro-channels (μCh) with the width in the range of 25 μm were developed, and cells were seeded and grown to develop tubular-like structures. The fabrication technique must be reproducible, easy to perform, rapid and allow the fabrication of relatively large scale sample. Among the potential micro-fabrication techniques, hot-embossing was chosen which is a template-based fabrication that involves a mold *in silicon* (SiM) containing line-pattern that are transferred to PC using a combination of pressure and temperature to develop μCh . The characterization of the patterned structures is performed using scanning electron microscopy (SEM) and profilometry to determine the dimensions of the pattern features.

2. Objective #2: Biofunctionalization

The second objective of this study is to functionalize the supporting material using natural polysaccharides. The supporting substrate should present a surface's charge, it should be transparent to facilitate cell observations, it should be molded in a fast, accurate and reproducible manner, and it should be cheap and available without limits in the production. As it presents all these characteristics, polycarbonate (PC) appeared as a very good candidate's material and was therefore selected as supporting material. In addition to its peculiar characteristics, the current studies were possible thanks to a collaboration with it4ip, a company expert on the development of PC films and membranes with the defined thickness. PC surface can be functionalized thanks to its negative net charge on the surface and it is compatible with a number of common microfabrication techniques such as hot embossing.

Our second objective includes two parts. The first one consists of the deposition of natural polysaccharides using the layer-by-layer (LbL) deposition approach, in order to develop a homogeneous 'cushion' on the PC surface, aiming at improving cellular adhesion and biorecognition. Biorecognition is possible thanks to the interactions between cell's receptors and the binding motifs present in natural polysaccharides like hyaluronic acid (HA) and chitosan (CHI). In addition to this, with the LbL approach, the thickness of the final cushion can be finely controlled depending on the number of deposited bilayers, as well as the degree of crosslinking performed. The final crosslinking density, in fact, influences not only the stability of the LbL cushion but also its mechanical properties, which can be tuned to properly mimic a more suitable substrate for endothelial cells to grow, proliferate and develop tube-like structures.

The second part of this first specific objective is the immobilization of bioactive molecules onto and into the LbL cushion. Two type of peptides; the cell-adhesive sequence arginine-glycine-aspartic acid (RGD) and two angiogenic sequences known as SVV and QK were chosen for this work. The RGD sequence is globally known to have a potent effect on improving cellular adhesion on material thanks to the presence of an integrin-binding-site in its sequence. HUVECs cells present the

integrin receptors on the surface of the cells' surface and therefore the binding between the integrin receptor with the RGD binding-motif would trigger an intracellular signaling that leads to adhesion of the cells. SVV peptide is known to contain the binding-site of osteopontin protein, and it was already demonstrated how the presence of this peptide immobilized on the surface of a material can induce the development of capillary vessels, especially in bone tissues where osteopontin normally is highly expressed. The last peptide, QK, was designed to mimic the binding site of the more complex Vascular endothelial growth factor (VEGF). This protein is known as a potent angiogenic factor and is currently used in a lot of studies to induce pre-vascularization into engineered constructs.

Regardless of the peptide sequence, all of them share some common characteristics, such as the presence of a terminal amino group, that can be used as the functional group to perform the immobilization of the peptides on the material surface. 1-Ethyl-3-(3-dimethylaminopropyl)carbodiimide (EDC) and N-hydroxysulfosuccinimide (sulfo-NHS) was used in order to activate the carboxylic groups present on the HA, and later let them react with the amino group present on the peptide to form a covalent amide bond. Surface characterization at this step was performed using ellipsometry, fluorescence microscopy, and confocal microscopy.

Last, a preliminary study with HUVECs is performed to check the difference in metabolic activity between the different samples' conditions combining two assays: XTT test for metabolic activity and PicoGreen test to quantify the DNA content of each sample.

3. Objective #3: Capillaries development

The third specific objective of this work is the guidance of HUVECs through the development of capillary vessels. Once the objectives #1 and #2 are achieved the biological studies with HUVECs are performed. Functionalizing the micro-channels, with LbL and peptides combination, is fundamental to provide simultaneously a three-dimensional microenvironment and a rich cell-matrix environment where endothelial cells can recreate capillary vessels structures.

PC microchannels substrates presenting three types of surface chemistry were chosen for the biological investigations: Polycarbonate functionalized only with HA/CHI layer-by-layer (abbreviated PC-LbL), PC bio-functionalized with HA/CHI LbL layer-by-layer onto which adhesive RGD peptide and angiogenic peptide SVV were covalently grafted (abbreviated PC-LbL-RGD+SVV), and polycarbonate bio-functionalized with HA-CHI LbL onto which adhesive RGD peptide and angiogenic peptide QK were covalently grafted (abbreviated PC-LbL-RGD+QK).

Cellular morphology inside the μ Ch was observed using confocal laser scanning microscopy (CLSM) in order to have a complete acquisition of the whole three-dimensional structure of HUVECs to determine the formation, or not, of tubular-like structures. The images were then elaborated with IMARIS software in order to reconstruct the three-dimensional acquisition and identify the presence of the lumen in the tubular structures.

The material's surface characteristics were investigated in order to evaluate which material would lead to a faster development of tubular-like structure and which would stabilize for longer such structure over the time. Investigations were performed following the evolution of HUVECs at different time-points to answer those questions.

4. Objective #4: Capillaries stabilization

The last fundamental objective of this work is the stabilization (and maturation) of the newly developed capillaries using a second cell line, like human pericytes derived from placenta (hPC-PL). Pericytes were selected according to their nature capability to stabilize capillary vessels *in vivo* in the human body, and therefore the co-culture composed of HUVECs and hPC-PL would better mimic the proper conditions also *in vitro*.

HUVECs morphology and hPC-PL localization inside the micro-channels were investigated using confocal laser scanning microscopy (CLSM). In specific, capillary structure and lumen formation were followed as in the objective 3 of this chapter, to determine the formation over the time using Fiji software and IMARIS software.

Later, once the capillary structures were formed, hPC-PL were seeded together with the HUVECs and followed for a longer time.

The material condition PC- μ Ch-RGD+SVV was chosen, with HUVECs:hPC-PL ratio of 2:1 and separate time for the seeding approach: first seeding HUVECs and after 2 hours seeding of hPC-PL.

5. Strategy and approach

In order to achieve these objectives, we established the following strategy. The most suitable method of biofunctionalization of the polycarbonate substrates was first selected. One important requirement was to choose a quite universal technique that could easily be transferred for the biofunctionalization of other substrates, more adequate for bone tissue engineering transplant. PC substrate used in the present work is therefore only a model template for evaluating the potential of our innovative approach in developing small capillary vessels. A versatile technique which presents the potential to be used on several substrates is the so-called polyelectrolyte layer-by-layer (LbL) deposition. Here, two naturally-derived polyelectrolytes with opposite charges were chosen in order to interact with each other and build up the LbL cushion. Hyaluronic acid (HA) was chosen as anionic polyelectrolyte according to its ubiquitous presence as a component of the ECM and its negative net charge at the desired pH thanks to the carboxylic group in its sequence. The second polyelectrolyte chosen is Chitosan (CHI) for its biocompatibility and because it presents a positive net charge at the pH used for the build-up of the LbL layer, thanks to the presence of amino groups in its structure. Once the HA/CHI LbL film reached the desired thickness, a stabilizing step is performed using carbodiimide chemistry with EDC/sulfo-NHS in order to crosslink the LbL film using the amino and carboxylic groups of CHI and HA, respectively.

After the LbL coating of the PC substrate, a further biofunctionalization is performed using small biomolecules to promote cell-material integration. The small molecules used in this work are peptides with precise sequences and defined structures which mimic larger proteins, without instability and denaturation

drawbacks. Regarding the immobilization of the peptides onto the HA/CH layers, we chose an already well-known protocol using carbodiimide chemistry allowing to form covalent bonds between amino and carboxylic groups, and therefore forming a stable immobilization of the peptides on the materials' surface. The type of peptide chosen falls into two categories: adhesive peptide or angiogenic peptide. The Arginine-Glycine-Aspartic acid (RGD) peptide sequence was chosen for our preliminary studies, as it is a peptide sequence found on many extracellular matrix proteins, such as fibronectin, vitronectin, and osteopontin. RGD is the specific region on those proteins and is recognized by integrins to facilitate cell-material interaction. RGD sequence has been largely investigated to improve cellular adhesion using several types of cells combined with several types of materials, and in our work, the Penta-sequence GRGDS was used [167]. Additionally, the mimetic peptide of osteopontin is chosen according to its angiogenic potential. The used sequence is composed of nine amino acids GDSVVYGLR since it was already successfully investigated in angiogenetic studies with HUVECs [166]. Last, mimetic peptide of vascular endothelial growth factor (VEGF) is used. VEGF is the most known and used protein for angiogenetic studies both *in vitro* and *in vivo*, and its active binding site for cellular receptor has been replicated into the 15-aa sequence KLTWQELYQLKYKGI. This sequence mimics the same angiogenic potential of the complex VEGF exploiting another mechanism of activation [248].

The second step was the selection of the micro-fabrication method in order to develop μ Ch. The pattern should be sufficiently large to allow HUVECs cells to grow inside, but not too large to lose the micro-environment of a natural capillary structure which ranges between 10 and 15 μ m. In addition, the μ Chs should be developed uniformly on a large-area surface without consuming a significant amount of time. Considering the characteristics of the polycarbonate material such as the glass transition temperature of 150°C, hot-embossing method was selected since satisfies all the requirements in terms of large patterning area and fast imprinting time. The hot embossing technique and protocols were initially investigated using larger micro-channel width and spacing, to conclude on a smaller pattern, closer to the final sizes of a capillary vessel but not too small to constrict the cells in terms of

migration and morphology change. Once the channels are fabricated, the biofunctionalization approach is performed using both LbL and immobilized peptides. After that, the LbL film is removed in the space between two channels using a metal blade, In order to avoid as much as possible cell adhesion outside the microchannels.

Then, the strategy for carrying out cell culture consists of the seeding on HUVECs cells using a centrifugation approach to collect the totality of cells at the bottom of the μ Ch. The used media is free from fetal bovine serum (FBS) and other growth/angiogenic factors in order to evaluate uniquely the effect of geometry and biofunctionalization on capillary vessel development. The culture is followed by confocal laser scanning microscopy (CLSM) at early time-points from 1h until 5h after HUVECs seeding with acquisition time each hour.

Last, co-culture with HUVECs and hPC-PL is performed to follow the improved stability of the capillary vessels structures inside the micro-channels biofunctionalized material. Also, in this case, the media used for the study is free of FBS and other growth/angiogenic factors. The culture is followed firstly seeding HUVECs during 2 hours, and later seeding hPC-PL in $\frac{1}{2}$ of the HUVECs concentration, and investigated with CLSM during two more hours.

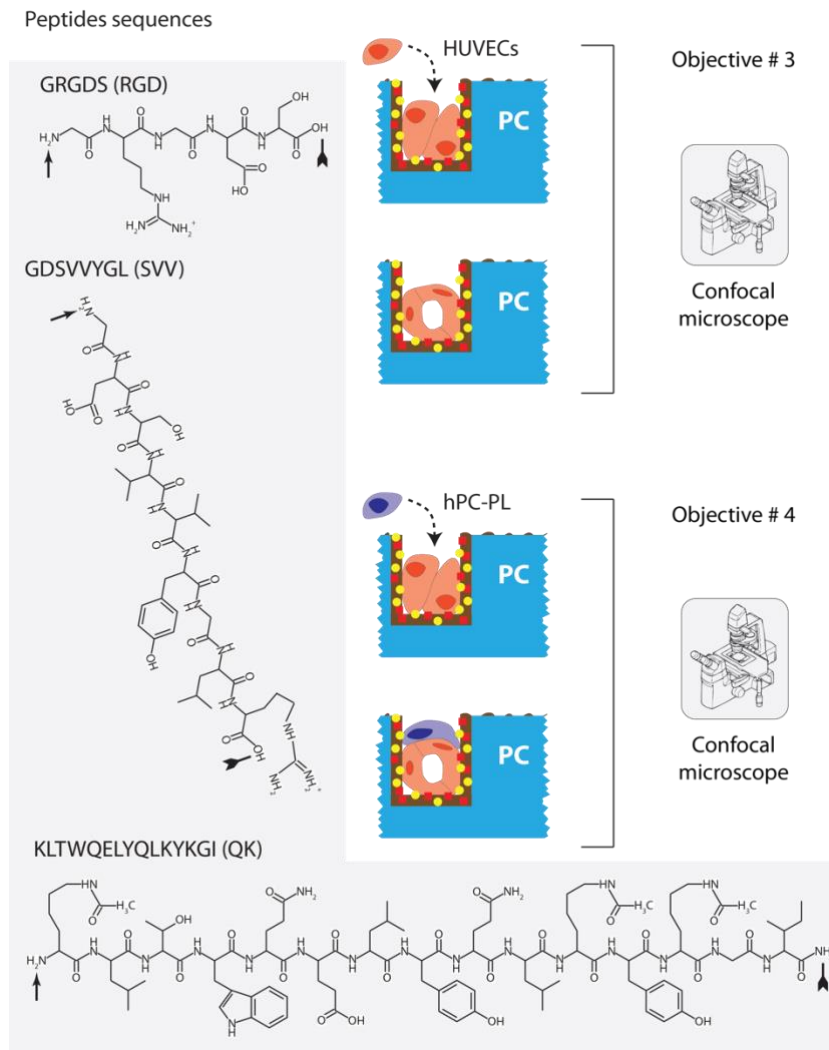


Figure II. 1 – The objectives of my work: Schematic summary of the steps used to achieve each objective of my work. First, biofunctionalization with polysaccharides and peptides is performed and characterized with ellipsometry and fluorospectrometry (Objective #1). Second, 3D-micro pattern is developed and functionalized and further characterized with scanning electron microscopy, profilometry and fluorescence microscopy (objective #2). HUVECs are seeded into the developed micro-channels to develop capillary-like structures; characterized with confocal laser scanner microscopy (CLSM) (objective #3). hPC-PL are seeded to stabilize the tube-like structure; HUVECs morphology and hPC-PL localization inside the micro-channels are investigated using CLSM (objective #4).

III. Materials and Methods

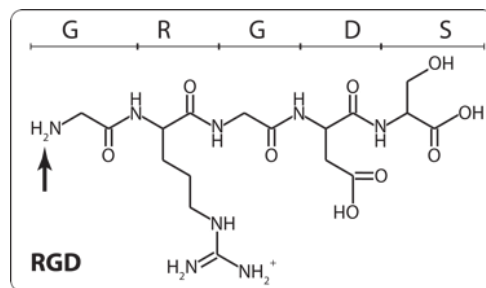
1. Materials

Polycarbonate (PC) films of 50 μm thickness were gently provided by it4ip, Belgium. Polyethyleneimine (PEI) with 25 kDa molecular weight was purchased from Aldrich (408727-100ML). Chitosan (CHI) with 50-150 kDa molecular weight was purchased from NovaMatrix with a deacetylation degree of >90%w (BP-08016-02, CL-114). Hyaluronic acid (HA) with 151-300 kDa molecular weight was purchased from Lifecore Biomedical (025841, HA200K-5). N-(3-Dimethylaminopropyl)-N'-ethylcarbodiimide hydrochloride (EDC), N-Hydroxysulfosuccinimide sodium salt (Sulfo-NHS), 4-(2-Hydroxyethyl)piperazine-1-ethanesulfonic acid (HEPES), fluor-shield 4',6-diamidino-2-phenylindole (DAPI), Cell Proliferation Kit II (XTT), Poly(2-hydroxyethyl methacrylate) (poly-HEMA), Rhodamine red, Sodium hydroxide (NaOH), and Hydrochloric acid (HCl) were purchased from Sigma-Aldrich (E7750-5G, 56485-1G, H3375-500G, F6057-20ML, 11465015001, P3932-10G, 83689-1G, S8045, and H1758 respectively). Sodium chloride (NaCl) was purchased from Fisher scientific (10428420-1KG). Fetal bovine serum (FBS), Trypsin-EDTA, Quant-iT™ PicoGreen™ dsDNA Assay Kit, CMTPX cell tracker, CMFDA cell tracker, and AlexaFluor-Phalloidin-564 were purchased from Thermo Fischer scientific (10500064, 25200072, P11496, C34552, C2925, and A22283 respectively). β -(N-Morpholino)ethanesulfonic acid (MES) was purchased from ACROS (32776-1000). Polycarbonate in powder was purchased from Lexan, General Electric (145). Ethanol 96%, 2-propanol, and acetone were purchased from VWR (83804.360, 20842.367 and 20066.365 respectively). Peptides were purchased from Genecust, with personal customize sequences: GRGDS (refer from now on as "RGD"), GDSVVYGLR (refer from now on as "SVV"), Ac-KLTWQELYQLK(Ac)YK(Ac)GI-amide (refer from now on as "QK"), GRGDSK-Fluorescein 5-isothiocyanate (refer from now on as "RGD-FITC"), GDSVVYGLRK-Fluorescein 5-isothiocyanate (refer from now on as "SVV-FITC"), and Ac-KLTWQELYQLK(Ac)YK(Ac)GIK-Fluorescein 5-isothiocyanate (refer from now on as "QK-FITC"). Human umbilical vein endothelial cells (HUVECs), human pericytes derived from placental (hPC-PL), endothelial basal medium 2 (EBM-2) with

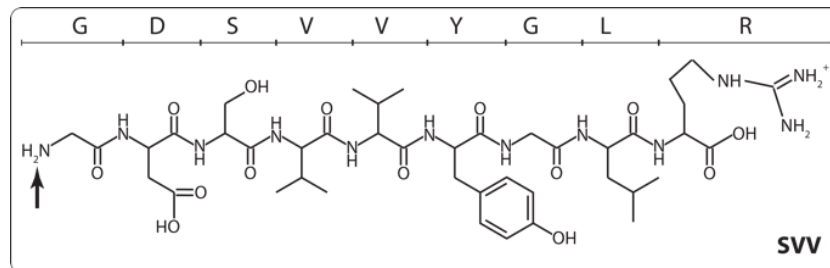
endothelial medium supplements, and pericytes growth medium (PGM) were purchased from Promocell (C-12203, C-22111, C-12980, and C-28040 respectively). Endothelial growth medium 2 (EGM-2) is created adding the endothelial medium supplements to the EBM-2. Silicone was purchased from HEMA (80805014). One-side-polished (100) silicon wafers were purchased from Wacker (Germany).

1.1. Molecular structures

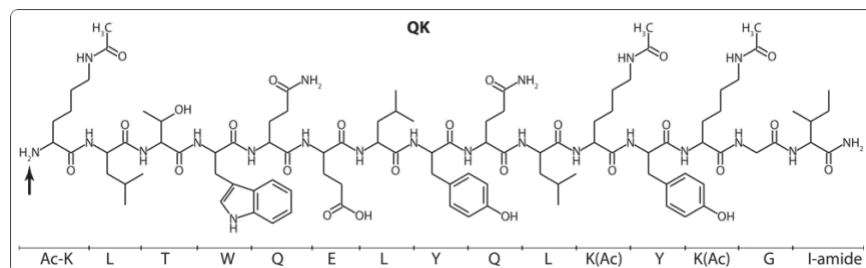
GRGDS peptide (RGD)



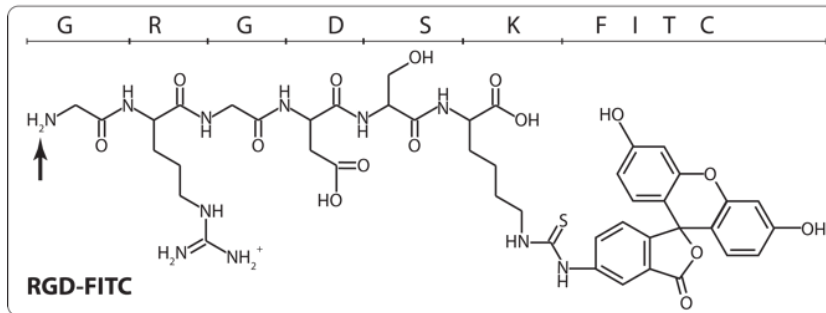
GDSVVYGLRK peptide (SVV)



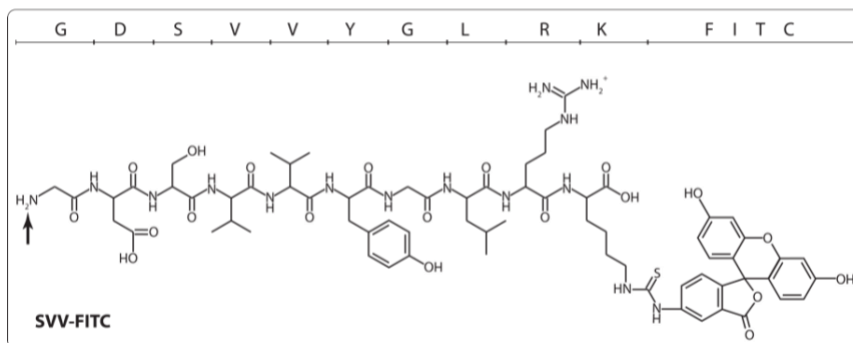
Ac-KLTWQELYQLK(Ac)YK(Ac)GI-amide peptide (QK)



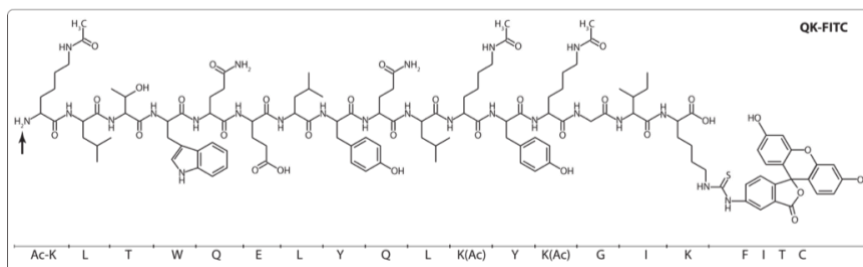
GRGDSK-Fluorescein 5-isothiocyanate conjugate peptide (RGD-FITC)



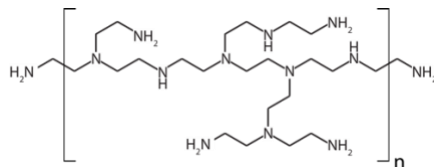
GDSVVYGLRK-Fluorescein 5-isothiocyanate conjugate peptide (SVV-FITC)



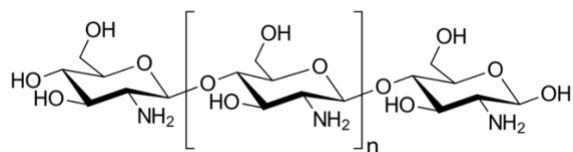
Ac-KLTWQELYQLK(Ac)YK(Ac)GIK-Fluorescein 5-isothiocyanate conjugate peptide (QK-FITC)



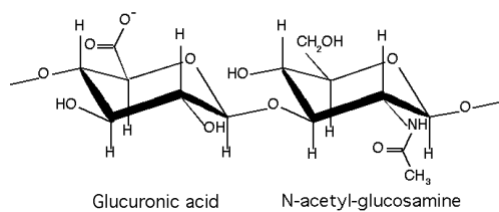
Polyethyleneimine (PEI)



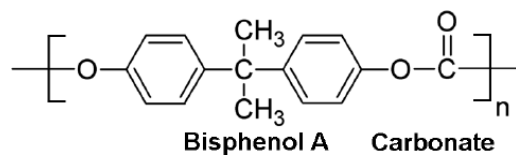
Chitosan (CHI)



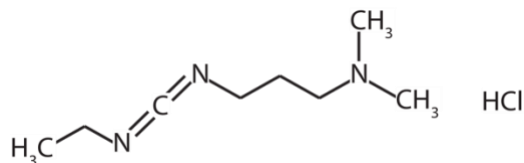
Hyaluronic acid (HA)



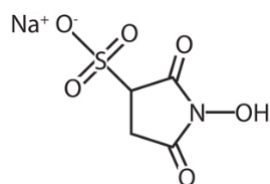
Polycarbonate (PC)



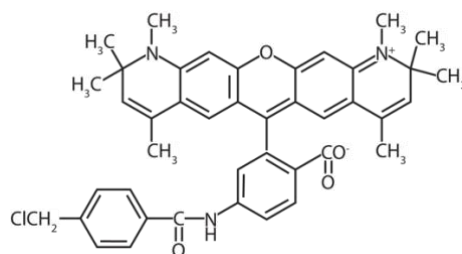
N-(3-Dimethylaminopropyl)-N'-ethyl-carbodiimide hydrochloride (EDC)



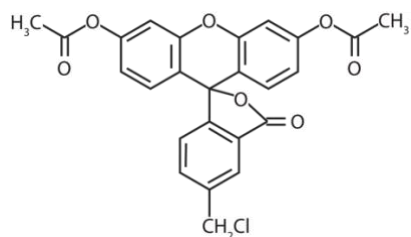
N-Hydroxysulfosuccinimide sodium salt (Sulfo-NHS)



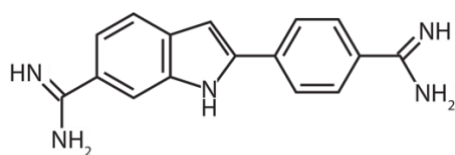
CMPX cell tracker



CMFA cell tracker



4',6-diamidino-2-phenylindole (DAPI)



1.2. Materials preparation

Hot embossing

Polycarbonate micro-channels (PC- μ Ch) were developed using hot embossing technique by pattern transfer from a silicon master (SiM) (Figure III. 1).

PC films were firstly washed by immersion in isopropanol for 10 minutes, and then dried blowing nitrogen gas with a pressure pistol. Parameters such as temperature, pressure (or force) and time were investigated to allow a complete PC mold transfer. Three types of line SiM patterns were used after the optimization step:

- Master with line pattern width (w) of 25 μ m, line spacing (s) of 100 μ m and line height (d) of 28 μ m (MICRO-L-25K-125K) represented in Figure III. 1 A. Periodicity is represented by the sum of width and spacing ($w+s$).

- Master with line pattern width (w) of 25 μ m, line spacing (s) of 50 μ m and line height (d) of 28 μ m (MICRO-L-25K-75K) represented in Figure III. 1 B. Periodicity is represented by the sum of width and spacing ($w+s$).

- Master with line pattern width (w) of 25 μ m, line spacing (s) of 25 μ m and line height (d) of 28 μ m (MICRO-L-25K-50K) represented in Figure III. 1 C. Periodicity is represented by the sum of width and spacing ($w+s$).

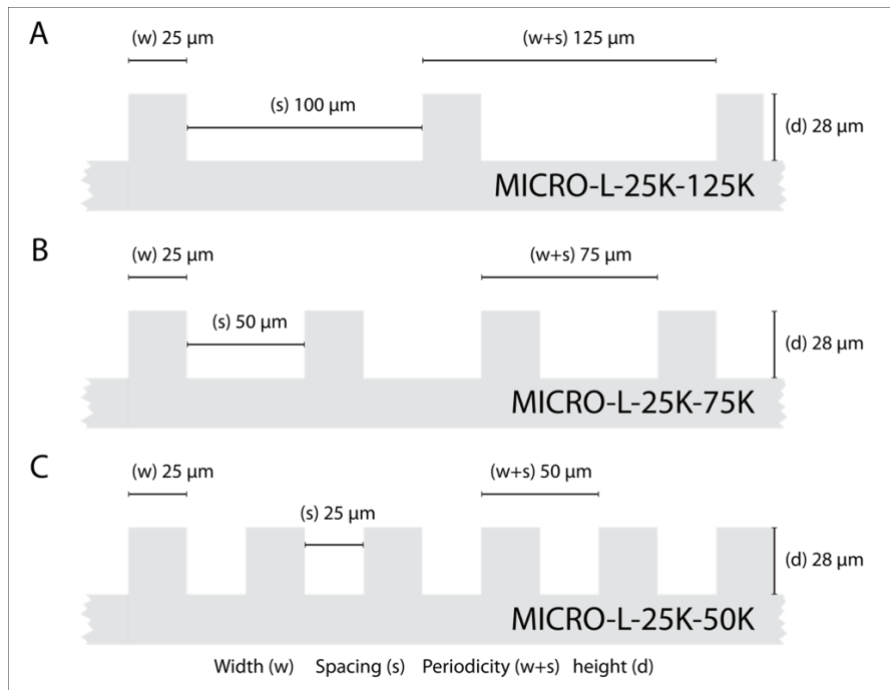


Figure III. 1 – Silicon master with micro-line pattern: Schematic representation of the three silicon masters used to develop micro-channels in polycarbonate. The line width (w) and height (d) is constant in all the masters, $25\mu\text{m}$ and $28\mu\text{m}$ respectively, but the spacing (s) between line differs: $s = 100\mu\text{m}$ (A), $s = 50\mu\text{m}$ (B) and $s = 25\mu\text{m}$ (C). The nomenclature of the silicon masters represent the micrometric scale pattern (MICRO) the type of pattern as line (L), the line width (w) and periodicity ($w+s$) of the pattern.

The molds were firstly washed by immersion in ethanol for 10 minutes and blow-dried using nitrogen gas to remove small particles before the imprinting process. Molding was performed using temperature- and pressure- controlled Fontijne hydraulic press (TP400, Fontijne, Holland) with the following protocol:

- Materials were aligned to fit in the embossing machine, according to Figure III.

2 A

- The “sandwich” of the components of printing is assembled according to Figure

III. 2 B

- Plates were brought in contact without applying force,
- The temperature was increased from room temperature (RT) until 200°C

- The sample was kept for 2 minutes at 200°C without force applied to equilibrate the system's temperature homogeneously.
- Force of 3 kN was applied
- After 2 minutes, the temperature was cooled down to 30°C, without reducing the applied force
- Finally, the applied force was removed by opening the plate of the press

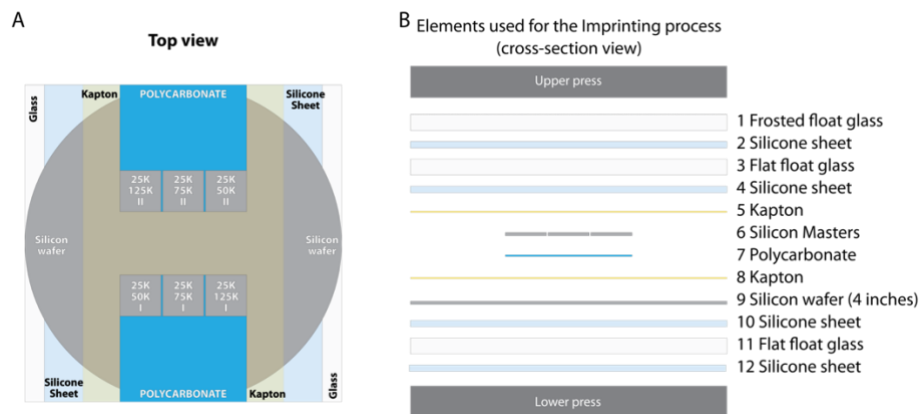


Figure III. 2 – Hot-embossing setup: Schematic representation of the setup for imprinting the materials. The top view (A) allows to visualize which silicon master was used and where is its location, as well as the location of the PC films and the other elements. The cross-section view (B) represents the type of “sandwich” of each element necessary for an homogeneous imprinting process.

After the hot embossing, the different PC films were gently peeled off from the SiM and stored into a fluoroware wafer carrier, while the SiM was washed with acetone and blow-dried, as previously described, before each imprinting process. Molded PC- μ Ch are named accordingly with the type of mold used: PC- μ Ch_(25K-125K), PC- μ Ch_(25K-75K) and PC- μ Ch_(25K-50K) (Figure III. 3).

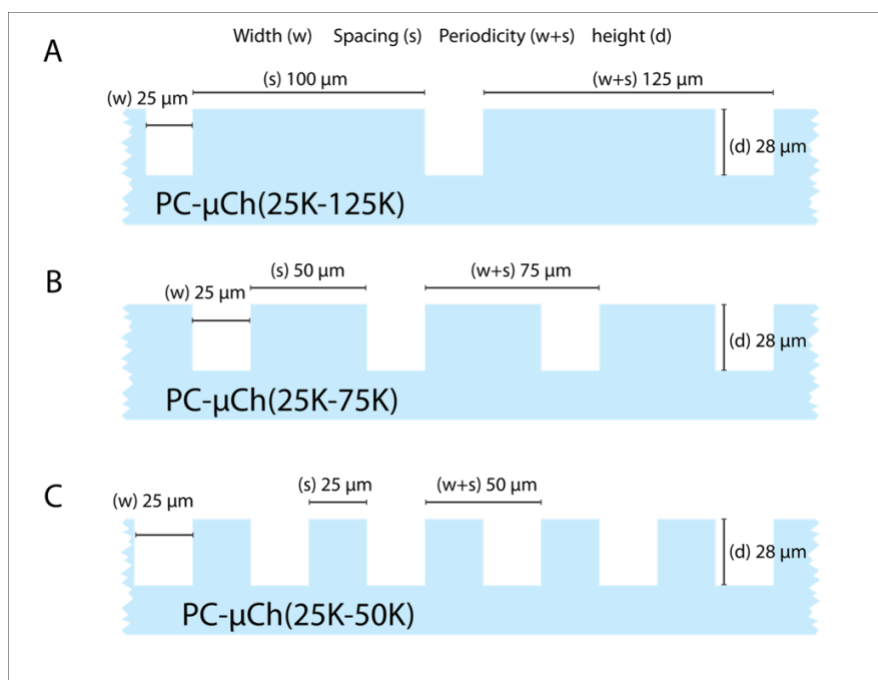


Figure III. 3 – Imprinted polycarbonate micro-channels: Schematic representation of the three polycarbonate micro-channel materials developed with the respective silicon masters previously represented. The line width (w) and height (d) of the micro-channels is constant in all the samples, 25 μm and 28 μm respectively, but the spacing (s) between line differs: $s = 100 \mu\text{m}$ (A), $s = 50 \mu\text{m}$ (B) and $s = 25\mu\text{m}$ (C). The nomenclature of the samples indicates the polycarbonate micro-channels (PC- μCh) with the the line width (w) and periodicity ($w+s$) of the pattern.

1.3. Material functionalization

1.3.1. Layer-by-layer deposition and crosslinking

Multilayered structures were built-up using the layer-by-layer (LbL) assembly technique, either on flat PC films or on PC- μCh . Hyaluronic acid (HA), chitosan (CHI) and polyethylenimine (PEI) were firstly freshly dissolved overnight under stirring conditions, at 1 mg/ml in 0.15M NaCl solution and buffered at pH 6.0-6.5 using NaOH and HCl 0.1M solutions. PC films or PC- μCh were firstly washed through 10 min

immersion in isopropanol followed by blow-drying step with nitrogen gas. Each deposition and rinsing steps were performed using a custom-made automatic dipping machine, holding the samples in a vertical orientation. Initially, a thin layer of PEI was deposited on the PC substrate, followed by three rinsing steps with NaCl 0.15 M pH 6.0 to coat the materials' surface with a homogenous positively charged layer (Figure III. 4). Afterwards the PC material was dipped alternatively in CHI and HA solutions for 5 min, each followed by three rinsing steps in NaCl 0.15 M, pH 6.0 solution (Figure III. 4). The multilayered films were then crosslinked by immersion of the modified PC substrates into freshly prepared EDC/sulfo-NHS (30 mM/50 mM in NaCl 0.15M pH 5.0-5.5) solution overnight at 4°C (Figure III. 4). After 16 h, the crosslinking reaction was stopped by performing eight washing steps of 20 min each in HEPES (20 mM in NaCl 0.15M pH 7.3-7.6) solution (Figure III. 4). For the initial characterization, different architectures of PC-PEI(HA/CHI)_n were developed with n ranging between 4 and 24. Each of these architectures were freshly crosslinked before performing further measurements. Once the characterization of the polyelectrolytes growth was performed, the architecture PC-PEI(HA/CH)_{12.5} was chosen as the definitive one, used for all further experiments on biofunctionalization, like peptide immobilization, and for the biological investigations as well. From now on, this specific architecture is referred to PC-LbL.

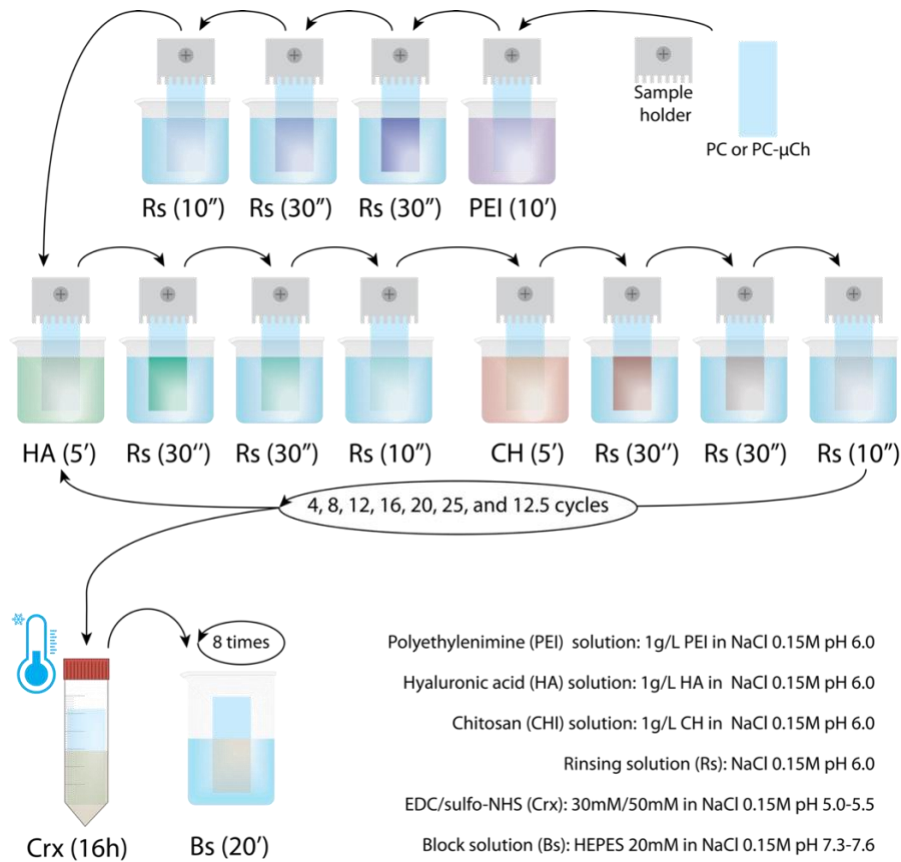


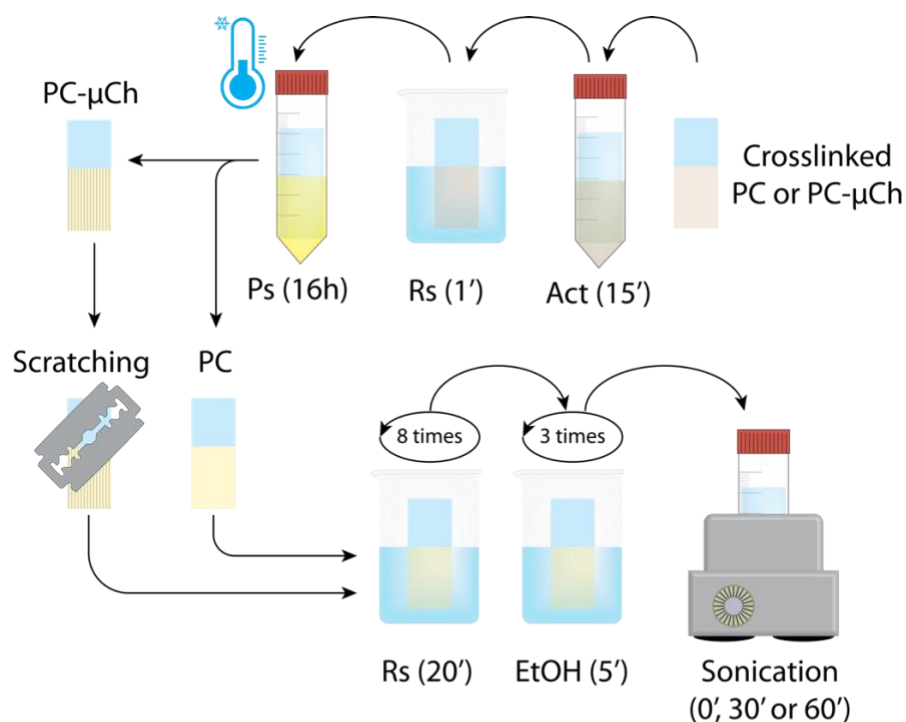
Figure III. 4 – Layer-by-layer functionalization: Schematic representation of the layer-by-layer deposition technique showing each step of deposition and rinsing. First, PC sample is fixed on the head of the automatic-dipping machine and the initial PEI deposition is performed, once. Then, the HA and CHI are deposited repetitively in cycle, each followed by three rinsing steps, in order to build up the polyelectrolytes layer-by-layer (LbL) film. Once the LbL reached the desired architecture, it was crosslinked at 4°C overnight and then washed extensively to remove the crosslinking solution. The type of solutions used for the deposition are indicated with particular attention on the salt concentration and pH.

1.3.2. Peptide grafting

PC-LbL was further functionalized by immobilizing six types of peptides on the LbL cushion. RGD, SVV, QK, RGD-FITC, SVV-FITC, and QK-FITC sequences alone or in

combination were immobilized using carbodiimide chemistry, same concentration as for the crosslinking of the LbL. Briefly, a quick activation of the polyelectrolyte LbL with EDC/sulfo-NHS was performed for 15 min at RT followed by one rinsing step in 0.1 M MES buffer (Figure III. 5). Then the activated PC-LbL substrates were immersed into a peptide solution (10^{-4} M in 0.1 M MES buffer at pH 5.0-5.5) overnight at 4°C. After 16 h, only for the PC- μ Ch-LbL samples, a further step of scratching with a metal blade was performed to remove the bioactive coating from the spacing between channels (Figure III. 5). Both flat PC-LbL or PC- μ Ch-LbL were washed eight times for 20 min each with 0.1 M MES buffer, followed by three rinsing steps of 5 min each in ethanol 50% (Figure III. 5). Last, samples underwent a sonication step (30 Hz, 100 W, Elmasonic P120H) of 0, 30 or 60 min to investigate the optimal time which allows a complete removal of unreacted peptides (Figure III. 5).

For the immobilization of peptide combination (such as RGD+SVV or RGD+QK) the same protocol as previously described was used with the presence of the two peptides in the equimolar concentration of 10^{-4} M each.



EDC/sulfo-NHS (Act): 30mM/50mM in MES 0.1M pH 5.0-5.5

Rinsing solution (Rs): MES 0.1M pH 5.0-5.5

Peptide solution (Ps): 10^{-4} M in MES 0.1M pH 5.0-5.5

Ethanol solution (EtOH): 50% Ethanol, 50% MilliQ water

Figure III. 5 – Peptide immobilization step: Schematic representation of the immobilization of peptides on polyelectrolytes LbL. First the LbL is activated and quickly rinsed. Then it is immersed in peptide solution overnight and the day after PC-μCh undergoes further scratching step. Both PC and PC-μCh undergoes two washing steps with MES buffer and ethanol. Last step of sonication, with a different exposition time, is performed to remove the unreacted peptides.

1.3.3. Biofunctionalized material sterilization

Approach A: Sterilization was performed placing the biofunctionalized materials in 48-well plate and immersed in ethanol 70% overnight. The day after, ethanol was removed and the samples were left under the laminar flow hood for 1h with the lid

open. Then three washed 10 min each was performed with sterile PBS, before the cell seeding.

Approach B: Sterilization was performed placing the biofunctionalized materials in 48-well plate and immersed in ethanol 70% for 15 min. After ethanol was removed and the samples were left under the laminar flow hood for 45 min with the lid open. Then three washed of 2 min each was performed with sterile PBS, before the cell seeding.

1.4. Materials characterization

1.4.1. Profilometry

SiM pattern's height and PC- μ Ch's depth were characterized by profilometry (Veeco Dektak 150). The scan of both features was performed perpendicularly to the direction of the features using the following parameters: Profile HillsAndValleys, ScanDuration 100 s, ScanLength 100 μ m, scan resolution 0,003 μ m, ScanType Standard Scan, StylusForce 4 mg, StylusScanRange, 524 μ m, StylusType Radius: 0,7 μ m. At least three measurements were acquired per each sample.

1.4.2. FE-SEM

PC- μ Ch were firstly coated with Pt/Pd depositing 10 nm thick layer (Cressington 208HR, thickness controller MTM-20). Both SiM and PC- μ Ch samples were observed at 15 keV with a Field Emission Scanning Electron Microscope (FE-SEM) (JSM- 7600F, Jeol Ltd.) in order to characterize the features' width and spacing.

1.4.3. Ellipsometry

HA/CHI multilayer growth was followed by ellipsometry (Jobin Yvon Horiba) using the same material preparation procedure, described in the material

functionalization part, with a little modification. Instead of using directly a PC film, the PC was firstly spin-coated (Laurell WS-650MZ) at 1 g/L on a 1 cm² silicon wafer surface (speed 4500 rpm, acceleration 2250 rpm and time 60 seconds), in order to create a homogeneous thin layer. Psi and Delta of each sample's architecture from 4<n<24 was measured. Later, Igor pro (6.3.7.2, Wavemetrics) software was used to simulate a curve model using isotropic film on isotropic substrate model and the following variables: number of layers = 1, wavelength= 632.8 nm, theta angle = 65.2 °C, Start value = 0, step size = 10, end value = 5000, silicon refraction (n_1)= 3.882, silicon absorption coefficient (k_1)= 0.019, air refraction (n_2) = 1, air absorption coefficient (k_2)= 0, silicon oxide refraction (n_3)= 1.455, silicon oxide absorption coefficient (k_3)= 0, PC refraction (n_4)= 1.5848, PC absorption coefficient (k_4)= 0 [302 1998.]. This model was used to fit the material's thickness and obtain the values for each measured architecture.

1.4.4. Spectrometry (TBO)

Free carboxylic groups available on PC-LbL samples were quantified using toluidine blue-0 (TBO) test [163]. The TBO method allows a selective dye staining of the deprotonated acid groups (COO⁻), present on the surface of the material, through ionic interaction at basic pH. It was already proven how 1 mole of TBO complex exactly with 1 mole of COO⁻ [303] and therefore the final concentration of COO⁻ groups was calculated. [163]. Briefly, 5 mM TBO solution in NaOH at pH=10 was freshly prepared and added to PC-LbL samples overnight. The day after, when the TBO has properly interacted with the COO⁻ groups, two quick rinsing steps in NaOH pH 10 solution and MilliQ water were performed followed by elution of the dye in acid pH condition, using acetic acid solution (50%). Thanks to the new acid conditions, the TBO present in the solution is proportional to the TBO linked to the COO⁻ groups on the material. 200 µl of the final solution was aliquoted into a transparent flat-bottom 96-well plate and absorbance was read at 633 nm (BioTek µQuant Gen5). The concentration of TBO was evaluated aliquoting 200 µl of TBO

standards from 10^{-4} to 10^{-8} M to create a calibration curve, reading the absorbance signal at 633 nm. Once the equation absorbance vs. concentration was developed, the unknown COO- concentrations were calculated knowing their absorbance intensity.

1.4.5. Fluorospectrometer (peptide grafting)

In order to quantify the density of the different peptides grafted on the LbL multilayer, fluorescent peptides: RGD-FITC, SVV-FITC, and QK-FITC, were grafted onto flat PC-LbL using the same procedure than for unlabeled peptides and using as control PC and PC-LbL without carbodiimide chemistry. Quantification was then performed using spectrofluorometer (CLARIOstar Excitation: 488 nm, Emission: 535 nm, gain: 600, 30x30 matrix scan method). A calibration curve was plotted reading the fluorescence signal of 100 μ l FITC-peptides aliquots in solution from 10^{-4} M to 10^{-8} M concentration range. From the fluorescence intensity of the known peptides' concentration is it possible to obtain the calibration curve. This was then used to evaluate the concentration of peptides grafted on the sample and, knowing the area of the sample, it was also possible to determine the concentrations reported in nmol/cm², pmol/cm², pmol/mm², and molecules/nm².

1.4.6. CLSM (LbL swelling)

PC-LbL-RGD-FITC samples were firstly rinsed in PBS, dipped in rhodamine red (Sigma-Aldrich 83689-1G) solution for 5 min and rinsed once in PBS. Then the materials were placed upside-down onto a glass slide for CLSM analysis at the confocal laser scanning inverted microscope (CLSM, ZEISS LSM 710). Images were acquired in green fluorescence (RGD-FITC) and red fluorescence (rhodamine red) with exposition time of 20 ms, oil objective 40 X scanning the entire thickness of the sample. Later a Z-reconstruction using Fiji (Schindelin J Nature methods 2012) software was performed to determine the penetration depth of the two-fluorophore used inside the LbL multilayers.

1.4.7. Fluorescence microscopy (scratching test)

PC- μ Ch-LbL-RGD-FITC samples were treated to remove the upper part of the LbL from the μ Ch spacing region. Removal of the top layer was performed on half of the sample, using a metal scalpel scratching in the direction of the channels. Later, fluorescence microscopy (LEICA DM5500B) was performed to identify the different regions of the partially scratched sample and the images were acquired using 10X objective. Images were analyzed using Fiji (Schindelin J Nature methods 2012) software and fluorescence signal was recorded.

2. Cell culture

2.1. Mono culture (or HUVEC)

2.1.1. Expansion

HUVECs were grown in a culture flask using EGM-2. Cells were sub-cultured using trypsin-EDTA and maintained in a humidified atmosphere containing 5 % CO₂ at 37 °C. Cells at passages 4–6 were used for experiments.

2.1.2. Cell detachment and counting

At the defined time-point of growth, HUVECs were detached using the trypsin-EDTA protocol which can briefly be summarized as follow: culture media containing FBS was removed and HUVECs were rinsed twice with warm PBS without Ca²⁺ and Mg²⁺. After PBS was removed and warm trypsin-EDTA was added and the sample incubated for 2-3 min in the cell incubator at 37°C and 5% CO₂. After that time, an aliquot of is collected and placed into the Malassez chamber for counting the number of total cells present in each sample under a brightfield microscopy [304].

Alternatively to the Malassez chamber, a more precise and reliable method can be used, based on the double-stranded DNA (dsDNA) quantification using PicoGreen kit (refer to paragraph 3.2 for more detail about PicoGreen method).

2.1.3. Culture on PC-LbL

Firstly, the wells of a 48-well plate were coated with anti-cell-adhesive polyHema 3% solution in ethanol 96% and dried overnight. Later, PC-LbL were placed on the coated wells and sterilized with ethanol 70% immersion for 15min, followed by ethanol removal and drying for 45 min. After, samples were washed using PBS three

times of 10 min each. 0.1 million HUVEC/cm² were then seeded in EBM-2 for 4 hours maintained in a humidified atmosphere containing 5 % CO₂ at 37 °C. After that, media was replaced with EGM-2 and incubated until the time-point was reached.

2.1.4. Culture on PC- μ Ch-LbL

Firstly, the wells of a 48-well plate were coated with anti-cell-adhesive polyHema 3% solution in ethanol 96% and dried overnight. Later, PC-LbL were placed on the coated wells and sterilized with ethanol 70% immersion for 15min, followed by ethanol removal and drying for 45 min. After, samples were washed using PBS three times of 10 min each. 0.1 million HUVEC/cm² were then seeded in EBM-2 and then centrifuged (Eppendorf 5810) using a swing-bucket rotor (Eppendorf A-2-DWP) for 2 min at 900 RPM. After samples were stored in a humidified atmosphere containing 5 % CO₂ at 37 °C until the time-points were reached.

2.2. Co-culture (or hPC-PL)

2.2.1. Expansion

hPC-PL were grown in a culture flask using PGM supplemented with 20% FBS and supplement kit. Cells were sub-cultured using trypsin-EDTA and maintained in a humidified atmosphere containing 5 % CO₂ at 37 °C. Cells at passages 4–6 were used for experiments.

2.2.2. Culture on PC- μ Ch-LbL

Firstly, the wells of a 48-well plate were coated with anti-cell-adhesive polyHema 3% solution in ethanol 96% and dried overnight. Later, PC-LbL were placed on the coated wells and sterilized with ethanol 70% immersion for 15min, followed by ethanol removal and drying for 45 min. In the meantime, HUVECs growing on the

culture flask were treated with CMTPX cell tracker for 45 min following the manufacturing instructions, while hPC-PL were treated with CMFDA cell tracker for 45 min following the manufacturing instructions. After, samples were washed using PBS three times of 10 min each. 0.1 million HUVEC/cm² were then seeded in EBM-2 and then centrifuged (Eppendorf 5810) using a swing-bucket rotor (Eppendorf A-2-DWP) for 2 min at 900 RPM. After samples were stored in a humidified atmosphere containing 5 % CO₂ at 37 °C for 2 hours. Later, 50'000 hPC-PL/cm² were seeded in EBM and placed again in the incubator until the prime-points were reached.

3. Biological characterization

3.1. Metabolic activity (XTT)

Metabolic activity test was performed after 18h of HUVECs incubation, according to manufacturer protocol. Two controls of PC and PC-LbL were tested together with the samples RGD, SVV, QK, RGD+SVV, and RGD+QK. Absorbance was read (BioTek μ Quant Gen5) at 650 and 450 nm after 4 hours incubation with the components of the kit.

3.2. DNA content (Pico green)

dsDNA content of the same samples from the XTT test were quantified using Pico-Green assay. Samples were firstly rinsed three times with PBS. Later 400 μ l of PBS were added and cells' membrane were lysate through 10s ultra-sonication (Micro-tip, Misomx ultrasonic processor XL) using 3 different power intensities and performed keeping the samples on ice. Later, dsDNA was extracted and quantified following the manufacturing instructions. Fluorescence signal (CLARIOstar, gain: 600) was measured at 520 nm and cell number was calculated considering that each cell contains on average 6.6 pg of dsDNA [305].

3.3. CLSM (tubulogenesis)

3.3.1. Mono-culture tubulogenesis

Three-dimensional organization of HUVECs was evaluated using CLSM (ZEISS LSM 710). At the desired time-points of 1h, 2h, 3h, 4h, and 5h, cells were fixed using PFA4% incubation for 15 min. After PBS rinsing, the samples were stained with Phalloidin-564 and mounted with Fluor shield DAPI in glass slide for CLSM analysis.

Images acquisition was performed with an oil objective at 40X in red and blue fluorescence.

3.3.2. Co-culture stabilization

Three-dimensional organization of HUVECs and hPC-PL were evaluated using CLSM (ZEISS LSM 710). At the desired time-points of 2h, 3h, and 4h cells were fixed using PFA4% incubation for 15 min. After PBS rinsing, the samples were mounted with Fluor shield DAPI in glass slide for CLSM analysis. Images acquisition was performed with an oil objective at 40X in red, green and blue fluorescence.

4. Software and statistical analysis

4.1. ImageJ / Fiji

Fiji 2.0 (Schindelin J Nature methods 2012) was used for measuring the feature pattern in SiM and PC- μ Ch, the thickness of the LbL after CLSM analysis, adjusting and adding scalebar to all the fluorescence microscopy images, and analyze all the CLSM of monoculture and co-culture experiment to identify the location of tubular-like structures.

4.2. IMARIS

IMARIS 9.0 (Oxford Instruments, <http://www.bitplane.com>) was used for the three-dimensional (3D) reconstruction of the confocal images and for analysis of the tubular structures of HUVECs into micro-channels.

4.3. PRISM (statistical software)

4.3.1. μ Ch development

A first two-tailed unpaired t-student test was performed between w and w' samples to compare if their mean were different. We assume gaussian distribution of the samples. Welch's correction was then performed, assuming not equal SD between samples. 95% confidence level was chosen.

A second two-tailed unpaired t-student test was performed between s and s' samples to compare if their mean were different. We assume gaussian distribution of the samples. Welch's correction was then performed, assuming not equal SD between samples. 95% confidence level was chosen.

A third two-tailed unpaired t-student test was performed between d and d' samples to compare if their mean were different. We assume gaussian distribution

of the samples. Welch's correction was then performed, assuming not equal SD between samples. 95% confidence level was chosen.

Results were considered to be significantly different starting from $p < 0.05$. Different p values were represented with different symbols: $p < 0.05$ (*) $p < 0.01$ (**) $p < 0.001$ (***) $p < 0.0001$ (****).

4.3.2. LbL growth

Non-linear fit with exponential growth was used. The selected fitting method was the least squares fit, without comparison or constraints. No weighting was considered, minimize the sum-of-squares of the distance of the points from the curve choosing when you expect the average distance between point and curve to be unrelated to the values of Y. We considered each replicate of Y as an individual point. The fit curve was performed for a maximum number of iterations 1000 and the goodness-of-fit was quantified using the R square and the sum-of-squares values.

4.3.3. TBO

The two-tailed unpaired t-student test was performed between the PC and PC-LbL samples to compare if their mean were different. We assume gaussian distribution of the samples. Welch's correction was then performed, assuming not equal SD between samples. 95% confidence level was chosen. Results were considered to be significantly different starting from $p < 0.05$. Different p values were represented with different symbols: $p < 0.05$ (*) $p < 0.01$ (**) $p < 0.001$ (***) $p < 0.0001$ (****).

Linear regression was performed on the standards to identify the equation of the calibration curve and interpolate the unknown samples from the standard curve.

4.3.4. Peptide grafting

Ordinary two-way ANOVA was performed comparing each cell mean with every other cell mean on the same column, as well as compare rows within each column. When F values for a given variable were found to be significant, the multiple comparison analysis was corrected with the Tukey test. Results were considered to be significantly different starting from $p < 0.05$. Different p values were represented with different symbols: $p < 0.05$ (*) $p < 0.01$ (**) $p < 0.001$ (***) $p < 0.0001$ (****).

Linear regression was performed on the standards to identify the equation of the calibration curve and interpolate the unknown samples from the standard curve.

4.3.5. Scratching test

A first two-tailed unpaired t-student test was performed between t and t' samples to compare if their mean were different. We assume gaussian distribution of the samples. Welch's correction was then performed, assuming not equal SD between samples. 95% confidence level was chosen.

A second two-tailed unpaired t-student test was performed between w and w' samples to compare if their mean were different. We assume gaussian distribution of the samples. Welch's correction was then performed, assuming not equal SD between samples. 95% confidence level was chosen.

A second two-tailed unpaired t-student test was performed between s and s' samples to compare if their mean were different. We assume gaussian distribution of the samples. Welch's correction was then performed, assuming not equal SD between samples. 95% confidence level was chosen.

Results were considered to be significantly different starting from $p < 0.05$. Different p values were represented with different symbols: $p < 0.05$ (*) $p < 0.01$ (**) $p < 0.001$ (***) $p < 0.0001$ (****).

4.3.6. Metabolic activity (XTT)

One-way ANOVA without matching or pairing was performed 95% confidence interval. We assume a gaussian distribution of the samples, comparing the mean of each sample with the mean of every other sample. When F values for a given variable were found to be significant, the multiple comparison analysis was corrected with the Tukey test. Results were considered to be significantly different starting from $p < 0.05$. Different p values were represented with different symbols: $p < 0.05$ (*) $p < 0.01$ (**) $p < 0.001$ (***) $p < 0.0001$ (****).

Linear regression was performed on the standards to identify the equation of the calibration curve and interpolate the unknown samples from the standard curve.

4.3.7. DNA content (Pico Green)

One-way ANOVA without matching or pairing was performed 95% confidence interval. We assume a gaussian distribution of the samples, comparing the mean of each sample with the mean of every other sample. When F values for a given variable were found to be significant, the multiple comparison analysis was corrected with the Tukey test. Results were considered to be significantly different starting from $p < 0.05$. Different p values were represented with different symbols: $p < 0.05$ (*) $p < 0.01$ (**) $p < 0.001$ (***) $p < 0.0001$ (****).

Linear regression was performed on the standards to identify the equation of the calibration curve and interpolate the unknown samples from the standard curve.

IV. Results and Discussion

The studies outlined in this thesis aim to understand the interactions between cells and biomaterials for tissue engineering applications focusing on angiogenesis. For this purpose, a three-dimensional micro-structured material presenting various forms of bioactivity was designed, to mimic the complex and rich extracellular matrix environment, naturally present in the human body. The combination of various surfaces' properties can influence the cell response in many ways.

In the first part of the results chapter, the fabrication and characterization of various elaborated flat and microstructured surfaces are presented. Three types of micro-channels in polycarbonate with different geometries were successfully fabricated, and the best among those was later functionalized with adhesive and/or angiogenic peptides through a polyelectrolytes cushion deposited in a layer-by-layer manner. The peptide sequence chosen to induce the initial cellular adhesion was the well-known Arg-Gly-Asp (RGD). Two peptides with angiogenic properties were also tested: SVV sequence derived from osteopontin protein, and QK sequence designed to mimic the vascular endothelial growth factor (VEGF) protein. Each step of the surface functionalization process was monitored through a variety of surface characterization techniques to ensure the validity of the used protocol. These techniques include profilometry to evaluate the depth of the developed μ -channels, scanning electron microscopy (SEM) to evaluate the width and spacing between channels, ellipsometry to investigate the polyelectrolytes growth on the PC material, absorption spectroscopy to quantify the amount of available carboxylic groups on the LbL cushion, fluoro-spectrometry to quantify the number of immobilized peptides in the LbL cushion, fluorescence microscopy to investigate the efficiency of functional layer removal out of the μ Ch, and confocal laser scanning microscopy (CLSM) to evaluate the thickness and the penetration of the peptides into the LbL cushion.

In the second part of this chapter, results on the evaluation of human umbilical vein endothelial cells (HUVECs) behavior on the adhesive and angiogenetic modified-surfaces with peptides are reported.

We first determine the cellular behavior on flat surfaces, functionalized to be adhesive and angiogenic. After, mono-culture conditions with HUVECs were tested

on μ Ch-functionalized materials to follow the development of tubular-like structures and to evaluate the impact of the surface chemistry used to functionalize the different samples while maintaining constant the three-dimensional geometry of the μ Ch. Finally, a co-culture experiment with HUVECS and hPC-PL was performed in order to assess if a stabilization of those tubular-like structures for a longer period of time can be obtained, compared to the monoculture conditions tested.

1. PART I: Fabrication of PC microchannels

In this study, three-dimensional channels with dimensions ranging at the micro-scale level, are developed in order to favor the formation of capillaries vessels on a total surface of 1 cm². In literature, various techniques are reported to fabricate micro-scale pattern on material surfaces such as photolithography, soft lithography, and hot embossing as already discussed in chapter I. Among those interesting techniques, hot-embossing offers a series of advantages related to its ease of processing, rapidity, reproducibility, and versatility depending on the polymeric material used. Hot-embossing belongs to the categories of techniques which require a template in order to transfer a pre-defined pattern into a multitude of materials' surfaces. In the present study, the template master mold is made of silicon (SiM) and the material surface is polycarbonate (PC). This imprinting method allows large areas to be patterned on the micro-scale without the need for other time-consuming processes. Moreover, surface features of micro-metric scale can be easily constructed without limit on geometry.

Two main types of surfaces were elaborated for biological assays: (1) flat polycarbonate films (PC) with and without functionalization, and functionalized polycarbonate micro-channels (PC- μ Ch). The PC materials do not require any processing and were thus only cleaned and washed prior to functionalization. Instead, the PC- μ Ch materials require an initial step of micro-fabrication in order to develop the three-dimensional geometry. For the micro-patterning of PC materials, three types of lines pattern were used, characterized by their width (w), the spacing between lines (s) and their depth (d).

Combination of scanning electron microscopy (SEM) and profilometry are used to fully characterize the pattern line on the SiM, used for the hot-embossing, and on the imprinted PC- μ Ch. More precisely SEM is used to characterize the line-channels width (w) and spacing (s) (Figure IV. 1 A, B, and C), while profilometry was used to characterize the line height or channel depth (d).

Three types of SiM were used in this study, with the following nomenclature: MICRO-L-25K-125K (Figure IV. 1 A), MICRO-L-25K-75K (Figure IV. 1 B) and MICRO-L-25K-50K (Figure IV. 1 C) which define their main features. And accordingly, three types of PC- μ Ch are generated from each mold named: PC- μ Ch_{25K-125K}, PC- μ Ch_{25K-75K}, and PC- μ Ch_{25K-50K}.

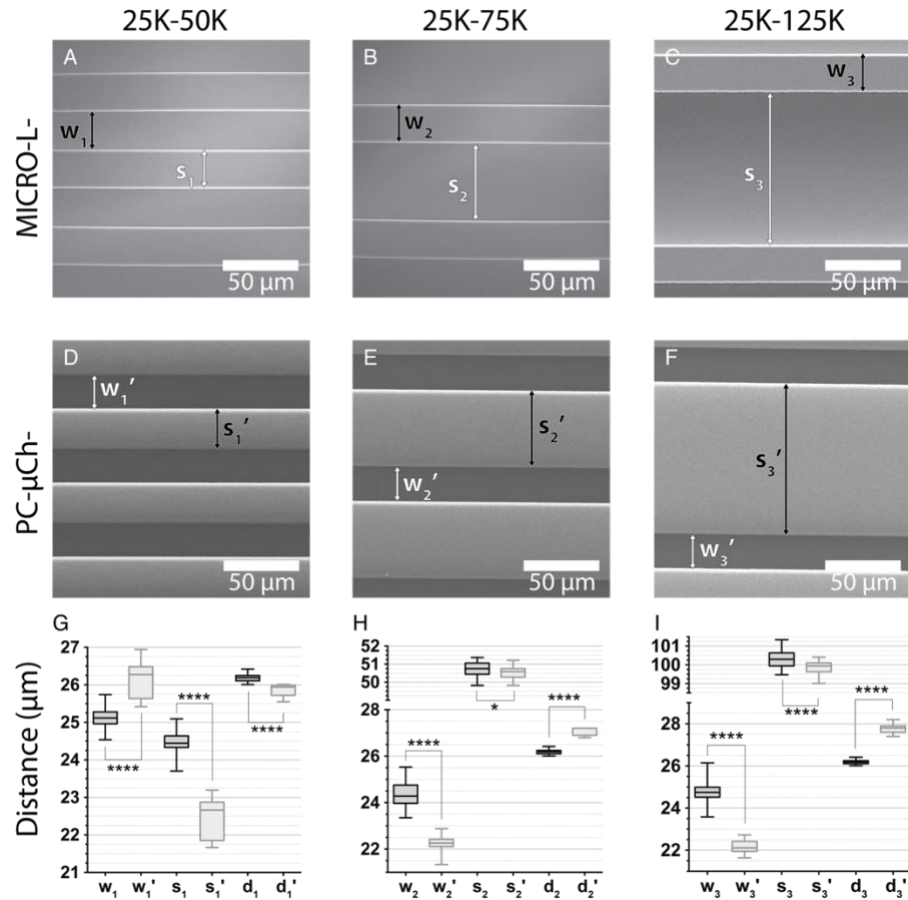


Figure IV. 1 – Silicon Master and Polycarbonate micro-channels geometries. Characterization of Silicon masters (SiM) and polycarbonate micro-channels (PC- μ Ch) using SEM and statistical analysis of the SEM and profilometry data for each molding type. (A) SiM MICRO-L-25K-50K image with marked details of line width (w_1) and spacing (s_1). (B) SiM MICRO-L-25K-75K image with marked details of line width (w_2) and spacing (s_2). (C) SiM MICRO-L-25K-125K image with marked details of line width (w_3) and spacing (s_3). (D) PC- μ Ch_{25K-50K} image with marked details of channel width (w_1') and spacing (s_1'). (E) PC- μ Ch_{25K-75K} image with marked details of channel width (w_2') and spacing (s_2'). (F) PC- μ Ch_{25K-125K} image with marked

details of channel width (w_3') and spacing (s_3'). Statistical analysis of the differences in features between SiM and PC- μ Ch for the pattern 25K-50K (G), 25K-75K (H) and 25K-125K (I).

1.1. 25K-125K geometry

The first SiM type investigated, MICRO-L-25K-125K, presents width (w_1) of $24,78 \pm 0,07 \mu\text{m}$, spacing (s_1) of $100,30 \pm 0,06 \mu\text{m}$ and height (d_1) of $26,19 \pm 0,01 \mu\text{m}$ (Figure IV. 1 A, G). The corresponding imprinted samples generated by this SiM are named PC- μ Ch_{25K-125K}. Those PC- μ Ch samples present micro-channel width (w_1') of $22,16 \pm 0,03 \mu\text{m}$, spacing (s_1') of $99,87 \pm 0,05 \mu\text{m}$ and depth (d_1') of $27,76 \pm 0,01 \mu\text{m}$ (Figure IV. 1 D, G). After the measurements of each feature of the two samples, a comparison is performed using three independent t-student test with PRISM software. The first comparison investigates if there is a statistical difference between the SiM line width (w_1) and the PC- μ Ch width (w_1'), resulting in a $p < 0.0001$ (****). The second comparison investigates if there is a statistical difference between the SiM line spacing (s_1) and the PC- μ Ch spacing (s_1'), resulting in a $p < 0.0001$ (****). The last comparison investigates if there is a statistical difference between the SiM line height (d_1) and the PC- μ Ch depth (d_1'), resulting in a $p < 0.0001$ (****). In this case, all the differences between SiM features and PC- μ Ch features result to be strongly significant (Figure IV. 1 G). To conclude the analysis of this sample, knowing the size of the mold, the total number of microchannels in the mold was calculated to be equal to 48 channels/mold.

1.2. 25K-75K geometry

The second SiM type investigated, MICRO-L-25K-75K, present width (w_2) of $24,33 \pm 0,07 \mu\text{m}$, spacing (s_2) of $50,75 \pm 0,06 \mu\text{m}$ and height (d_2) of $26,19 \pm 0,01 \mu\text{m}$ (Figure IV. 1 B, H). The corresponding imprinted samples generated by this SiM are named PC- μ Ch_{25K-75K}. Those PC- μ Ch samples present micro-channel width (w_2') of $22,27 \pm 0,03 \mu\text{m}$, spacing (s_2') of $50,57 \pm 0,04 \mu\text{m}$ and depth (d_2') of $27,00 \pm 0,03 \mu\text{m}$ (Figure

IV. 1 E, H). After the measurements of each feature of the two samples, a comparison was performed using three independent t-student test with PRISM software, reporting the results in the same way as for the previous geometry. For this investigated sample, width and depth differences between SiM features and PC- μ Ch features result to be strongly significant (****), while the spacing difference between SiM line and PC- μ Ch result to be significant (*) (Figure IV. 1 H). In the present case, the total number of microchannels in the mold was estimated to be 80 channels/mold.

1.3. 25K-50K geometry

The last SiM type investigated, MICRO-L-25K-50K, present width (w_3) of $25,13 \pm 0,03 \mu\text{m}$, spacing (s_3) of $24,47 \pm 0,04 \mu\text{m}$ and height (d_3) of $26,19 \pm 0,01 \mu\text{m}$ (Figure IV. 1 C, I),. The corresponding imprinted samples generate by these SiMs are named PC- μ Ch_{25K-50K}. Those PC- μ Ch samples present micro-channel width (w_3') of $26,09 \pm 0,07 \mu\text{m}$, spacing (s_3') of $22,40 \pm 0,07 \mu\text{m}$ and depth (d_3') of $25,86 \pm 0,05 \mu\text{m}$ (Figure IV. 1 F, I). After the measurements of each feature of the two samples, a comparison is performed using three independent t-student test with PRISM software reporting the results in the same way as for the previous geometry. In this case, all the differences between SiM features and PC- μ Ch features result to be strongly significant (****) (Figure IV. 1 I). For this mold, the total number of microchannels which is equal to 120 channels.

These data confirm what was already reported in the literature, that hot embossing is an easy and highly reproducible procedure capable of transferring a pattern from a master to a polymeric material using a combination of temperature and pressure [306]. However, this pattern transferring does not result in a perfect matching between the features of the initial master and the polymeric material. Those little modifications are common in the application of hot embossing and are due to the thermal shrinking of the polymer, occurring during the cooling step which follows the molding phase [307]. Nevertheless, the reduced size of the micro-

channels compared with the original line width, would not affect the biological experiments, since the range of interest for the development of capillaries structures is preserved [29, 264].

For further experiments, the geometry 25K-50K with the μCh width of 26 μm and μCh spacing of 22 μm was chosen. This choice results from the fact that the overall width of the μCh was identical for the three types of geometry but, the SiM MICRO-L-25K-50K allows to produce more μCh per unit of surface compared to the other two types, resulting in a higher surface area where capillary-like structures can be developed. From now on, polycarbonate material with this geometry will be simply indicated as PC- μCh .

2. PART II: Biofunctionalization

2.1. Layer-by-layer biofunctionalization

To immobilize peptides on the various polycarbonate surfaces, we firstly deposited a polyelectrolyte multilayered film using the well-known layer-by-layer (LbL) deposition technique. Hyaluronic acid (HA) and chitosan (CHI) were chosen as polyelectrolytes based on their biocompatibility, their net charge at the working pH and the availability of free carboxylic groups to further graft the peptides of interest. First, the build-up of the LbL made of HA and CHI was followed by ellipsometry.

One of the peculiarities of ellipsometry measurements is the requirement of a smooth surface, to limit the scattering of the laser beam during the measurements. Therefore, the ellipsometry study using PC films spin-coated on a 1x1 cm² silicon wafer. Different concentrations of PC solution were prepared and spin-coated in order to determine which one would provide a homogeneous, thin and smooth layer. Concentrations of 0.5 g/L, 1 g/L, and 2 g/L were tested (Figure IV. 2 A), and the layer thickness was calculated based on the fitting of the simulation resulting in 4.4 ± 0.03 , 6.1 ± 0.08 and 10.3 ± 0.3 nm, respectively (Figure IV. 2 B).

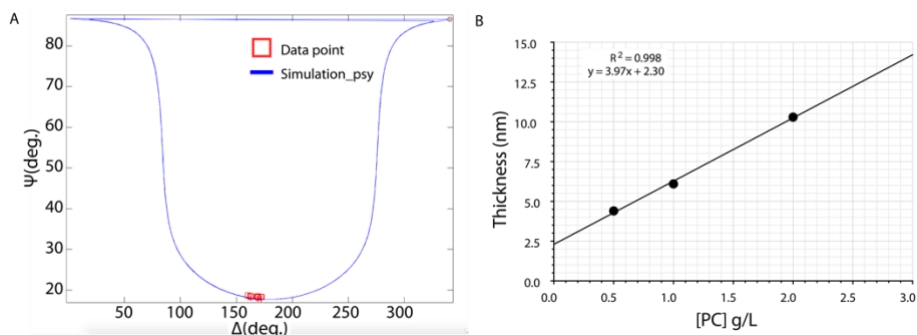


Figure IV. 2 - Ellipsometry measurements for PC-spin coated on the silicon wafer. (A) the Ψ and Δ values are given by the ellipsometer for 0.5, 1 and 2 g/L spin-coated PC with also the simulation curve of the material's characteristics. (B) XY plot with linear regression to evaluate the correlation between PC film thickness and PC solution concentration. Detail of the R^2 and equation of the line used.

Figure IV. 2B shows that the resulting PC film thickness is linearly correlated with the concentration of the PC starting solution. To investigate polyelectrolytes growth by ellipsometry, we used the 6 nm thick PC layer obtained from the 1g/L PC solution for the spin-coating step.

Prior to the deposition of HA/CHI bilayers, a first anchoring PEI layer was deposited onto the PC spin-coated film based on previous investigations [308]. When the precursor layer of PEI is adsorbed on the material surfaces, it enhances the polyelectrolytes multilayer film thickness and the amount of adsorbed polymer, regardless the materials' substrate [308]. Since the first layer works as anchoring precursor for the further LbL deposition, the type of polymer used to anchor plays an important role, affecting the stability of the whole film [308]. The general architecture of the grown multilayers can be represented in this form: PC-PEI(HA/CHI)_n, with n indicating the number of deposited HA/CHI polyelectrolytes bilayers. (HA/CHI)_n multilayer with n ranging between 4 and 24 bilayers were grown. All samples were freshly prepared and crosslinked with carbodiimide chemistry prior to each measurement, in order to preserve their stability. The LbL thickness with n= 4, 8, 12, 16, 20, and 24 bilayers result in 16.8 ± 0.1 , 43.2 ± 0.2 , 112.0 ± 0.8 , $159.0 \pm$

0.9, 260.2 ± 0.4 , 373.8 ± 0.6 nm thick multilayers, respectively (Figure IV. 3 A). The final architecture is schematically represented in Figure IV. 3 B, with the particular interest in the repetitive alternation of CHI and HA typical of the LbL approach. The thickness of the final PC-PEI(HA/CHI)_{12.5} architecture in liquid conditions was measured after sample immersion in PBS/rhodamine red solution overnight, recording the fluorescence signal (Chapter II.1.4.6) resulting in 6 ± 1 μm thickness. The thickness of the final polyelectrolytes film depends, as previously investigated, on several parameters such as the salt concentration, the pH of the solution, the temperature, the nature of the polyelectrolytes, and the time of swelling [118, 119].

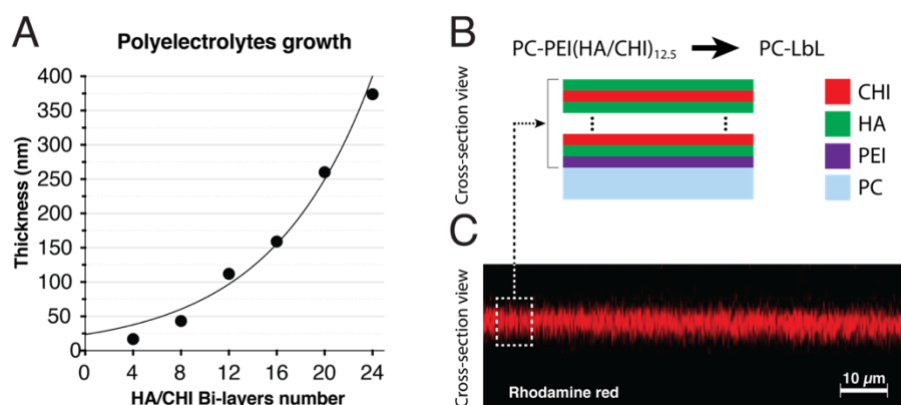


Figure IV. 3 - Layer-by-layer deposition characterization.(A) Polyelectrolytes growth while increasing the number of deposited bilayers measured in dry conditions using ellipsometer. (B) Schematic representation of the final PC-PEI(HA/CHI)_{12.5} architecture, named from now on PC-LbL (or PC- μCh -LbL). (C) CLSM cross-section view of LbL swelling in wet conditions using rhodamine red fluorescence. Measurements were performed after 16h incubation in PBS/rhodamine red solution at 4°C.

LbL is an attractive method for surface modification since it can be potentially applied to any type of substrate and provides support and multiple signals for cell adhesion and interactions [309]. In the present work, HA and CHI were used as natural polyelectrolytes for the build-up of the LbL coating onto PC substrates. The salt concentration of 0.15 M NaCl and pH 6 were chosen as build-up conditions, according to a previous publication showing that HA solubility decreases with increasing salt concentration [119]. The evolution of (HA/CHI)_n coating thickness in

terms of the number of deposited bilayers, presented in Figure IV. 3, proves that the LbL assembly of HA and CHI was successful under these conditions and that, as previously reported that the growth mechanism follows an exponential curve [119].

Richert *et al.* investigate the buildup process of hyaluronic acid/poly(L-lysine) (HA/PLL) multilayers formed by electrostatic self-assembly. This polyelectrolyte film constitutes one of the best known exponential growth system, where the thickness increases exponentially with the number of deposited layers. This exponential growth regime was shown to result from an 'in' and 'out' diffusion of PLL chains through the film during the buildup process. PLL diffuses throughout the film down to the substrate after each new PLL deposition and out of the film after each rinsing step and further after each HA deposition. As PLL reaches the outer layer of the film, it interacts with the incoming negatively charged HA, forming a new PLL/HA layer. Consequently, the thickness of the new formed PLL/HA layer is proportional to the amount of PLL that diffuses out of the film during the buildup step, which explains the exponential growth regime [119].

Covalent cross-link within the film was made in order to create covalent amide bonds between the carboxyl groups of the HA with the amine groups of the CHI. This protocol was taken from previous publications [119, 310] since it was applied already on CHI/HA LbL and characterized in terms of mechanical properties and film adhesive properties. It was also investigated how one micrometer thick films are sufficiently thick to do not allow cells to experience the underlying material [311].

For all further experiments, the architecture PC-PEI(HA/CHI)_{12.5}, corresponding to a coating thickness of about 120 nm, was used and, labeled as PC-LbL when applied on PC films, or PC- μ Ch-LbL when applied to PC with μ Ch (Figure IV. 3 B). We focus on the PC-PEI(HA/CHI)_{12.5} architecture for two main reasons: 12 deposition cycles were chosen according to previous investigations in which was shown how 120nm of CHI/HA bilayers develop a uniform film on the materials' surface [119]. HA was used as the last layer in order to have a top surface richer in carboxylic acid groups to further perform peptides grafting using carbodiimide chemistry.

After the determination of the thickness dry conditions, using ellipsometry, we focused on the swelling degree of the LbL when exposed to salt conditions, which

better mimic the real environment experienced during biological test analysis. In these wet conditions, the PC-LbL thickness measured by CLSM was 6 μm (Figure IV. 3 C). This means that the multilayer swells by a factor of about 60 when going from the dry to the wet conditions. The swelling of the LbL was homogeneous without any small islets that would be characteristic of inhomogeneous polyelectrolytes build up [119]. The high degree of swelling observed in our work indicates that the degree of crosslinking remains rather low and that, consequently, not all the carboxylic groups of HA are involved in linking with amine groups of CHI but some are still available for the further grafting of peptides. We, therefore, decided to maintain the functionalization focus on this architecture for the further chemical-immobilization studies and the biological investigations.

2.2. Immobilization and penetration of peptides on materials' surface

The next step was the immobilization of adhesive and angiogenic peptides on the newly deposited PC-LbL surface. First, the amount of available carboxylic groups was determined using toluidine blue (TBO) test, reading the absorbance at 633 nm with a spectrometer. Results show a high concentration of carboxylic groups, on the PC-LbL sample with $73 \pm 4 \text{ pmol/mm}^2$.

In order to investigate whether the peptides were physically adsorbed on the LbL cushion or covalently grafted on it using carbodiimide chemistry, a test with different washing sonication steps was performed after the grafting steps of RGD-FITC peptide. Three materials' chemistry were used and, for each of them, three different sonication exposition time were tested (0, 30, and 60 min) (Figure IV. 4 A). (1) PC films without biofunctionalization and without EDC/sulfo-NHS activation step (Chapter II.1.3.2) were immersed in RGD-FITC solution. Later, physically adsorbed peptide concentration was evaluated resulting in $0.9 \pm 0.3 \text{ pmol/mm}^2$, corresponding to 0 min sonication time. After the first wash time of 30 min, concentration results in $0.1 \pm 0.05 \text{ pmol/mm}^2$. Finally, after 60 min of sonication time, the concentration results in $0.4 \pm 0.1 \text{ pmol/mm}^2$. After the statistical analysis, no significant differences

were found for the PC material (Figure IV. 4 A). (2) PC films coated with HA/CHI LbL multilayer without the addition of the activating EDC/sulfo-NHS compound, named PC-LbL (Chapter II.1.3.2) were immersed in RGD-FITC solution. Physically adsorbed peptide concentration (0 min sonication) was evaluated resulting in 7 ± 2 pmol/mm². After the first wash time of 30 min concentration result in 0.7 ± 0.1 pmol/mm². Finally, after 60 min of sonication time, the concentration results in 0.9 ± 0.1 pmol/mm². Using this material PC-LbL, the statistical analysis identifies a significant difference (*) between the 0 min sonication and each of the two other sonication step of 30 and 60 min (Figure IV. 4 A(3) PC films coated with HA/CHI LbL multilayer with addition of the activating EDC/sulfo-NHS compound, named PC-RGD (Chapter II.1.3.2) were immersed in RGD-FITC solution. Physically adsorbed peptide concentration (0 min sonication) was evaluated resulting in 18 ± 3 pmol/mm². After the first wash time of 30 min, concentration results in 18 ± 2 pmol/mm². Finally, after 60 min of sonication time, the concentration results in 21 ± 2 pmol/mm². After the statistical analysis, no significant differences were found for the PC-RGD material (Figure IV. 4 A).

Another important investigation was performed to evaluate the efficiency of peptides penetration into the LbL cushion (Figure IV. 4 B). In this case, RGD-FITC peptide was grafted as reported in the previous section (Chapter II.1.3.2) and analyzed at the CLSM (Chapter II.1.4.6) resulting in a 6 ± 1 μ m (Figure IV. 4 B). To efficiently evaluate if the penetration of peptide corresponds to the whole LbL cushion thickness, we merge the signal with the Rhodamine red test (Figure IV. 3 C) resulting in a complete overlap (Figure IV. 4 C).

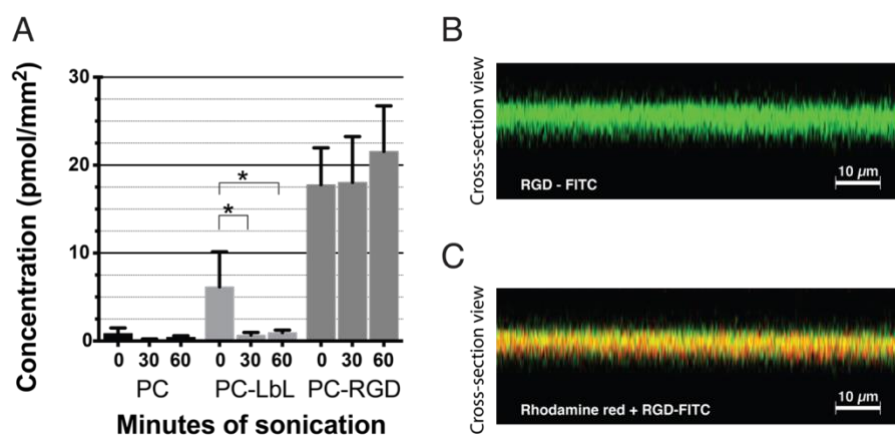


Figure IV. 4 - Characterization of immobilized-peptides.(A) Fluorescence quantification of peptides physically adsorbed on PC and on PC-LbL before and after sonication steps, as well as quantification of immobilized peptides on PC-RGD before and after sonication steps. (B) CLSM cross-section of RGD-FITC peptides penetration and (C) comparison with the LbL thickness shown in Figure IV. 3 C resulting in a merge of the fluorescent signal. Measurements were performed after 16h incubation in PBS solution at 4°C.

Peptides were chosen to induce adhesion and induce angiogenesis/tube-like formation. In the specific case of RGD sequence, this peptide is already largely investigated in tissue engineering application to improve cell adhesion even after immobilization onto materials' surfaces [1, 312]. However, in order to determine the number of peptides that were covalently immobilized on the PC substrates and to verify that our protocol of washing the physically adsorbed peptides was efficient, a quantification was performed at different sonication times.

In order to determine the number of peptides that were covalently immobilized on the PC substrates, and to verify that our protocol of washing the physically adsorbed peptides was efficient, a quantification was performed at different sonication times.

Only the PC-LbL presents a significant difference of immobilized peptide density before and after sonication (Figure IV. 4 A). As previously reported for PLL/PGA LbL composition [313], our PC-LbL material based on CHI/HA is expected to adsorb peptides in the LbL cushion. The removal of physically adsorbed peptides was

successfully proven by the difference in fluorescence intensity between the untreated sample and sonicated sample for 30 min, considering equal signal acquisition method per each measure. This result, justify perfectly the effectiveness of the sonication step for the adsorbed peptides removal. In addition, the constant level of fluorescence intensity after 60 min of sonication, compared to the 30 min of sonication, proofs how all the physically adsorbed peptides were already efficiently removed after the initial first 30 min of sonication, and therefore this time was selected for the further experiments.

On the contrary, on the virgin PC film between 0 and 30 min sonication time, there are no significant differences in fluorescence intensity, since the absence of a LbL cushion does not allow the adsorption of a high amount of peptides on the surface. In addition to this point, we can conclude that the sonication step does not affect the stability of the LbL cushion, resulting in an efficient and non-destructive method to remove only the physically adsorbed peptides and not affecting the bi-layer architecture. As a proof of what was just discussed, the high-intensity signal found in the sample treated with carbodiimide chemistry, PC-RGD, persists both before and after the two sonication steps, without any significant difference in the quantification of the fluorescent signal. From this, we can evince how the immobilization of the peptide was successful and not altered by the sonication steps, even during the longest exposition time.

Another key point of the in materials' surface characterization is to deeply understand the distribution of the immobilized molecules in it. In fact, immobilization of peptides could be superficial, following a gradient of penetration or being homogeneously dispersed. In order to understand how our peptide would be immobilized on the LbL cushion, two tests were performed. RGD-FITC penetration after immobilization in the LbL was characterized in 0.15M NaCl pH6.0 using confocal laser scanning microscopy (CLSM) (Figure IV. 4 B). We compared the thickness, resulting from the penetration of the peptide, with the total thickness of the swelled LbL previously investigated with Rhodamine red at point 1.2 of this chapter and showed in Figure IV. 3 C. It results how the signal from peptide penetration and LbL thickness is perfectly overlapping, indicating that the peptides during the

immobilization step were able to penetrate completely into the entire LbL thickness, resulting in a total thickness of $6 \pm 1 \mu\text{m}$ (Figure IV. 4 C). From this important result, we conclude that the impact of the peptides on the cells would be determined only by the homogenous immobilization of them, and not by a gradient in the LbL cushion.

2.3. Quantification of RGD, SVV and QK peptides on PC-LbL

Peptides are potent small molecules which can specifically trigger intracellular signaling, affecting the cellular activity and morphology [158, 230-232, 234, 238, 241-243, 246, 248]. In our work three main fluorescent-peptides are used (Chapter II.1.1.) to quantify their concentration after immobilization: RGD-FITC, SVV-FITC, and QK-FITC.

Considering that our system has a third dimension in space which is the not-negligible thickness of the LbL, it would have been more appropriate to report the peptide concentration in volume units (cm^3 or mm^3) instead of the surface units (cm^2 or mm^2). However, as we did not find any reported peptide grafting density per unit of volume in the literature that would allow comparisons, we also reported the peptide grafting per unit of surface area.

The immobilized peptide density was quantified using the corresponding calibration curve for each peptide used (Figure IV. 5). Data are presented in Table IV. 1. The lowest grafted peptide density results from PC-RGD sequence immobilization ($18 \text{ pmol}/\text{mm}^2$), followed by PC-SVV sequence immobilization which results in an intermediate density ($34 \text{ pmol}/\text{mm}^2$), and the highest grafting density was obtained with PC-QK sequence immobilization ($55 \text{ pmol}/\text{mm}^2$).

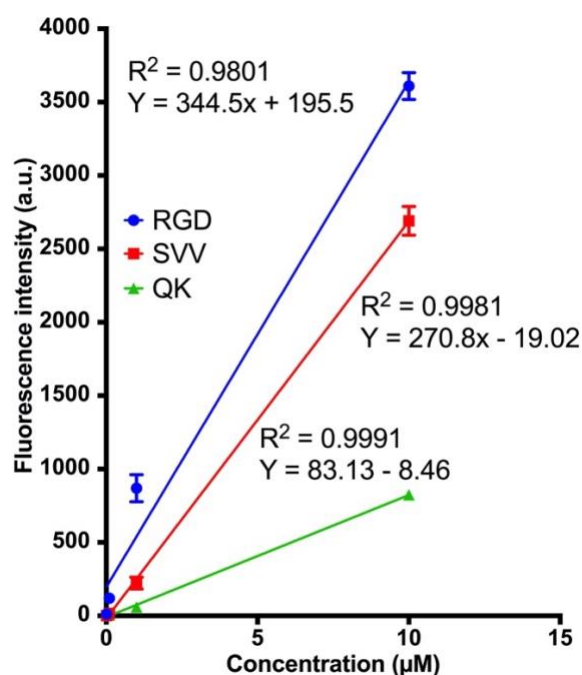


Figure IV. 5 - Calibration curve of fluorescent RGD, SVV and QK. Curves of RGD-FITC in blue, SVV-FITC in red and QK-FITC in green. For each curve are also represented the goodness of fit (R^2) and their equation are also presented.

Table IV. 1 – Quantification of immobilized peptides Peptide density for RGD-FITC, SVV-FITC, and QK-FITC. The density is measured in the different type of units to allow a comparison with the different resources found in the literature.

	Mean \pm standard error	Mean \pm standard error	Mean \pm standard error
Concentration	nmol/cm ²	pmol/cm ²	molecules/nm ²
RGD-FITC	1.8 \pm 0.3	1800 \pm 310	11 \pm 2
SVV-FITC	3.4 \pm 0.4	3400 \pm 370	20 \pm 2
QK-FITC	5.5 \pm 0.2	5500 \pm 150	33 \pm 1

In order to predict the effect of the second functionalization with peptides immobilization, we compared some previously published works in which the focus was based on the immobilization of the same peptide sequences, but on different material. RGD is the most known and used peptide which improve cellular adhesion, especially when immobilized on surfaces. Previous work demonstrated how cells

require a density as low as 1 fmol/mm² to adhere and spread on glass surface [314]. In other works using polyethylene terephthalate (PET) [171] or titanium [315] RGD density was reported as 1.8 and 6 pmol/mm² respectively. In a previous work of Gribova *et al.* the amount of RGD grafted onto an LbL of (PGA/PLL)_{6.5} was evaluated 3 pmol/mm² [316]. Chua PH *et al.*, instead quantify the amount of RGD grafted on Ti-(HA/CHI)₅ as high as 0.15 pmol/mm². Laslie-Barbick *et al.* were able to immobilize RGD peptide PEG hydrogels at peptide density of 80 pmol/mm² [317].

In the present work, the RGD (GRGDS sequence) grafting density is evaluated to be 18 ± 3 pmol/mm². This value lies in between the one reported by Gribova *et al.* (CGPKGDRGDAGPKGA sequence) [316] and the one reported by Laslie-Barbick *et al.* (RGDS sequence) [317] and is much higher than the minimum RGD density required for cell adhesion reported by Massia. *et al.* [314]. Our results also demonstrate that the RGD-FITC peptide penetrates into the entire swollen LbL in wet conditions. As among the different tested peptides, RGD-FITC showed the lower grafting density but a complete penetration into the LbL film, it is highly probable that the other two peptides SVV-FITC and QK-FITC, which present a higher grafting density, also fully penetrate into the LbL cushion.

Concerning angiogenesis and capillary-like formation, SVV and QK peptides were used in our work based on literature reviews of previous works. SVV peptide was already used as a potent angiogenic factor with a similar impact as VEGF in solution inducing the formation of capillaries [318], however, when grafted onto a surface material it was able to acquire both cell adhesion properties and promote neovascularization in artificial bone marrow scaffold [165-167, 242]. SVV peptide was already successfully grafted onto a modified gold substrate using EDC/NHS chemistry resulting in 1.6 ± 0.2 pmol/mm² [319], and on PET surface using same chemistry resulting in 20 pmol/mm² [167].

Regarding the PC-SVV, our SVV peptide density results in 34 ± 4 pmol/mm² which is, as for the case of PC-RGD higher than previously investigated. Therefore, we expect to have a significant impact of immobilized SVV peptide when grafted to the LbL cushion in the development of tubular-like structures. In addition, also, in this

case, the consideration of a three-dimensional substrate where peptide was successfully grafted is still valid.

QK peptide, the most used VEGF-mimetic peptide, is largely studied when used in solution *in vitro* for activation of VEGF receptors (VEGFRs) [248] and *in vivo* to enhance neovascularization of burn wounds in mice [247, 249]. Even after immobilization, it was shown how QK peptide preserve the bioactive properties in terms of angiogenic potential [317, 320] [321]. Chan *et al.* demonstrate a local increase of HUVEC tubulogenesis and increased endothelial sprouting with immobilized QK peptide of 55 pmol/mm² onto 2D collagen substrate [320]. Laslie-Barbick *et al.* demonstrate how covalently immobilized QK increased *in vitro* HUVECs migration and tubulogenesis and *in vivo* angiogenesis. In their studies 23 pmol/mm² of QK were immobilized on PEG hydrogels [317].

Concerning PC-QK material, our peptide density results in 55 pmol/mm² which is equal with the density achieved by Chan *et al.* and comparable with the range investigated in the PEG hydrogels by Laslie-Barbick *et al.* Therefore, like in the case of SVV, we expect to have a significant impact of immobilized QK peptide when grafted to the LbL cushion in the development of tubular-like structures.

Further studies should be performed in order to investigate exactly the ratio between the grafting of peptide combinations (like in the case of RGD+SVV and RGD+QK). It would indeed be interesting to evaluate, how the presence of one peptide would influence the grafting of the other peptide and in which ratio the two peptides would coexist on the materials' surfaces. It is surprising how the longest peptides used, QK, presents as well the highest concentration after grafting, while the intermediate SVV peptide presents an intermediate concentration, and finally, the shortest sequence of RGD presents also the smallest concentration after grafting. Logically, one would have expected that the shortest peptide RGD presents the highest concentration, thanks to better diffusion into the LbL film. One potential explanation can be that the presence of large FITC molecule could influence the efficiency of the formation of amide bonds during the grafting due to charges or steric hindrance.

2.4. Preserving a selective functionalization into μCh

To selectively preserve the functionalization only inside the μCh of the sample, a scratch test was performed on half of the materials' surface using a metal blade on LbL-RGD-FITC samples. Fluorescence microscopy was used in order to measure differences in fluorescence intensity between the half materials' surface scratched and the half not scratched (Figure IV. 6). The signal differences were evaluated between the top part of the material with scratch and without the scratch, as well as between the bottom part of the material inside the μCh with scratch and without the scratch. The signal from the top of the not-scratched region differs significantly with the region scratched with $p < 0.0001$ (****). In the case of the bottom of the μCh , the signal in the region not-scratched and the one scratched do not present any significant difference (Figure IV. 6 E).

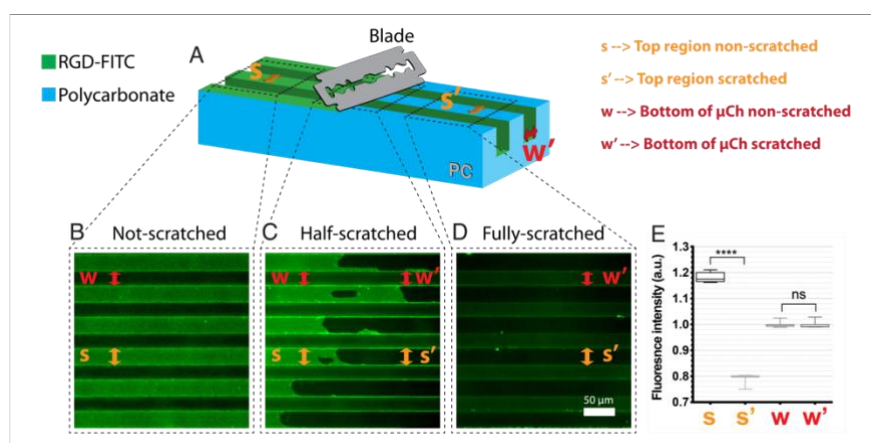


Figure IV. 6 - Selective functionalization of micro-channels. (A) Schematic representation of a half scratched sample of PC- μCh -LbL-RGD-FITC with a particular focus on the green region (FITC) or light blue region (PC). (B) In the region not scratched the brighter region represent the spacing (s) between channels (w) which are less bright. (C) In the region where the scratch started spacing non-scratched (s), spacing scratched (s'), channel not scratched (w), and channel scratched (w') can be identified. (D) In this region spacing (s') and channel (w') fully scratched can be identified. (E) The t-test for spacing results significantly different in the fluorescence intensity, compared to the non-significant difference between the channels regions.

The region of PC- μ Ch-RGD-FITC sample not scratched shows a stronger signal between the micro-channels, in the spacing region (s), this is due to the type of focus used for the image acquisition, which results in a larger light component coming from the top part of the sample, compared to the region deep inside the micro-channels (w). The resulting fluorescent signal is homogeneous between the spacing region and is homogenous also between the channel regions, but they do not correspond to the same signal intensity between themselves (Figure IV. 6 B, E). In the region, half-scratched (Figure IV. 6 C), large differences are observed between the spacing which underwent a scratch (s) and the one which did not (s'). This difference is confirmed by the quantification and it results in a significantly strong difference (Figure IV. 6 C, E). Regarding the signal change between the channel which underwent scratching (w) and the one which did not (w'), there is no evidence of a statistical difference (Figure IV. 6 E). Finally, the region fully-scratched present a very low signal on the spacing area (s') compared to the micro-channels area (w') which do not show the higher intensity in the overall picture (Figure IV. 6 E). It is important to notice how the micro-channel signal results in a homogenous surface, without any trace of scratch or peptide removal.

Therefore, we can conclude from the scratching assay that it is possible to get a selective removal of the LbL-RGD-FITC cushion only in the upper part of the sample where the spacing between channel exists, without affecting the functionalization inside the channels, which is the region of interest for the future biological evaluations in the development of capillary-like structures.

3. PART III: Capillaries development

3.1. Sterilization protocol for HUVEC adhesion

In order to successfully seed HUVECs cells on the material, and on the tissue control plate (TCP) as control, two sterilization process of the material have to be optimized (Chapter III.1.3.3.). The first approach, named approach A was chosen according to the previously investigated sterilization method with PET material (Figure IV. 7) [166, 167]. Preliminary results using HUVECs on PC materials, identify a consistent cellular death in both; the functionalized materials, and the surrounding TCP without the biofunctionalized materials. The second approach investigates named approach B, is a variation of the first one, with modifications in the exposition time to ethanol and the drying plus washing steps (Figure IV. 7). Using the second approach, no cellular death was identified in neither the samples or the surrounding TCP.

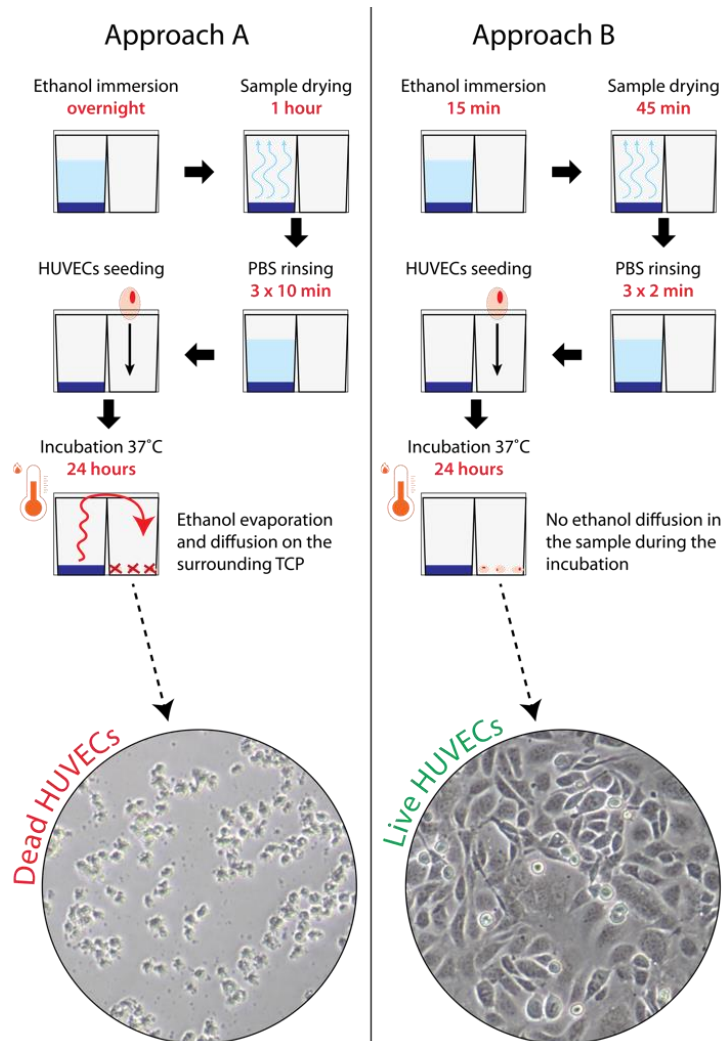


Figure IV. 7 - Two sterilization approaches. Approach A uses an overnight immersion in ethanol 70% followed by 1 hour of drying step and three washing steps of 10 min each with PBS. After HUVECs seeding and 24h incubation a massive cell death was found. Approach B use 15 min immersion in ethanol 70% followed by 45 min of drying step and three washing steps 2 min each with PBS. After HUVECs seeding and 24h incubation, cells were alive and adhered on the TCP material.

The model which we used to explain the initial cell death involved the evaporation and diffusion of the ethanol entrapped into the PC film which is released after incubation at 37°C (Figure IV. 7). The sterilization with approach A result in a

toxic condition for the surrounding HUVECs, leading to massive cell death due to the evaporation of the ethanol entrapped into the polymer when exposed for a long time at 37°C in the cell incubator. In fact, it is known that ethanol is absorbed by PC up to 0.08 g/g of polymer [322] Considering the small diffusion coefficient of ethanol in glassy PC of 10^{-12} cm²/sec [323], we can estimate that it would probably take the same time (overnight) to remove completely the ethanol inside the PC than for the immersion in ethanol. Therefore the exposition time to ethanol and the drying step were changed.

The optimized sterilization approach, approach B (Figure IV. 7), do not present any toxicity, and in addition, no contaminations were reported in the tested samples, indicating both the successful sterilization of the materials and the non-toxicity linked to ethanol entrapment. Therefore, the approach B was used for all the future cellular experiments.

3.2. Counting of HUVEC. Malassez vs Pico green (sonication tests also)

In order to properly quantify the number of cells adhering both on the biofunctionalized materials or the TCP, a precise and reliable method has to be used. Two main techniques were investigated in this work, preliminary on TCP material: Malassez chamber counting (Chapter III.2.1.2.) and Pico Green assay (Chapter III.3.2.). A preliminary result, to investigate which technique is the most precise, HUVECs cells were let adhere on the TCP material for 24h, detached, counted and compared with the initial amount of HUVECs seeded.

The first technique, based on trypsin detachment and brightfield microscopy counting with Malassez chamber, corresponds to the most common method used. In our case on TCP, after 24h of seeding 100'000 HUVECs only 49'632 ± 1'757 cells were effectively counted under the microscope. For 50'000 HUVECs seeded, only 33'169 ± 1'602 cells were counted and for 25'000 HUVECs seeded, 27'280 ± 1'016 cells were counted (Figure IV. 8 A).

The second technique is based on a selective interaction between a fluorescent-DNA-intercalant and fluorescent quantification signal, later converted in cell number (Figure IV. 8 B). Using this technique, the dsDNA extraction is the crucial step, and therefore to optimize the amount of extracted dsDNA three power-mode were selected, according to the ultra-sonicator characteristics: power 3 (P3), power 4 (P4) and power 5 (P5) (Figure IV. 8 B). To help in visualizing the theoretical value of cells counted per each seeding concentration, three different dash-lines are represented in Figure IV. 8, indicating 100'000, 50'000, and 25'000 cells in blue, red and green respectively. The DNA quantification, converted in cell number, is summarized in Table IV. 2 indicating the amount of cell counted per each power-mode selected.

Table IV. 2 – Correlation of HUVECs count and sonication power used. Number of HUVECs counted using different ultra-sonication power after 24h seeding in 48-well plate.

HUVECs seeding	Power 3: # HUVECS ± SEM	Power 4: # HUVECS ± SEM	Power 5: # HUVECS ± SEM
100'000	66'348 ± 3'169	70'628 ± 1'688	90'012 ± 3'062
50'000	43'301 ± 337	39'569 ± 2'175	50'710 ± 2'546
25'000	20'112 ± 494	19'210 ± 1'211	23'130 ± 2'031

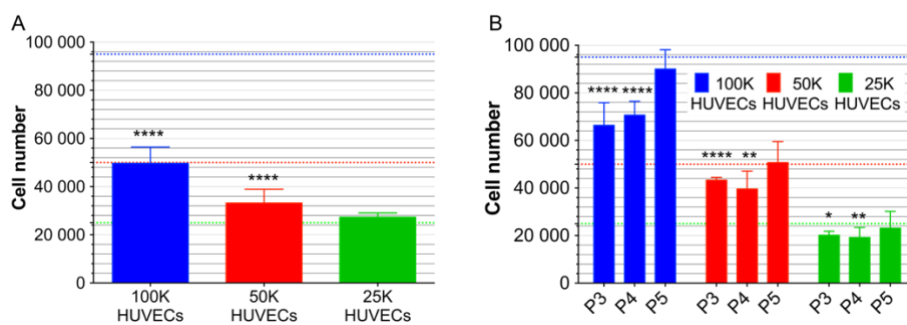


Figure IV. 8 - Number of HUVECs counted after 24h seeding using two techniques. (A) Counting with Malassez chamber under the microscope, according to three different initial seeding concentrations. (B) Quantification with Pico Green assay after ultra-sonication step

at three different power mode. Also, in this case, three different initial seeding concentration were tested. Blue-dash line report the maximum confluent value for the 48-well plate used, reported to be 95'000 cells. The red-dash line indicates 50'000 cells level. Green-dash line indicates 25'000 cells level.

Determine with precision the number of cells is crucial in biological investigations such as adhesion studies or metabolic activity studies. Therefore a precise protocol needs to be defined to determine whether one sample contains more cells than another one. Firstly, the common approach of detaching adhesive cells using trypsin-EDTA was used counting the cells with the Malassez chamber. However, the large difference between the cell-seeded originally, and the cells detached after 24h of incubation was too large to be considered reliable for the further biological investigations. The difference is significantly evident for the highest cell seeding condition with $p < 0.0001$ (****), showing a 48% reduction between the theoretical value of cell confluency 95'000 cells and the cells counted. As well, the second seeding condition presents a strong statistical difference with $p < 0.0001$ (****) and decrees of 34% from the initial seeding of 50'000 cells. Contrariwise, the lowest concentration does not present any difference between the cell initially seeded and the one counted after 24h.

This might indicate that at high cellular density, trypsin does not work efficiently with highly confluent cells, to allow a complete detachment from the 48-well tissue culture plate (TCP).

To overcome the problem, another approach was used, lysing the cells directly on the well plate, without a need for a detachment step. In this case, three instrumental setting were tested increasing the power of the ultra-sonicator. There is a significant difference between the power used to lysate the cells, and the quantification of cells, through their DNA. In fact, we can notice how the P3 and P4 set-up give a significantly lower number of counted cells, compared to the expected one for all the three seedings' concentration used. However, the P5 set-up shows no significant difference *versus* the relative theoretical cell density, per each used condition, resulting in the most reliable approach for an accurate count of cells. Therefore, considering an equal cellular adhesion in each sample, at the different

seeding concentration, the efficiency of dsDNA extraction using the ultra-sonication with power 5, is much higher than the other two. And as result, the number of HUVECs counted correspond to the number of HUVECs initially seeded.

3.3. Metabolic activity of HUVECs

Metabolic activity was measured after 18 hours using XTT kit on HUVECs cells, seeded on flat PC, flat PC-LbL and flat PC-LbL functionalized with RGD (PC-RGD), SVV (PC-SVV), QK (PC-QK) peptides and their combinations, as well as in the 48-well plate (TCP) as control (Figure IV. 9 A). The first investigation reports how the cells grown on TCP show the highest signal, significantly different against all the others with $p < 0.0001$ (****) in each case. The second highest signal comes from PC-RGD sample presenting a strong statistical difference against PC-LbL and the other single-peptide materials PC-SVV and PC-QK, with $p < 0.0001$ (****). Then the samples containing a combination of peptides PC-RGD+SVV and PC-RGD+QK present a similar signal compared with PC-RGD sample, with significant difference against the single-peptide samples PC-SVV and PC-QK with $p < 0.01$ (**) and $p < 0.05$ (*) respectively (Figure IV. 9 A).

Then the second analysis reveals the number of cells present in each sample, using the PicoGreen assay developed previously. In this case, the highest cell density was found in the TCP with a strong significant difference compared with all the other samples with $p < 0.0001$ (****). Then sample PC-RGD show the second highest concentration with strong significant difference against all the other samples with $p < 0.0001$ (****). All the other samples do not present a significant difference between each other (Figure IV. 9 B).

The last analysis, results in the adjustment of the metabolic activity signal, against the number of counted cells per each material condition. We define this new value as corrected absorbance. In this case, the signal from TCP sample reduced considerably being not different from PC-LbL or PC-RGD. However, the samples with peptide combination PC-RGD+SVV and PC-RGD+QK show a significant increment, resulting as the two highest conditions tested with a significant difference against all

the other samples presenting only one peptide PC-RGD, PC-SVV, and PC-QK (Figure IV. 9 C).

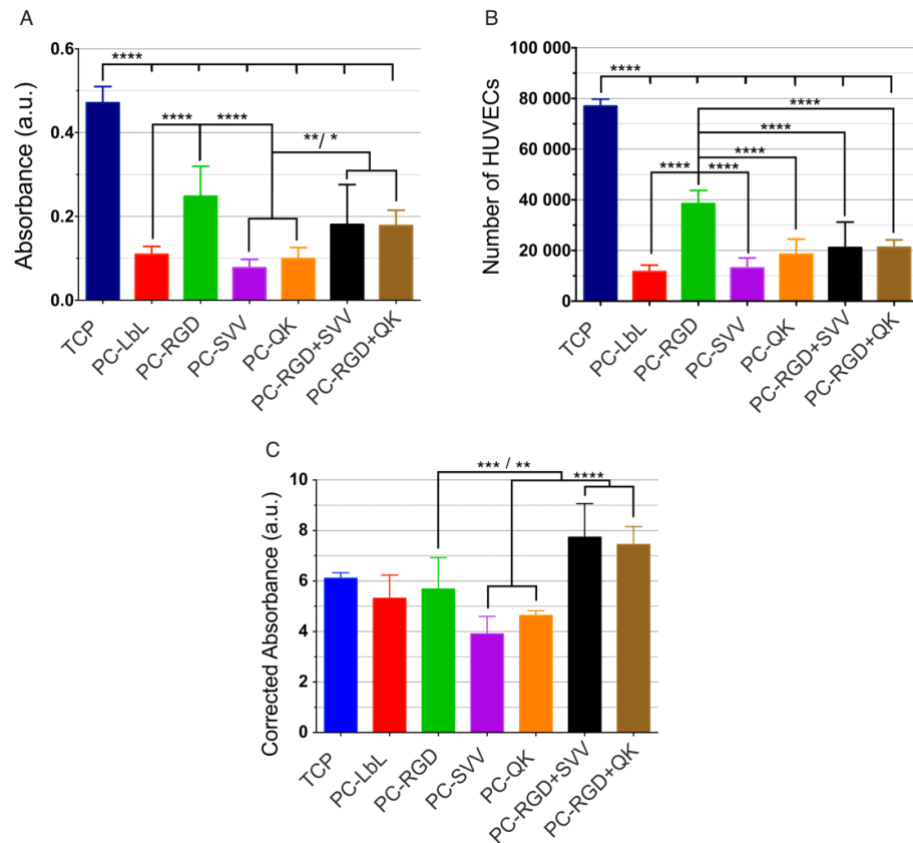


Figure IV. 9 - Biological evaluation on metabolic activity. (A) The absorbance recorded directly after XTT test. (B) The number of cells counted in each sample using PicoGreen assay (power P5). (C) Metabolic activity of HUVECs after the correction for the relative cell number per each sample.

In our studies, cells were seeded into a serum-free medium for the initial 4h of incubation in the case of XTT metabolic activity. This removes any possibility of the presence of adsorbed proteins which would enhance cell adhesion, and allow us to ensure a specific interaction between the cells' receptors and the peptides used. HUVECs are largely used for angiogenesis study and formation of vessel-like structures in vascular tissue engineering [324-326]. The studies on metabolic activity, after correction, showed a higher metabolism for peptide combination of RGD+QK

or RGD+SVV compared to each single-peptide version (Figure IV. 9 C). Further experiments are needed to fully understand the impact of the double peptide combination, however, some previous studies have been investigated the effect of co-immobilized RGD with VEGF [327] bFGF [328] and insulin [329] proving a synergistic effect on endothelial cells' adhesion and proliferation compared to only RGD immobilization. Also, the crosstalk between the receptor 2 for VEGF and RGD-binding integrins have been previously investigated [330-333] leading to a possible synergistic effect between the two in terms of cellular adhesion (Chapter I.4.2.1.), focal adhesion order, integrin activation, and migration speed. Le Saux *et al.* in a previous work reported an enhanced endothelial cells response depending on the grafting density of RGD [331]. Noel *et al.* reported a successful grafting of RGD peptide (1nmol/cm²) and VEGF protein (50fmol/cm²) showing a clear evidence of the additive effect of their combination [327].

Based on our investigations, would be interesting to answer the question about how deep cells' receptors would be capable of binding the peptides entrapped into the LbL film. In fact, investigating how much of the LbL-peptides would be "visible" by HUVECs would help to investigate also the minimum thickness of LbL-peptides, in order to trigger the desired development of capillaries structures, with the minimum waste of polysaccharides and peptides to efficiently move the application to a closer clinical approach. However, more sophisticated studies would be required to answer this question, and therefore for the lack of time, it was not possible to study deeper this aspect.

3.4. Centrifuge-based seeding approach of HUVECs

In order to specifically seed HUVECs inside the micro-channels of polycarbonate, a centrifugation approach was developed and investigated. After HUVECs seeding, centrifugation was applied resulting in a perpendicular force which forces the HUVECs on the spacing between channels, to fall into the channels (Figure IV. 10 A). This allows both to selectively focus the work inside the micro-channels and at the same time, increase the density of HUVECs into them to increase the number of

tube-like structures. To effectively prove that the approach was working efficiently, a bright field image was acquired immediately after centrifugation (Figure IV. 10 B). Three important regions can be identified in the Figure IV. 10 B which are the border of the sample, without channels (red arrow), the spacing between channels (blue arrow) and the micro-channels (green arrow). We can clearly appreciate how there are no HUVECs laying in the spacing region between channels, while all the HUVECs are laying inside the micro-channels.

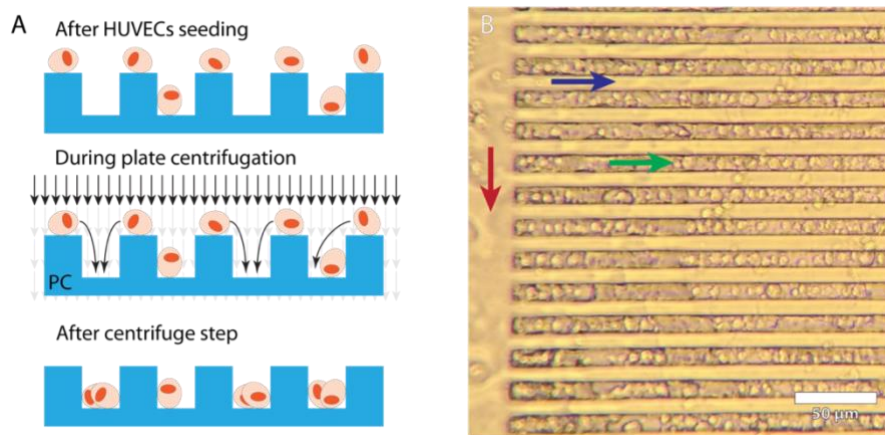


Figure IV. 10 - Investigation of centrifugation seeding approach. (A) Schematic representation of the seeding approach showing the initial condition of HUVECs after their seeding on the materials, the forces applied on the cells during the centrifugation step, and their new localization at the end of the centrifugation step. (B) Bright field image of HUVECs seeded uniquely inside the micro-channels after the centrifugation step. Green arrow indicate the micro-channels, blue arrow indicate the space between two channels and the red arrow indicate the flat region, without channel at the edge of the sample.

Raghavan *et al.* developed a microchannel structure in PDMS and seeded HUVECs cells into the channels using a similar approach to ours [65]. They reported that after the microchannels development, the material was immersed in liquid collagen and later, HUVECs resuspended in liquid collagen were seeded on the material surface and centrifugated to drive them into the channels (Figure I. 20) [65].

3.5. Time lapse epi- fluorescence microscopy

The very first evaluation of tube formation using HUVECs in PC- μ Ch functionalized materials was performed using the fluorescent microscope (LEICA DM5500B), equipped with the cell-culture chamber to maintain the proper temperature and CO₂ level constant. Lei *et al.* developed a time-lapse acquisition for 12 hours to investigate the development of capillary-like structures on flat-patterned PET material [166]. In this work the aim was to follow the evolution of the capillary formation in two-dimensional conditions, investigating the optimal time for the development of capillaries. However, in our experiment, an epifluorescence microscopy does not have enough resolution to visualize the complex three-dimensional structure developed inside the micro-channels of the PC. In addition to this, it is impossible in our case to define a priori one single focal plane to follow the three-dimensional evolution of the capillaries during the entire time of the experiment. On top of those limitations, the microscopy presents a focus drift which generates a shift in the imaged focal plane, altering the initial parameters selected to follow the capillary formation and making impossible to perform a precise analysis. For all those reasons, CLSM with higher resolution (Chapter III.3.3.1.) in the cross-view reconstruction and reduced focal drift was chosen for the further experiments.

3.6. Time-lapse confocal microscopy

In order to obtain a better resolution for the image analysis, CLSM (Chapter III.3.3.1.) was performed with a setup for long-term cell culture (Figure IV. 11). The setup consists of a temperature controller to maintain 37°C, and a 5% CO₂ supplier. A time-lapse acquisition was performed on multiple PC-QK biomaterials and on multiple micro-channels of the same sample from 10 minutes after cell seeding, to 840 min after cell seeding (Figure IV. 11). Our work wanted to follow the evolution of HUVECs during the development of capillaries structure, like in a previous work of Moon *et al.*, which report a time-lapse confocal video-microscopy of HUVECs alone

or HUVECs and 10T1/2 cells encapsulated in PEG-hydrogels to follow endothelial tubule formation for about 70 hours [91].

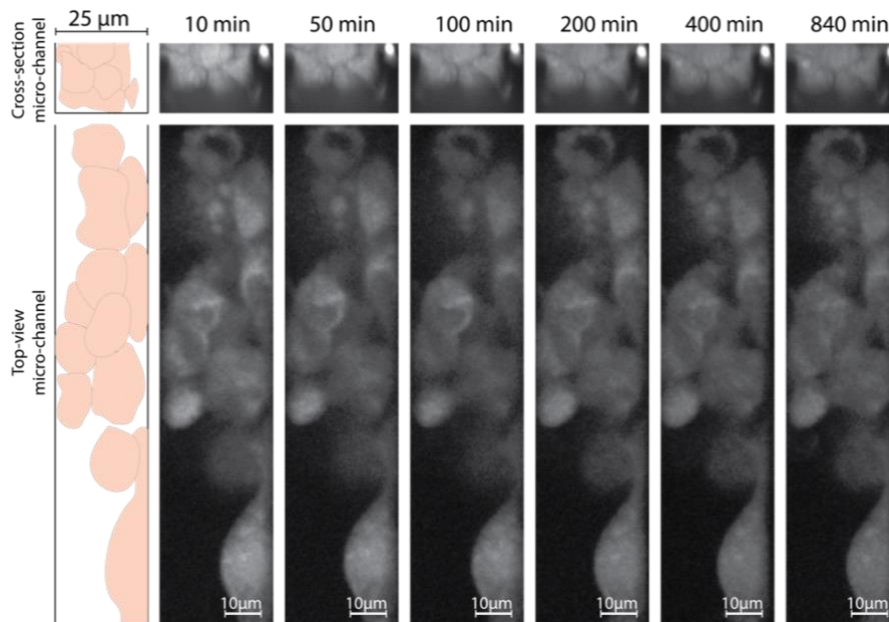


Figure IV. 11 – Time-lapse acquisition of HUVECs on PC- μ Ch-QK. Scheme of HUVECs seeded into PC- μ Ch-QK (first left) and CLSM images of time-lapse acquisition showing the cross section and top views at different time-points from 10 min after seeding up to 840 min after seeding.

Two different conclusions we can report from this analysis. The first one is concerning the auto-focus adjustment, in fact, no focus drift was detected during more than 13 hours of exposition resulting in a reliable method to maintain a stable acquisition.

The second conclusion is that cells are not moving during the entire time-set of acquisition, a clear indication of cell death from the beginning of the experiment. Therefore, even after implementing the set-up for the time-lapse acquisition in collaboration with the Bordeaux Imaging Center, it was not possible to reproduce experiments in a reliable way with this approach.

Two main causes can be identified. First, the transfer of cells between our cell culture facility and the facility of Bordeaux Imaging Center which resulted in a

stressful condition, due to long transfer without temperature and CO₂ supply. This leads to cell death even before starting the experiment. Second, even though a culture performed in-loco, cells underwent a rapid death and detachment within 30 min after the beginning of the experiment, indicating that some of the environmental parameters like temperature or the level of CO₂ were not adequately precise to ensure a long-lasting time-lapse experiment. Unfortunately, the insufficient time did not allow us to solve the problems linked to the culture transport and the environmental controls. However, the experiment was repeated using fixed time-points instead of a time-lapse, explained in the next section of this same chapter.

3.7. HUVECs on functionalized PC- μ Ch: late time-point investigation

In order to assess the proper time-point in which HUVECs would develop a tube-like structure, several samples were fixed at different times from 18 hours to 26 hours in the sample PC- μ Ch-RGD+QK. As result, HUVECs cells are able to grow both inside the micro-channels region (Figure IV. 12 brown arrows) and between two channels, in the upper space (Figure IV. 12 green arrows). However, the percentage of HUVECs growing between two channels is higher than the percentage of HUVECs growing inside the micro-channels. In fact, there seems to be a driving force for the HUVECs to migrate from the bottom of the channels, in which they were originally seeded through centrifugation approach, to the top of the channel spacing. This effect might be due to constriction of the small size of the channels or simply a migration effect from a higher concentrated region to a lower concentrated region and the fact that micro-channels were left open, inevitably allow to HUVECs a free degree of freedom to migrate.

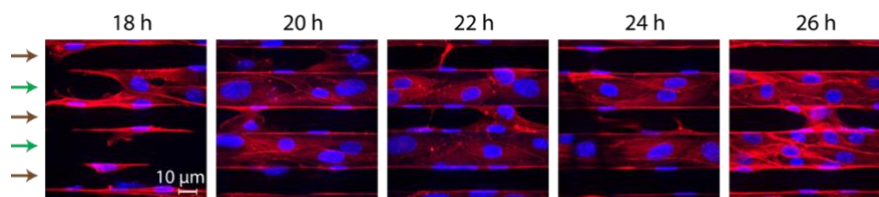


Figure IV. 12 – Fixed HUVECs cultured on PC- μ Ch-RGD+QK. CLSM images of HUVECs culture growing on PC- μ Ch-RGD+QK sample and fixed each 2 hours starting from 18h, ending at 26h after seeding. Brown arrows represent the micro-channel region, green arrows indicate the regions between two micro-channels. Nuclei colored in blue, and cytoskeleton in red.

After image analysis, no tubular-like structures were found both inside the micro-channels, nor in the spacing between channels, indicating that the following range of time-points would not suit for the development of those structures. A previous publication, however, showed how the initial formation of tubes around 21 hours was visualized when HUVECs are embedded into PEG-hydrogels [91] and after 24 hours for HUVECs embedded into collagen matrix and seed inside micro-channel structure of PDMS [65].

3.8. HUVECs on functionalized PC- μ Ch: wide time-point investigation

After the previous analysis with 5 time-points in the sample PC- μ CH-RGD+QK, a new experiment was performed to investigate a more broad range of possible time-points and evaluate the formation of tube-like structures in the different sample PC- μ Ch-RGD+SVV. Therefore, 11 time-points were acquired and analyzed using CLSM and Fiji software (Chapter III.4.1) in order to evaluate the spatial organization of cells inside and outside the micro-channels. HUVECs initially lay only inside the micro-channels (Figure IV. 13 4 h) both at the bottom and at the side of them, later they start to slowly migrate more on the side of the channels (Figure IV. 13 6 h, 8 h, 10 h) until they reach the upper part of the sample, in the interspace between two channels (Figure IV. 13 12 h). Starting from this point HUVECs start to be less present

inside the micro-channels and more present in the spacing region (Figure IV. 13 14 h, 16 h, 18 h), until the moment in which there is almost a complete migration of cells in the spacing between channels (Figure IV. 13 20 h, 22 h, 24 h).

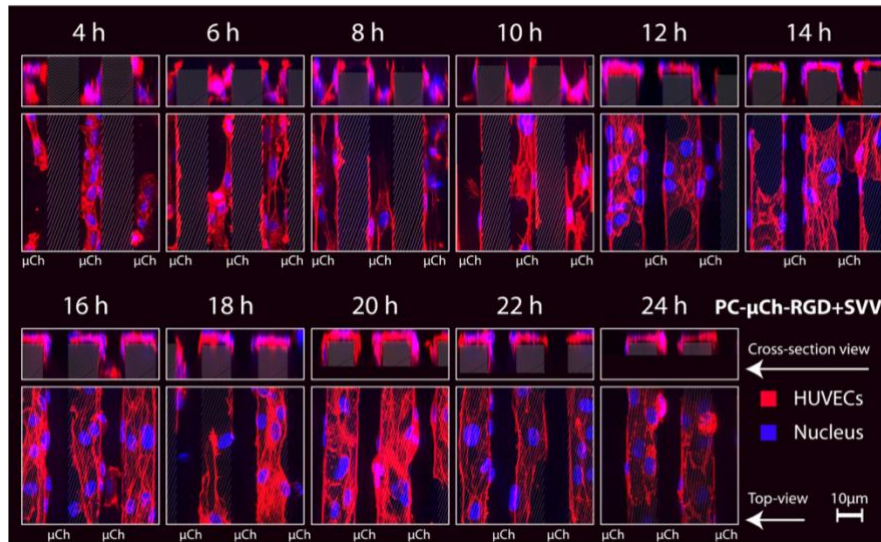


Figure IV. 13 - Fixed HUVECs cultured on PC- μ Ch-RGD+SVV. CLSM of HUVECs growing and migrating in PC- μ Ch-RGD+SVV sample. Indicated fixed samples from 4 hours after seeding up to 24 hours after seeding. Per each time-point, the upper rectangular image represent the cross-section view, while the square image represent the top-view of the sample. The white rectangles drawn upon each image represent the region with PC while micro-channels are indicated using their abbreviation (μ Ch). HUVECs were stained with red-cell tracker and the nucleus with DAPI.

The wide time-points analysis, unfortunately, did not show the expected formation of tube-like structures in any of the analyzed samples. However, a more clear understanding of cell migration was achieved following the general trend of HUVECs. In fact, HUVECs move from the bottom of the channels, which are originally confined thanks to the centrifugation seeding, to the side, and then the top part of the sample. Surprisingly, even if the spacing area between channels was previously scratched to remove the LbL and the immobilized peptides, seems that HUVECs found the way to interact with that material and migrate consequently.

3.9. HUVECs on functionalized PC- μ Ch: early time-point investigation

CLSM was performed on HUVECs cells, fixed each hour for 5 hours respectively to observe the formation of tubular structures with the empty lumen in the middle (Figure IV. 14 white arrows details). From the first sample, functionalized with RGD and QK peptides after 1 hour of HUVECs incubation cells just started the adhesion process inside the microchannels, as can be seen by their morphological shape which is still mostly round but with the presence of adhesion sites. In addition, all the cells are localized inside the channels, preferentially at the bottom of the channels (Figure IV. 14 A, 1h). After 2 hours HUVECs are already able to migrate from the bottom of the channels to the side and close the structure in a tubular-like morphology (Figure IV. 14 A, 2h white arrow). From the top view, the location of the tubular-like structure is indicated with a white dash line. After 3 hours HUVECs maintain their characteristic tubular-like structure (Figure IV. 14 A, 3h white arrow) but also they start to migrate between two channels in the inter-distance space region (Figure IV. 14 A, 3h). After 4 hours the presence of tubular-like structure is maintained (Figure IV. 14 A, 4h) and more HUVECs are migrating between two channels (Figure IV. 14 4h). After 5 hours all the HUVECs show the same morphology spreading both inside and outside the micro-channels, without the presence of tubular-like structure (Figure IV. 14 T5h).

The sample functionalized with RGD and SVV peptides after 1 hour of HUVECs incubation cells just started the adhesion process like in the previous material, mostly inside the microchannels (Figure IV. 14 1h). After 2 hours, HUVECs show the same morphological tubular-like structure as in the previous sample (Figure IV. 14 2h white arrow). After 3 hours HUVECs lose their capability to maintain the tubular-like structure and adhere on the materials' microchannels both on the bottom and the two sides (Figure IV. 14 3h white arrow) showing a reduced migration effect between the channels. After 4 hours HUVECs spread more outside of the channels, migrating from the channels to the top of the material (Figure IV. 14 B, 4h). After 5

hours all the HUVECs show an indiscriminate growth both inside and outside of the channels without the presence of tubular-like structure (Figure IV. 14 B, 5h).

The sample which is functionalized with LbL but without any adhesion nor angiogenic peptide, the formation of the tubular-like structure is completely absent during all the time points (Figure IV. 14 C). In all the time points analyzed, HUVECs preserve their round-shape morphology, showing a very limited capability of adhesion or migration from the bottom of the channels (Figure IV. 14 C, 1h-5h). Even at the last time point, HUVECs did not migrate between the channels, as shown for the other two materials.

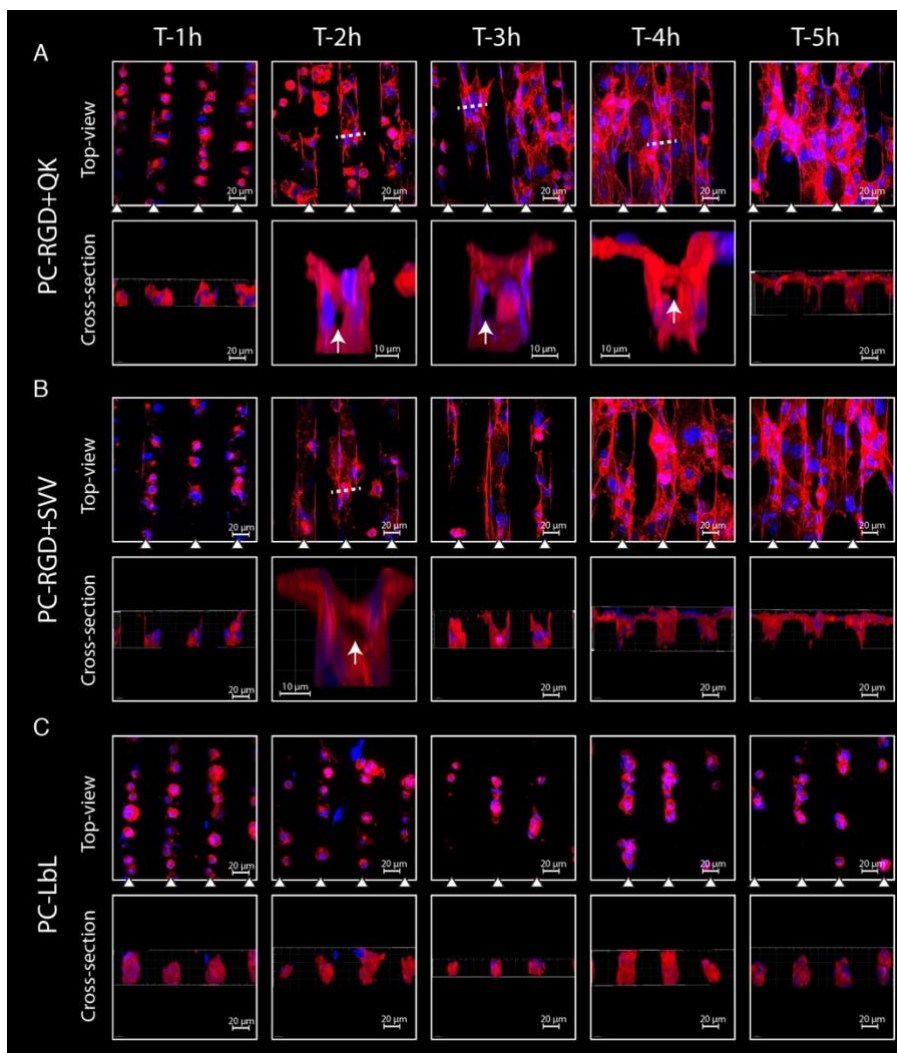


Figure IV. 14 – Tube-like structure formation on functionalized biomaterials. CLSM of HUVECs grown in three functionalized PC- μ Ch for 1 to 5 hours to evaluate the formation of tube-like structures. (A) PC- μ Ch-RGD+QK material induces the formation of tube-like structures (white arrows) after 2, 3 and 4 hours. (B) PC- μ Ch-RGD+SVV material induces the formation of tube-like structures after only 2 hours. (C) The PC-LbL material does not induce the formation of any tube-like structure. The little triangle indicate where micro-channels are located in the images.

HUVECs cells have been already investigated within micro-channels for transendothelial studies after reaching confluency [334]. In addition, Mori *et al.*

developed an interesting system of perfusable channels to supplement a skin-equivalent graft by seeding HUVECs in channels made of collagen of about 500 μm width [335]. Tocchio A *et al.* developed a perfusable micro-channels system using sacrificial templates fabrication and 2-hydroxyethyl methacrylate (HEMA), agarose and gelatin methacrylate (GelMA) seeded with HUVECs [336]. Those studies investigate the formation of microvasculature using larger channel size about 300 μm width, while our work focus on the smallest limit of a capillary vessel which present vessel diameter between 10 and 15 μm [29].

Thanks to the preparation of the proper size microchannels and functionalization with LbL and peptide the capillary tubes formation test was performed on three chemical conditions, using the same micro-channels structure size. Compared to the PC-LbL material, the peptides combinations largely improve HUVECs behave in term of adhesion onto the surface in the bottom but also sides of the micro-channels. In addition, with the time is clearly noticeable a migration effect of HUVECs through the side of the channels to the top of the sample, after 5h incubations. The formation of the tubular-like structure was more prominent after 2h incubation for both samples contains peptides, but only the PC-RGD+QK material allows the formation of the tubular-like structure for longer time-up to 4h after incubation.

In their previous investigation, Tsvirkun *et al.* reported a complete endothelialization of their PDMS micro-channels of 30-40 μm diameter. They used a microfluidic approach to seed HUVECs over two days and later incubate them for two weeks to see the complete coverage of the micro-channel lumen with endothelial cells [72]. Zheng *et al.* used a similar approach developing a complete endothelialized surface of their 200 μm micro-channels after 1 week of culture. Their approach involved the usage of collagen type I to favor the cellular adhesion and obtain a complete coverage of HUVECs in a shorter time [68]. Sivarapatna *et al.* used a microfluidic chip fabricated with PDMS with micro-channels of 200 μm , to seed HUVECs cells embedded in Collagen type I enriched with VEGF to obtain capillary structures after only 4 days of incubation under a constant flow [66]. Finally, Raghavan *et al.* used micro-channels of about 50 μm in size developed in PDMS. They embedded HUVECs in collagen type I, later seeded by centrifugation approach inside

the channels and they were able to observe the formation of capillary structures after only 24h of incubation using enriched media with bFGF and VEGF [65]. In our work, we substitute the VEGF factor with the more stable approach of mimetic peptide immobilization on a biofunctionalized layer-by-layer of Chitosan and Hyaluronic acid. In addition, we reduced the size of the microchannel and seed HUVECs non-embedded directly into the micro-channels using centrifugation approach. As result, the development of the first tube-like structure was observed after only 2 hours of HUVECs seeding. Therefore, the combination of biofunctionalization with LbL approach and peptide functionalization, together with the geometry and size of micro-channels seems an optimal substrate where HUVECs can change their morphology to develop a tube-like structure.

4. PART IV: Capillaries stabilization

4.1. HUVECs and hPC-PL stabilize tube-like structures

Co-culture experiments of HUVECs with hPC-PL were performed on PC- μ Ch-LbL-RGD+SVV samples and CLSM was performed on fixed cells to evaluate the formation and stabilization of tube-like structures during 2, 3 and 4 hours (Figure IV. 15). In this experiment, we focus on the interest in the cells located inside the μ Ch and we analyze the cross-section of each image to identify the tube-like structures. After 2 hours of monoculture with HUVECs, the formation of the tube-like structure with lumen component was observed (Figure IV. 15 upper image dash circle). When only HUVECs are present in the μ Ch, no lumen formation was observed at 3 and 4 hours (Figure IV. 15 left images). Once hPC-PL are introduced in the culture, the formation of lumen structure was observed both at 3 and 4 hours of incubation (Figure IV. 15 right images). However, no pericytes were found lying above HUVECs in the region presenting lumen, but they were located in a more distant place.

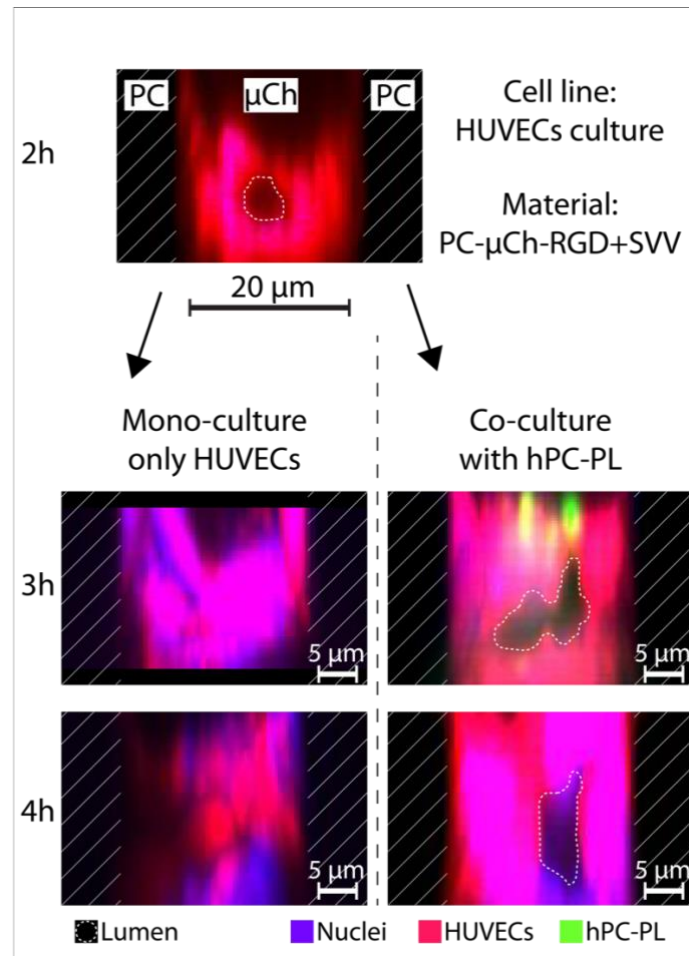


Figure IV. 15 – Tube-like structure stabilization by co-culture. CLSM of co-culture with HUVECs and hPC-PL. Mono-culture (left) and co-culture (right) were performed to compare the potential of stabilizing tube-like structures in the presence of pericytes. Blue marking with DAPI for cell nuclei, red marking for HUVECs cytoplasm with CMTPX and green marking for hPC-PL cytoplasm with CMFDA.

Co-culture systems, combining HUVECs with multiple cell lines have been already investigated for the stabilization of capillary-like structures [337]. In literature, the approaches which involve co-culture system between HUVECs and PCs are numerous and different. Therefore there is not a real agreement in the ratio between the two cells types, nor in the timing of seeding. Few examples can be

reported among the vast number of existing works. Tourovskaia *et al.* performed co-culture with HUVECS and PCs in ratio 3:1 into a microfluidic device which allows a constant perfusion [88]. Their approach involves an initial HUVECs seeding for 30 min followed by 4 days perfusion. After, PC were seeded and let adhere for 15 min before reconnecting to the perfusion system again. They report a successful angiogenesis in which PCs were recruited to the ECs vessels in presence of VEGF gradient with increasing sprout length (Figure I. 25 D). In another work, Morin *et al.* performed a co-culture with HUVECS and PCs in ratio 5:1 encapsulating both cell types at the same time in fibrin gel and culturing the system for 3 days [89]. The results reported in their work demonstrated the ability of HUVECs and PCs to form fully interconnected microvascular networks in fibrin gel developing longer structures with longer average length. In addition, the type of media used influence significantly the recruitment of PCs (Figure I. 27). Kim *et al.* used a microfluidic chip with different channels to investigate angiogenic sprout of HUVECS in the presence or not of hPC-PL [90]. Firstly, HUVECs were seeded for 30 min in the lateral micro-channels resuspended in their media, later hPC-PL were resuspended in fibrinogen-thrombin solution and injected into the central channel at ratio 10:1 [90]. They reported how after 4 days of co-culture, PCs were frequently found adjacent to the capillaries vessels with stretched morphology to cover the abluminal surface of endothelium. Particular detail also in the pericytes attachment to the endothelial-derived collagen IV basement membrane (Figure I. 28).

In our work, in order to prolong the tube-like structure in the PC-SVV+QK material for longer than 2 hours, a co-culture system of HUVECs and hPC-PL was developed. Analyzed samples show indeed the presence of tube-like structures only when the co-culture system is used, compared with HUVECs alone up to 4 hours after HUVECs incubation. This is an evidence on the formation of the tube-like structure after 2 hours of HUVECs culture, which persists up to 4 hours only when hPC-PL are added to the culture. The mechanism of stabilization in our case remains unclear, however, samples with tube-like structured did not require hPC-PL to be physically in contact with HUVECs, instead, they were located in a distal position than the tube, probably stabilizing the tube-like structure with released factors. It was indeed already proven

how HUVECs and pericytes communicate through the release of several factors such as angiopoietin1 and 2 through the TIE2 receptor [338]. In the work of Zhang *et al.* presented in Chapter I, the AngioChip represent an elegant experiment in which the contact between HUVECs and pericytes was prevented, but not their interaction through the released factors [94].

v. Conclusion and Perspectives

1. Conclusions

In this study, we fabricated micro-channels functionalized with adhesive peptide RGD, and angiogenic peptides SVV and QK, using an LbL assembled-thin film of naturally-derived polyelectrolytes hyaluronic acid and chitosan as anchoring layer. A variety of techniques were used to characterize the surface thickness, the molecular density, the physical and chemical topography of materials' surfaces for both flat and micro-channel biofunctionalized materials. Human umbilical vein endothelial cells (HUVECs) were cultured on flat and micro-channels biofunctionalized materials with and without peptides for various time points and the formation of tubular-like structures was observed. Specifically, we evaluated the metabolic activity of the cells, their organization in the material surface and their three-dimensional rearrangement inside the micro-environment. In addition, human pericytes derived from placenta (hPC-PL) were used to stabilize the tubular-like structures in order to improve the original approach and perform longer-term experiments. The general conclusions are as follow.

1.1. Regarding materials preparation and surface functionalization

Through the development of surface micropatterns and the functionalization method, we demonstrated that large-area surfaces of ordered arrays of microchannels can be fabricated on polycarbonate substrates using hot-embossing. Specifically, we succeeded in the development of three types of micro-channels geometry: (1) width of 22 μm , spacing of 100 μm and depth of 28 μm , (2) width of 22 μm , spacing of 50 μm and depth of 27 μm , and (3) width of 26 μm , spacing of 22,40 μm and depth of 25,86 μm . All those three geometries can be produced in a rapid and highly reproducible way. The current state-of-the-art in micro-vasculature focused most on the development of three-dimensional structure as small as 40 μm

and as large as 200 μm [65, 66, 72]. However, those structures differ from the size of capillaries *in vivo* and therefore can be classified as giant capillaries [69-71]. In this work, we succeeded to produce as small as 26 μm micro-channels, to better mimic the physiological conditions *in vivo* for capillaries size, representing therefore an original progress in the micro-vasculature development.

In addition, the homogeneous film of polysaccharides can be achieved on the PC substrate through layer-by-layer deposition. In fact, LbL films including a different number of hyaluronic acid and chitosan bilayers (4, 8, 12, 16, 20, and 24 bilayers) were successfully built up resulting in multilayered films with thickness ranging from 17 to 374 nm. Moreover, we investigated more deeply the LbL thickness for the architecture PC-PEI(HA/CHI)_{12.5}, used for the further biofunctionalization experiments. We showed that in liquid conditions, the 12.5 bi-layers swelled over 50 times, reaching a thickness of 6 μm . Taken together, these results confirm the previously investigated CHI/HA coating and the final thickness of the LbL cushion, demonstrating a reliable reproducibility of the technique for surface biofunctionalization [119]. Next, peptides of varying lengths were successfully grafted onto the layer-by-layer cushion using carbodiimide chemistry reaction. Firstly, the grafting conditions were optimized for the RGD sequence. Later, SVV and QK peptides were also immobilized and their grafted amount was quantified. Quantification of peptide grafting in the LbL would be more adequately represented as peptide/ cm^3 or mm^3 instead of peptide/ cm^2 or mm^2 , due to the non-negligible thickness of the LbL. However, as we did not find any reported peptide grafting density per unit of volume in the literature that would allow comparisons, we also reported the peptide grafting per unit of surface area. In the present work, the RGD grafting density was evaluated to be 18 ± 3 pmol/ mm^2 (11 molecules/ nm^2), between the one reported by Gribova *et al.* [316] and Leslie-Barbick *et al.* [317]. The SVV grafting density was evaluated to be 34 ± 4 pmol/ mm^2 (21 molecules/ nm^2) which was higher than previously investigated by Le Saux *et al.* [319] and Zouani *et al.* [170]. Finally, the QK grafting density was evaluated to be 55 pmol/ mm^2 (33 molecules/ nm^2) which was equal with the density achieved by Chan *et al.* [320] and

comparable with the range investigated in the PEG hydrogels by Leslie-Barbick *et al.* [317].

Finally, the selective functionalization into the microchannels, through the removal of the LbL from the inter-channel space was proven by the difference of the fluorescence signal from the scratched region and the non-scratched region of the same sample.

Hence, the successful fabrication of micro-channels and their biofunctionalization, allow proceeding for the biological investigations in terms of HUVECs adhesion and capillary tube-like formation and stabilization.

1.2. Regarding mono-culture on functionalized PC materials

In terms of culture on materials without micro-channels, HUVECs were cultured on PC-LbL, PC-RGD, PC-SVV, PC-QK, PC-RGD+SVV, PC-RGD+QK in order to evaluate which material would give a higher cell metabolism as well as which material would allow an higher cell adhesion. More HUVECs adhere initially on PC-RGD surface, compared to the other grafted peptides or without peptides, and therefore the overall metabolic activity of the sample result higher. Once the metabolic activity is corrected for the cell number per each sample, a clear evidence of higher material's impact result for peptides combination of RGS+SVV and RGS+QK. A definitive conclusion that this material would be the best condition for our experiment cannot be taken at this step, however, this preliminary result helps us to focus on the peptides-combination materials conditions for the further experiments.

HUVECs were cultured on three PC- μ Ch functionalized materials: LbL, RGD+SVV, and RGD+QK. Formations of tubular-like structures were observed only in the samples containing the peptides and only during the early stage of seeding. Specifically, monoculture condition in RGD+QK allows the formation of tube-like structure starting from 2h, up to 4h after HUVECs seeding. The material condition with RGD+SVV peptide showed a similar tube-like formation at 2h after seeding but not further in the time-points. Therefore, in terms of material functionalization, for

the monoculture condition, the combination of peptides RGD+QK provide a stronger stabilization of the tubular structure for a longer time than the other tested conditions. This exciting result introduces new possibility of functionalization to obtain a rapid development of tubular-like structures after just 2 hours of cell seeding, compared to the previously investigated approach in which lumen formation was observed only later than 12 hours [65, 66, 68, 72] We expected to have a positive formation of tubular structure using QK, as previously reported in literature, however, the very rapid development found in our work provides an original appealing strategy to further develop a more stable system.

1.3. Regarding co-culture on functionalized PC materials

In terms of co-culture condition with HUVECs and hPC-PL, the material PC- μ Ch-RGD+SVV was tested in order to evaluate a stabilization of the tube-like structures with the time. Firstly, the formation of the tube-like structure was newly evaluated for monoculture condition with only HUVECs as the negative control for tube like-formation later than 2h. After this proof, co-culture was tested seeding HUVECs first, and after 2h the hPC-PL for other 2h. Compared with previous works [90, 91, 93] we reported for the first time an early development of capillary structure and persistence at very early time-point of the investigation. In fact, the formation of the tube-like structure was found both after 3h and 4h after HUVECs seeding, indicating an effective stabilization operated by the second cell line. However, in the previously reported work, the tube-like structures were investigated also for late-time point, as long as 69 hours [91], which we could not achieve in our case for equipment and time limitations. In our studies, the confocal images reveal how the pericytes are not strictly required to be in contact with the tube-like structure in order to stabilize it, and therefore a mechanism which involves soluble factors is likely to happen.

2. Perspectives and future work

2.1. Comparison with single-peptide functionalization

We plan to perform the same experiments of mono- and co-culture previously explained, using the material PC-RGD in order to assess if the absence of angiogenic peptides would lead to the formation of capillaries, even if unlikely possible since RGD is well known in processes of cellular adhesion and not for angiogenic properties. In addition, the materials PC-SVV, and PC-QK could be tested to evaluate if the angiogenic effect of the peptides, even in the absence of a strong adhesion normally enhanced by RGD sequence, would be sufficient to induce the formation of tube-like structures.

2.2. Investigate genetic pathways involved in angiogenesis

We also originally planned to perform real-time quantitative polymerase chain reaction (RT-qPCR) together with the tube-like observation at the CLSM, investigating pathways involved in angiogenesis. This would assess if the combination of geometry and chemistry would trigger the activation of angiogenic pathways such as Vascular Endothelial Growth Factor Receptor 2 (KDR) [200], Vascular Endothelial Growth Factor Receptor 1 (FLT1) [200, 339], Angiopoietin-1 Receptor (TEK) [339], Fibroblast Growth Factor 2 (FGF2) [194], Platelet And Endothelial Cell Adhesion Molecule 1 (PECAM1) [340], and Tyrosine Kinase With Immunoglobulin-Like And EGF Like Domains 1 (TIE1) [339]. The process of angiogenesis is controlled by a complex expression of proteins which directly influences and guide cellular signals through the interaction of their receptors. VEGF and FGF-2 have been utilized frequently to develop new capillary vessels, as well as the angiopoietins family. Therefore, the gene expression of the receptors capable of

recognizing and triggering the intracellular signal is fundamental to complete our studies of tube-like development, performed with CLSM.

2.3. Time-lapse analysis for tube-like formation

Once the best conditions for mono- and co-culture would be confirmed by the combination of CLSM and RT-qPCR, a deep investigation of the formation of the tube-like structure can be performed using time-lapse CLSM. We already started the preliminary experiments to define the optimal parameters in order to perform the experiment, however, the cell survival was not sufficient to allow a stable culture. The problem of cell death was most probably caused by two different conditions: first, the transfer of the biofunctionalized material with the cell culture between the biological laboratory to the Bordeaux Imaging Center facility for time-lapse acquisition, inevitably induced cell stress due to lack of constant temperature and CO₂ level. Second, the cell-culture chamber mounted on the CLSM was probably not precisely adjusted at the 37°C and 5% CO₂ level, fundamental for a long-lasting cell culture incubation. Therefore, performing the cell-seeding in the same facility as the CLSM, and improving the cell-culture chamber conditions at the CLSM would lead to a successful acquisition of time-lapse video to follow the development of the capillary-like structures inside the biofunctionalized micro-channels.

2.4. Choice of cell line for the endothelial line and supporting cells

Primary endothelial cells are constantly used for the purpose of investigating and reproducing vascularization. However, the final choice of which type of endothelial cell can differ, depending on the aim of the experiments [26]. HUVECs are in fact the most commonly used for *in vitro* studies and fundamental studies. Another possibility is the use of human adipose microvascular endothelial cells (HAMECs)

which are mature primary endothelial cells easily isolated from adults (and therefore practical for autologous procedures). In addition, they showed impressive angiogenic and vasculogenesis capacities, both *in vitro* and *in vivo* [26, 341]. Endothelial progenitor cells (EPCs) constitute another promising source of endothelial cells, in fact, it is possible to isolate them directly from the peripheral blood [342] with high angiogenic capacities [26]. There are two main sub-population of EPCs named early EPCs and outgrowth endothelial cells (OECs) [343].

Apart from the endothelial cells, all types of vessels also include supporting mural cells such as pericytes. In order to create *in vitro* long-lasting, stable blood vessels, endothelial cells must be co-cultured with mural cell [26]. Therefore, pericytes have been largely used, but not exclusively. In fact, fibroblasts [344] and smooth muscle cells [345] were used as well together with other mesenchymal stem cells [341]. However, there is not yet an agreement on which supporting mural cell would be the best for a stable vascular structure *in vitro* or *in vivo* [26].

2.5. Application of microfluidic system

The creation of a microfluidic chip of Polycarbonate could push forward the research for a stable development of functional capillary vessels, under constant flow conditions to mimic more accurately the physiological environment of the human body, such as the shear stress. In fact, several studies in literature prove how the shear stress triggers specific mechano-receptors on the endothelial cell's surface, improving their alignment, change in morphology, migration, development of capillary structure and finally the stabilization of such structures [54, 61, 66, 76]. A microfluidic chip is a pattern of microchannels molded or engraved in which at least two output holes are built through the chip and serve as inlet and outlet for the flow of the liquid [346]. Microfluidic chips can easily handle fluids no matter the area of application. The design of the microchannels network must be adapted to meet the requirements, thus, the materials for microfluidic chips employed should also be adequate and present the appropriate properties. In our case PC have been used to successfully produce micro-channels with hot-embossing techniques. Although

some scientists successfully built PC chips, they used thermal bonding procedures which are unfortunately known to be a process that doesn't provide good bonds even when the temperature is slightly too low [346]. Moreover, thermal bonding also significantly alters the geometry of the channels when the temperature is high enough to ensure bonding [346]. Therefore, optimizations are firstly required to properly develop a microfluidic chip in the PC.

Through the microfluidic approach, it would be possible to bio-functionalize selectively the microchannels with the LbL of Chitosan/hyaluronic acid and in addition immobilize the adhesive RGD peptide and the angiogenic SVV and QK peptides. Finally, HUVECs can be seeded and let adhere for some time, before applying the constant physiological flow. In addition, co-culture could be performed seeding hPC-PL together with the HUVECs or in a second moment, investigating which procedure would allow a faster and more stable formation of capillary vessels.

2.6. Moving towards clinical application

Our novel approach is not yet properly optimized to be transferred to a clinical approach. However, some considerations can be already done for a possible future perspective approach in clinics.

The model material used in this study, Polycarbonate, is biocompatible but not biodegradable and therefore, a proper substitute should be investigated to not-implant directly this material *in vivo*, even if, nowadays, the best candidate has not been found yet.

To work efficiently, immediately after implantation, the micro-vasculature should be surgically connected to the macro vasculature of the patient. This is nowadays not possible due to technical and surgical limitations. However, in the future, the possibility to develop a more complex vascular network composed of both capillaries, arterioles, and arteries, would allow the surgeon to micro-surgically join the own patient's blood vessels with the newly implanted vessel network.

Another interesting approach would be to properly remove the developed capillary vessels from the three-dimensional micro-channels, without compromising their

structure or function. Two main approaches can be used to achieve this goal: the peeling out of the capillaries using a solution collagen after crosslinking, as previously reported in the work of Raghavan *et al.* [65]. Alternatively, the usage of the thermo-responsive system can be used, such as poly(N-isopropylacrylamide). This interesting polymer has been already used to harvest cell sheets, briefly, above its lower critical solution temperature (LCST) cells are capable of adhesion and growth. But below the LCST, the polymer undergoes a structural transition changing from the hydrophobic to the hydrophilic state, allowing an efficient cell detachment [347]. We could transfer this technology into the microchannel and modify the temperature of the system to efficiently release the capillaries when mature.

Appendices

1. Appendix 1: Scientific communication

Scientific publications

- ❖ Bruno Aor, Irfan Khan, Karine Glinel, Alain M. Jonas, Sophie Demoustier-Champagne, Marie-Christine Durrieu. Microchannel Molding and Layer-by-layer Approach for the Formation of 3D Tube-like Structures by Endothelial Cells. Under submission to BIOMATERIALS journal.

Oral and poster presentations

2016

- Engineering micro-channels for vascularization in bone tissue engineering (Oral communication), Bruno Aor, Laurent Plawinski, Karine Glinel, Alain M. Jonas, Sophie Demoustier-Champagne, Marie-Christine Durrieu. EJD-FunMat training school 2016, Bordeaux – France, March 13th-18th 2016.
- Engineering micro-channels for vascularization in bone tissue engineering (Poster session), Bruno Aor, Laurent Plawinski, Karine Glinel, Alain M. Jonas, Sophie Demoustier-Champagne, Marie-Christine Durrieu. 2nd Workshop of Regenerative Medicine in Bordeaux, Bordeaux – France, October 24th - 26th 2016.

2017

- Engineering micro-channels for vascularization in bone tissue engineering (Oral communication), Bruno Aor, Laurent Plawinski, Karine Glinel, Alain M. Jonas, Sophie Demoustier-Champagne, Marie-Christine Durrieu. EJD-FunMat training school 2017, Aveiro - Portugal.

- Engineering micro-channels for vascularization in bone tissue engineering (Poster session), Bruno Aor, Laurent Plawinski, Karine Glinel, Alain M. Jonas, Sophie Demoustier-Champagne, Marie-Christine Durrieu. EJD-FunMat training school 2017, Aveiro - Portugal, March 26th-31st 2017.
- Engineering micro-channels for vascularization in bone tissue engineering (Poster session), Bruno Aor, Laurent Plawinski, Karine Glinel, Alain M. Jonas, Sophie Demoustier-Champagne, Marie-Christine Durrieu. 10 Years of Research at CBMN, Talence - France, April 6th-7th 2017.
- Engineering micro-channels for vascularization in bone tissue engineering (Poster session), Bruno Aor, Laurent Plawinski, Karine Glinel, Alain M. Jonas, Sophie Demoustier-Champagne, Marie-Christine Durrieu. 19e Journée de l'École Doctorale des Sciences Chimiques de l'Université de Bordeaux, Bordeaux – France, May 5th 2017.
- Engineering micro-channels for vascularization in bone tissue engineering (Oral communication), Bruno Aor, Laurent Plawinski, Karine Glinel, Alain M. Jonas, Sophie Demoustier-Champagne, Marie-Christine Durrieu. Young scientist day FR TransBioMed with TecSan, Bordeaux Cedex – France, May 17th 2017.
- Engineering micro-channels for vascularization in bone tissue engineering (Flash-Poster session), Bruno Aor, Laurent Plawinski, Karine Glinel, Alain M. Jonas, Sophie Demoustier-Champagne, Marie-Christine Durrieu. Journée Scientifique de la FR TecSan, Bordeaux – France, June 22nd 2017.
- Engineering micro-channels for vascularization in bone tissue engineering (Oral presentation with Poster), Bruno Aor, Laurent Plawinski, Karine Glinel, Alain M. Jonas, Sophie Demoustier-Champagne,

Marie-Christine Durrieu. Summer School 2017: PhD program in Biomedical Engineering "Nanomedicine", Saas-Fee – Switzerland, June 25th-30th 2017.

- Behavior of human umbilical vein endothelial cells on polysaccharide coatings grafted with adhesive and angiogenetic peptides (Flash-Poster session), Bruno Aor, Laurent Plawinski, Karine Glinel, Alain M. Jonas, Sophie Demoustier-Champagne, Marie-Christine Durrieu. 28th annual conference of the european society for biomaterials, Athens, Greece, 4-8 September 2017.

2018

- A novel potential approach to develop capillary vessels (Oral communication), Bruno Aor, Laurent Plawinski, Karine Glinel, Alain M. Jonas, Sophie Demoustier-Champagne, Marie-Christine Durrieu. EJD-FunMat training school 2018, Luxembourg, March 18th - 23rd 2018.
- Behavior of human umbilical vein endothelial cells on polysaccharide coatings grafted with adhesive and angiogenetic peptides (Poster), Bruno Aor, Laurent Plawinski, Karine Glinel, Alain M. Jonas, Sophie Demoustier-Champagne, Marie-Christine Durrieu. EJD-FunMat training school 2018, Luxembourg, March 18th - 23rd 2018.

Reference

1. Sadtler, K., et al., *Design, clinical translation and immunological response of biomaterials in regenerative medicine*. Nature Reviews Materials, 2016. **1**(7): p. 16040.
2. Krafs, K.P., *Tissue repair: The hidden drama*. Organogenesis, 2010. **6**(4): p. 225-233.
3. Xia, H., et al., *Tissue repair and regeneration with endogenous stem cells*. Nature Reviews Materials, 2018: p. 1.
4. Kumar, V., et al., *Robbins and Cotran pathologic basis of disease, professional edition e-book*. 2014: elsevier health sciences.
5. Chen, F.-M. and X. Liu, *Advancing biomaterials of human origin for tissue engineering*. Progress in polymer science, 2016. **53**: p. 86-168.
6. Tang, D., et al., *Biofabrication of bone tissue: approaches, challenges and translation for bone regeneration*. Biomaterials, 2016. **83**: p. 363-382.
7. Loi, F., et al., *Inflammation, fracture and bone repair*. Bone, 2016. **86**: p. 119-130.
8. Liu, M., et al., *Injectable hydrogels for cartilage and bone tissue engineering*. Bone research, 2017. **5**: p. 17014.
9. Albrektsson, T. and C. Johansson, *Osteoinduction, osteoconduction and osseointegration*. European spine journal, 2001. **10**(2): p. S96-S101.
10. Chang, W.G. and L.E. Niklason, *A short discourse on vascular tissue engineering*. NPJ Regenerative medicine, 2017. **2**(1): p. 7.
11. González-Molina, M., et al., *Immune response and histology of humoral rejection in kidney transplantation*. nefrologia, 2016. **36**(4): p. 354-367.
12. Assenmacher, A.T., et al., *Long-term outcomes after osteochondral allograft: a systematic review at long-term follow-up of 12.3 years*. Arthroscopy: The Journal of Arthroscopic & Related Surgery, 2016. **32**(10): p. 2160-2168.
13. Goldberg, V.M., *Natural history of autografts and allografts*, in *Bone implant grafting*. 1992, Springer. p. 9-12.
14. Oryan, A., et al., *Bone regenerative medicine: classic options, novel strategies, and future directions*. Journal of orthopaedic surgery and research, 2014. **9**(1): p. 18.
15. JP, L.R.V., *Tissue engineering*. Science, 1993. **260**(5110): p. 920-926.
16. Williams, D.F., *The biomaterials conundrum in tissue engineering*. Tissue Engineering Part A, 2014. **20**(7-8): p. 1129-1131.
17. Williams, D.F., *On the nature of biomaterials*. Biomaterials, 2009. **30**(30): p. 5897-5909.
18. Williams, D.F., *On the mechanisms of biocompatibility*. Biomaterials, 2008. **29**(20): p. 2941-2953.
19. J. Gordon Betts, T.J.C., et al., *Anatomy and Physiology*, ed. OpenStax. 2013.
20. Novosel, E.C., C. Kleinhans, and P.J. Kluger, *Vascularization is the key challenge in tissue engineering*. Advanced drug delivery reviews, 2011. **63**(4-5): p. 300-311.
21. Brockport, C.A., et al., *Anatomy and Physiology II*, O.e. access, Editor., Lumen learning: Lumen learning.
22. Buschmann, I. and W. Schaper, *The pathophysiology of the collateral circulation (arteriogenesis)*. The Journal of pathology, 2000. **190**(3): p. 338-342.

23. Murohara, T., *Therapeutic vasculogenesis using human cord blood-derived endothelial progenitors*. Trends in cardiovascular medicine, 2001. **11**(8): p. 303-307.
24. Adams, R.H. and R. Klein, *Eph receptors and ephrin ligands: essential mediators of vascular development*. Trends in cardiovascular medicine, 2000. **10**(5): p. 183-188.
25. Lindner, V. and T. Maciag, *The putative convergent and divergent natures of angiogenesis and arteriogenesis*. 2001, Am Heart Assoc.
26. van Hinsbergh, V.W., *Angiogenesis: Basics of Vascular Biology*, in *Vascularization for Tissue Engineering and Regenerative Medicine*. 2016, Springer. p. 1-29.
27. Peirce, S.M. and T.C. Skalak, *Microvascular remodeling: a complex continuum spanning angiogenesis to arteriogenesis*. Microcirculation, 2003. **10**(1): p. 99-111.
28. Burri, P.H. and V. Djonov, *Intussusceptive angiogenesis—the alternative to capillary sprouting*. Molecular aspects of medicine, 2002. **23**(6): p. 1-27.
29. Kannan, R.Y., et al., *The roles of tissue engineering and vascularisation in the development of micro-vascular networks: a review*. Biomaterials, 2005. **26**(14): p. 1857-1875.
30. Takuwa, Y., et al., *Roles of sphingosine-1-phosphate signaling in angiogenesis*. World journal of biological chemistry, 2010. **1**(10): p. 298.
31. Marenzana, M. and T.R. Arnett, *The key role of the blood supply to bone*. Bone research, 2013. **1**(3): p. 203.
32. Muylaert, D.E., et al., *Early in-situ cellularization of a supramolecular vascular graft is modified by synthetic stromal cell-derived factor-1 α derived peptides*. Biomaterials, 2016. **76**: p. 187-195.
33. Gui, L., et al., *Implantable tissue-engineered blood vessels from human induced pluripotent stem cells*. Biomaterials, 2016. **102**: p. 120-129.
34. Best, C., et al., *Deconstructing the tissue engineered vascular graft: evaluating scaffold pre-wetting, conditioned media incubation, and determining the optimal mononuclear cell source*. ACS biomaterials science & engineering, 2016. **3**(9): p. 1972-1979.
35. Mitchell, G.M. and W.A. Morrison, *In vitro and in vivo approaches for pre-vascularization of 3-dimensional engineered tissues*, in *Vascularization for Tissue Engineering and Regenerative Medicine*. 2017, Springer. p. 1-27.
36. Zhu, W., et al., *Direct 3D bioprinting of prevascularized tissue constructs with complex microarchitecture*. Biomaterials, 2017. **124**: p. 106-115.
37. Kang, H.-W., et al., *A 3D bioprinting system to produce human-scale tissue constructs with structural integrity*. Nature biotechnology, 2016. **34**(3): p. 312.
38. Carmeliet, P. and R.K. Jain, *Angiogenesis in cancer and other diseases*. nature, 2000. **407**(6801): p. 249.
39. Folkman, J. and M. Hochberg, *Self-regulation of growth in three dimensions*. Journal of Experimental Medicine, 1973. **138**(4): p. 745-753.
40. Zhu, W., Y.J. Chuah, and D.-A. Wang, *Bioadhesives for Internal Medical Applications: A Review*. Acta biomaterialia, 2018.

41. Mazzitelli, D., et al., *Complete aortic valve cusp replacement in the pediatric population using tissue-engineered bovine pericardium*. The Annals of thoracic surgery, 2015. **100**(5): p. 1923-1925.
42. Takazawa, K., et al., *Evaluation of magnetic resonance imaging and clinical outcome after tissue-engineered cartilage implantation: prospective 6-year follow-up study*. Journal of Orthopaedic Science, 2012. **17**(4): p. 413-424.
43. Raya-Rivera, A., et al., *Tissue-engineered autologous urethras for patients who need reconstruction: an observational study*. The lancet, 2011. **377**(9772): p. 1175-1182.
44. Shevchenko, R., et al., *A step towards an artificial skin: a novel supermacroporous anisotropic cryogel for wound healing applications*. International Journal of Artificial Organs, 2010. **33**(7): p. 426-427.
45. Lokmic, Z. and G.M. Mitchell, *Engineering the microcirculation*. Tissue Engineering Part B: Reviews, 2008. **14**(1): p. 87-103.
46. Lab, K. *Angiogenesis - Overview of the role of Angiopoietins and VEGF*. Available from: http://people.duke.edu/~cdkontos/Kontos_Lab/Angiogenesis_8.html.
47. Holthoner, W., et al., *Vascularization for Tissue Engineering and Regenerative Medicine*. 2019: Springer International Publishing. 400.
48. Di Cio, S. and J.E. Gautrot, *Cell sensing of physical properties at the nanoscale: Mechanisms and control of cell adhesion and phenotype*. Acta biomaterialia, 2016. **30**: p. 26-48.
49. Khalili, A.A. and M.R. Ahmad, *A review of cell adhesion studies for biomedical and biological applications*. International journal of molecular sciences, 2015. **16**(8): p. 18149-18184.
50. Black, A.F., et al., *In vitro reconstruction of a human capillary-like network in a tissue-engineered skin equivalent*. The FASEB Journal, 1998. **12**(13): p. 1331-1340.
51. Black, A., et al., *A novel approach for studying angiogenesis: a human skin equivalent with a capillary-like network*. Cell biology and toxicology, 1999. **15**(2): p. 81-90.
52. Nguyen, L.L. and P.A. D'Amore, *Cellular interactions in vascular growth and differentiation*. 2001.
53. Pinney, E., et al., *Human three-dimensional fibroblast cultures express angiogenic activity*. Journal of cellular physiology, 2000. **183**(1): p. 74-82.
54. Iruela-Arispe, M.L. and G.E. Davis, *Cellular and molecular mechanisms of vascular lumen formation*. Developmental cell, 2009. **16**(2): p. 222-231.
55. Jones, E.A., F. le Noble, and A. Eichmann, *What determines blood vessel structure? Genetic prespecification vs. hemodynamics*. Physiology, 2006. **21**(6): p. 388-395.
56. MBinfo, *Mechanisms of tube formation*.
57. Avraamides, C.J., B. Garmy-Susini, and J.A. Varner, *Integrins in angiogenesis and lymphangiogenesis*. Nature Reviews Cancer, 2008. **8**(8): p. 604.
58. Jaffe, E.A., et al., *Culture of human endothelial cells derived from umbilical veins. Identification by morphologic and immunologic criteria*. The Journal of clinical investigation, 1973. **52**(11): p. 2745-2756.

59. Perry, L., et al., *Co-culture systems for vasculogenesis*. *Vascularization for Tissue Engineering and Regenerative Medicine*, 2017: p. 1-29.
60. Bouïs, D., et al., *Endothelium in vitro: a review of human vascular endothelial cell lines for blood vessel-related research*. *Angiogenesis*, 2001. **4**(2): p. 91-102.
61. Park, H.-J., et al., *Human umbilical vein endothelial cells and human dermal microvascular endothelial cells offer new insights into the relationship between lipid metabolism and angiogenesis*. *Stem cell reviews*, 2006. **2**(2): p. 93-101.
62. Burns, M.P. and N. DePaola, *Flow-conditioned HUVECs support clustered leukocyte adhesion by coexpressing ICAM-1 and E-selectin*. *American Journal of Physiology-Heart and Circulatory Physiology*, 2005. **288**(1): p. H194-H204.
63. Kokura, S., et al., *Molecular mechanisms of neutrophil-endothelial cell adhesion induced by redox imbalance*. *Circulation Research*, 1999. **84**(5): p. 516-524.
64. Zhang, W., et al., *Communication between malignant glioma cells and vascular endothelial cells through gap junctions*. *Journal of neurosurgery*, 2003. **98**(4): p. 846-853.
65. Raghavan, S., et al., *Geometrically controlled endothelial tubulogenesis in micropatterned gels*. *Tissue Engineering Part A*, 2010. **16**(7): p. 2255-2263.
66. Sivarapatna, A., et al., *Engineered Microvasculature in PDMS Networks Using Endothelial Cells Derived from Human Induced Pluripotent Stem Cells*. *Cell transplantation*, 2017. **26**(8): p. 1365-1379.
67. Hohenwarter, O., et al., *Expression of SV40 tumour antigens enables human endothelial cells to grow independently from foetal calf serum and exogenous growth factors*. *Journal of biotechnology*, 1994. **34**(2): p. 205-211.
68. Zheng, Y., et al., *In vitro microvessels for the study of angiogenesis and thrombosis*. *Proceedings of the National Academy of Sciences*, 2012. **109**(24): p. 9342-9347.
69. Warren, B., et al., *The microcirculation in two transplantable melanomas of the hamster II. Scanning electron microscopy*. *Cancer letters*, 1978. **4**: p. 117-124.
70. Monticone, G., et al., *Quantitative nailfold capillary microscopy findings in patients with acrocyanosis compared with patients having systemic sclerosis and control subjects*. *Journal of the American Academy of Dermatology*, 2000. **42**(5): p. 787-790.
71. Vayssairat, M., et al., *Clinical significance of subcutaneous calcinosis in patients with systemic sclerosis. Does diltiazem induce its regression?* *Annals of the rheumatic diseases*, 1998. **57**(4): p. 252-254.
72. Tsvirkun, D., et al., *Microvasculature on a chip: study of the Endothelial Surface Layer and the flow structure of Red Blood Cells*. *Scientific reports*, 2017. **7**: p. 45036.
73. Covas, D.T., et al., *Multipotent mesenchymal stromal cells obtained from diverse human tissues share functional properties and gene-expression profile with CD146+ perivascular cells and fibroblasts*. *Experimental hematology*, 2008. **36**(5): p. 642-654.

74. Murray, I.R., et al., *Natural history of mesenchymal stem cells, from vessel walls to culture vessels*. Cellular and Molecular Life Sciences, 2014. **71**(8): p. 1353-1374.
75. Crisan, M., et al., *A perivascular origin for mesenchymal stem cells in multiple human organs*. Cell stem cell, 2008. **3**(3): p. 301-313.
76. Gökçinar-Yagci, B., D. Uçkan-Çetinkaya, and B. Çelebi-Saltik, *Pericytes: properties, functions and applications in tissue engineering*. Stem Cell Reviews and Reports, 2015. **11**(4): p. 549-559.
77. Crisan, M., et al., *Perivascular cells for regenerative medicine*. Journal of cellular and molecular medicine, 2012. **16**(12): p. 2851-2860.
78. Nees, S., et al., *Isolation, bulk cultivation, and characterization of coronary microvascular pericytes: the second most frequent myocardial cell type in vitro*. American Journal of Physiology-Heart and Circulatory Physiology, 2011. **302**(1): p. H69-H84.
79. Andreeva, E., et al., *Continuous subendothelial network formed by pericyte-like cells in human vascular bed*. Tissue and Cell, 1998. **30**(1): p. 127-135.
80. Goumans, M.J., et al., *Balancing the activation state of the endothelium via two distinct TGF- β type I receptors*. The EMBO journal, 2002. **21**(7): p. 1743-1753.
81. Sato, T.N., et al., *Distinct roles of the receptor tyrosine kinases Tie-1 and Tie-2 in blood vessel formation*. Nature, 1995. **376**(6535): p. 70.
82. Maisonpierre, P.C., et al., *Angiopoietin-2, a natural antagonist for Tie2 that disrupts in vivo angiogenesis*. Science, 1997. **277**(5322): p. 55-60.
83. Hoch, R.V. and P. Soriano, *Roles of PDGF in animal development*. Development, 2003. **130**(20): p. 4769-4784.
84. Darland, D.C. and P.A. D'Amore, *Blood vessel maturation: vascular development comes of age*. The Journal of clinical investigation, 1999. **103**(2): p. 157-158.
85. Kitahara, T., et al., *Mesangial cells stimulate differentiation of endothelial cells to form capillary-like networks in a three-dimensional culture system*. Nephrology Dialysis Transplantation, 2004. **20**(1): p. 42-49.
86. Nehls, V., E. Schuchardt, and D. Drenckhahn, *The effect of fibroblasts, vascular smooth muscle cells, and pericytes on sprout formation of endothelial cells in a fibrin gel angiogenesis system*. Microvascular research, 1994. **48**(3): p. 349-363.
87. Sims, D.E., *Diversity within pericytes*. Clinical and Experimental Pharmacology and Physiology, 2000. **27**(10): p. 842-846.
88. Tourovskaia, A., et al., *Tissue-engineered microenvironment systems for modeling human vasculature*. Experimental biology and medicine, 2014. **239**(9): p. 1264-1271.
89. Morin, K.T., et al., *Aligned human microvessels formed in 3D fibrin gel by constraint of gel contraction*. Microvascular research, 2013. **90**: p. 12-22.
90. Kim, S., et al., *Engineering of functional, perfusable 3D microvascular networks on a chip*. Lab on a Chip, 2013. **13**(8): p. 1489-1500.
91. Moon, J.J., et al., *Biomimetic hydrogels with pro-angiogenic properties*. Biomaterials, 2010. **31**(14): p. 3840-3847.

92. Pinney, D.F. and C.P. Emerson Jr, *10T1/2 cells: an in vitro model for molecular genetic analysis of mesodermal determination and differentiation*. Environmental health perspectives, 1989. **80**: p. 221.
93. Westein, E., et al., *Atherosclerotic geometries exacerbate pathological thrombus formation poststenosis in a von Willebrand factor-dependent manner*. Proceedings of the National Academy of Sciences, 2013. **110**(4): p. 1357-1362.
94. Zhang, B., et al., *Biodegradable scaffold with built-in vasculature for organ-on-a-chip engineering and direct surgical anastomosis*. Nature materials, 2016. **15**(6): p. 669.
95. Hallmann, R., et al., *Expression and function of laminins in the embryonic and mature vasculature*. Physiological reviews, 2005. **85**(3): p. 979-1000.
96. Dejana, E., et al., *Fibrinogen induces endothelial cell adhesion and spreading via the release of endogenous matrix proteins and the recruitment of more than one integrin receptor*. Blood, 1990. **75**(7): p. 1509-1517.
97. Sahni, A. and C.W. Francis, *Vascular endothelial growth factor binds to fibrinogen and fibrin and stimulates endothelial cell proliferation*. Blood, 2000. **96**(12): p. 3772-3778.
98. Sahni, A., et al., *FGF-2 binding to fibrin (ogen) is required for augmented angiogenesis*. Blood, 2006. **107**(1): p. 126-131.
99. Peniche, C., W. Argüelles-Monal, and F. Goycoolea, *Monomers, polymers and composites from renewable resources*. Amsterdam: Elsevier, 2008: p. 517-542.
100. Rao, S.B. and C.P. Sharma, *Use of chitosan as a biomaterial: studies on its safety and hemostatic potential*. Journal of Biomedical Materials Research: An Official Journal of The Society for Biomaterials and The Japanese Society for Biomaterials, 1997. **34**(1): p. 21-28.
101. Kumirska, J., et al., *Biomedical activity of chitin/chitosan based materials— influence of physicochemical properties apart from molecular weight and degree of N-acetylation*. Polymers, 2011. **3**(4): p. 1875-1901.
102. Tomihata, K. and Y. Ikada, *In vitro and in vivo degradation of films of chitin and its deacetylated derivatives*. Biomaterials, 1997. **18**(7): p. 567-575.
103. Croll, T.I., et al., *A blank slate? Layer-by-layer deposition of hyaluronic acid and chitosan onto various surfaces*. Biomacromolecules, 2006. **7**(5): p. 1610-1622.
104. He, X., et al., *The production of fully deacetylated chitosan by compression method*. The Egyptian Journal of Aquatic Research, 2016. **42**(1): p. 75-81.
105. Collins, M.N. and C. Birkinshaw, *Hyaluronic acid based scaffolds for tissue engineering—A review*. Carbohydrate polymers, 2013. **92**(2): p. 1262-1279.
106. Mero, A. and M. Campisi, *Hyaluronic acid bioconjugates for the delivery of bioactive molecules*. Polymers, 2014. **6**(2): p. 346-369.
107. Jiang, D., J. Liang, and P.W. Noble, *Hyaluronan in tissue injury and repair*. Annu. Rev. Cell Dev. Biol., 2007. **23**: p. 435-461.
108. Eenschooten, C., et al., *Novel self-associative and multiphasic nanostructured soft carriers based on amphiphilic hyaluronic acid derivatives*. Carbohydrate polymers, 2012. **87**(1): p. 444-451.
109. Moreland, L.W., *Intra-articular hyaluronan (hyaluronic acid) and hylans for the treatment of osteoarthritis: mechanisms of action*. Arthritis Res Ther, 2003. **5**(2): p. 54.

110. Davidenko, N., et al., *Collagen–hyaluronic acid scaffolds for adipose tissue engineering*. *Acta biomaterialia*, 2010. **6**(10): p. 3957-3968.
111. Wang, T.-W. and M. Spector, *Development of hyaluronic acid-based scaffolds for brain tissue engineering*. *Acta biomaterialia*, 2009. **5**(7): p. 2371-2384.
112. Campos, J., M. Varas-Godoy, and Z.S. Haidar, *Physicochemical characterization of chitosan-hyaluronan-coated solid lipid nanoparticles for the targeted delivery of paclitaxel: a proof-of-concept study in breast cancer cells*. *Nanomedicine*, 2017. **12**(5): p. 473-490.
113. Silva, J.M., R.L. Reis, and J.F. Mano, *Biomimetic extracellular environment based on natural origin polyelectrolyte multilayers*. *Small*, 2016. **12**(32): p. 4308-4342.
114. del Hoyo-Gallego, S., et al., *Construction of antibacterial poly (ethylene terephthalate) films via layer by layer assembly of chitosan and hyaluronic acid*. *Carbohydrate polymers*, 2016. **143**: p. 35-43.
115. Hammond, P.T., *Recent explorations in electrostatic multilayer thin film assembly*. *Current Opinion in Colloid & Interface Science*, 1999. **4**(6): p. 430-442.
116. Bertrand, P., et al., *Ultrathin polymer coatings by complexation of polyelectrolytes at interfaces: suitable materials, structure and properties*. *Macromolecular rapid communications*, 2000. **21**(7): p. 319-348.
117. Decher, G., *Fuzzy nanoassemblies: toward layered polymeric multicomposites*. *science*, 1997. **277**(5330): p. 1232-1237.
118. Shiratori, S.S. and M.F. Rubner, *pH-dependent thickness behavior of sequentially adsorbed layers of weak polyelectrolytes*. *Macromolecules*, 2000. **33**(11): p. 4213-4219.
119. Richert, L., et al., *Layer by layer buildup of polysaccharide films: physical chemistry and cellular adhesion aspects*. *Langmuir*, 2004. **20**(2): p. 448-458.
120. Ladam, G., et al., *In situ determination of the structural properties of initially deposited polyelectrolyte multilayers*. *Langmuir*, 2000. **16**(3): p. 1249-1255.
121. Ruths, J., et al., *Polyelectrolytes I: polyanion/polycation multilayers at the air/monolayer/water interface as elements for quantitative polymer adsorption studies and preparation of hetero-superlattices on solid surfaces*. *Langmuir*, 2000. **16**(23): p. 8871-8878.
122. Elbert, D.L., C.B. Herbert, and J.A. Hubbell, *Thin polymer layers formed by polyelectrolyte multilayer techniques on biological surfaces*. *Langmuir*, 1999. **15**(16): p. 5355-5362.
123. Picart, C., et al., *Buildup mechanism for poly (L-lysine)/hyaluronic acid films onto a solid surface*. *Langmuir*, 2001. **17**(23): p. 7414-7424.
124. Lavallo, P., et al., *Comparison of the structure of polyelectrolyte multilayer films exhibiting a linear and an exponential growth regime: An in situ atomic force microscopy study*. *Macromolecules*, 2002. **35**(11): p. 4458-4465.
125. Detzel, C.J., A.L. Larkin, and P. Rajagopalan, *Polyelectrolyte multilayers in tissue engineering*. *Tissue Engineering Part B: Reviews*, 2011. **17**(2): p. 101-113.
126. Rodrigues, J.R., N.M. Alves, and J.F. Mano, *Biomimetic polysaccharide/bioactive glass nanoparticles multilayer membranes for guided tissue regeneration*. *RSC Advances*, 2016. **6**(79): p. 75988-75999.

127. Moura, D., et al., *Chitosan nanocomposites based on distinct inorganic fillers for biomedical applications*. Science and Technology of advanced Materials, 2016. **17**(1): p. 626-643.
128. Lu, H. and N. Hu, *Loading behavior of {chitosan/hyaluronic acid} n layer-by-layer assembly films toward myoglobin: an electrochemical study*. The Journal of Physical Chemistry B, 2006. **110**(47): p. 23710-23718.
129. Correia, C.R., et al., *Chitosan scaffolds containing hyaluronic acid for cartilage tissue engineering*. Tissue Engineering Part C: Methods, 2011. **17**(7): p. 717-730.
130. Chua, P.-H., et al., *Surface functionalization of titanium with hyaluronic acid/chitosan polyelectrolyte multilayers and RGD for promoting osteoblast functions and inhibiting bacterial adhesion*. Biomaterials, 2008. **29**(10): p. 1412-1421.
131. Liu, Y., et al., *Multilayer-assembled microchip for enzyme immobilization as reactor toward low-level protein identification*. Analytical chemistry, 2006. **78**(3): p. 801-808.
132. Salem, A.K., et al., *Interactions of 3T3 fibroblasts and endothelial cells with defined pore features*. Journal of Biomedical Materials Research: An Official Journal of The Society for Biomaterials, The Japanese Society for Biomaterials, and The Australian Society for Biomaterials and the Korean Society for Biomaterials, 2002. **61**(2): p. 212-217.
133. Grigoriev, T., et al., *Effect of Molecular Characteristics and Morphology on Mechanical Performance and Biocompatibility of PLA-Based Spongy Scaffolds*. BioNanoScience, 2018: p. 1-7.
134. Sung, H.-J., et al., *The effect of scaffold degradation rate on three-dimensional cell growth and angiogenesis*. Biomaterials, 2004. **25**(26): p. 5735-5742.
135. Anderson, J.M., A. Rodriguez, and D.T. Chang. *Foreign body reaction to biomaterials*. in *Seminars in immunology*. 2008. Elsevier.
136. Padera, R.F. and C.K. Colton, *Time course of membrane microarchitecture-driven neovascularization*. Biomaterials, 1996. **17**(3): p. 277-284.
137. Brauker, J.H., et al., *Neovascularization of synthetic membranes directed by membrane microarchitecture*. Journal of biomedical materials research, 1995. **29**(12): p. 1517-1524.
138. Sieminski, A.L. and K.J. Gooch, *Biomaterial-microvasculature interactions*. Biomaterials, 2000. **21**(22): p. 2233-2241.
139. Schnell, H., *Linear aromatic polyesters of carbonic acid*. Industrial & Engineering Chemistry, 1959. **51**(2): p. 157-160.
140. Ogończyk, D., P. Jankowski, and P. Garstecki, *Functionalization of polycarbonate with proteins; open-tubular enzymatic microreactors*. Lab on a Chip, 2012. **12**(15): p. 2743-2748.
141. Park, D.-W., et al., *A titer plate-based polymer microfluidic platform for high throughput nucleic acid purification*. Biomedical microdevices, 2008. **10**(1): p. 21-33.
142. Wu, J., Q. Chen, and J.-M. Lin, *Microfluidic technologies in cell isolation and analysis for biomedical applications*. Analyst, 2017. **142**(3): p. 421-441.

143. Yoon, J.J., et al., *Heparin-immobilized biodegradable scaffolds for local and sustained release of angiogenic growth factor*. Journal of Biomedical Materials Research Part A, 2006. **79**(4): p. 934-942.
144. Chen, R., et al., *The use of poly (l-lactide) and RGD modified microspheres as cell carriers in a flow intermittency bioreactor for tissue engineering cartilage*. Biomaterials, 2006. **27**(25): p. 4453-4460.
145. Connelly, J.T., A.J. García, and M.E. Levenston, *Inhibition of in vitro chondrogenesis in RGD-modified three-dimensional alginate gels*. Biomaterials, 2007. **28**(6): p. 1071-1083.
146. Petrie, T.A., et al., *Integrin specificity and enhanced cellular activities associated with surfaces presenting a recombinant fibronectin fragment compared to RGD supports*. Biomaterials, 2006. **27**(31): p. 5459-5470.
147. Alimperti, S., et al., *Three-dimensional biomimetic vascular model reveals a RhoA, Rac1, and N-cadherin balance in mural cell–endothelial cell-regulated barrier function*. Proceedings of the National Academy of Sciences, 2017. **114**(33): p. 8758-8763.
148. Costa, P.F., et al., *Mimicking arterial thrombosis in a 3D-printed microfluidic in vitro vascular model based on computed tomography angiography data*. Lab on a Chip, 2017. **17**(16): p. 2785-2792.
149. Bosman, F.T. and I. Stamenkovic, *Functional structure and composition of the extracellular matrix*. The Journal of Pathology: A Journal of the Pathological Society of Great Britain and Ireland, 2003. **200**(4): p. 423-428.
150. Almubarak, S., et al., *Tissue engineering strategies for promoting vascularized bone regeneration*. Bone, 2016. **83**: p. 197-209.
151. Black, C.R., et al., *Bone tissue engineering*. Current molecular biology reports, 2015. **1**(3): p. 132-140.
152. Shin, H., S. Jo, and A.G. Mikos, *Biomimetic materials for tissue engineering*. Biomaterials, 2003. **24**(24): p. 4353-4364.
153. Fields, G.B., et al., *Proteinlike molecular architecture: biomaterial applications for inducing cellular receptor binding and signal transduction*. Peptide Science, 1998. **47**(2): p. 143-151.
154. Hlady, V. and J. Buijs, *Protein adsorption on solid surfaces*. Current Opinion in Biotechnology, 1996. **7**(1): p. 72.
155. Lhoest, J.B., et al., *Fibronectin adsorption, conformation, and orientation on polystyrene substrates studied by radiolabeling, XPS, and ToF SIMS*. Journal of Biomedical Materials Research: An Official Journal of The Society for Biomaterials, The Japanese Society for Biomaterials, and the Australian Society for Biomaterials, 1998. **41**(1): p. 95-103.
156. Keselowsky, B.G., D.M. Collard, and A.J. García, *Surface chemistry modulates fibronectin conformation and directs integrin binding and specificity to control cell adhesion*. Journal of Biomedical Materials Research Part A: An Official Journal of The Society for Biomaterials, The Japanese Society for Biomaterials, and The Australian Society for Biomaterials and the Korean Society for Biomaterials, 2003. **66**(2): p. 247-259.
157. Collier, J.H. and T. Segura, *Evolving the use of peptides as components of biomaterials*. Biomaterials, 2011. **32**(18): p. 4198-4204.

158. Dettin, M., et al., *Effect of synthetic peptides on osteoblast adhesion*. Biomaterials, 2005. **26**(22): p. 4507-4515.
159. Hersel, U., C. Dahmen, and H. Kessler, *RGD modified polymers: biomaterials for stimulated cell adhesion and beyond*. Biomaterials, 2003. **24**(24): p. 4385-4415.
160. Ryu, J.-J., et al., *Effects of anodized titanium with Arg-Gly-Asp (RGD) peptide immobilized via chemical grafting or physical adsorption on bone cell adhesion and differentiation*. International Journal of Oral & Maxillofacial Implants, 2013. **28**(4).
161. Hirano, Y. and D.J. Mooney, *Peptide and protein presenting materials for tissue engineering*. Advanced materials, 2004. **16**(1): p. 17-25.
162. thermoFisher, *Sulfo-NHS plus EDC (carbodiimide) crosslinking reaction scheme*.
163. Chollet, C., et al., *RGD peptides grafting onto poly (ethylene terephthalate) with well controlled densities*. Biomolecular engineering, 2007. **24**(5): p. 477-482.
164. Chollet, C., et al., *Impact of peptide micropatterning on endothelial cell actin remodeling for cell alignment under shear stress*. Macromolecular bioscience, 2012. **12**(12): p. 1648-1659.
165. Lei, Y., et al., *Peptide immobilization on polyethylene terephthalate surfaces to study specific endothelial cell adhesion, spreading and migration*. Journal of Materials Science: Materials in Medicine, 2012. **23**(11): p. 2761-2772.
166. Lei, Y., et al., *Geometrical microfeature cues for directing tubulogenesis of endothelial cells*. PloS one, 2012. **7**(7): p. e41163.
167. Lei, Y., et al., *Modulation of lumen formation by microgeometrical bioactive cues and migration mode of actin machinery*. Small, 2013. **9**(7): p. 1086-1095.
168. Zouani, O.F., et al., *Differentiation of pre-osteoblast cells on poly (ethylene terephthalate) grafted with RGD and/or BMPs mimetic peptides*. Biomaterials, 2010. **31**(32): p. 8245-8253.
169. Zouani, O.F., et al., *Altered nanofeature size dictates stem cell differentiation*. J Cell Sci, 2012: p. jcs. 093229.
170. Zouani, O.F., et al., *Effect of BMP-2 from matrices of different stiffnesses for the modulation of stem cell fate*. Biomaterials, 2013. **34**(9): p. 2157-2166.
171. Chollet, C., et al., *The effect of RGD density on osteoblast and endothelial cell behavior on RGD-grafted polyethylene terephthalate surfaces*. Biomaterials, 2009. **30**(5): p. 711-720.
172. Chollet, C., et al., *Impact of RGD micro-patterns on cell adhesion*. Colloids and Surfaces B: Biointerfaces, 2010. **75**(1): p. 107-114.
173. Liu, Y. and J. Yu, *Oriented immobilization of proteins on solid supports for use in biosensors and biochips: a review*. Microchimica Acta, 2016. **183**(1): p. 1-19.
174. Silva, R.R., et al., *Programa de Pos-Graduacao em Inovacao Terapeutica, Universidade Federal de Pernambuco, 50670-901 Recife, PE, Brasil, 2 Departamento de Bioquímica, Universidade Federal de Pernambuco, 50670-901, Recife, PE, Brasil, 3 Centro de Analise Proteomicas e Bioquimicas de Brasilia, Universidade Catolica de Brasilia, 71966-700, Brasilia, DF, Brasil*. Frontiers in Bioscience, 2016. **8**: p. 129-142.

175. Mattiasson, B., *Immobilization methods*, in *Immobilized cells and organelles*. 2018, CRC Press. p. 3-26.
176. Ahmad, R. and M. Sardar, *Enzyme immobilization: an overview on nanoparticles as immobilization matrix*. *Biochemistry and Analytical Biochemistry*, 2015. **4**(2): p. 1.
177. Rouwkema, J., N.C. Rivron, and C.A. van Blitterswijk, *Vascularization in tissue engineering*. *Trends in biotechnology*, 2008. **26**(8): p. 434-441.
178. Laschke, M.W., et al., *Angiogenesis in tissue engineering: breathing life into constructed tissue substitutes*. *Tissue engineering*, 2006. **12**(8): p. 2093-2104.
179. Demirdögen, B., A.E. Elçin, and Y.M. Elçin, *Neovascularization by bFGF releasing hyaluronic acid–gelatin microspheres: in vitro and in vivo studies*. *Growth Factors*, 2010. **28**(6): p. 426-436.
180. Borselli, C., et al., *Bioactivation of collagen matrices through sustained VEGF release from PLGA microspheres*. *Journal of Biomedical Materials Research Part A: An Official Journal of The Society for Biomaterials, The Japanese Society for Biomaterials, and The Australian Society for Biomaterials and the Korean Society for Biomaterials*, 2010. **92**(1): p. 94-102.
181. Prokop, A., et al., *Towards retrievable vascularized bioartificial pancreas: induction and long-lasting stability of polymeric mesh implant vascularized with the help of acidic and basic fibroblast growth factors and hydrogel coating*. *Diabetes technology & therapeutics*, 2001. **3**(2): p. 245-261.
182. De Boer, R., et al., *In vitro and in vivo release of nerve growth factor from biodegradable poly-lactic-co-glycolic-acid microspheres*. *Journal of Biomedical Materials Research Part A*, 2010. **95**(4): p. 1067-1073.
183. Karal-Yilmaz, O., et al., *Preparation and in vitro characterization of vascular endothelial growth factor (VEGF)-loaded poly (D, L-lactic-co-glycolic acid) microspheres using a double emulsion/solvent evaporation technique*. *Journal of microencapsulation*, 2011. **28**(1): p. 46-54.
184. Geiger, F., et al., *VEGF producing bone marrow stromal cells (BMSC) enhance vascularization and resorption of a natural coral bone substitute*. *Bone*, 2007. **41**(4): p. 516-522.
185. Yang, J., et al., *Effects of myocardial transplantation of marrow mesenchymal stem cells transfected with vascular endothelial growth factor for the improvement of heart function and angiogenesis after myocardial infarction*. *Cardiology*, 2007. **107**(1): p. 17-29.
186. Andrae, J., R. Gallini, and C. Betsholtz, *Role of platelet-derived growth factors in physiology and medicine*. *Genes & development*, 2008. **22**(10): p. 1276-1312.
187. Thurston, G., *Complementary actions of VEGF and angiopoietin-1 on blood vessel growth and leakage*. *Journal of anatomy*, 2002. **200**(6): p. 575-580.
188. Hervé, M.-A., et al., *Overexpression of vascular endothelial growth factor 189 in breast cancer cells leads to delayed tumor uptake with dilated intratumoral vessels*. *The American journal of pathology*, 2008. **172**(1): p. 167-178.
189. Yao, C., et al., *The effect of cross-linking of collagen matrices on their angiogenic capability*. *Biomaterials*, 2008. **29**(1): p. 66-74.

190. Go, D.P., et al., *Porous PLGA microspheres tailored for dual delivery of biomolecules via layer-by-layer assembly*. Journal of Biomedical Materials Research Part A, 2015. **103**(5): p. 1849-1863.
191. Li, W., et al., *In vitro and in vivo evaluation of a novel collagen/cellulose nanocrystals scaffold for achieving the sustained release of basic fibroblast growth factor*. Journal of biomaterials applications, 2015. **29**(6): p. 882-893.
192. Subbiah, R., et al., *Osteogenic/angiogenic dual growth factor delivery microcapsules for regeneration of vascularized bone tissue*. Advanced healthcare materials, 2015. **4**(13): p. 1982-1992.
193. Wang, K., et al., *Enhanced vascularization in hybrid PCL/gelatin fibrous scaffolds with sustained release of VEGF*. BioMed research international, 2015. **2015**.
194. Cao, R., et al., *Angiogenic synergism, vascular stability and improvement of hind-limb ischemia by a combination of PDGF-BB and FGF-2*. Nature medicine, 2003. **9**(5): p. 604.
195. Kano, M.R., et al., *VEGF-A and FGF-2 synergistically promote neoangiogenesis through enhancement of endogenous PDGF-B–PDGFR β signaling*. J Cell Sci, 2005. **118**(16): p. 3759-3768.
196. Ley, C.D., et al., *Angiogenic synergy of bFGF and VEGF is antagonized by Angiopoietin-2 in a modified in vivo Matrigel assay*. Microvascular research, 2004. **68**(3): p. 161-168.
197. Rophael, J.A., et al., *Angiogenic growth factor synergism in a murine tissue engineering model of angiogenesis and adipogenesis*. The American journal of pathology, 2007. **171**(6): p. 2048-2057.
198. Richardson, T.P., et al., *Polymeric system for dual growth factor delivery*. Nature biotechnology, 2001. **19**(11): p. 1029.
199. Ferrara, N., et al., *Molecular and biological properties of the vascular endothelial growth factor family of proteins*. Endocrine reviews, 1992. **13**(1): p. 18-32.
200. Holmes, D.I. and I. Zachary, *The vascular endothelial growth factor (VEGF) family: angiogenic factors in health and disease*. Genome biology, 2005. **6**(2): p. 209.
201. Alvarez, R.H., et al., *Bevacizumab treatment for advanced breast cancer*. The oncologist, 2011: p. theoncologist. 2011-0113.
202. Tischer, E., et al., *The human gene for vascular endothelial growth factor. Multiple protein forms are encoded through alternative exon splicing*. Journal of Biological Chemistry, 1991. **266**(18): p. 11947-11954.
203. Houck, K.A., et al., *The vascular endothelial growth factor family: identification of a fourth molecular species and characterization of alternative splicing of RNA*. Molecular endocrinology, 1991. **5**(12): p. 1806-1814.
204. Celletti, F.L., et al., *Vascular endothelial growth factor enhances atherosclerotic plaque progression*. Nature medicine, 2001. **7**(4): p. 425.
205. Ware, J.A. and M. Simons, *Angiogenesis in ischemic heart disease*. Nature medicine, 1997. **3**(2): p. 158-164.
206. Carmeliet, P., *Angiogenesis in life, disease and medicine*. Nature, 2005. **438**(7070): p. 932.

207. Felmeden, D., A. Blann, and G. Lip, *Angiogenesis: basic pathophysiology and implications for disease*. European Heart Journal, 2003. **24**(7): p. 586-603.
208. Ozawa, C.R., et al., *Microenvironmental VEGF concentration, not total dose, determines a threshold between normal and aberrant angiogenesis*. The Journal of clinical investigation, 2004. **113**(4): p. 516-527.
209. Benjamin, L.E., I. Hemo, and E. Keshet, *A plasticity window for blood vessel remodelling is defined by pericyte coverage of the preformed endothelial network and is regulated by PDGF-B and VEGF*. Development, 1998. **125**(9): p. 1591-1598.
210. Baluk, P., et al., *Regulated angiogenesis and vascular regression in mice overexpressing vascular endothelial growth factor in airways*. The American journal of pathology, 2004. **165**(4): p. 1071-1085.
211. Yu, W.-L., et al., *Enhanced osteogenesis and angiogenesis by mesoporous hydroxyapatite microspheres-derived simvastatin sustained release system for superior bone regeneration*. Scientific reports, 2017. **7**: p. 44129.
212. Feng, X., et al., *Injectable cartilaginous template transformed BMSCs into vascularized bone*. Scientific reports, 2018. **8**(1): p. 8244.
213. Barati, D., et al., *Spatiotemporal release of BMP-2 and VEGF enhances osteogenic and vasculogenic differentiation of human mesenchymal stem cells and endothelial colony-forming cells co-encapsulated in a patterned hydrogel*. Journal of Controlled Release, 2016. **223**: p. 126-136.
214. Schweigerer, L., et al., *Capillary endothelial cells express basic fibroblast growth factor, a mitogen that promotes their own growth*. Nature, 1987. **325**(6101): p. 257.
215. Nabel, E.G., et al., *Recombinant fibroblast growth factor-1 promotes intimal hyperplasia and angiogenesis in arteries in vivo*. Nature, 1993. **362**(6423): p. 844.
216. Barger, A.C., et al., *Hypothesis: vasa vasorum and neovascularization of human coronary arteries: a possible role in the pathophysiology of atherosclerosis*. New England Journal of Medicine, 1984. **310**(3): p. 175-177.
217. Unger, E.F., et al., *Effects of a single intracoronary injection of basic fibroblast growth factor in stable angina pectoris*. The American journal of cardiology, 2000. **85**(12): p. 1414-1419.
218. Sprugel, K., et al., *Effects of growth factors in vivo. I. Cell ingrowth into porous subcutaneous chambers*. The American journal of pathology, 1987. **129**(3): p. 601.
219. Peter, S., et al., *Polymer concepts in tissue engineering*. Journal of biomedical materials research, 1998. **43**(4): p. 422-427.
220. Xiong, S., et al., *A gelatin-sulfonated silk composite scaffold based on 3D printing technology enhances skin regeneration by stimulating epidermal growth and dermal neovascularization*. Scientific reports, 2017. **7**(1): p. 4288.
221. Ross, R., et al., *A platelet-dependent serum factor that stimulates the proliferation of arterial smooth muscle cells in vitro*. Proceedings of the National Academy of Sciences, 1974. **71**(4): p. 1207-1210.
222. Kohler, N. and A. Lipton, *Platelets as a source of fibroblast growth-promoting activity*. Experimental cell research, 1974. **87**(2): p. 297-301.

223. Johnsson, A., et al., *The c-sis gene encodes a precursor of the B chain of platelet-derived growth factor*. The EMBO journal, 1984. **3**(5): p. 921-928.
224. Bowen-Pope, D.F., et al., *Platelet-derived growth factor in vivo: levels, activity, and rate of clearance*. Blood, 1984. **64**(2): p. 458-469.
225. Grotendorst, G., et al., *Platelet-derived growth factor is a chemoattractant for vascular smooth muscle cells*. Journal of cellular physiology, 1982. **113**(2): p. 261-266.
226. Seppä, H., et al., *Platelet-derived growth factor is chemotactic for fibroblasts*. The Journal of cell biology, 1982. **92**(2): p. 584-588.
227. Ross, R., E.W. Raines, and D.F. Bowen-Pope, *The biology of platelet-derived growth factor*. Cell, 1986. **46**(2): p. 155-169.
228. Berk, B.C., et al., *Vasoconstriction: a new activity for platelet-derived growth factor*. Science, 1986. **232**(4746): p. 87-90.
229. Santos, M.I. and R.L. Reis, *Vascularization in bone tissue engineering: physiology, current strategies, major hurdles and future challenges*. Macromolecular bioscience, 2010. **10**(1): p. 12-27.
230. Dalby, M.J., A.J. García, and M. Salmeron-Sanchez, *Receptor control in mesenchymal stem cell engineering*. Nature Reviews Materials, 2018. **3**: p. 17091.
231. von der Mark, K., et al., *Nanoscale engineering of biomimetic surfaces: cues from the extracellular matrix*. Cell and tissue research, 2010. **339**(1): p. 131.
232. Rosso, F., et al., *Smart materials as scaffolds for tissue engineering*. Journal of cellular physiology, 2005. **203**(3): p. 465-470.
233. Singh, M., C. Berkland, and M.S. Detamore, *Strategies and applications for incorporating physical and chemical signal gradients in tissue engineering*. Tissue Engineering Part B: Reviews, 2008. **14**(4): p. 341-366.
234. Rao, S.S. and J. Winter, *Adhesion molecule-modified biomaterials for neural tissue engineering*. Frontiers in neuroengineering, 2009. **2**: p. 6.
235. Sreejalekshmi, K.G. and P.D. Nair, *Biomimeticity in tissue engineering scaffolds through synthetic peptide modifications—Altering chemistry for enhanced biological response*. Journal of biomedical materials research Part A, 2011. **96**(2): p. 477-491.
236. Briquez, P.S., et al., *Design principles for therapeutic angiogenic materials*. Nature Reviews Materials, 2016. **1**(1): p. 15006.
237. Park, K.M., et al., *In situ SVVYGLR peptide conjugation into injectable gelatin-poly (ethylene glycol)-tyramine hydrogel via enzyme-mediated reaction for enhancement of endothelial cell activity and neo-vascularization*. Bioconjugate chemistry, 2012. **23**(10): p. 2042-2050.
238. Hamada, Y., et al., *Osteopontin-derived peptide SVVYGLR induces angiogenesis in vivo*. Dental materials journal, 2004. **23**(4): p. 650-655.
239. Barry, S.T., et al., *Analysis of the α 4 β 1 integrin-osteopontin interaction*. Experimental cell research, 2000. **258**(2): p. 342-351.
240. Green, P.M., et al., *Structural elements of the osteopontin SVVYGLR motif important for the interaction with α 4 integrins*. FEBS letters, 2001. **503**(1): p. 75-79.
241. Yokosaki, Y., et al., *The integrin α 9 β 1 binds to a novel recognition sequence (SVVYGLR) in the thrombin-cleaved amino-terminal fragment of osteopontin*. Journal of Biological Chemistry, 1999. **274**(51): p. 36328-36334.

242. Hamada, Y., et al., *Synthetic osteopontin-derived peptide SVVYGLR can induce neovascularization in artificial bone marrow scaffold biomaterials*. Dental materials journal, 2007. **26**(4): p. 487-492.
243. Egusa, H., et al., *Enhanced bone regeneration via multimodal actions of synthetic peptide SVVYGLR on osteoprogenitors and osteoclasts*. Biomaterials, 2009. **30**(27): p. 4676-4686.
244. Grant, D.S., et al., *Interaction of endothelial cells with a laminin A chain peptide (SIKVAV) in vitro and induction of angiogenic behavior in vivo*. Journal of cellular physiology, 1992. **153**(3): p. 614-625.
245. D'Andrea, L.D., et al., *Targeting angiogenesis: structural characterization and biological properties of a de novo engineered VEGF mimicking peptide*. Proceedings of the National Academy of Sciences, 2005. **102**(40): p. 14215-14220.
246. Parthiban, S.P., et al., *Covalently immobilized VEGF-mimicking peptide with gelatin methacrylate enhances microvascularization of endothelial cells*. Acta biomaterialia, 2017. **51**: p. 330-340.
247. Fu, J. and D.-A. Wang, *In Situ Organ-Specific Vascularization in Tissue Engineering*. Trends in biotechnology, 2018.
248. Di Stasi, R., et al., *VEGFR recognition interface of a proangiogenic VEGF-mimetic peptide as determined in vitro and in presence of endothelial cells by NMR spectroscopy*. Chemistry—A European Journal, 2018.
249. Santulli, G., et al., *In vivo properties of the proangiogenic peptide QK*. Journal of translational medicine, 2009. **7**(1): p. 41.
250. Chen, C., et al., *Research trends in biomimetic medical materials for tissue engineering: 3D bioprinting, surface modification, nano/micro-technology and clinical aspects in tissue engineering of cartilage and bone*. Biomaterials research, 2016. **20**(1): p. 10.
251. Borenstein, J.T., et al., *Microfabrication of three-dimensional engineered scaffolds*. Tissue engineering, 2007. **13**(8): p. 1837-1844.
252. Khademhosseini, A., et al., *Microscale technologies for tissue engineering and biology*. Proceedings of the National Academy of Sciences, 2006. **103**(8): p. 2480-2487.
253. Moon, J.J., et al., *Micropatterning of poly (ethylene glycol) diacrylate hydrogels with biomolecules to regulate and guide endothelial morphogenesis*. Tissue Engineering Part A, 2008. **15**(3): p. 579-585.
254. Jeong, H.J., et al., *The future of optical lithography*. Solid State Technology, 1994. **37**(4): p. 39-45.
255. Kane, R.S., et al., *Patterning proteins and cells using soft lithography*, in *The Biomaterials: Silver Jubilee Compendium*. 2006, Elsevier. p. 161-174.
256. Xia, Y. and G.M. Whitesides, *Soft lithography*. Angewandte Chemie International Edition, 1998. **37**(5): p. 550-575.
257. Becker, H. and U. Heim. *Silicon as tool material for polymer hot embossing*. in *Micro Electro Mechanical Systems, 1999. MEMS'99. Twelfth IEEE International Conference on*. 1999. IEEE.
258. Becker, H. and U. Heim, *Hot embossing as a method for the fabrication of polymer high aspect ratio structures*. Sensors and Actuators A: Physical, 2000. **83**(1-3): p. 130-135.

259. Deng, Y., et al., *Experimental investigation on the large-area fabrication of micro-pyramid arrays by roll-to-roll hot embossing on PVC film*. Journal of Micromechanics and Microengineering, 2014. **24**(4): p. 045023.
260. Worgull, M., et al., *Hot embossing of microstructures: characterization of friction during demolding*. Microsystem Technologies, 2008. **14**(6): p. 767-773.
261. Saha, B., et al., *Hot-embossing performance of silicon micromold coated with self-assembled n-octadecyltrichlorosilane*. Sensors and Actuators B: Chemical, 2011. **160**(1): p. 207-214.
262. Weigand, A., et al., *Acceleration of vascularized bone tissue-engineered constructs in a large animal model combining intrinsic and extrinsic vascularization*. Tissue Engineering Part A, 2015. **21**(9-10): p. 1680-1694.
263. Young, D., K. Greulich, and H. Weier, *Species-specific in situ hybridization with fluorochrome-labeled DNA probes to study vascularization of human skin grafts on athymic mice*. The Journal of burn care & rehabilitation, 1996. **17**(4): p. 305-310.
264. Cassell, C.O., et al., *Vascularisation of tissue-engineered grafts: the regulation of angiogenesis in reconstructive surgery and in disease states*. British journal of plastic surgery, 2002. **55**(8): p. 603-610.
265. Balamurugan, A., et al., *Bioartificial pancreas transplantation at prevascularized intermuscular space: effect of angiogenesis induction on islet survival*. Pancreas, 2003. **26**(3): p. 279-285.
266. Elcin, A.E. and Y.M. Elcin, *Localized angiogenesis induced by human vascular endothelial growth factor-activated PLGA sponge*. Tissue engineering, 2006. **12**(4): p. 959-968.
267. Elçin, Y.M., V. Dixit, and G. Gitnick, *Extensive in vivo angiogenesis following controlled release of human vascular endothelial cell growth factor: implications for tissue engineering and wound healing*. Artificial organs, 2001. **25**(7): p. 558-565.
268. Hiraoka, Y., et al., *In situ regeneration of adipose tissue in rat fat pad by combining a collagen scaffold with gelatin microspheres containing basic fibroblast growth factor*. Tissue engineering, 2006. **12**(6): p. 1475-1487.
269. Lee, H., et al., *Local delivery of basic fibroblast growth factor increases both angiogenesis and engraftment of hepatocytes in tissue-engineered polymer devices*. Transplantation, 2002. **73**(10): p. 1589-1593.
270. Miki, A., et al., *Maintenance of neovascularization at the implantation site of an artificial device by bFGF and endothelial cell transplant*. Cell transplantation, 2006. **15**(10): p. 893-901.
271. Perets, A., et al., *Enhancing the vascularization of three-dimensional porous alginate scaffolds by incorporating controlled release basic fibroblast growth factor microspheres*. Journal of Biomedical Materials Research Part A: An Official Journal of The Society for Biomaterials, The Japanese Society for Biomaterials, and The Australian Society for Biomaterials and the Korean Society for Biomaterials, 2003. **65**(4): p. 489-497.
272. Peters, M.C., et al., *Release from alginate enhances the biological activity of vascular endothelial growth factor*. Journal of Biomaterials Science, Polymer Edition, 1998. **9**(12): p. 1267-1278.

273. Tabata, Y., et al., *De novo formation of adipose tissue by controlled release of basic fibroblast growth factor*. Tissue engineering, 2000. **6**(3): p. 279-289.
274. Tremblay, P.L., et al., *Inosculation of tissue-engineered capillaries with the host's vasculature in a reconstructed skin transplanted on mice*. American journal of transplantation, 2005. **5**(5): p. 1002-1010.
275. Chen, X., et al., *Rapid anastomosis of endothelial progenitor cell-derived vessels with host vasculature is promoted by a high density of cotransplanted fibroblasts*. Tissue Engineering Part A, 2009. **16**(2): p. 585-594.
276. Laschke, M.W., et al., *Improvement of vascularization of PLGA scaffolds by inosculation of in situ-preformed functional blood vessels with the host microvasculature*. Annals of surgery, 2008. **248**(6): p. 939-948.
277. Auger, F.A., L. Gibot, and D. Lacroix, *The pivotal role of vascularization in tissue engineering*. Annual review of biomedical engineering, 2013. **15**: p. 177-200.
278. Mian, R., et al., *Formation of new tissue from an arteriovenous loop in the absence of added extracellular matrix*. Tissue engineering, 2000. **6**(6): p. 595-603.
279. Lokmic, Z., et al., *An arteriovenous loop in a protected space generates a permanent, highly vascular, tissue-engineered construct*. The FASEB Journal, 2007. **21**(2): p. 511-522.
280. Koepfle, C., U. Kneser, and V.J. Schmidt, *Microsurgical Approaches for In Vivo Prevascularization*. Vascularization for Tissue Engineering and Regenerative Medicine, 2017: p. 1-18.
281. Risau, W., *Mechanisms of angiogenesis*. nature, 1997. **386**(6626): p. 671.
282. Polykandriotis, E., et al., *Intrinsic axial vascularization of an osteoconductive bone matrix by means of an arteriovenous vascular bundle*. Plastic and reconstructive surgery, 2007. **120**(4): p. 855-868.
283. Tanaka, Y., et al., *Generation of an autologous tissue (matrix) flap by combining an arteriovenous shunt loop with artificial skin in rats: preliminary report*. British journal of plastic surgery, 2000. **53**(1): p. 51-57.
284. Tanaka, Y., et al., *Tissue engineering skin flaps: which vascular carrier, arteriovenous shunt loop or arteriovenous bundle, has more potential for angiogenesis and tissue generation?* Plastic and reconstructive surgery, 2003. **112**(6): p. 1636-1644.
285. Nicosia, R.F. and A. Ottinetti, *Modulation of microvascular growth and morphogenesis by reconstituted basement membrane gel in three-dimensional cultures of rat aorta: a comparative study of angiogenesis in matrigel, collagen, fibrin, and plasma clot*. In Vitro Cellular & Developmental Biology, 1990. **26**(2): p. 119-128.
286. Cassell, O.C., et al., *The influence of extracellular matrix on the generation of vascularized, engineered, transplantable tissue*. Annals of the New York Academy of Sciences, 2001. **944**(1): p. 429-442.
287. Bezenah, J.R., Y.P. Kong, and A.J. Putnam, *Evaluating the potential of endothelial cells derived from human induced pluripotent stem cells to form microvascular networks in 3D cultures*. Scientific reports, 2018. **8**(1): p. 2671.
288. Théry, M., *Micropatterning as a tool to decipher cell morphogenesis and functions*. J Cell Sci, 2010. **123**(24): p. 4201-4213.

289. Ingber, D.E., *Tensegrity I. Cell structure and hierarchical systems biology*. Journal of cell science, 2003. **116**(7): p. 1157-1173.
290. Ingber, D.E., *Tensegrity II. How structural networks influence cellular information processing networks*. Journal of cell science, 2003. **116**(8): p. 1397-1408.
291. Ingber, D.E., *Cellular mechanotransduction: putting all the pieces together again*. The FASEB journal, 2006. **20**(7): p. 811-827.
292. Johnson, K.R., J.L. Leight, and V.M. Weaver, *Demystifying the effects of a three-dimensional microenvironment in tissue morphogenesis*. Methods in cell biology, 2007. **83**: p. 547-583.
293. Fraley, S.I., et al., *A distinctive role for focal adhesion proteins in three-dimensional cell motility*. Nature cell biology, 2010. **12**(6): p. 598.
294. Shafiee, A. and A. Atala, *Tissue engineering: toward a new era of medicine*. Annual review of medicine, 2017. **68**: p. 29-40.
295. Laschke, M.W. and M.D. Menger, *Life is 3D: boosting spheroid function for tissue engineering*. Trends in biotechnology, 2017. **35**(2): p. 133-144.
296. Ng, J., et al., *Biomimetic approaches for bone tissue engineering*. Tissue Engineering Part B: Reviews, 2017. **23**(5): p. 480-493.
297. Song, H.-H.G., et al., *Vascular tissue engineering: progress, challenges, and clinical promise*. Cell stem cell, 2018. **22**(3): p. 340-354.
298. Laschke, M.W. and M.D. Menger, *Prevascularization in tissue engineering: current concepts and future directions*. Biotechnology advances, 2016. **34**(2): p. 112-121.
299. Rouwkema, J. and A. Khademhosseini, *Vascularization and angiogenesis in tissue engineering: beyond creating static networks*. Trends in biotechnology, 2016. **34**(9): p. 733-745.
300. Roseti, L., et al., *Scaffolds for Bone Tissue Engineering: State of the art and new perspectives*. Materials Science and Engineering: C, 2017. **78**: p. 1246-1262.
301. Trappmann, B., et al., *Matrix degradability controls multicellularity of 3D cell migration*. Nature communications, 2017. **8**(1): p. 371.
302. Palik, E.D., *Handbook of Optical Constants of Solids, Author and Subject Indices for Volumes I, II, and III*. 1998: Elsevier.
303. Uchida, E., Y. Uyama, and Y. Ikada, *Surface graft polymerization of ionic monomers onto poly (ethylene terephthalate) by UV-irradiation without degassing*. Journal of applied polymer science, 1993. **47**(3): p. 417-424.
304. Oehmichen, L.e.E.t. *UTILISER UNE CELLULE DE MALASSEZ*. Available from: https://lycee-etienne-oehmichen.fr/contenu/discipline/svt/01_Pour_Observation2/Utiliser_une_cellule_de_Malassez.pdf.
305. Coufal, N.G., et al., *L1 retrotransposition in human neural progenitor cells*. Nature, 2009. **460**(7259): p. 1127.
306. Debono, M., et al., *One-step fabrication of microchannels with integrated three dimensional features by hot intrusion embossing*. Sensors, 2016. **16**(12): p. 2023.

307. Guckenberger, D.J., et al., *Micromilling: a method for ultra-rapid prototyping of plastic microfluidic devices*. Lab on a Chip, 2015. **15**(11): p. 2364-2378.
308. Trybała, A., L. Szyk-Warszyńska, and P. Warszyński, *The effect of anchoring PEI layer on the build-up of polyelectrolyte multilayer films at homogeneous and heterogeneous surfaces*. Colloids and Surfaces A: Physicochemical and Engineering Aspects, 2009. **343**(1-3): p. 127-132.
309. Monge, C., et al., *Spatio-temporal control of LbL films for biomedical applications: from 2D to 3D*. Advanced healthcare materials, 2015. **4**(6): p. 811-830.
310. Picart, C., *Polyelectrolyte multilayer films: from physico-chemical properties to the control of cellular processes*. Current medicinal chemistry, 2008. **15**(7): p. 685-697.
311. Schneider, A., et al., *Polyelectrolyte multilayers with a tunable Young's modulus: influence of film stiffness on cell adhesion*. Langmuir, 2006. **22**(3): p. 1193-1200.
312. Kapp, T.G., et al., *A comprehensive evaluation of the activity and selectivity profile of ligands for RGD-binding integrins*. Scientific reports, 2017. **7**: p. 39805.
313. Picart, C., et al., *Primary cell adhesion on RGD-functionalized and covalently crosslinked thin polyelectrolyte multilayer films*. Advanced Functional Materials, 2005. **15**(1): p. 83-94.
314. Massia, S.P. and J.A. Hubbell, *An RGD spacing of 440 nm is sufficient for integrin alpha V beta 3-mediated fibroblast spreading and 140 nm for focal contact and stress fiber formation*. The Journal of cell biology, 1991. **114**(5): p. 1089-1100.
315. Porté-Durrieu, M.-C., et al., *Cyclo-(DfKRG) peptide grafting onto Ti-6Al-4V: physical characterization and interest towards human osteoprogenitor cells adhesion*. Biomaterials, 2004. **25**(19): p. 4837-4846.
316. Gribova, V., et al., *Effect of RGD functionalization and stiffness modulation of polyelectrolyte multilayer films on muscle cell differentiation*. Acta biomaterialia, 2013. **9**(5): p. 6468-6480.
317. Leslie-Barbick, J.E., et al., *The promotion of microvasculature formation in poly (ethylene glycol) diacrylate hydrogels by an immobilized VEGF-mimetic peptide*. Biomaterials, 2011. **32**(25): p. 5782-5789.
318. Hamada, Y., et al., *Angiogenic activity of osteopontin-derived peptide SVVYGLR*. Biochemical and biophysical research communications, 2003. **310**(1): p. 153-157.
319. Le Saux, G., et al., *Surface bound VEGF mimicking peptide maintains endothelial cell proliferation in the absence of soluble VEGF in vitro*. Journal of Biomedical Materials Research Part A, 2016. **104**(6): p. 1425-1436.
320. Chan, T.R., P.J. Stahl, and S.M. Yu, *Matrix-Bound VEGF Mimetic Peptides: Design and Endothelial-Cell Activation in Collagen Scaffolds*. Advanced functional materials, 2011. **21**(22): p. 4252-4262.
321. Koepsel, J.T., E.H. Nguyen, and W.L. Murphy, *Differential effects of a soluble or immobilized VEGFR-binding peptide*. Integrative Biology, 2012. **4**(8): p. 914-924.
322. Sarti, G.C. and M.G. De Angelis, *Calculation of the solubility of liquid solutes in glassy polymers*. AIChE Journal, 2012. **58**(1): p. 292-301.

323. Kambour, R., *Structure and properties of crazes in polycarbonate and other glassy polymers*. *Polymer*, 1964. **5**: p. 143-155.
324. Suntornnond, R., et al., *A highly printable and biocompatible hydrogel composite for direct printing of soft and perfusable vasculature-like structures*. *Scientific reports*, 2017. **7**(1): p. 16902.
325. Datta, P., B. Ayan, and I.T. Ozbolat, *Bioprinting for vascular and vascularized tissue biofabrication*. *Acta biomaterialia*, 2017. **51**: p. 1-20.
326. Ma, Y.-H.V., et al., *A review of microfluidic approaches for investigating cancer extravasation during metastasis*. *Microsystems & Nanoengineering*, 2018. **4**: p. 17104.
327. Noel, S., et al., *Co-immobilization of adhesive peptides and VEGF within a dextran-based coating for vascular applications*. *Acta biomaterialia*, 2016. **37**: p. 69-82.
328. Lee, Y.B., et al., *Polydopamine-mediated immobilization of multiple bioactive molecules for the development of functional vascular graft materials*. *Biomaterials*, 2012. **33**(33): p. 8343-8352.
329. Hatakeyama, H., et al., *Bio-functionalized thermoresponsive interfaces facilitating cell adhesion and proliferation*. *Biomaterials*, 2006. **27**(29): p. 5069-5078.
330. Eliceiri, B.P., *Integrin and growth factor receptor crosstalk*. *Circulation research*, 2001. **89**(12): p. 1104-1110.
331. Le Saux, G., et al., *Spacing of integrin ligands influences signal transduction in endothelial cells*. *Biophysical journal*, 2011. **101**(4): p. 764-773.
332. Byzova, T.V., et al., *A mechanism for modulation of cellular responses to VEGF: activation of the integrins*. *Molecular cell*, 2000. **6**(4): p. 851-860.
333. Traub, S., et al., *The promotion of endothelial cell attachment and spreading using FNIII10 fused to VEGF-A165*. *Biomaterials*, 2013. **34**(24): p. 5958-5968.
334. Hebeiss, I., et al., *Novel three-dimensional Boyden chamber system for studying transendothelial transport*. *Lab on a Chip*, 2012. **12**(4): p. 829-834.
335. Mori, N., Y. Morimoto, and S. Takeuchi, *Skin integrated with perfusable vascular channels on a chip*. *Biomaterials*, 2017. **116**: p. 48-56.
336. Tocchio, A., et al., *Versatile fabrication of vascularizable scaffolds for large tissue engineering in bioreactor*. *Biomaterials*, 2015. **45**: p. 124-131.
337. Kim, J., et al., *Engineering of a biomimetic pericyte-covered 3D microvascular network*. *PloS one*, 2015. **10**(7): p. e0133880.
338. Teichert, M., et al., *Pericyte-expressed Tie2 controls angiogenesis and vessel maturation*. *Nature communications*, 2017. **8**: p. 16106.
339. Puri, M., et al., *The receptor tyrosine kinase TIE is required for integrity and survival of vascular endothelial cells*. *The EMBO journal*, 1995. **14**(23): p. 5884-5891.
340. Cao, G., et al., *Involvement of human PECAM-1 in angiogenesis and in vitro endothelial cell migration*. *American Journal of Physiology-Cell Physiology*, 2002. **282**(5): p. C1181-C1190.

341. Freiman, A., et al., *Adipose-derived endothelial and mesenchymal stem cells enhance vascular network formation on three-dimensional constructs in vitro*. Stem cell research & therapy, 2016. **7**(1): p. 5.
342. Asahara, T., et al., *Isolation of putative progenitor endothelial cells for angiogenesis*. Science, 1997. **275**(5302): p. 964-966.
343. Medina, R.J., et al., *Outgrowth endothelial cells: characterization and their potential for reversing ischemic retinopathy*. Investigative ophthalmology & visual science, 2010. **51**(11): p. 5906-5913.
344. Shandalov, Y., et al., *An engineered muscle flap for reconstruction of large soft tissue defects*. Proceedings of the National Academy of Sciences, 2014. **111**(16): p. 6010-6015.
345. Wang, Z., et al., *Rapid vascularization of tissue-engineered vascular grafts in vivo by endothelial cells in co-culture with smooth muscle cells*. Journal of Materials Science: Materials in Medicine, 2012. **23**(4): p. 1109-1117.
346. Ogończyk, D., et al., *Bonding of microfluidic devices fabricated in polycarbonate*. Lab on a Chip, 2010. **10**(10): p. 1324-1327.
347. Patel, N.G. and G. Zhang, *Responsive systems for cell sheet detachment*. Organogenesis, 2013. **9**(2): p. 93-100.

Titre: Synthèse de microcanaux bioactifs pour la vascularization

Résumé: *In vitro*, la formation de structures de type tubulaire avec des cellules endothéliales de veine ombilicale humaine (HUVEC) a été étudiée en combinant la fonctionnalisation de la chimie des matériaux et le développement de la géométrie tridimensionnelle. Le polycarbonate (PC) a été utilisé comme modèle pour le développement de l'échafaud. Le film de polysaccharide naturel, basé sur un dépôt alternatif couche par couche (LbL) d'acide hyaluronique (HA) et de chitosane (CHI), a d'abord été appliqué sur une surface PC et caractérisé en termes de croissance d'épaisseur par microscopie à balayage laser (CLSM). Cette première fonctionnalisation se traduit par un revêtement complet de la couche PC. Une biofonctionnalisation supplémentaire avec un peptide adhésif (RGD) et deux peptides angiogénétiques (SVV et QK) a été étudiée, immobilisant ces peptides sur le groupe carboxylique de HA précédemment déposé, en utilisant la chimie bien connue du carbodiimide. La version marquée de chaque peptide a été utilisée pour caractériser l'immobilisation et la pénétration des peptides dans les couches de polyélectrolytes, aboutissant à une greffe réussie avec une pénétration complète dans toute l'épaisseur du LbL. Des tests *in vitro* ont été effectués à l'aide de cellules HUVEC pour évaluer leur efficacité d'adhésion et leur activité métabolique sur la LbL avec et sans immobilisation de peptides, ce qui a permis d'améliorer l'activité préliminaire lorsque des combinaisons de peptides sont utilisées. Enfin, les micro-canaux PC (μ Ch) ont été développés et caractérisés pour la première fois, et les autres expériences ont été réalisées sur un micromètre de 25 μ m de largeur, fonctionnalisé avec une architecture (HA / CHI) 12,5 (PC-LbL) avec des peptides RGD et QK (RGD + QK) ou avec des peptides RGD et SVV (PC-RGD + SVV). Notre première expérience de tubulogénèse a montré de manière surprenante la formation de structures de type tubulaire déjà après 2h d'incubation en utilisant la combinaison double-peptides, mais uniquement avec PC-RGD + QK. Les tubes étaient également présents après 3 et 4 heures de culture. L'expérience de co-culture avec des péricytes humains dérivés du placenta (hPC-PL) montre comment la stabilisation des tubes a été améliorée après 3 et 4 heures également pour l'échantillon de PC-RGD + SVV. Globalement, notre matériel bio-fonctionnel avec les peptides PC-RGD + QK et PC-RGD + SVV

permet la formation d'une structure de type tubulaire à la fois dans une expérience de monoculture et de co-culture.

Mots clés: estampage à chaud, fonctionnalisation de surface, microcanaux, dépôt couche par couche, bioactivité, cellules endothéliales de la veine ombilicale humaine, péricytes humains, peptides, structure capillaire.

Title: Engineered microchannels for vascularization in bone tissue engineering

Abstract: *In vitro*, tubular-like structures formation with human umbilical vein endothelial cells (HUVECs) was investigated by combining material chemistry functionalization and three-dimensional geometry development. Polycarbonate (PC) was used as a template for the development of the scaffold. Natural polysaccharide's film based on alternate layer-by-layer (LbL) deposition of hyaluronic acid (HA) and chitosan (CHI), was first applied to PC surface and characterized in terms of thickness growth both, in dry conditions using ellipsometry, and confocal laser scanning microscopy (CLSM). This first functionalization results in a complete coating of the PC layer. Further biofunctionalization with one adhesive peptide (RGD) and two angiogenic peptides (SVV and QK) was investigated, immobilizing those peptides on the carboxylic group of HA previously deposited, using the well-known carbodiimide chemistry. The labeled version of each peptide was used to characterize the peptides' immobilization and penetration into the polyelectrolyte layers, resulting in a successful grafting with complete penetration through the entire thickness of the LbL. *In vitro* tests were performed using HUVECs to assess their adhesion efficiency and their metabolic activity on the LbL with and without peptide immobilization, resulting in a preliminary improved activity when peptide-combinations is used. Finally, PC micro-channels (μ Ch) were first developed and characterized, and the rest of the experiments were performed on μ Ch of 25 μ m width, functionalized with (HA/CHI)_{12.5} architecture (PC-LbL) with RGD and QK peptides (PC-RGD+QK) or with RGD and SVV peptides (PC-RGD+SVV). Our first tubulogenesis experiment surprisingly showed the formation of tubular-like

structures already after 2h of incubation using the double-peptides combination but only using PC-RGD+QK the tubes were present also after 3 and 4 hours of culture. The co-culture experiment with human pericytes derived from placenta (hPC-PL) demonstrates how the stabilization of the tubes was improved after 3 and 4 hours also for the PC-RGD+SVV sample. Globally our bio-functional material with PC-RGD+QK and PC-RGD+SVV peptides allow the formation of tubular-like structure in both mono and co-culture experiment.

Keywords: hot-embossing, surface functionalization, micro-channels, layer-by-layer, bioactivity, human umbilical vein endothelial cells, human pericytes, peptides, capillary structure.

UNITÉ DE RECHERCHE

CBMN - UMR 5248 Chemistry And Biology Des Membranes Et Des Nano-Objets

3Bio's Lab; 1 Allée Geoffroy Saint-Hilaire, 33600 Pessac (France)

IMCN - Institut de la Matière Condensée et des Nanosciences

Bio- and Soft Matter lab; Croix du Sud, 1 B-1348 Louvain-la-Neuve, (Belgique)